Topological Order and Glassy Properties of Flux Line Lattices in Disordered Superconductors

Inaugural-Dissertation
zur
Erlangung des Doktorgrades
der Mathematisch-Naturwissenschaftlichen Fakultät
der Universität zu Köln

vorgelegt von

Jan Kierfeld

aus Essen

Köln 1997

Berichterstatter: Prof. Dr. T. Nattermann
Priv.-Doz. Dr. H. Rieger

Tag der mündlichen Prüfung: 20. Dezember 1996

Contents

1 Introduction **1**

I Topological Order in the Vortex Glass Phase of High Temperature Superconductors **9**

2 Introduction **11**
2.1 Topological Defects and Melting 12
2.2 Dislocations in the Presence of Disorder 18

3 The Bragg Glass Phase, Random Manifolds and Random Forces **23**
3.1 Elasticity Theory and Interaction-induced Length Scale L^* 23
3.2 Pinning Energy 27
3.3 Random Force Regime and Larkin Length L_ξ 28
3.4 Random Manifold Regime and Positional Correlation Length L_l 30
3.5 Bragg Glass and 2D Random Field XY Model 33

4 Variational Calculation for a Layered Superconductor in a Parallel Field **43**
4.1 Hamiltonian for the Layered Uniaxial Geometry 44
4.2 Elastic and Decoupled Limit 47
4.3 Variational Calculation 52

5 Scaling Arguments **63**
5.1 The Layered, Uniaxial Model 64
5.2 Scaling Approach to Realistic Models 71

5.3 Lindemann Criteria 75

6 Phase Diagram for a Typical HTSC **79**
6.1 Experimental Facts 79
6.2 Positional Correlation Length R_l 80
6.2.1 Interaction-Induced Length Scale L^* 81
6.2.2 Larkin Length L_ξ 81
6.2.3 Positional Correlation Length R_l 83
6.3 Phase Diagram 84

7 Conclusion **89**

II Planar Arrays of Steps and Lines in Random Media: The 2D Random Field XY Model **93**

8 Introduction **95**

9 Renormalization of a Generalized Replica Hamiltonian of the Vortex-Free 2D RFXY Model **105**
9.1 Replica Hamiltonian 105
9.2 Renormalization 106
9.3 Correlation Functions 111
9.4 Free Energy 112

10 Replica Symmetry Breaking and Renormalization of the Vortex-Free 2D RFXY Model **115**
10.1 Replica Symmetry Breaking in Renormalization 115
10.1.1 RG Analysis of a One-Step RSB 118
10.1.2 Correlations 122
10.1.3 Free Energy 125
10.1.4 Comparison with Variational RSB Approach 127
10.2 Self-Consistent Diagrammatic Approach 130
10.2.1 Replica Symmetric Solution 133
10.2.2 One-Step RSB Solution 135

11 Two Interacting Arrays of Lines and Steps in Random Media **139**

12 Conclusion **151**

A Part I **155**
A.1 Random Force, Bragg Glass and Random Manifold Regime 155
A.1.1 Correlations and Larkin Lengths in the Random Force and Bragg Glass Regime 155
A.1.2 Correlations in the Random Manifold Regime 159
A.2 Details of the Variational Calculation 161
A.2.1 Self-Consistency Equation 161
A.2.2 Quantitative Analysis of the Self-Consistency Equation for $T = 0$ and $\tau \gtrapprox 0$ 165
A.3 Elastic Moduli 169

Acknowledgments **177**

Zusammenfassung **I**

Errata **IX**

Chapter 1

Introduction

As opposed to type-I superconductors which have a direct phase transition from the superconducting Meissner phase to the normal phase, type-II superconductors exhibit the so-called *mixed phase* [Figure 1.1]. Upon increasing the magnetic field above a lower critical field H_{c1}, the diamagnetic Meissner effect ceases to be complete, and the magnetic field penetrates the sample in form of *vortices* or *flux lines* carrying each a magnetic flux quantum $\phi_0 = hc/2e$. At the upper critical field H_{c2}, the Meissner effect is lost and the transition to the normal phase takes place. As predicted by Abrikosov [1], the vortices arrange themselves at low temperatures in a triangular *Abrikosov lattice*, which bears his name since. After the discovery of the high-T_c superconductors by Bednorz and Müller in 1986 [2], theoretical and experimental interest in the properties of the vortex lattice strongly revived. In the first place, this is due to the *technological* importance of the new class of materials discovered by Bednorz and Müller, which opens up a possibility to generate dissipation-free currents at relatively high temperatures (up to 125K, i.e., above the temperature of liquid nitrogen). Unfortunately, as we will see, a current causes motion of vortices in the mixed phase, which leads to dissipation. In order to produce a technological useful high-T_c superconductor, *disorder* has to be introduced, i.e., defects in the superconductor that "pin" flux lines and hinder them from moving. These processes require a more profound theoretic understanding of the physics of flux lines in a disordered superconductor, to which this thesis hopefully can contribute a little.

From the phenomenological point of view, that we want to take throughout this thesis, superconductors can be described by the Ginzburg-Landau theory [3]. This theory starts from a free energy functional describing the superconducting electrons in terms of a complex *order parameter* Ψ, that can be interpreted as the macroscopic wave function of the condensate of Cooper pairs and that couples to the *electromagnetic vector potential* $\mathbf{A}$. In the mean-field theory, minimizing the Ginzburg-Landau functional, one finds the superconductor in the ideal Meissner phase at low temperatures and low fields [Figure 1.2]. The superconductor exhibits a perfect diamagnetism with $\mathbf{A} = 0$, and all electrons

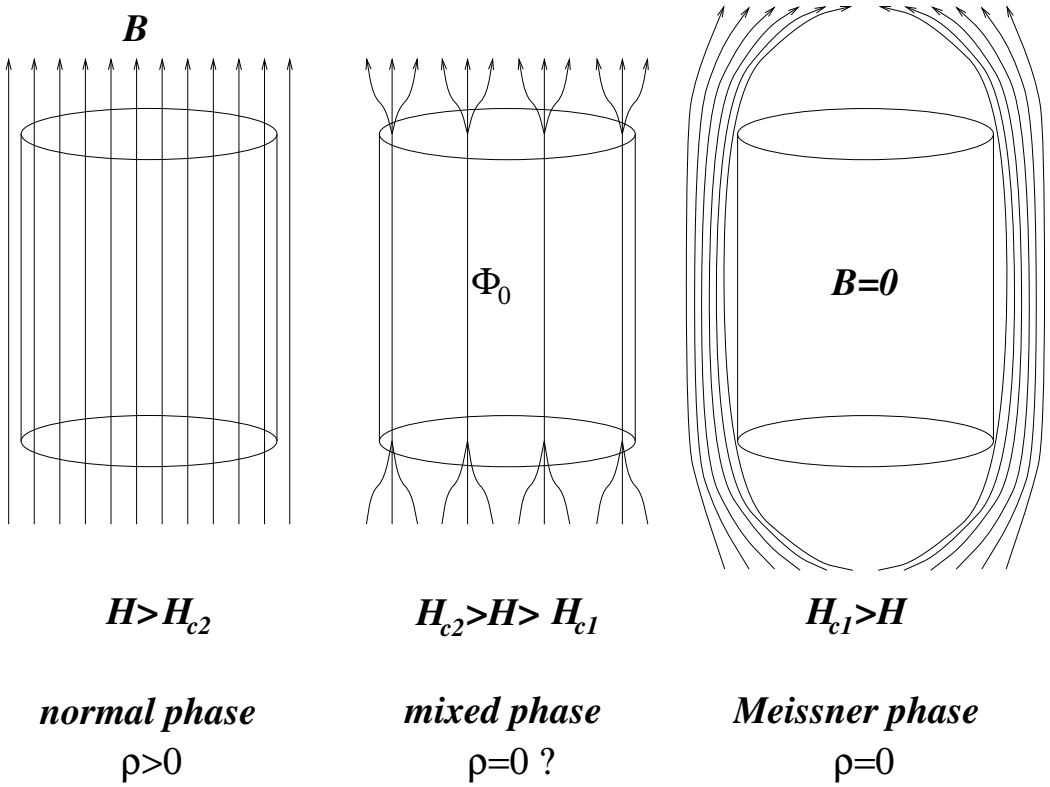

Figure 1.1: The three phases of a type-II superconductor. Left: In the *normal phase* at $H > H_{c2}$, the magnetic field penetrates the sample and the resistivity is non-zero $\rho > 0$. Right: In the *Meissner phase* at $H < H_{c1}$, the magnetic field is excluded and the superconductor is a diamagnet with $\rho = 0$. Middle: In the *mixed phase* at $H_{c2} > H > H_{c1}$, magnetic flux penetrates in form of *flux lines* carrying each an elementary flux quantum Φ_0.

are paired into Cooper pairs and condensed into *one* quantum state such that $|\Psi| = 1$. Much of the physics contained in the Ginzburg-Landau functional is determined by the interplay of two basic length scales. The *magnetic penetration depths* λ is the typical scale for variations of $\mathbf{A}$, and the *coherence length* ξ gives the correlation length of the Cooper pairs and sets the scale for variations in the order parameter Ψ. In particular, the ratio λ/ξ determines the "sensitivity" of the superconductor to fluctuations allowing a local penetration of the magnetic field and reduction of the order parameter: For $\lambda/\xi > 1/\sqrt{2}$, the superconductor becomes of type-II, and magnetic flux penetrates above a *lower critical field* $H_{c1}(T)$ [Figure 1.2] in form of the flux lines. Increasing the magnetic field further, more flux lines penetrate, and at the *upper critical field* $H_{c2}(T)$, the flux lines start to overlap and the superconductivity is lost [Figure 1.2]. The ratio $H_{c2}/H_{c1} \propto (\lambda/\xi)^2$ is given

by the two basic length scales of the superconductor. The signatures of high-T_c materials are extremely *large penetration depths* λ and *short coherence lengths* ξ with $\lambda/\xi \approx 100$, and a very *pronounced anisotropy* due to a layered crystal structure such that λ can change by a factor of 100 depending on the direction probed in the experiment. In addition, we have *high transition temperatures* typically around 100K. From these values alone, it is evident that virtually the whole region of the phase diagram, that is relevant for applications, is dominated by the presence of *flux lines* and, moreover, strong *fluctuation* effects of the vortex lattice can be expected. These fluctuations can be caused by *thermal* excitation of the vortices or by *disorder*, on which we focus in this thesis. An understanding of the disorder-induced fluctuation effects, which lead to the above mentioned pinning of the flux lines, is necessary for any technological progress in this field.

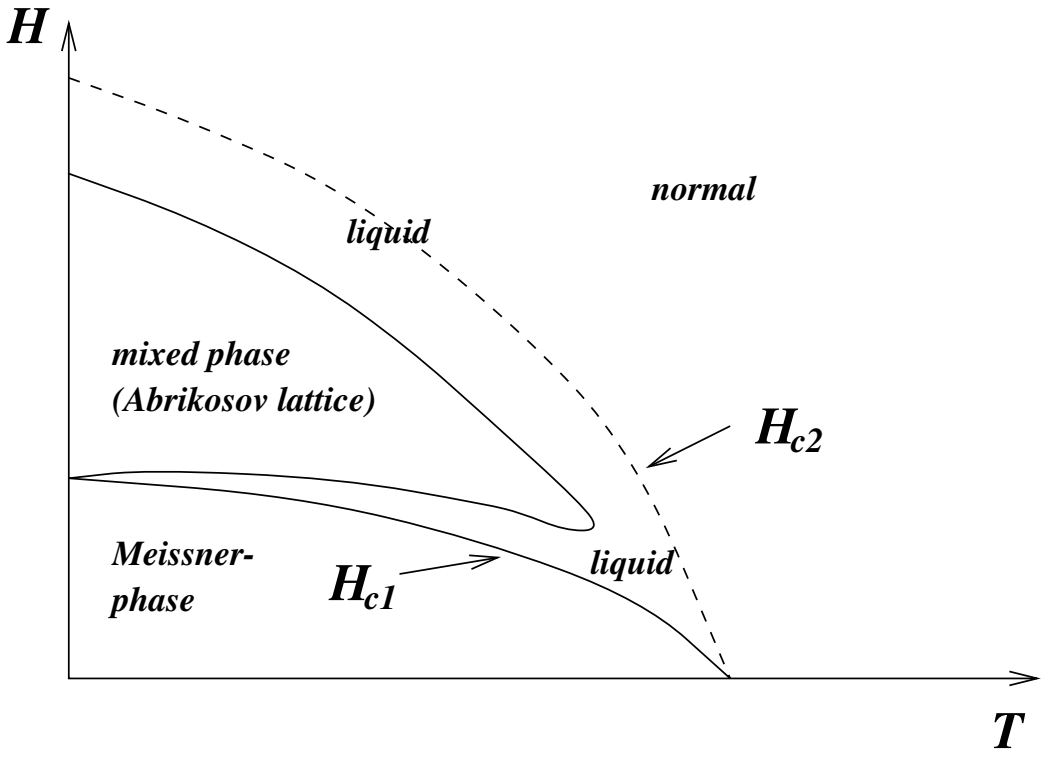

Figure 1.2: Schematic phase diagram of a pure type-II superconductor. Mean-field theory predicts an ideal Meissner phase for $H < H_{c1}$ and a mixed phase with an Abrikosov vortex *lattice* for $H_{c1} < H < H_{c2}$. Thermal fluctuations *melt* the lattice into a flux *liquid* beyond the indicated melting line.

The Abrikosov vortex lattice of the mixed phase can be described in wide parts of the phase diagram much like a crystal by an elasticity theory in the displacements of the lines with elastic moduli, which can be calculated from the Ginzburg-Landau theory [4].

Though even less microscopic than the Ginzburg-Landau theory, this is a very fruitful way of looking at the Abrikosov lattice and allows a quite detailed study of fluctuation effects. Virtually all calculations performed in this thesis are based on such an elastic description of the flux line lattice, and the whole first part of this work is devoted to estimate the region in the phase diagram where it is internally consistent in the presence of disorder.

First, let us consider a clean sample of a high-T_c superconductor. The mean-field phase diagram, represented by the lines $H_{c1}(T)$ and $H_{c2}(T)$ in Figure 1.2, has to be strongly modified already due to the presence of thermal fluctuations. When the vortex lattice becomes "soft", or the shear modulus small, it is likely to *melt* by thermal fluctuations. This happens for low vortex densities near H_{c1}, where the interactions become weak (like in an "ordinary" crystal), or close to H_{c2}, where the order parameter ϕ is reduced and thermal fluctuations are strong [Figure 1.2].

For technological aspects, the "performance" of a superconductor is mainly determined by its dynamic properties when an external current $\mathbf{j}$ is applied. Also from a theoretical point of view, the behaviour of the *resistivity* ρ clearly marks the differences between the phases in a clean sample. In the normal conducting phase, we have a *finite* resistivity $\rho > 0$ as in the flux liquid, which turns out not to be thermodynamically distinct from the normal phase due to the strong vortex motion leading to $\langle \Psi \rangle = 0$. By contrast, we find a genuinely superconducting state with $\rho = 0$ in the Meissner phase. However, this is *not* the case in the mixed phase: An applied current causes a Lorentz force, since the vortex lattice carries a magnetization $B = (\#\text{vortices}) \cdot \Phi_0$. Under the action of the Lorentz force $\mathbf{f_L} = \mathbf{j} \times \mathbf{B}/c$, the flux lines start to *move* in the direction of f_L. Moving flux lines with a velocity $\mathbf{v}$ generate in turn an electric field $\mathbf{E} = \mathbf{B} \times \mathbf{v}/c$. Because $\mathbf{j} \parallel \mathbf{E}$, *dissipation* appears. This mechanism causes a non-zero resistance $\rho > 0$ so that an ideally clean sample of a high-T_c superconductor would be of very limited use: Due to the large extent of the mixed phase ($H_{c2}/H_{c1} \sim \mathcal{O}(10^4)$), one has a non-zero resistivity in the parts of the phase diagram, that are of interest with regard to novel applications.

However, dissipation can be prevented when the sample is disordered, i.e., it contains defects such as point impurities, columnar defects from heavy-ion irradiation or twin-planes. Defects represent favorable regions for the normal-conducting cores of the flux lines and thus exert a *pinning force* f_{pin} on the vortices. As soon as $f_{pin} > f_L$, the flux lattice is pinned and dissipation stops. The equilibrium properties of the pinned flux line lattice can be described as "glassy" in the framework of the theory of disordered systems and have led to the term "vortex glass phase" for this thermodynamic state of the disordered flux line array [5]. Another characteristic of the high-T_c materials is their stoichiometry, which is such that the presence of oxygen vacancies in the crystal, and thus pinning of flux lines, is an *intrinsic* property of these materials, and their technological usefulness is reestablished. These oxygen vacancies are in most of the cases the dominant source of disorder and can be theoretically treated as *weak* point defects. Throughout this thesis, we are dealing only

with such point defects and do not consider higher dimensional defects such as columnar defects. In combination with the above mentioned elasticity theory for the pure flux line lattice, this allows to describe the mixed state of a high-T_c on a phenomenological basis as what has been termed in the theory of disordered systems a *pinned elastic manifold*.

The concept of the pinned elastic manifold provides a link between theory and experiment where, on the one hand, one of the most-studied models in the theory of disordered systems can be applied to the phenomenology of vortex arrays in high-T_c superconductors and, on the other hand, almost the entire theoretical field becomes experimentally accessible. It is also the starting point for the work performed in this thesis. From a statistical mechanics point of view, in particular regarding the phase diagram and possible phase transitions of the vortex lattice, it is most important to identify the different universality classes of pinned elastic manifolds, which are characterized by physical properties probing the asymptotic large scale behaviour. For example, the technologically relevant depinning current $j_c = cf_{pin}/B$ of the flux line lattice (the current where f_L starts to exceed f_{pin}) is such a quantity for weak disorder. With regard to their universal large scale features, elastic manifolds in a random medium can be characterized by only a few parameters, which are (i) the dimensionality d of the manifold, (ii) its codimension, i.e., the number n of components of the displacement-field, and (iii) its coupling to the disorder.

A large variety of combinations of these three parameters can be realized in a disordered superconductor [4], of which a few are considered in this work. The most obvious application is certainly the Abrikosov lattice itself with $d = 3$ and $n = 2$. However, as we will work out in more detail in chapter 3, the coupling to the disorder has to be treated in three different ways depending on the size of the regions under consideration. On the shortest scales, disorder can be modeled as short-range correlated random forces, and the instability of the Abrikosov-lattice with respect to arbitrarily weak point disorder below $d = 4$ has first been demonstrated by Larkin [6] within this approximation. On larger scales, disorder is overestimated in such a model, and the so-called "random manifold" model with a short-ranged disorder potential in the displacements is appropriate. On the largest scales, the periodicity of the Abrikosov lattice has to be retained, and the elastic manifold is modeled as "living" in a *periodic random medium*. This regime is called "Bragg Glass" or charge density wave regime. Such periodic random media are what is considered mainly in this thesis, for $d = 3$ in part I and for $d = 2$ in part II. There, we study extensively the case $d = 2$ and $n = 1$ in a periodic random medium, which is experimentally realized for *planar* arrays of vortex lines. Because of the intrinsic layering of most of the high-T_c superconductors, planar arrays of vortex lines occur when the layers of the material are *parallel* to the applied magnetic field. Another important realization of pinned elastic manifolds in a superconductor occurs close to H_{c1}, where the flux line density is low enough that we can approximate the vortex array by a collection of *single* flux lines, which are pinned elastic manifolds in $d = 1$ or, in other words,directed paths in

a random medium.

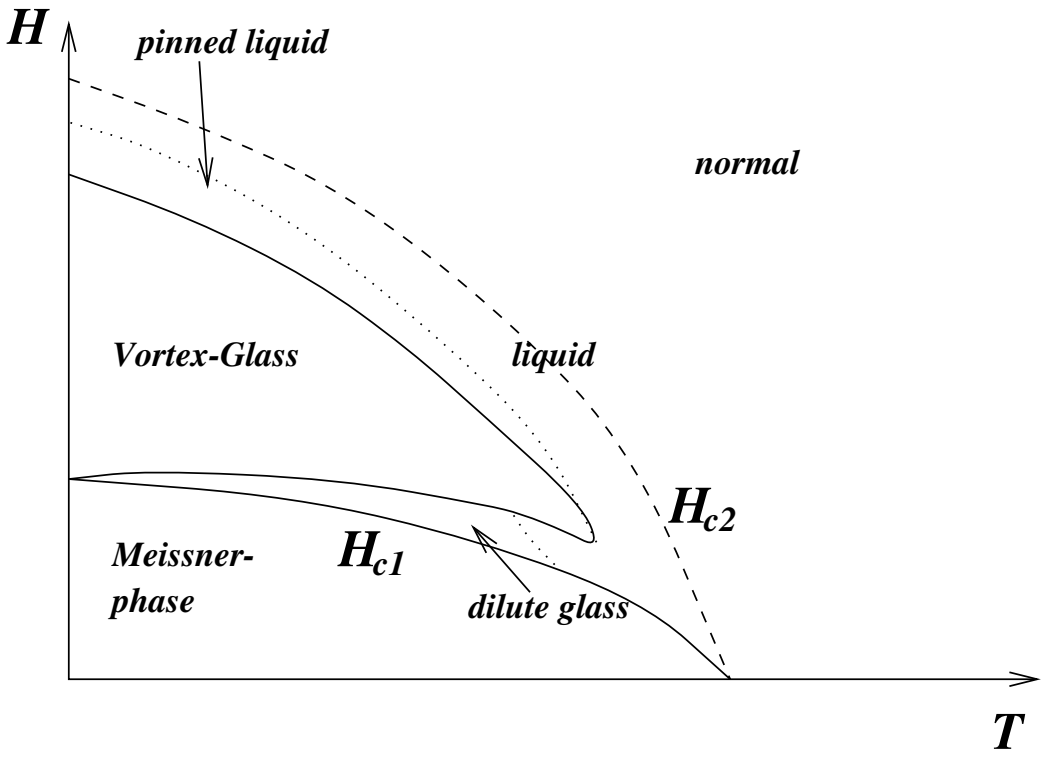

Figure 1.3: Schematic phase diagram of a high-T_c superconductor in the presence of *point disorder* as proposed by a description as pinned elastic manifold.

Let us summarize very briefly the basic results of the theory of pinned elastic manifolds regarding the phase diagram for a disordered superconductor (as compared to the clean limit [Figure 1.2]) [4]. As already mentioned, the Abrikosov lattice has been shown to be unstable with respect to disorder [6] and is believed to be replaced by a pinned glassy phase, the *vortex glass phase* [5] [Figure 1.3], which is in the framework of the theory of pinned elastic manifolds the above mentioned Bragg glass phase. By the term "glassy" one usually refers quite losely to a bunch of properties all of which are connected in one or the other way to some anomalous fluctuations in the free energy on large scales due to the disorder. These fluctuations give rise to energy barriers U between different low-lying metastable configurations of the disordered flux line array. For the dynamics it is this property which reestablishes the vanishing linear resistivity. Driving the flux lines with a small current j probes the large scale properties, and one finds *diverging* energy barriers $U(j) \sim U_c(j_c/j)^\mu$ for small j with an exponent $\mu > 0$. With an activated dynamics, this leads directly to a "glassy" non-linear current voltage relation $V \propto \exp\left[-(U_c/T)(j_c/j)^\mu\right]$ such that $\rho(j \downarrow 0) = 0$. Such a behaviour is as well obtained for single flux lines so that

also in the regime of low flux line densities close to H_{c1}, we expect to find some "diluted vortex glass" [Figure 1.3]. On the other hand, the liquid phase close to H_{c2} is essentially stable to weak disorder because entropic effects dominate over the pinning energies. This short overview leads to the schematic phase diagram in Figure 1.3.

Pinned elastic manifolds are one of the most-studied objects in the statistical physics of disordered systems [7]. Apart from superconductors, they occur in many other physical systems, among which are domain walls in disordered magnetic systems, pinned charge density waves and, for $d = 2$, numerous applications in surface physics (one of the latter will be studied in detail in chapter 11). A good deal of this knowledge will be available for a theoretical study of the properties of the disordered flux line array, leading to a phase diagram as depicted in Figure 1.3, if the treatment by an elasticity theory is internally *consistent*, in particular in the presence of disorder. This consistency may break down if the topological order of the vortex lattice – that is tacitly assumed to be intact in writing down an elastic energy – is destroyed by topological defects of the line lattice such as *dislocation loops*. In the pinned glassy phase of the flux line lattice, dislocation loops may occur when the flux lines optimize their configuration but are pinned by the impurities in the sample at the same time. Such an instability with respect to dislocation loop formation has been conjectured by Fisher, Fisher and Huse [8] for the vortex glass phase in $d = 3$, however, quantitative arguments have not been brought forth in past approaches [8, 9]. Part I is devoted entirely to this important subject, and we will find a simple Lindemann-like criterion giving the range of applicability of the elastic approach in the presence of point disorder or, in other words, the region in the phase diagram 1.3, where the vortex glass is indeed a topologically ordered Bragg glass [see Figure 6.1].

In part II, we consider in detail the glassy equilibrium properties of the two-dimensional random field XY model, which corresponds in the above classification to $d = 2$, $n = 1$ and a periodic randomness. As mentioned above, it models a disordered planar array of vortex lines and is the only system for which the existence of a glassy low-temperature phase can be shown analytically due to the topological perfection of a planar system. It were essentially the properties of the low-temperature phase of the two-dimensional random field XY model, which led to the first conjecture of a vortex glass phase by Fisher [5]. Though it is one of the simplest possible models describing many interacting flux lines in a random medium, there is only a general agreement regarding the existence of a glassy or pinned low-temperature phase. However, the properties of this glassy phase are less clear and an agreement regarding for example the basic question of the shape of displacement-correlations has not yet been reached. These issues will be the subject of part II.

Part I

Topological Order in the Vortex Glass Phase of High Temperature Superconductors

Chapter 2

Introduction

The first part of this work is devoted to the issue of topological defects, in particular dislocations, in a flux line (FL) array in the presence of "point disorder", i.e., point defects exerting pinning forces on the FLs. This issue is of special interest with regard to the nature of the disordered FL array. Whereas it is well-known [6] that the FL array is unstable to weak point disorder beyond the Larkin length, the nature of the FL array on larger scales is still subject of intense studies [4]. It has been conjectured that the FL array is *collectively pinned*, forming a *vortex glass* (VG) phase [5, 8, 10, 11] with zero linear resistivity at low temperatures. This conjecture is supported by a number of experiments on disordered samples of high-T_c superconductors [12, 13, 14, 15, 16], where a continuous transition to a phase with zero linear resistivity was found upon cooling. However, Refs. [8, 10, 11] make very different statements regarding the positional order of the FL array and, intimately related to that issue, the role of dislocation loops on scales beyond the Larkin length. Refs. [10, 11] describe the disordered FL array as an *elastic* system subject to a disorder potential, so they consider an explicitly *dislocation-free* system. On the other hand, it is argued in Ref. [8] by using an Imry-Ma-type argument that dislocation loops are *always* relevant beyond the Larkin length and that a purely elastic description of the FL array is therefore inadequate.

The *dislocation-free*, *elastic* FL array in a random medium [9, 10, 11, 17] is one of the best studied disordered systems being very similar to the randomly-pinned charge-density waves and the random-field XY model, which have been studied extensively in the past decades [18, 19, 20, 21, 22, 23]. A variety of approximate methods have been used to obtain the conclusion that the presence of weak point disorder leads to a glass phase with the remarkable property that the transverse displacements of the FLs exhibit only logarithmic fluctuations. This implies the existence of quasi-long-range positional order in the glass phase of the dislocation-free flux array. This property is especially interesting in view of recent experiments on pinned FL arrays, where Bitter-decoration [24], neutron scattering [25, 26], and μSR [27] experiments on weakly disordered samples have all indicated some

long-range order of the FL array. This suggests [9] that such a topologically ordered glass may actually exist as a *stable* thermodynamic phase for some range of parameters in the cuprate superconductors. Recently, related numerical studies of the random field-XY model [28] and a layered model superconductor [29] further supported this scenario.

On the other hand, in neutron diffraction experiments by Cubitt et al. [25] it has been observed that upon increasing the magnetic field, the topologically ordered glass phase becomes *unstable*. In addition, critical current measurements of Khaykovich et al. [30] show a sharp drop in the (local) critical current j_c upon decreasing the magnetic induction below a critical value. This can be attributed to the existence of a *topological phase transition*, where topological order is regained upon lowering the magnetic field. The existence of such a transition has also been demonstrated in the numerical studies in Refs. [28, 29] in good agreement with the experimental results in Ref. [25]. An understanding of these signatures of a topological transition where topological defects, i.e., dislocations, proliferate requires a quantitative analysis of the stability of the topologically ordered, elastic VG phase.

Whereas the issue topological defects in the FL lattice is quite well understood for disorder-free case [31, 32], it is on a *quantitative* level still essentially unresolved for a disordered sample, when the FL array is in the VG phase. This is due to the fact that the issue of spontaneous formation of topological defects, i.e., dislocation loops involves a complicated interplay between elastic energies and disorder as we will see below. We try to close this gap and explore quantitatively the possibility of a dislocation-free, elastic VG phase.

However, before addressing the disordered system, it is useful to review shortly some general facts about topological defects in line lattices. Thereafter, we discuss how the melting of the *disorder-free* FL lattice can be understood qualitatively in terms of a proliferation of dislocations. It is instructive to compare the physical mechanism underlying the thermal melting of the disorder-free FL lattice by dislocations with the mechanism of the "disorder-induced melting" by dislocations in the pinned FL array.

2.1 Topological Defects and Melting

There are various kinds of possible defects in a line lattice: *Interstitials* and *vacancies*, *edge* and *screw dislocations* [33]. As we will see, only the latter have a long-range, non-local effect on the deformation of the lattice and are for this reason more important. We start with a short review of their properties in a perfect, i.e., disorder-free line lattice. For definiteness, we take the z-direction as the direction of the lines so that the lattice, e.g. the hexagonal Abrikosov lattice, is in the xy-plane; displacements $\mathbf{u}(\mathbf{r})$ of the lines are lying in the xy-plane then. Mathematically speaking, *dislocations* are *topologically stable* line defects with a non-zero *topological charge*. The integral $\int_C d\mathbf{u} = -\mathbf{b}$, measuring

the increase in the displacement $\mathbf{u}$ along a contour C around the dislocation line, is non-zero and equals the *Burgers vector* $\mathbf{b}$, which is a lattice vector (for the energetically most favorable dislocations, it is a primitive lattice vector) [Figure 2.1]. The Burgers vector $\mathbf{b}$ is the topological (vector) charge of the dislocation. Denoting the tangent vector of the dislocation line with $\boldsymbol{\tau}$, an *edge dislocation* is defined by $\boldsymbol{\tau} \perp \mathbf{b}$ and a *screw dislocation* by $\boldsymbol{\tau} \parallel \mathbf{b}$.

An *edge dislocation* is created by inserting or removing a half-plane or "sheet" of lines in the lattice, the edge of which is after relaxation the dislocation line [Figure 2.1]. In a line lattice, dislocations are subject to more constraints than, for example, in a usual crystal lattice, because we want to exclude that a line splits into two or two lines merge into one [which is for FLs in a type-II superconductor forbidden due to the flux quantization]. This requires that *no* edge dislocation can occur in the xy-plane, i.e., $\boldsymbol{\tau} \parallel \hat{\mathbf{z}}$.

A *screw dislocation* can be created by cutting the line lattice along a half-plane in the xy-plane, displacing one side of the half-plane parallel to the plane by a lattice vector, joining the two sides again, and letting the lattice relax. The edge of the half-plane is the dislocation line [Figure 2.1]. From this construction follows that screw dislocations always lie in the xy-plane, i.e., $\boldsymbol{\tau} \perp \hat{\mathbf{z}}$. Both sorts of dislocations are combined when a *dislocation loop* is formed [Figure 2.1]. Because the edge components of the loop must not lie in the xy-plane, loops are constrained to fulfill

$$\boldsymbol{\tau} \cdot (\hat{\mathbf{z}} \times \mathbf{b}) = 0 \ . \tag{2.1}$$

Hence, they always lie in a single plane of the lattice spanned by $\hat{\mathbf{z}}$ and $\mathbf{b}$.

However, this topological constraint is weakened in the presence of another kind of defect, *interstitials* or *vacancies* [32]. Analogously to crystal defects, an *interstitial/vacancy* is created by adding/removing a single line and letting the lattice relax. The main difference to crystals lies in the line nature of the lattice constituents themselves. Hence, in a line lattice interstitials/vacancies are not point defects but line defects. Interstitials/vacancies are line defects with zero topological charge and therefore not subject to the topological constraint (2.1) as opposed to a dislocation. By absorbing or emitting interstitials/vacancies, a dislocation loop can circumvent the above planarity restriction and "climb" gradually out of the $\hat{\mathbf{z}}\mathbf{b}$-plane it was confined to originally. Henceforth, we exclude interstitials/vacancies for simplicity and comment on this subject later.

It is well-known that many phase transitions in two dimensions are in the Kosterlitz-Thouless universality class and can be described by the occurrence of free (or unbound) topological defects, which destroy the quasi-long-range order of the low-temperature phase [35]. In a similar way, it is one possibility to describe the melting of the three-dimensional line lattice by the proliferation of unbound dislocation loops [considering a cut through the system in a xy-plane, intersections of a dislocation line with the plane represent indeed topological defects in two dimensions with the Burgers vector as topological charge]. With

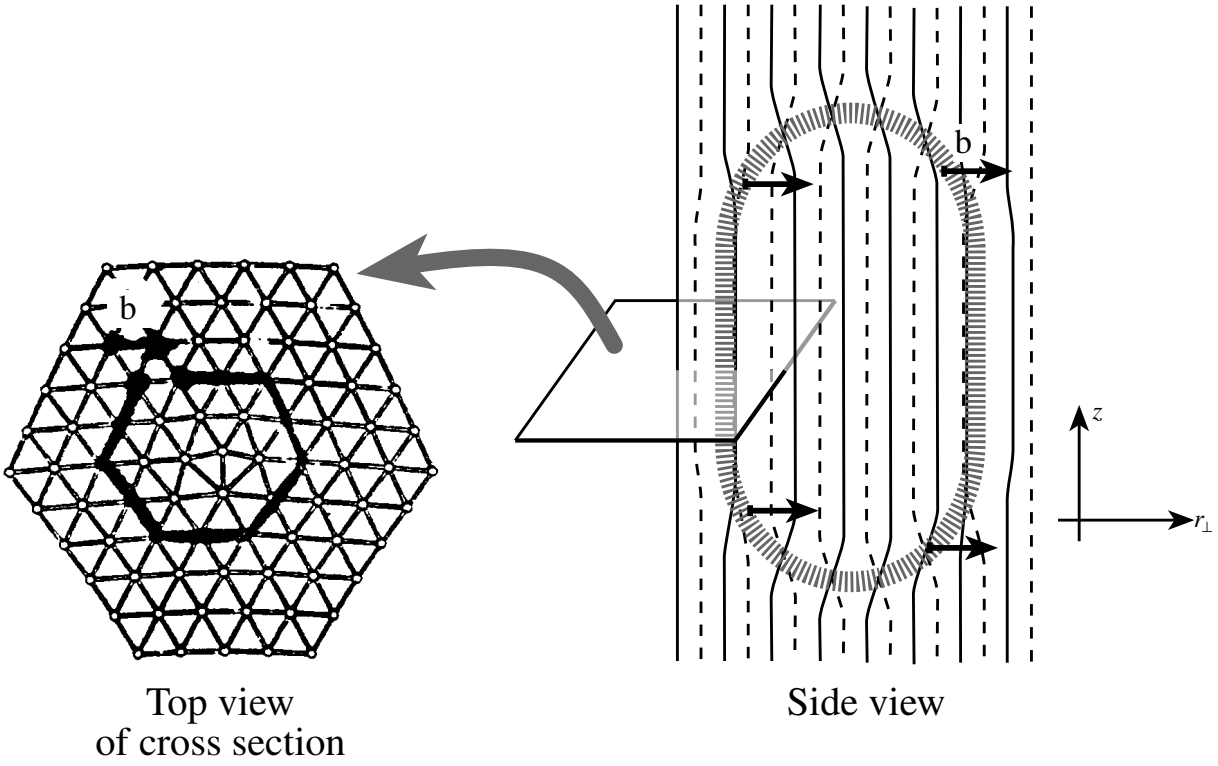

Figure 2.1: Dislocation loop in the hexagonal Abrikosov flux line lattice with Burgers vector **b**. Left: Contour C around the dislocation line measuring the increase $\int_C d\mathbf{u} = -\mathbf{b}$. Right: The part of the dislocation loop $\parallel \hat{\mathbf{z}}$ is an *edge dislocation*, the part $\perp \hat{\mathbf{z}}$ a *screw dislocation*. Dashed lines represent flux lines in the next crystal plane behind the figure plane. [The Figure is taken from Ref. [34].]

an "unbound" or "free" dislocation loop, we denote an *arbitrary large* or *infinite* loop; upon cutting the loop, it can alternatively be viewed as a free, infinitely long, stretched dislocation line threading the whole system [cutting in a xy-plane, this is the analog of free, unpaired defects in two dimensions, as they occur in the high-temperature phase above a Kosterlitz-Thouless transition].

Why is the melting of the line lattice mediated by free dislocation loops? A physical answer to this question is that free dislocations are capable of providing a mechanism for relaxing elastic stress, in particular shear stress: Upon applying shear stress on a single dislocation loop, a so-called *Peach-Köhler force* is generated, which tends to expand the loop. By plastic deformation, the dislocation loop starts to expand through the sample along a "gliding plane", the plane spanned by $\hat{\mathbf{z}}$ and **b** [31, 36]. This important property of a dislocation loop drives the shear modulus of the lattice to zero and destroys the translational order when unbound loops occur. This can be checked analytically by studying the

downward renormalization of the shear modulus by dislocations or the translational order parameter

$$\langle \rho_{\mathbf{K}} \rangle = \langle \exp\left(i\mathbf{K}\mathbf{u}\right) \rangle \tag{2.2}$$

($\mathbf{K}$ is a reciprocal lattice vector), which is also driven to zero by dislocations reflecting the loss of translational order [31]. But these two properties just characterize a *hexatic flux liquid*, which is distinguished from an *isotropic flux liquid* only by the persistence of the bond-orientational order [dislocation loops cannot destroy the bond-orientational order [31]]. Therefore, a proliferation of unbound dislocation loops can indeed describe a melting of the lattice, at least into a hexatic liquid.

The nature of such a phase transition, i.e., whether it is first or second order, will be determined by the details of what we just called "proliferation". If there is a jump in the density of free dislocations upon increasing the temperature beyond a the transition temperature, a first order transition will occur. If the density increases continuously from zero, we will have a second order phase transition. Let us consider an ensemble of free dislocation loops or, equivalently, infinitely long dislocation lines threading the whole system with an average areal density ρ in the xy-plane, which can be expressed in terms of their average distance in the xy-plane L as $\rho = 1/L^2$. In a first order phase transition, the density jumps to $\Delta\rho$ at the transition, so that *many* ($L = 1/\sqrt{\Delta\rho}$ is finite at the transition) unbound dislocations occur at the transition. The second order phase transition can be described by the formation of a *single* ($L \to \infty$ at the transition) unbound dislocation. The spacing of the dislocation loops L also sets an upper bound for the correlation length of the system. Again, a second order phase transition with a diverging correlation length can occur only if a single loop is formed at the transition.

On our way to a discussion of the effects of dislocations on the disordered, pinned vortex lattice, it is instructive to consider first the *disorder-free case*, and we want to discuss the melting of the disorder-free FL lattice by thermal fluctuations in terms of dislocations qualitatively [31, 35, 37]. Of course, there are also other possibilities to describe this transition: Phenomenologically, it can be described by the Lindemann-criterion [38], which, however, does not give any information about the nature of the transition. Following a very general mean-field argument of Landau [39], the liquid to crystal transition should be first order. The most elaborated approaches [40, 41] start from the Ginzburg-Landau mean-field theory, take into account fluctuations in the order parameter at the upper critical field and obtain an unstable renormalization group (RG) flow indicating a first order melting transition. [From these theoretical approaches and recent experiments, the general believe today is that the melting transition is of first order [42].]

Let us start investigating the second order melting scenario, i.e., the free energy of a single, large dislocation loop of size L. Generation of a single stretched dislocation line involves insertion or cutting of a whole plane in the line lattice so that dislocations

cause a *global* elastic rearrangement, i.e., a long-ranged stress-field decaying as $1/r$ from the dislocation. Therefore, the elastic energy cost (per length) E_{el} of a single, straight dislocation line is diverging logarithmically with system size:

$$E_{el} \sim cb^2 \, L \ln (L/l) \, , \tag{2.3}$$

where c is an elastic constant [1] and l the short-distance cutoff, i.e., the FL distance. In addition, the core of the dislocation costs an energy of the order

$$E_{core} \sim c' b^2 \, L \tag{2.4}$$

(with $c' \approx c$), because $\nabla u \approx b/l$ in the core region of extent $\mathcal{O}(l^2)$. The dislocation loop will occur at high enough temperatures if the total energy cost $E_{el} + E_{core}$ can be balanced by the entropy gain due to meandering of the dislocation. The entropy gain can be estimated from the number of configurations a dislocation line of length L can explore typically. Let us neglect the loop-nature for the moment and consider a dislocation of length L stretched along the z-direction. We assume that there is a typical scale ℓ in the z-direction on which the dislocation line performs a "hop" of one lattice spacing l in the xy-plane. Due to the planarity constraint (2.1) there are 2 possibilities for each "hop" and we obtain an entropy[2]

$$S \sim \ln \left(2^{L/\ell}\right) \sim (\ln 2) \, L/\ell \, . \tag{2.5}$$

Thus, the free energy of a single, large loop of size L is

$$F_{loop} = (E_{el} + E_{core}) - TS \sim L \, \left(cb^2 (\ln (L/l)) - T \, (\ln 2)/\ell\right) \, . \tag{2.6}$$

Clearly, the elastic energy cost dominates for large L due to its additional logarithmic divergence, and $F_{loop}(L \to \infty) > 0$ always, so that *no* second order melting transition can take place. But we see already that the free energy of a *finite* loop can become negative for high enough temperature indicating the possibility of a first order melting transition.

In a first order melting scenario, many dislocation loops with a finite density will occur above the transition. On the one hand, this can be favorable because the logarithmic divergence in the elastic energy can be screened but, on the other hand, also the entropy gain is reduced because the dislocations start to collide. To study this scenario, we consider an ensemble of dislocations loops with areal density ρ. In the dislocation ensemble, the logarithmic divergence of the elastic energy cost (2.3) is cut off at the distance to the next dislocation, which is of order $L = 1/\sqrt{\rho}$. The density of the elastic energy cost is thus

$$e_{el} \sim cb^2 \rho \ln (1/l^2 \rho) \, . \tag{2.7}$$

[1] For simplicity in the qualitative discussion, we assume that we can make the elastic energy isotropic by rescaling, so that we have only one elastic constant.

[2] $k_B \equiv 1$

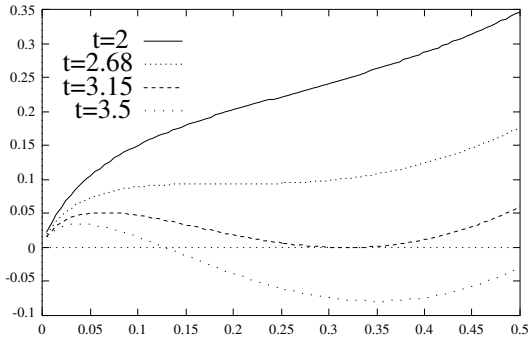

Figure 2.2: The free energy (2.11) $f \cdot l^2/cb^2$ as function of the density $\rho \cdot l^2$ for different temperatures $t = T \cdot (\ln 2)/cb^2\ell$. The transition is first order.

The density of the energy cost for the cores (2.4) is

$$e_{core} \;\sim\; c'b^2\rho \;, \tag{2.8}$$

and the density of the entropy gain (2.5) is for independent dislocation loops

$$s \;\sim\; (\ln 2)\rho/\ell \tag{2.9}$$

for the ensemble. However, following up the argumentation leading to (2.5), the dislocations are random walkers in 1+1 dimensions (i.e., with a roughness exponent $\zeta = 1/2$) and start to collide on scales $L_{col} \simeq \ell/l^2\rho$ (in the z-direction). This leads in turn to an effective entropy *loss* of $S_{col} \sim (\ln 2)L/L_{col}$ or a corresponding entropy density loss

$$s_{col} \;\sim\; (\ln 2)\rho^2 l^2/\ell \;. \tag{2.10}$$

The free energy density for a dislocation ensemble of density ρ is then (in Ref. [37], the authors give a more rigorous derivation by a mapping onto a tight-binding model)

$$\begin{aligned} f &= e_{el} + e_{core} - T(s - s_{col}) \\ &\sim A\rho \ln(1/l^2\rho) + B(T)\rho + C(T)\rho^2 \end{aligned} \tag{2.11}$$

with $A = cb^2$, $B(T) = c'b^2 - T(\ln 2)/\ell$ and $C(T) = T(\ln 2)l^2/\ell$. Such a free energy yields a first order melting [Figure 2.2] at a temperature

$$T_m \;\simeq\; \alpha\, \frac{cb^2\ell}{\ln 2} \tag{2.12}$$

with a jump in the equilibrium density of dislocations from zero to

$$\Delta\rho \simeq \frac{1}{\alpha}\,\frac{1}{l^2}\;, \tag{2.13}$$

where $\alpha \approx 3.15$ is a number[3]. For high enough temperatures $T > T_m$, the entropy gain $s - s_{col}$ from the meandering of the dislocation lines is big enough to compensate for the cost in core energy and elastic energy. At the transition a rather dense ensemble of dislocations occurs with distances $L \sim l/\sqrt{\alpha}$. The dislocations have to be sufficiently dense to screen the logarithmically diverging elastic energy. It is interesting to note that the first order transition is only obtained because the cost in elastic energy (per length) of a dislocation is logarithmically diverging: Defects with zero topological charge (like interstitials/vacancies) induce only a local, short ranged elastic deformation and thus, have only a finite elastic and core energy (per length) cost. They proliferate in a second order phase transition as can be shown by a similar argument [32].

2.2 Dislocations in the Presence of Disorder

What happens to this scenario in the presence of disorder? First of all, the dislocation-free lattice is no longer an ideal line lattice but a *pinned* FL array, where point defects, e.g. oxygen vacancies in high-T_c superconductors (HTSCs), lead to a collective pinning of the FLs, and a glassy state on large scales. The statistical properties of the dislocation-free FL array pinned by point disorder are highly non-trivial in themselves. It has been found by using an elastic description of the FL array that the dislocation-free, pinned FL array exhibits glassy properties with logarithmic displacement correlations on the largest scales [9, 11, 17]. Hence, the glassy FL array has quasi-long-range order with a disorder-averaged translational order parameter $\overline{\langle \rho_{\mathbf{K}} \rangle}$ (see (2.2)), which decays algebraically resulting in quasi Bragg peaks in scattering experiments, the reason why this pinned, elastic phase bears the name *Bragg glass* [17, 9]. These Bragg peaks can indeed be observed in neutron diffraction experiments on $Bi_2Sr_2CaCu_2O_{8+x}$ (BSCCO) at low magnetic fields [25]. A proliferation of dislocation loops will destroy the elastic Bragg glass in a *topological phase transition*. Signatures of such a transition have been observed in neutron diffraction experiments by Cubitt et al. [25], where the Bragg peaks vanish upon increasing the magnetic field, indicating an instability of the Bragg glass phase. Furthermore, the critical current measurements of Khaykovich et al. [30], that show a sharp drop in the (local) critical current j_c upon decreasing the magnetic induction below a critical value, can be explained by the existence of a topological transition, where FLs "disentangle" when topological order is regained. The existence of such a transition has also been demonstrated in the numerical studies in Refs. [28, 29]. In the closely related 3D XY model in a random field, vortex loops occur in a topological phase transition at a critical strength of the random field [28]. In simulations of disordered FL arrays [29], a proliferation of dislocation lines has been found at a critical magnetic field in good agreement with the experimental results in Ref. [25]. As in

[3] α is a solution of $\alpha = \exp(\alpha - 2)$.

the disorder-free line lattice, the bond orientational order can nevertheless persist, so that upon the instability of the Bragg glass phase the system will either "melt" into an amorphous *hexatic glass* with bond-orientational order as discussed in [43] but with vanishing shear modulus, or it undergoes directly a melting into an isotropic disordered flux liquid.

Let us give a short summary of the main results along with an outline of the remainder of part I. For the Bragg glass, one finds a $T=0$ fixed point in the RG calculation, indicating that thermal fluctuations are irrelevant for the large scale properties. This means that the free energy is equal to the energy of a large dislocation loop, and the entropy gain of the dislocation loop by meandering does *not* lead to a free energy gain in the disordered system. However, the dislocation loop can gain a disorder energy E_{dis} by allowing the line array a more optimal adjustment to the disorder configuration by its occurrence. [This change in the physical mechanisms underlying the behavior of a line-like object when switching from the disorder-free system with a Gaussian, entropy-dominated finite temperature RG fixed point to the point disordered system with a disorder dominated $T = 0$ RG fixed point is a common phenomenon in disordered systems. For example, it occurs in a very similar manner in the localization problem of a directed polymer by a columnar pin, which delocalizes in the disorder-free system entropy-driven and in the presence of point disorder driven by the energy gain from the point defects [44, 45].] We make use of this mechanism in scaling arguments presented in **chapter 5**, where we consider the dislocation loop as the result of a partial relaxation of the system. Thus, the long-range elastic rearrangement that the dislocation induces must not be interpreted as an energy cost in the disordered system. Rather, it has to be seen as the mechanism enabling an *optimally configured* dislocation line to gain disorder energy by giving the FL array the possibility to re-optimize its configuration. Of course, a dislocation loop has still to pay the core energy E_{core} due to the displacement gradients of order unity in the dislocation core. This suggests that in a disordered system the (free) energy of a dislocation loop is determined by a quite different mechanism as compared to (2.11):

$$F_{loop} \;=\; E_{loop} \;=\; E_{core} - E_{dis} \;. \tag{2.14}$$

In chapter 5, we will study the scaling of the different energies in (2.14) with the size L of the dislocation loop in detail. This leads to an Imry-Ma-type argument based on the energy balance (2.14) at $T = 0$. In (2.14) we consider a single, optimally configured, large loop of size L. As discussed above, a second order phase transition, similar to a Kosterlitz-Thouless transition, can occur when $F_{loop}(L) < 0$ for large $L \to \infty$.

We will study first a strongly layered model of a HTSC in a parallel field in chapter 5. In this model the FLs are confined by a strong pinning potential in between the CuO-planes of the HTSC (we assume a value of the magnetic field such that the Abrikosov lattice is commensurate with the layer spacing of the HTSC). Displacements are then effectively uniaxial, i.e., a scalar field. Our result from a detailed scaling analysis for the uniaxial

system is for a dislocation loop with fractal dimension D (i.e., a loop of linear dimension L has a length L^D):

$$E_{core} \sim L^D \tag{2.15}$$
$$E_{dis} \sim L^{\omega(D)} . \tag{2.16}$$

E_{core} is proportional to the loop length as above in (2.4). For the exponent $\omega(D)$, we will argue that an upper bound is $\omega(D) \leq 1$ and $\omega(D = 3/2) = 1$; furthermore, $\omega(D)$ should be monotonously increasing with D so that $\omega(D) < D$ for $D > 1$ and $\omega(D = 1) \leq 1$. This yields $F_{loop}(L \to \infty) > 0$ for $D > 1$ excluding a second order melting of the Bragg glass by dislocations with fractal dimensions > 1. Though from this argumentation it is tempting to assume that $\omega(D = 1) < 1$ holds, excluding a second order melting of the Bragg glass by dislocations, also $\omega(D = 1) = 1$ is well possible. This is a sort of "worst case"-scenario for the stability of the Bragg glass with respect to dislocation loop formation, and therefore maybe the preferred "channel" for an instability. In this "worst case", it depends on the prefactors in (2.4) and (2.16), whether dislocations will form, which will be studied in detail in chapter 5.

On the other hand, as we have seen above in the treatment of the disorder-free case, even if we have $F_{loop}(L \to \infty) > 0$, there is still the possibility of a first order melting, where dislocations occur with a finite density at the transition. In **chapter 4**, we perform a variational calculation of an effective shear modulus for the layered, uniaxial model. Instead of an elastic inter-layer coupling characterized by the shear modulus of elasticity theory for the FL lattice, we generalize to a coupling allowing a formation of dislocations and determine an effective shear modulus self-consistently in a variational approach. However, the generalized coupling allows only a simultaneous formation of dislocation loops in between *every* layer, i.e., on the shortest scale, the layer spacing. This is typical for a first order phase transition, which is indeed found in the variational calculation where, upon reducing the inter-layer coupling, the effective shear modulus drops to zero with a finite jump. This can be assigned to a downward renormalization of the shear modulus due to a proliferation of dislocation loops with a distance of the order of the layer spacing, i.e., the FL spacing in the direction perpendicular to the layers. However, in this model only loops parallel to the planes can occur. In the usual experimental situation, where the FLs are perpendicular to the planes, each dislocation is planar due to (2.1), but dislocations can occur in all planes of the lattice with *three* possible orientations instead of one in the layered model. Because in the layered model the in-plane order cannot be destroyed by the dislocations, we obtain rather a first order melting into a *smectic glass* with an in-plane quasi-long-range translational order, but without translational order in the direction perpendicular to the layers.

The scaling approach for a single, large loop with $D = 1$ and $\omega(D = 1) = 1$ (the "worst case" for the stability of the Bragg glass) and the variational approach to the

strongly layered system produce a stability criterion of the same form for the Bragg glass. Assuming a stretched loop with $D = 1$ and $\omega(D = 1) = 1$, the scaling argument is generalized from the uniaxial model to the usual experimental situation with the magnetic field perpendicular to the layers and two-component displacements of the FLs in chapter 5. This yields a generalized criterion, which can be viewed as the disordered analog of the *Lindemann criterion* [38]:

$$R_l \;>\; c^{1/2\zeta} \cdot \max(l, \lambda) \;, \tag{2.17}$$

where l is the FL spacing and λ the *magnetic penetration depth* of the superconductor (which has to be further specified for the geometry at hand). R_l is the *positional correlation length* of the FL array and defined as the transverse (to the FLs) scale, on which the typical (disorder-induced) displacement of a FL is of the order of the FL spacing l, i.e., $u(R_l) \sim l$. The Bragg glass exists only on scales larger than R_l, because it is characterized by the property that FLs start to compete for the same defects, which happens for $u \gtrsim l$. R_l has to be distinguished from another crossover length, the *Larkin length* R_ξ, which is smaller than R_l and gives the scale up to which perturbation theory in the disorder potential is valid (i.e., the typical displacement of a FL is smaller than the scale, on which the disorder varies), so that the pinning of the FL array can be described by *random forces* on smaller length scales. On intermediate (transverse) scales between the positional correlation length R_l and the *Larkin length* R_ξ, the FL array is in the so-called *random manifold regime*. In this regime, we have glassiness but FLs do not compete for the same defects and every line "lives" in an independent disorder. The criterion (2.17) is called "Lindemann-like" because it compares the positional correlation length R_l characterizing the strength of the disorder-induced fluctuations with the length scale of the FL spacing set by the ordered state of the lattice. c is a number playing a similar role as the Lindemann-number in the conventional Lindemann-criterion [38]. The variational calculation (where we ignore the existence of the random manifold regime) yields $c \approx \mathcal{O}(50)$. Finally, ζ is the roughness exponent in the random manifold regime, i.e., for a 3-dimensional random manifold with a 2-component displacement field, the best estimate for which is $\zeta = 1/5$ [7].

In the case of $\omega(D) < D$, the scaling argument excludes an instability with respect to the formation of a single, large dislocation loop. For $D = 1$ and $\omega(D = 1) = 1$, we are in the marginal case of the scaling argument for a single dislocation loop, and the stability of a free dislocation depends on the prefactors of the involved energies. From the energy balance (2.14), one obtains a criterion of the above form (2.17) but the value of the numerical factor c is beyond the scope of a scaling argument. Though such an instability with respect to a single loop is of course a *sufficient* criterion for the destruction of the Bragg glass phase, namely in a second order transition, a first order melting by the occurrence of *many* loops at the transition may well be favorable, as it is in the disorder-free case discussed above. The variational calculation, where a first order melting on the shortest scale of a FL distance is

realized, yields a value $c \approx \mathcal{O}(50)$. In formulating the Lindemann-criterion (2.17), we take this value for c obtained from the variational calculation. In chapter 5 we show by using a scaling relation that the criterion (2.17) is indeed equivalent to a criterion in the form suggested originally by Lindemann [38],

$$u(l) > c^{-1} \cdot l \ , \tag{2.18}$$

where $u(l)$ is the average FL displacement on the *shortest scale* of a FL spacing l (as opposed to thermal melting, $u(l)$ is in wide parts of the phase diagram purely *disorder-induced* here). We can read off the relation

$$c \simeq 1/c_L^2 \ , \tag{2.19}$$

between the number c and the *Lindemann-number* c_L. Indeed, the relation (2.19) produces a good agreement between the value $c \approx \mathcal{O}(50)$ from the variational calculation and the value $c_L \approx 0.1 - 0.2$ widely used in the literature. This equivalence to a melting induced by fluctuations on the shortest scale l and described by a Lindemann-criterion suggests that, much like in the disorder-free case, the Bragg glass melts in a first order transition as it is obtained in the variational calculation. At this transition, *stretched* dislocation loops (i.e., non-fractal loops with $D = 1$) should occur with a *finite* density. However, the nature of the transition cannot be determined unambiguously [in analogy to the role, the Lindemann criterion plays in describing melting transitions in a disorder-free system: It has proved to be a very effective tool to obtain information about a melting curve without giving any knowledge about the nature of the transition].

The Lindemann-like criterion (2.17) will be the central result of this chapter. In the next **chapter 3**, we give a short review of the properties of the dislocation-free Bragg glass phase, and introduce the models we use throughout part I. The **chapters 4 and 5** are devoted to the detailed derivation of the Lindemann-criterion (2.17) by means of the variational approach and Imry-Ma-type scaling arguments, respectively, as they were outlined in this inroduction. Thereafter, we will use (2.17) to obtain a phase diagram for a typical HTSC (e.g. BSCCO) in **chapter 6**.

Chapter 3

The Bragg Glass Phase, Random Manifolds and Random Forces

The purpose of this chapter is to introduce the models of *pinned elastic manifolds* for the disordered FL array which are relevant for what follows in the next chapters 4 and 5. Pinned elastic manifolds give a consistent description of the disordered FL array in the *absence* of dislocations and are thus the starting point of all considerations in chapters 4 and 5. In particular, we review shortly the properties of the dislocation-free *Bragg glass phase*, which describes the asymptotic large scale properties of the dislocation-free disordered FL array. But also the crossover between the different pre-asymptotic regimes of the dislocation-free disordered FL array, as well described as pinned elastic manifolds, will play an important role in the subsequent chapters 5 and 6. These crossovers are induced by the interplay between the FL interaction, the periodicity of the FL lattice, and the disorder potential, which are in addition affected by thermal fluctuations, and lead to essentially two different pre-asymptotic regimes: The perturbative or *random force regime* on the shortest scales, the *random manifold regime* on intermediate scales before the asymptotic large scale behaviour of the Bragg glass phase sets in. The associated crossover scales and the properties of the pre-asymptotic regimes are reviewed as well in this chapter.

3.1 Elasticity Theory and Interaction-induced Length Scale L^*

We want to describe the disorder- and dislocation-free FL array by *elasticity theory* (see Ref. [4] for a review). The relevant degrees of freedom of the FL array are the positions of the vortices in this approach. Then, all configurations can be parameterized by allowing for two-component displacements of each FL element from its equilibrium position in the two directions transverse to the FL. The undistorted FLs are straight lines forming the

hexagonal Abrikosov lattice. The z-coordinate is chosen parallel to the undistorted FLs; the lattice formed by the undistorted FLs in the xy-plane is described by lattice vectors $\mathbf{R}_{\boldsymbol{\nu}}$ (with inverse lattice vectors $\mathbf{K}_{\boldsymbol{\nu}}$) with unit cell volume $l^2 = \phi_0/B$. Furthermore, we define the vector $\mathbf{r}$ as $\mathbf{r} = (\mathbf{R}_{\boldsymbol{\nu}}, z) \to (\mathbf{R}, z)$ when we switch to a continuous representation in the vector $\mathbf{R}$ transverse to the FLs (or in momentum space $\mathbf{k} = (\mathbf{K}_{\boldsymbol{\nu}}, k_z) \to (\mathbf{K}, k_z)$). Let us begin with the usual experimental situation of an anisotropic HTSC in a magnetic field perpendicular to the CuO-planes ($\mathbf{H} \parallel \hat{\mathbf{c}} \perp \mathbf{ab}$); the lattice in the xy-plane, which is then identical to the ab-plane of the HTSC, is a hexagonal lattice with $\mathbf{R}_{\boldsymbol{\nu}} = \mathbf{R}_{(i,j)} = (\ (2i+j)l_0/2\ ,\ j\sqrt{3}l_0/2\ )$ with a FL distance $l_0 \approx l$ [$l^2 = \phi_0/B = \sqrt{3}/2l_0^2$]. Displacements are parameterized by $\mathbf{u} = \mathbf{u}_{\boldsymbol{\nu}}(z)$, or in a continuum description with $\mathbf{R} = (x, y)$ by

$$\mathbf{u} \ = \ \mathbf{u}(\mathbf{R}, z) \ = \ \int_{BZ} \frac{d^2\mathbf{K}}{(2\pi)^2}\, e^{i\mathbf{K}\cdot\mathbf{R}}\ \ l^2 \sum_{\boldsymbol{\nu}}\ e^{-i\mathbf{K}\cdot\mathbf{R}_{\boldsymbol{\nu}}}\ \mathbf{u}_{\boldsymbol{\nu}}(z). \tag{3.1}$$

In elasticity theory, the following three-dimensional Hamiltonian in the two-component displacement field $\mathbf{u}$ describes the disorder- and dislocation-free FL array:

$$\begin{aligned} \mathcal{H}_{el}^{3D}[\mathbf{u}] \ &= \ \frac{1}{2}\int_{BZ} \frac{d^2\mathbf{K}}{(2\pi)^2} \int \frac{dk_z}{2\pi} \left\{ c_{11}\left[\mathbf{K}\cdot\mathbf{u}(\mathbf{K},k_z)\right]^2 + c_{66}\left[\mathbf{K}\times\mathbf{u}(\mathbf{K},k_z)\right]^2 + \right. \\ &\qquad \left. c_{44}\left[k_z\mathbf{u}(\mathbf{K},k_z)\right]^2 \right\} \qquad (3.2) \\ &= \ \frac{1}{2}\int d^2\mathbf{R} \int dz\ \left\{ c_{11}\left[\boldsymbol{\nabla}_{\mathbf{R}}\cdot\mathbf{u}(\mathbf{R},z)\right]^2 + c_{66}\left[\boldsymbol{\nabla}_{\mathbf{R}}\times\mathbf{u}(\mathbf{R},z)\right]^2 + \right. \\ &\qquad \left. c_{44}\left[\partial_z\mathbf{u}(\mathbf{R},z)\right]^2 \right\}\ , \qquad (3.3) \end{aligned}$$

where we switched to a continuum description in the last equation. The elastic energy of the possible distortion-modes is characterized by the three elastic moduli: The *compression modulus* c_{11}, the *shear modulus* c_{66}, and the *tilt modulus* c_{44}.

For a two-component displacement field, two elastic modes are possible with the free energy (3.2): (i) A *longitudinal* mode ($\mathbf{u} \parallel \mathbf{K}$) involving compression and tilt and (ii) a *transversal* mode ($\mathbf{u} \perp \mathbf{K}$) involving shear and tilt. Because for $\mathbf{H} \parallel \hat{\mathbf{c}}$ the compression modulus c_{11} is over a wide range of inductions much bigger than the shear modulus c_{66} (only in the dilute limit $l \gg \lambda_{ab}$, c_{11} becomes of the order of c_{66} and approaches $c_{11} \approx 3c_{66}$), we can neglect the longitudinal (compression) modes to a good approximation and treat the FL array as *incompressible*, i.e., $c_{11} \uparrow \infty$. $\mathbf{u}(\mathbf{k})$ consists then only of a transversal part $\mathbf{u}(\mathbf{k}) = \mathbf{u}_T(\mathbf{k})$.

In the subsequent discussion, we use the symbols

$$\begin{aligned} L \ &= \ \text{longitudinal length scale} \parallel \text{FL} \\ R \ &= \ \text{transversal length scale} \perp \text{FL} \end{aligned}$$

when we consider fluctuations in the displacements $\mathbf{u}$ on a certain length scale (or, alternatively, put the system in a box of linear dimensions R and L).

In general, the proper elasticity theory describing the FL array is *non-local*, as soon as the FLs interact over a range λ exceeding the FL distance l so that elastic distortions on scales R smaller than the interaction range become possible. When the elastic theory becomes non-local, the elastic moduli exhibit *dispersion*, that is they have a k-dependence $c_{xx} = c_{xx}[\mathbf{k}]$ in (3.2). In the *local limit*, we have $c_{xx} = \hat{c}_{xx} := c_{xx}[k = 0]$. However, c_{66} is always *dispersion-free* $c_{66} \equiv \hat{c}_{66}$ [shear modes are volume preserving and thus not changing for a given FL the number of FLs in its interaction range; thus, the non-locality cannot affect the value of c_{66}]. Results in the literature for the relevant moduli $c_{44}[\mathbf{k}]$ and c_{66} for $\mathbf{H} \parallel \hat{\mathbf{c}}$ are given in Appendix A.3 for future use. c_{44} obeys to a good approximation a dispersion relation [4]

$$c_{44}[K] \simeq \hat{c}_{44} \frac{1}{1 + K^2 \tilde{\lambda}_c^2} \ . \tag{3.4}$$

The length scale for the onset of dispersion is

$$\tilde{\lambda}_c \ := \ \frac{\lambda_c}{(1 - B/B_{c2})^{1/2}} \ , \tag{3.5}$$

because with the magnetic field perpendicular to the CuO-planes (ab-planes), non-locality occurs for $R < \lambda_c$, when the interaction range λ_c for tilted FL-elements lying in the ab-planes exceeds the scale R for variations in the FL displacement. At higher magnetic fields, λ_c has to be modified to the effective $\tilde{\lambda}_c$ in non-local elasticity theory [46, 47]. Neglecting an additional weak dispersion in k_z, the result (3.4) crosses over to the *single vortex tilt modulus* c_{44}^s on the shortest scales $R \sim 1/K \lesssim l$:

$$c_{44}^s \ \approx \ l^2 \, c_{44}[K \simeq \frac{2\pi}{l}] \ . \tag{3.6}$$

Using these approximations, we can rewrite the three-dimensional elastic Hamiltonian as

$$\mathcal{H}_{el}^{3D}[\mathbf{u}] \ \approx \ \frac{1}{2} \int_{BZ} \frac{d^2\mathbf{K}}{(2\pi)^2} \int \frac{dk_z}{2\pi} \ \Big\{ c_{66} \ \left[K^2 |u_T(\mathbf{K}, k_z)|^2\right] + c_{44}[K] \ \left[k_z^2 |u_T(\mathbf{K}, k_z)|^2\right] \Big\} \ . \tag{3.7}$$

From (3.7) and (3.4), we can deduce immediately the scaling relation between longitudinal scales L and transversal scales R induced by the elastic Hamiltonian, i.e., the typical "aspect ratio" of fluctuations involving elastic deformation:

$$L \ \sim \ \left(\frac{c_{44}[2\pi/R]}{c_{66}} \right)^{1/2} \ R \ . \tag{3.8}$$

The three-dimensional elastic Hamiltonian (3.2) is valid only on scales $R \gtrsim l$ or

$$L \gtrsim L^* := \left(\frac{c_{44}[2\pi/l]}{c_{66}} \right)^{1/2} \ l \approx \left(\frac{c_{44}^s}{c_{66}} \right)^{1/2} \tag{3.9}$$

using (3.8) and (3.6). Because transversal fluctuations on scales $R \lesssim l$ are not possible, the interaction between FLs becomes irrelevant on scales $L \lesssim L^*$, and a description in terms of single, non-interacting FLs is appropriate: The system crosses over to a *single vortex regime*. In this regime, i.e., on length scales $R \lesssim l$ smaller than the FL spacing, each FL can be described by one-dimensional elasticity theory in the displacement $\mathbf{u}(z)$ with only one elastic modulus, the "line tension" or single vortex tilt modulus c_{44}^s [note that at $R \sim l$, $c_{44}[2\pi/R]$ crosses over to the single vortex tilt modulus, see (3.6), which is approximately *dispersion-free*]:

$$\mathcal{H}_{el}^{s}[\mathbf{u}] \;=\; \frac{1}{2}\int dk_z\;\left\{c_{44}^{s}\;\left[k_z\mathbf{u}(k_z)\right]^2\right\}\;. \tag{3.10}$$

In other words, the longitudinal length scale L^* given by (3.9) (corresponding to a transversal scale equal to the FL spacing l) separates a regime of "single vortex" behaviour on scales $L < L^*$ or $R < l$ from a regime of "collective" behaviour on larger scales $L > L^*$ or $R > l$ [see Figure 3.3].

From a statistical physics perspective, it is useful to introduce the generalization of (3.2, 3.10) to the case of a d-dimensional elastic manifold with n codimensions, i.e., with a n-component displacement field $\mathbf{u}(\mathbf{R}, z) \in \mathbb{R}^n$ with $\mathbf{R} \in \mathbb{R}^{d-1}$ by going over to $d-1$ transversal dimensions. As in $d = 3$, we allow only in the tilt modulus associated with the one longitudinal dimension for a dispersion of the form (3.4):

$$\begin{aligned}\mathcal{H}_{el}^{(d,n\geq 2)}[\mathbf{u}] \;=\; \frac{1}{2}\int_{BZ}\frac{d^{d-1}\mathbf{K}}{(2\pi)^{d-1}}\int\frac{dk_z}{2\pi}\left\{c_{66}\;\left[K^2|u(\mathbf{K},k_z)|^2\right]\;+\right.\\ \left.+\;c_{44}[K]\;\left[k_z^2|u(\mathbf{K},k_z)|^2\right]\right\}.\end{aligned} \tag{3.11}$$

[To keep the notation simple, we write henceforth for $n \geq 2$ simply $\mathbf{u}$ for $\mathbf{u}_T$ but keep in mind that the FL lattice is incompressible and only the transversal part of $\mathbf{u}$ is subject to fluctuations for $n \geq 2$.] We can identify $\mathcal{H}_{el}^{3D} = \mathcal{H}_{el}^{(3,2)}$ and $\mathcal{H}_{el}^{s} = \mathcal{H}_{el}^{(1,2)}$. Note that the scaling relation (3.8) between longitudinal scales L and transversal scales R induced by the elastic Hamiltonian $\mathcal{H}_{el}^{(d,n\geq 2)}$ is unchanged.

However, this generalization, based on the approximation of an incompressible FL array, is only valid for $n \geq 2$. For $n = 1$ or *uniaxial* displacements, say $\mathbf{u} = u \cdot \hat{\mathbf{x}}$, there is only one mode involving shear *and* compression, and we have to consider ($K_\parallel := \mathbf{K}\cdot\hat{\mathbf{x}}$ and $\mathbf{K}_\perp := \mathbf{K}\times\hat{\mathbf{x}}$)

$$\begin{aligned}\mathcal{H}_{el}^{(d,n=1)}[\mathbf{u}] \;=\; \frac{1}{2}\int_{BZ}\frac{d^{d-2}\mathbf{K}_\perp}{(2\pi)^{d-2}}\int_{BZ}\frac{dK_\parallel}{2\pi}\int\frac{dk_z}{2\pi}\left\{c_{11}[K]\;\left[K_\parallel^2|u(\mathbf{K},k_z)|^2\right]\;+\right.\\ \left.+\;c_{66}\;\left[K_\perp^2|u(\mathbf{K},k_z)|^2\right]\;+\;c_{44}[K]\;\left[k_z^2|u(\mathbf{K},k_z)|^2\right]\right\}.\end{aligned} \tag{3.12}$$

In this chapter, we focus mainly on the generic case $n \geq 2$. The treatment of the uniaxial case $n = 1$ is analogous.

3.2 Pinning Energy

Let us consider now a disordered superconductor, where the Hamiltonian for the disordered, dislocation-free FL array contains also a disorder energy:

$$\mathcal{H}[\mathbf{u}] \;=\; \mathcal{H}_{el}[\mathbf{u}] + \mathcal{H}_{d}[\mathbf{u}] \quad . \tag{3.13}$$

In the disordered superconductor, point-like pinning centers, e.g. oxygen vacancies in a HTSC, generate a pinning potential acting on the FLs. Because the pinning force exerted by each defect on a FL has a range approximately equal to the coherence length ξ (which is ξ_{ab} for the magnetic field perpendicular to the CuO-planes), fluctuations in the pin-density generate a Gaussian distributed disorder potential $v(\mathbf{r})$ acting on a *single* FL [i.e., the pinning energy is $E_{pin}[\mathbf{u_0}] = \int dz v(\mathbf{u_0}(z), z)$]. The disorder potential has mean zero $\overline{v} = 0$ (the overbar denotes the quenched average over the disorder configurations) and fluctuations correlated only over a distance ξ_{ab}

$$\overline{v(\mathbf{u}, z)v(\mathbf{u}', z')} \;=\; g_0 \; \delta_\xi^2(\mathbf{u} - \mathbf{u}')\delta_\xi^1(z - z') \;, \tag{3.14}$$

where the parameter g_0 measures the strength of the disorder. It is convenient to define an associated energy Δ_{pin} with Δ_{pin}^2 being the mean square pinning energy in a volume ξ_{ab}^3

$$\Delta_{pin}^2 \;:=\; (n_{pin} f_{pin}^2 \xi_{ab}^2)\xi_{ab}^3 \;=\; g_0 \xi_{ab}^{-1} \;, \tag{3.15}$$

where n_{pin} is the density of pinning centers and f_{pin} the maximum pinning force exerted by a single pinning center for $\mathbf{H} \perp \mathbf{ab}$. Then, the disorder energy of the FL *array* can be written

$$\mathcal{H}_d^{3D}[\mathbf{u}] \;=\; \sum_{\boldsymbol{\nu}} \int dz \; v(\mathbf{R}_{\boldsymbol{\nu}} + \mathbf{u}_{\boldsymbol{\nu}}(z), z) \tag{3.16}$$

$$\;=\; \int d^3\mathbf{r} \; v(\mathbf{r}) \; \rho[\mathbf{r}, \mathbf{u}(\mathbf{r})] \;, \tag{3.17}$$

where $\rho[\mathbf{r}, \mathbf{u}(\mathbf{r})] = \sum_{\boldsymbol{\nu}} \delta^2(\mathbf{R} - \mathbf{R}_{\boldsymbol{\nu}} - \mathbf{u}_{\boldsymbol{\nu}}(z))$ is the FL density. The Hamiltonian $\mathcal{H} = \mathcal{H}_{el}^{3D} + \mathcal{H}_d^{3D}$ models the FL array as an elastic manifold of dimension $d = 3$ with $n = 2$ components of the displacement field in a random medium. However, the $n = 2$ "codimensions" of the manifold are physically *identical* to the 2 transversal of the $d = 3$ dimensions. This leads to important consequences for the asymptotic behaviour and to the existence of essentially three physically different regimes: (i) The *Larkin* or *random force regime*, (ii) the *random manifold regime*, and (iii) the *Bragg glass phase* or *charge density wave (CDW) regime* on large scales. These regimes are existing on different length scales; the crossover scale between (i) and (ii) is the *Larkin length* L_ξ and the crossover scale between (ii) and (iii) the *positional correlation length* L_l [see Figure 3.3]. We will discuss each regime in its

appropriate generalization to $d-1$ transversal dimensions and n-component displacements $\mathbf{u}$ [the single vortex disorder potential $v(\mathbf{u}, z)$ has then correlations analogously to (3.14) with

$$g_0 = \Delta_{pin}^2 \xi_{ab}^{n-1} \ , \tag{3.18}$$

where we want to define Δ_{pin}^2 as the mean square pinning energy in a volume ξ_{ab}^{1+n} for consistency]. The three regimes are distinguished by the scaling behaviour of their *roughness*

$$\begin{aligned} \overline{\langle |\mathbf{u}(\mathbf{r}) - \mathbf{u}(\mathbf{r}')|^2 \rangle} &\propto |\mathbf{r} - \mathbf{r}'|^{2\zeta} \qquad \text{or} \\ \overline{\langle u^2 \rangle}(R, L) \simeq \frac{1}{2} \overline{\langle |\mathbf{u}(\mathbf{R}, L) - \mathbf{u}(\mathbf{0})|^2 \rangle} &\propto L^{2\zeta} \propto R^{2\zeta} \end{aligned} \tag{3.19}$$

$[\overline{\langle \ldots \rangle}(R, L)$ denotes an average for a system in a box of transversal and longitudinal dimensions R and L, respectively, where R and L are related by (3.8)], characterized by the *roughness-exponent* ζ. As usual in disordered systems, also the scaling of the free-energy fluctuations, either sample-to-sample fluctuations or fluctuations within a single sample, will be of importance. Due to the anomalous roughness in a disordered system $\zeta > \zeta_{th} = (2-d)/2$ compared to the thermally induced roughness ζ_{th}, we expect anomalously large fluctuations in the elastic energy

$$\overline{\langle H_{el}^{(d,n)} \rangle}(R, L) \propto L^{2\zeta+d-2} \propto R^{2\zeta+d-2} \tag{3.20}$$

(and similar sample-to-sample fluctuations of the free energy), determining much of the physics in each of the three regimes.

3.3 Random Force Regime and Larkin Length L_ξ

In the *Larkin* or *random force (RF) regime* of Larkin and Ovchinnikov [6, 48], the displacements are small enough that perturbation theory in the displacements $\mathbf{u}$ is valid. This is the case if a FL stays within *one* minimum of the disorder potential $v(\mathbf{r})$. Because $v(\mathbf{r})$ varies typically on a scale ξ_{ab} for $\mathbf{H} \perp \mathbf{ab}$, given by the range of the pinning forces, this is the case for sufficiently small displacements $u \lesssim \xi_{ab}$ [Figure 3.1].

Thus, we can expand the disorder energy (3.16) in the displacements $\mathbf{u}$

$$\begin{aligned} \mathcal{H}_{d,RF}^{3D}[\mathbf{u}] &\approx \sum_{\boldsymbol{\nu}} \int dz \ \left(v|_{(\mathbf{R}_{\boldsymbol{\nu}}, z)} + \boldsymbol{\nabla}_{\mathbf{u}} v|_{(\mathbf{R}_{\boldsymbol{\nu}}, z)} \cdot \mathbf{u}_{\boldsymbol{\nu}}(z) + \ldots \right) \\ \mathcal{H}_{d,RF}^{(d,n)}[\mathbf{u}] &\approx \int d^{d-1}\mathbf{R} \int dz \ \mathbf{f}(\mathbf{R}, z) \cdot \mathbf{u}(\mathbf{R}, z) \end{aligned} \tag{3.21}$$

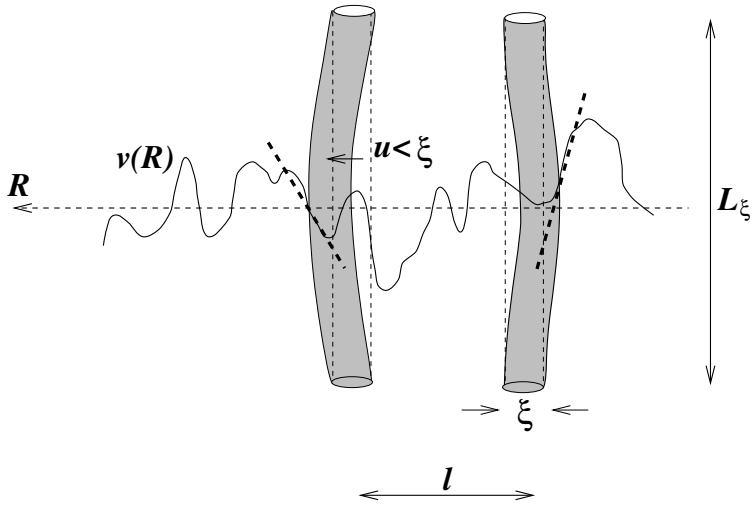

Figure 3.1: In the random force regime on scales $L < L_\xi$, the typical FL displacement is $u \lesssim \xi_{ab}$: Perturbation theory in the displacements leads to random forces (tangents on the disorder potential v).

and obtain a coupling of the FL-displacements to the (n-dimensional) random forces $\mathbf{f}(\mathbf{R}, z) = l^{-(d-1)} \boldsymbol{\nabla}_{\mathbf{u}} v|_{(\mathbf{0},z)}$. The random forces $\mathbf{f}(\mathbf{r})$ are Gaussian distributed with mean zero $\overline{\mathbf{f}} = 0$, uncorrelated components $\overline{f_i f_j} = 0$ (for $i \neq j$), and correlations

$$\overline{\mathbf{f}(\mathbf{R}, z) \cdot \mathbf{f}(\mathbf{R}', z')} \;=\; f_0^2 \; \delta_\xi^{d-1}(\mathbf{R} - \mathbf{R}') \; \delta_\xi^1(z - z') \tag{3.22}$$

$$f_0^2 \xi_{ab}^2 \;=\; n \; g_0 \xi_{ab}^{-n} l^{-(d-1)} \;=\; n \; \Delta_{pin}^2 \xi_{ab}^{-1} l^{-(d-1)} \; . \tag{3.23}$$

This leads for the Hamiltonian $\mathcal{H}^{(d,n)}[\mathbf{u}] = \mathcal{H}_{el}^{(d,n)}[\mathbf{u}] + \mathcal{H}_{d,RF}^{(d,n)}[\mathbf{u}]$ in momentum-space to a k^{-4}-divergence in the Fourier-transformed $\overline{\langle uu \rangle}$-correlations at low temperatures (see Ref. [6] and Appendix A.1.1). From this divergence, it follows a roughness exponent

$$\zeta_{RF} \;=\; \frac{4-d}{2} \tag{3.24}$$

and the upper critical dimension $d_> = 4$, above which random forces are irrelevant.

The *Larkin lengths* L_ξ and R_ξ ($L_\xi \simeq (c_{44}[2\pi/R_\xi]/c_{66})^{1/2} R_\xi$ by (3.8)) of the FL array are defined as the crossover length scales where the mean square FL displacements become of the order of the range ξ_{ab}^2 of the elementary pinning forces (at low temperatures)

$$\overline{\langle (\mathbf{u}(R_\xi, L_\xi) - \mathbf{u}(\mathbf{0}))^2 \rangle} \;\simeq\; 2\overline{\langle u^2 \rangle}(R_\xi, L_\xi) \;\simeq\; \xi_{ab}^2 \; , \tag{3.25}$$

and perturbation theory in the displacements, i.e., a description by random forces becomes

inapplicable. Thus the $\overline{\langle uu \rangle}$-displacements are of the form

$$2\overline{\langle u^2 \rangle}(R,L) \;\simeq\; \xi_{ab}^2 \left(\left(\frac{R}{R_\xi} \right)^2 + \left(\frac{L}{L_\xi} \right)^2 \right)^{\zeta_{RF}} \quad . \tag{3.26}$$

The Larkin lengths are calculated in Appendix A.1.1, formula (A.10), where we obtain for dispersion-free elastic constants, i.e., $c_{44}[K] = \hat{c}_{44}$,

$$\begin{aligned} L_\xi \;&\simeq\; \bar{c}_d \; \xi_{ab} \left(\frac{\hat{c}_{44}^{(5-d)/2} c_{66}^{(d-1)/2} \xi_{ab}^d}{f_0^2 \xi_{ab}^2} \right)^{1/(4-d)} \\ &\simeq\; R_\xi \left(\frac{\hat{c}_{44}}{c_{66}} \right)^{1/2} \quad . \end{aligned} \tag{3.27}$$

When the disorder increases, the Larkin length R_ξ decreases and finally becomes comparable to the FL spacing l for strong enough disorder or, in the longitudinal direction, $L_\xi \simeq L^*$ with L^* given by (3.9). Then the interaction between FLs becomes irrelevant in the whole RF regime, each FL can be described by a single vortex Hamiltonian $\mathcal{H}[\mathbf{u_0}] = \mathcal{H}_{el}^s[\mathbf{u_0}] + \mathcal{H}_{d,RF}^{(1,2)}[\mathbf{u_0}]$, and L_ξ crosses over to the *single vortex Larkin length* (A.12)

$$L_\xi^s \;\sim\; \xi_{ab} \left(\frac{{c_{44}^s}^2 \xi_{ab}^2}{\Delta_{pin}^2} \right)^{1/3} \quad . \tag{3.28}$$

Upon further increasing the disorder, $L_\xi^s \lesssim L^*$ becomes smaller than L^*, and each FL is pinned *independently* with an irrelevant FL-interaction in the RF regime, a situation we want to call *single vortex pinning*, as opposed to a *collective pinning* when $L_\xi \gtrsim L^*$ for weak disorder. The length scales and displacements associated with both situations are depicted in Figure 3.3. In the high-T_c materials like the Bi-compounds, the disorder is typically so strong that single vortex pinning is the generic situation, as we will see in chapter 6.

The pinning is weakened by thermal fluctuations, which will lead to an increase of the Larkin length above the so-called *depinning temperature* T_{dp}. With regard to experiments, we are mainly interested in extreme high-T_c materials like BSCCO, where we have single vortex pinning. Therefore, the role of thermal fluctuations will be reviewed shortly in chapter 6 for single vortex pinning (i.e., for $d = 1$, $n = 2$).

3.4 Random Manifold Regime and Positional Correlation Length L_l

In the *random manifold (RM) regime* [9, 49], perturbation theory breaks down, and every line explores many minima of the disorder potential, giving rise to a much more complicated

physics on scales exceeding the Larkin length. However, the typical displacements of the FLs are still smaller than the FL distances $u \lesssim l$, such that each line "sees" a different disorder configuration and does not compete with neighbouring lines for the same pinning centers or the same minima of the disorder potential [Figure 3.2].

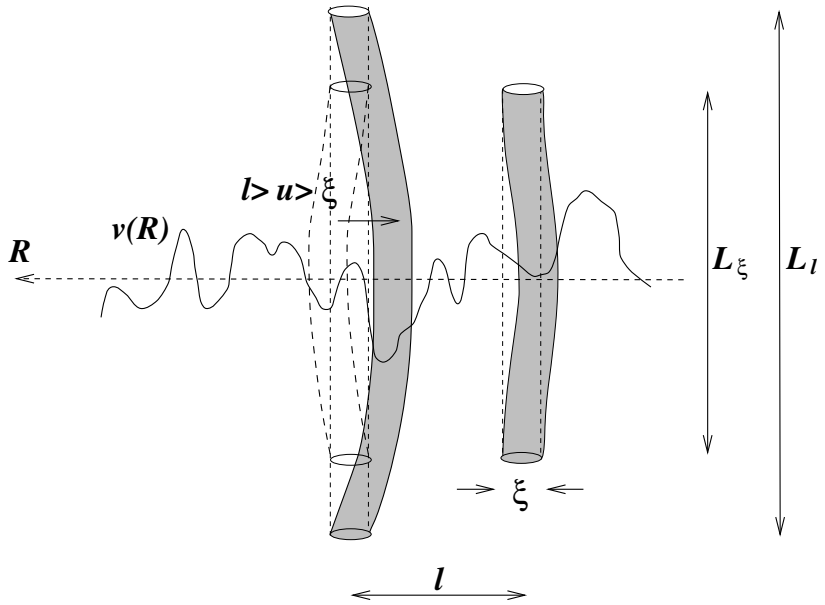

Figure 3.2: In the random manifold regime on scales $L_\xi < L < L_l$, the typical FL displacement is $\xi_{ab} \lesssim u \lesssim l$: FLs explore many minima of the disorder potential v (alternative dashed configuration of the left FL) but do not compete for the same minima.

Then, we can treat the n codimensions of the RM approximately as physically *independent* from the the $d-1$ transversal dimensions of the FLs:

$$\begin{aligned} \mathcal{H}^{3D}_{d,RM}[\mathbf{u}] &\approx \sum_{\boldsymbol{\nu}} \int dz\; v_{\boldsymbol{\nu}}(\mathbf{u}_{\boldsymbol{\nu}}(z), z) \\ \mathcal{H}^{(d,n)}_{d,RM}[\mathbf{u}] &\approx \int d^{d-1}\mathbf{R} \int dz\; V(\mathbf{R}, z, \mathbf{u}(\mathbf{R}, z)) \;, \end{aligned} \tag{3.29}$$

where $\overline{v_{\boldsymbol{\nu}} v_{\boldsymbol{\mu}}} = 0$ for $\boldsymbol{\nu} \neq \boldsymbol{\mu}$, and thus $V(\mathbf{r}, \mathbf{u})$ is Gaussian distributed with mean zero $\overline{V} = 0$ and second moment

$$\begin{aligned} \overline{V(\mathbf{r}, \mathbf{u}) V(\mathbf{r}', \mathbf{u}')} &= g_{RM}\; \delta^d_\xi(\mathbf{r} - \mathbf{r}')\; \delta^n_\xi(\mathbf{u} - \mathbf{u}') \\ g_{RM} &= g_0 l^{-(d-1)} = \Delta^2_{pin} \xi^{n-1}_{ab} l^{-(d-1)}. \end{aligned} \tag{3.30}$$

The Hamiltonian $\mathcal{H}^{(d,n)}[\mathbf{u}] = \mathcal{H}^{(d,n)}_{el}[\mathbf{u}] + \mathcal{H}^{(d,n)}_{d,RM}[\mathbf{u}]$ is the natural generalization of the classic problem of a directed path in a random medium ($d = 1$) to higher dimensions and known

as "random manifold" problem. This problem has been extensively studied in the past [7], and various attempts have been made to deal with the correct treatment of the many solutions of the Euler-Lagrange equations and its consequences for the calculation of large scale properties, though only the case $d = n = 1$ can be solved exactly. For $d = 1$, the mapping onto the quantum mechanical time evolution of a particle in n dimensions in a random potential, which can be described by a stochastic partial differential equation, the KPZ-equation [50], provides an exact solution, but only in $d = n = 1$ [7]. For the RM in higher dimensions ($d > 1$), two methods have been particularly successful, the functional renormalization group (FRG) analysis in replica space [51] and a Hartree-Fock like variational calculation (which becomes exact for $n \uparrow \infty$) using a replica symmetry breaking (RSB) Ansatz for the propagator [52]. To access also the dense limit $l \lesssim \lambda_c$ of higher magnetic fields, it is necessary to include the dispersion (3.4) of the tilt modulus in the elastic Hamiltonian (3.11) in our treatment. This is incorporated most easily when taking a relatively simple scaling approach, which uses a so-called "Flory-argument" [52]. This simple scaling argument, equating disorder and elastic energy on *one* dominant scale, allows nevertheless to reproduce the roughness-exponents obtained with the variational calculation using RSB and is presented in the Appendix A.1.2 in detail, where we obtain the result (A.26)

$$\overline{\langle u^2 \rangle}(R) \;\sim\; R^{2\zeta(d,n)} \left(1 + \frac{\tilde{\lambda}_c^2}{R^2}\right)^{\zeta(d,n)/(4-d)} \tag{3.31}$$

[the dispersion-free results are regained by letting $\tilde{\lambda}_c \downarrow 0$]. $\zeta(d,n)$ is the roughness-exponent for the RM regime, for which the Flory-argument gives $\zeta(d,n) = (4-d)/(4+n)$ (see (A.27)) in accordance with the variational RSB approach [52] [the upper critical dimension for the RM is again $d_> = 4$]. Flory-type arguments are known not to reproduce the correct roughness-exponents $\zeta(d,n)$ because they consider only one dominant scale; therefore we will use the values for $\zeta(d,n)$ obtained from the above mentioned more elaborate approaches using the FRG when we make contact to experiments in chapter 6. The best available estimates are [7]

$$\begin{aligned} \zeta(1,n) &\approx \frac{(3+n)}{2(2+n)} \\ \zeta(d,n) &\approx \frac{2(4-d)}{8+n} \;. \end{aligned} \tag{3.32}$$

The *positional correlation lengths* R_l and L_l ($L_l \simeq (c_{44}[2\pi/R_l]/c_{66})^{1/2} R_l$ by (3.8)) of the FL array are defined as the crossover scales where the RM regime becomes inapplicable because the mean square FL displacements become of the order of the FL distance l^2:

$$\overline{\langle (\mathbf{u}(R_l, L_l) - \mathbf{u}(\mathbf{0}))^2 \rangle} \;\simeq\; 2\overline{\langle u^2 \rangle}(R_l, L_l) \simeq l^2 \;. \tag{3.33}$$

They are related via the scaling (3.31) of the displacement correlations in the RM regime to the Larkin lengths R_ξ and L_ξ (3.25). We will give the detailed derivation of this relation in chapter 6 and give here only the general picture of the different scales associated with the RM regime, which becomes crucial for an understanding of the quantitative details of the Lindemann-criterion in chapter 5 and is visualized in Figure 3.3.

We have to distinguish between the two above mentioned cases of single vortex pinning in the RF regime for relatively strong disorder, as it is the common situation in high-T_c materials like the Bi-compounds, and collective pinning in the RF regime for a weak disorder. In other words, we have to consider the role of the additional length scale L^* (3.9) set by the interaction strength between FLs: For collective pinning, we have $L^* < L_\xi < L_l$ or $l < R_\xi < R_l$, whereas for single vortex pinning, we have $L_\xi^s < L^* < L_l$. [Notice that the positional correlation length R_l *always* exceeds the FL spacing l, otherwise the elastic approach itself (which is based on small gradients $\overline{\langle(\mathbf{u}(R=l)-\mathbf{u}(R=0))^2\rangle} < l^2$) breaks down as follows from (3.33).]

For weak disorder and collective pinning on scales $L^* < L < L_\xi$ or $l < R < R_\xi$ in the RF regime, there is only one "collective RM regime" on scales $L_\xi < L < L_l$ or $R_\xi < R < R_l$, where FLs are pinned collectively and $d = 3$, $n = 2$. For strong disorder and single vortex pinning in the RF regime on scales $L < L_\xi^s$, a "single vortex RM regime" occurs previous to the collective RM regime on scales $L_\xi^s < L < L^*$, where the FL-interaction is still irrelevant and each vortex behaves *independently* as an RM with $d = 1$, $n = 2$. On scales $L^* < L < L_l$ or $l < R < R_l$, the FL array crosses over to the above collective RM regime.

3.5 Bragg Glass and 2D Random Field XY Model

In the *Bragg glass phase* or *charge density wave (CDW) regime* [9, 11, 53], the average FL displacement becomes bigger than the FL spacing ($u \gtrsim l$), and lines not only explore many minima of the disorder potential but also start to *compete* for the same pinning centers or minima of the disorder potential [Figure 3.4].

The Bragg glass is the asymptotic regime on the largest scales exceeding the positional correlation lengths R_l of L_l, and determines the nature of the dislocation-free phase of the disordered FL array. When FLs start to compete for the same pinning centers, it becomes crucial that the n codimensions of the elastic manifold coincide with n of the d dimensions (usually n of the transverse dimensions). Therefore, care has to be taken that the discrete translational symmetry under $\mathbf{u} \to \mathbf{u} + \mathbf{R}_{\boldsymbol{\mu}}$ in (3.16) [the invariance of (3.16) under $\mathbf{u} \to \mathbf{u} + \mathbf{R}_{\boldsymbol{\mu}}$ follows immediately by a relabeling of the lines] is preserved [11, 53] for any approximation of the FL density ρ in (3.17); otherwise wrong asymptotic behaviours could be obtained (see the comment in Ref. [9] on Ref. [49]). Starting from a

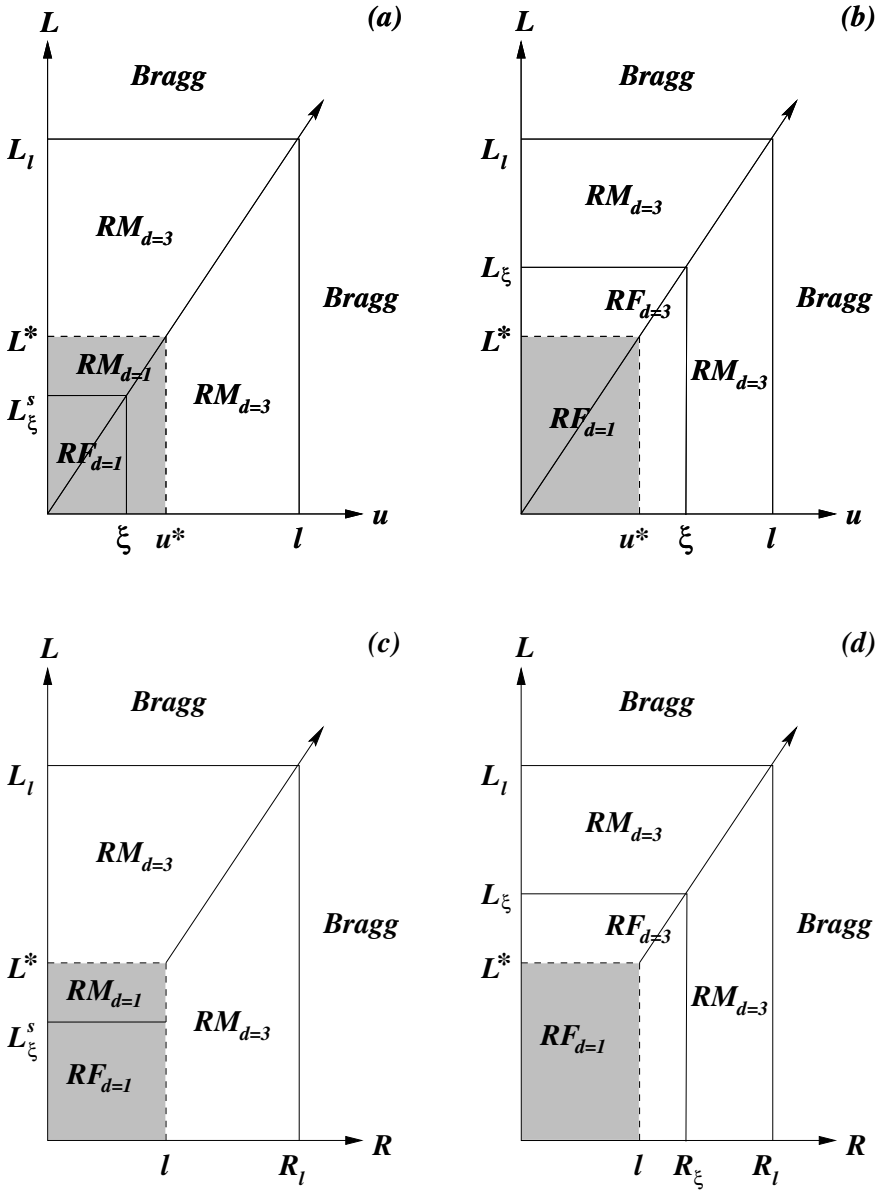

Figure 3.3: Graph of the different physical regimes of the FL array depending on the longitudinal scale L and the typical displacement u [(a)&(b)] or the transversal scale R [(c)&(d)]. The 3 longitudinal crossover length scales $L = L^*, L_\xi, L_l$ are shown together with the corresponding typical displacement $u = u^*, \xi, l$ [(a)&(b)] and their transversal counterparts $R = l, R_\xi, R_l$ [(c)&(d)]. (a)&(c) show the situation of "single vortex pinning", which realized in extreme HTSCs as BSCCO and which we will focus on in this work; (b)&(d) show the situation for "collective pinning". The shaded regime always marks the single vortex regime ($d = 1$), in the unshaded regime the FL array exhibits collective behaviour ($d = 3$).

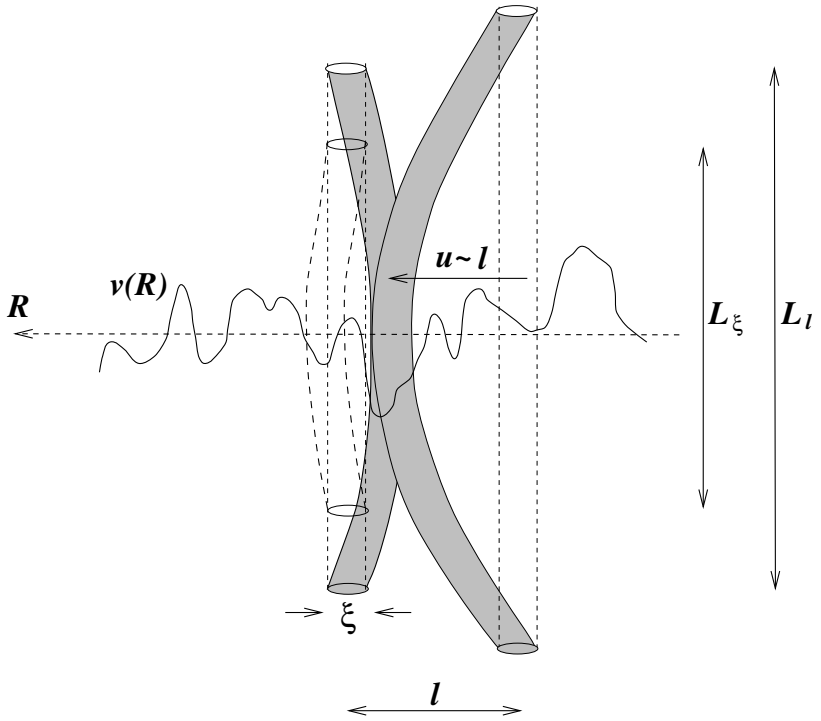

Figure 3.4: In the Bragg glass regime on scales $L_l < L$, the typical FL displacement is $l \lesssim u$: FLs start to compete for the *same* minimum of the disorder potential v.

discrete description as a sum of peaks, we use the Poisson formula to switch to a continuum description and obtain

$$\begin{aligned}\rho[\mathbf{r}, \mathbf{u}(\mathbf{r})] &= \sum_{\boldsymbol{\nu}} \delta^2(\mathbf{R} - \mathbf{R}_{\boldsymbol{\nu}} - \mathbf{u}_{\boldsymbol{\nu}}(z)) \\ &= \int d^2\mathbf{R}' \;\; \rho_0 \sum_{\boldsymbol{\nu}} e^{i\mathbf{K}_{\boldsymbol{\nu}}\cdot\mathbf{R}'} \;\; \delta^2(\mathbf{R} - \mathbf{R}' - \mathbf{u}(\mathbf{R}', z)) \\ &\simeq \rho_0(1 - \boldsymbol{\nabla}_{\mathbf{R}} \cdot \mathbf{u}(\mathbf{r})) \left(1 + \sum_{\boldsymbol{\nu}>0} 2\cos\left(\mathbf{K}_{\boldsymbol{\nu}} \cdot (\mathbf{R} - \mathbf{u}(\mathbf{r}))\right)\right), \end{aligned} \tag{3.34}$$

where $\rho_0 = 1/l^2 = B/\phi_0$ is the mean FL density. Above two dimensions, the $\boldsymbol{\nabla}_{\mathbf{R}} \cdot \mathbf{u}$-term in (3.34) measuring the large scale fluctuations in the density gives only a sub-dominant contribution to the mean square displacements [9] so that we will neglect this term in the following except for the treatment of the case $d = 2$ below. To obtain the large scale physics on scales exceeding R_l, we can limit ourselves to the first harmonic of the density fluctuations, i.e., with the smallest primitive inverse lattice vector $\mathbf{K}_0$ (we define a coordination number $z \leq d-1$ as the number of primitive inverse lattice vectors of size $|\mathbf{K}_0|$, which we label by $\mathbf{K}_{0i}$, $i = 1, \ldots, z$). However, via (3.17), this amounts to letting the

disorder vary effectively on scales $2\pi/K_0 \simeq l$, and we loose some "fine structure" on scales smaller than R_l, because the actual disorder potential (3.14) varies on a much smaller scale ξ_{ab}. This leads to the loss of the RM regime in this approximation because we have an effective range of the disorder potential $\xi_{ab,B} \simeq l$, and the Larkin lengths become equivalent to the positional correlation lengths. Keeping only the smallest inverse lattice vectors in (3.34), we obtain from (3.17) a disorder Hamiltonian

$$\begin{aligned} \mathcal{H}_{d,B}^{(d,n)}[\mathbf{u}] &= \int d^3\mathbf{r}\; v(\mathbf{r})\; \rho[\mathbf{r}, \mathbf{u}(\mathbf{r})] \\ &\approx \int d^{d-1}\mathbf{R} \int dz\; W_B[(\mathbf{R}, z), \mathbf{u}(\mathbf{R}, z)] \end{aligned} \tag{3.35}$$

for the Bragg glass, where $W_B[(\mathbf{R}, z), \mathbf{u}(\mathbf{R}, z)]$ is a Gaussian distributed *periodic* disorder potential with $\overline{W_B} = 0$ and (we neglect fast oscillating terms)

$$\overline{W_B[\mathbf{r}, \mathbf{u}] W_B[\mathbf{r}', \mathbf{u}']} = 2 g_B \sum_{i=1}^{z} \cos\left(\mathbf{K}_{0i} \cdot (\mathbf{u} - \mathbf{u}')\right) \delta^d(\mathbf{r} - \mathbf{r}') \; . \tag{3.36}$$

$\mathbf{K}_{0i}$ is now the projection of the $(d-1)$-dimensional inverse lattice vector down to the n-dimensional displacement space. The disorder strength g_B is

$$g_B = g_0 l^{-(n+d-1)} = \Delta_{pin}^2 \xi_{ab}^{n-1} l^{-(n+d-1)} = \frac{f_0^2 \xi_{ab}^2}{n} \xi_{ab}^n l^{-n} \; . \tag{3.37}$$

[1]Note that upon expanding in the displacements $\mathbf{u}$ we recover the RF regime on scales $R < R_\xi = R_l$, but with an effective range $\xi_{ab,B} \simeq l$ of the random forces, so that we have a direct crossover from the RF regime to the Bragg glass in the "Bragg glass model" defined by (3.35, 3.36): As already mentioned, the RM regime is "skipped" (this is checked explicitly in Appendix A.1.1), and

$$R_\xi = R_l \quad \text{and} \quad L_\xi = L_l \; . \tag{3.38}$$

The resulting Hamiltonian, which is very similar to a Hamiltonian for randomly-pinned charge-density waves, has been studied in detail by a variety of methods: A position-space renormalization group (RG) treatment [20], a Flory-type argument [11], a functional RG (FRG) [9, 17], and a variational approach with RSB [9, 17, 21]. In $d = 2$ dimensions (with $n = 1$ displacement components), which marks the lower critical dimension of the Bragg glass, the Hamiltonian is equivalent to the (vortex-free) 2D XY model in a random symmetry breaking field [53], which has also been intensively studied in the past [18, 19, 20, 22, 23] and is treated in part II of this work in detail.

[1]In the elastic part of the Hamiltonian we can limit ourselves to local elasticity in the asymptotic regime of large length scales where the Bragg glass phase is valid: $c_{44}[K < 1/\tilde{\lambda}_c] \approx \hat{c}_{44}$.

The upper critical dimension for the Bragg glass phase is $d_> = 4$, above which disorder is irrelevant. For $2 < d < 4$, disorder is relevant and the system is in a *glassy* phase. In the FRG analysis this manifests in a stable $T = 0$ fixed-point with non-analycities in the disorder correlator governing the behaviour of the system, and in the variational approach with RSB in the stability of a continuous RSB result for the propagator, indicating the occurrence of a hierarchically organized set of metastable states [9]. Displacements are found to grow logarithmically

$$\zeta_B \;=\; \mathcal{O}(\sqrt{\log}) \;, \tag{3.39}$$

corresponding to a k^{-d}-divergence in the Fourier-transformed $\overline{\langle uu\rangle}$-correlations. The precise form of the displacement correlations is

$$\overline{\langle (u(\mathbf{R},L)-u(\mathbf{R}',L))^2\rangle} \;=\; 2An(4-d)\frac{1}{K_0^2}\ln\left(\frac{|\mathbf{R}-\mathbf{R}'|^2}{R_l^2}+\frac{(L-L')^2}{L_l^2}\right)^{1/2}, \tag{3.40}$$

where A is a numerical constant of order unity. The variational calculation with RSB yields a value $A = 1$, slightly smaller than the result from the FRG, $A = \pi^2/9$ [9]. This discrepancy can be assigned to the fact that variational calculations tend to underestimate fluctuations. The relatively weak logarithmic divergence can be understood most easily from the CDW-type coupling to the disorder in $\mathcal{H}_{d,B}^{(d,n)}$ via the periodic density (3.34), again by using a Flory-type argument due to Nattermann [11]. Large displacements u cost an elastic energy increasing as u^2; the disorder energy gained from the pinning, however, is bounded because it is periodic in u and the FL array "sees" the same disorder configuration whenever it is displaced by a full FL spacing. Actually, assuming Gaussian displacement fluctuations, the mean square pinning energy determined from (3.35, 3.36) decays exponentially

$$(\overline{\langle(\mathcal{H}_{d,B}^{(d,n)})^2\rangle})^{1/2}(R) \;\sim\; R^{d/2}\exp\left(-\frac{K_0^2}{2}(\overline{\langle u^2\rangle}(R,L))\right) , \tag{3.41}$$

which leads upon equating to the elastic energy on the scale R,

$$\overline{\langle\mathcal{H}_{el}^{(d,n)}\rangle}(R,L) \;\sim\; R^{d-2} \;, \tag{3.42}$$

to the above logarithmic $\overline{\langle uu\rangle}$-displacements [again, the scaling relation between L and R is given by (3.8) $L \sim (\hat{c}_{44}/c_{66})^{1/2}R$].

Due to the logarithmic displacements, the correlations in the disorder-averaged translational order parameter decay algebraically

$$\begin{aligned}\overline{\langle\rho_{\mathbf{K}}(\mathbf{r})\rho_{\mathbf{K}}^*(\mathbf{r}')\rangle} \;&=\; \overline{\langle\exp\left(i\mathbf{K}(\mathbf{u}(\mathbf{r})-\mathbf{u}(\mathbf{r}'))\right)\rangle} \\ &\sim\; \left(\frac{|\mathbf{R}-\mathbf{R}'|}{R_l}\right)^{-A(4-d)K^2/K_0^2}\end{aligned} \tag{3.43}$$

(where $\mathbf{K}$ is a reciprocal lattice vector). This results in a structure factor

$$S(\mathbf{k}) \sim \frac{1}{|\mathbf{k}-\mathbf{K}|^{d-j^2\cdot A(4-d)}} \tag{3.44}$$

at the j^{th} reciprocal lattice vector $\mathbf{k} \approx \mathbf{K} = j \cdot \mathbf{K}_0$. Therefore, algebraically decaying Bragg peaks should be obtained in scattering experiments, and this phase bears the name "Bragg glass" [9, 17]. These Bragg peaks have been observed in neutron diffraction experiments by Cubitt et al. [25].

The lower critical dimension of the Bragg glass is $d_< = 2$, below which thermal fluctuations induce stronger fluctuations than the disorder [the FRG eigenvalue of the temperature is $2-d$]. For $d = 2$ and $n = 1$, we have a planar FL array, which is a chain of FLs confined to a plane, i.e., the magnetic field is *parallel* to the plane. [In other words we consider an $d = 1 + 1$ dimensional FL array, which has to be distinguished from the widely studied "pancake vortices" corresponding to $d = 2$ and $n = 2$, i.e., to $d = 2 + 0$ dimensions]. Such a system can be experimentally realized in disordered thin type-II superconducting films or for Josephson vortices in a planar, inhomogeneous Josephson junction. In the following chapter, this type of system will serve as building block to model a layered HTSC in a magnetic field parallel to the superconducting CuO-planes, where each layer of Josephson-type vortices between two CuO-planes can be described by an FL array with $d = 2$ and $n = 1$. At the marginal dimension $d = 2$, disorder and thermal fluctuations lead both to logarithmic growth of the displacements and to the existence of a transition temperature, above which thermal fluctuations dominate, and disorder is renormalized to zero, whereas in the low temperature phase the system exhibits "glassy" properties. The two-dimensional disordered FL array with uniaxial displacements ($n = 1$) can be mapped [53] onto a (vortex-free) 2D XY model in a random symmetry breaking field (2D RFXY model henceforth), for which the existence of the transition to a disorder-dominated low temperature phase with glassy properties has been demonstrated by a variety of methods [18, 19, 21, 22].

In fact, the glassy low-temperature phase of the two-dimensional FL array is the only vortex glass (VG) phase whose existence has been proven analytically [actually, based on this result for $d = 2$, Fisher [5] originally conjectured the existence of a VG phase for higher dimensions]. This is due to the fact that topological defects are excluded in a planar FL array in $d = 2$ because the original labeling of the lines and thus the displacement field are always unambiguously defined; hence, the elastic description cannot be invalidated. This is the essential difference to higher dimensions, which makes all our considerations in this part I necessary.

To switch to the "language" of the 2D XY model in a random symmetry breaking field (with a p-fold symmetry) for $d = 2$ and $n = 1$ (and $z = 1$), we introduce a *phase-field* ϕ

instead of the scalar displacement-field u ($\mathbf{u} = u \cdot \hat{\mathbf{x}}$)

$$\phi(\mathbf{r}) \;:=\; \frac{K_0}{p}\, u(\mathbf{r}) \;=\; \frac{2\pi}{pl}\, u(\mathbf{r})\;. \tag{3.45}$$

Note that the elastic part of the Hamiltonian $\mathcal{H}_{el}^{(2,1)}$ is now given by (3.12), and contains only a tilt (c_{44}) and a compression (c_{11}) term. Because we are interested mainly in the asymptotic long wavelength properties, we use the *local* limit of the elastic Hamiltonian and take the *non-dispersive* elastic constants $c_{44/11}[K] \approx \hat{c}_{44/11}$. We switch to an *isotropic* elastic Hamiltonian by rescaling

$$z' \;=\; \left(\frac{\hat{c}_{11}}{\hat{c}_{44}}\right)^{1/2} z \quad \text{and} \quad L' \;=\; \left(\frac{\hat{c}_{11}}{\hat{c}_{44}}\right)^{1/2} L \;=\; R\,, \tag{3.46}$$

which leads to a Hamiltonian[2]

$$\mathcal{H}^{2D}[\phi] \;=\; \mathcal{H}_{el}^{2D}[\phi] + \mathcal{H}_{d}^{2D}[\phi] \tag{3.47}$$

with an elastic part of the Hamiltonian characterized by the isotropic elastic constant K given in (3.53)

$$\beta\mathcal{H}_{el}^{2D}[\phi] \;=\; \frac{1}{2}\int d^2\mathbf{r}\;\left\{K(\boldsymbol{\nabla}\phi)^2\right\}\;. \tag{3.48}$$

In the disorder part of the Hamiltonian, we have to consider in $d = 2$ dimensions also the marginally relevant gradient term in the density (see (3.34) with the smallest inverse lattice vector $\mathbf{K}_0 = (2\pi/l)\hat{\mathbf{x}}$ only and $\rho_0 = 1/l$)

$$\rho[\mathbf{r}, \phi(\mathbf{r})] \;\approx\; \rho_0\left(1 - \frac{pl}{2\pi}\partial_x\phi(\mathbf{r}) + 2\cos\left(\frac{2\pi}{l}x - p\phi(\mathbf{r})\right)\right)\;, \tag{3.49}$$

which leads to an additional random bond term compared to (3.35):

$$\beta\mathcal{H}_{d}^{2D}[\phi] \;=\; \int d^2\mathbf{r}\;\left\{W[\mathbf{r}, \phi(\mathbf{r})] \;-\; \mathbf{w}[\mathbf{r}]\cdot\boldsymbol{\nabla}\phi\right\} \tag{3.50}$$

with

$$\overline{W[\mathbf{r}, \phi]W[\mathbf{r}', \phi']} \;=\; 2g\;\cos\left(p(\phi - \phi')\right)\,\delta^2(\mathbf{r} - \mathbf{r}') \tag{3.51}$$

$$\overline{w_i[\mathbf{r}]w_j[\mathbf{r}']} \;=\; \Delta\;\delta_{ij}\delta^2(\mathbf{r} - \mathbf{r}') \tag{3.52}$$

[2] $\beta \equiv 1/T$

(W and $\mathbf{w}$ are Gaussian distributed with mean zero and uncorrelated $\overline{\mathbf{w}W} = 0$), where we anticipated in (3.52) that the random bond terms become isotropic on large scales in the thermodynamic limit. Furthermore, we have absorbed all temperature dependencies into

$$K = (\hat{c}_{44}\hat{c}_{11})^{1/2} \left(\frac{pl}{2\pi}\right)^2 \frac{1}{T} \tag{3.53}$$

$$g = (\hat{c}_{44}/\hat{c}_{11})^{1/2} g_B \frac{1}{T^2} \tag{3.54}$$

$$\Delta = \frac{p^2 l^2}{8\pi^2}\, g\ . \tag{3.55}$$

The such defined 2D RFXY model is studied in the absence of vortices in the ϕ-field, which would correspond to FLs ending in a layer. This is assumed to cost a large amount of magnetic energy [the FL has to either "tunnel" to some other nearby layer, or to end in a magnetic monopole] and thus to be forbidden. Though it has been studied intensively analytically [9, 17, 18, 19, 20, 22, 23, 21, 54, 55, 56] and numerically [57, 58, 59, 60], some properties of the 2D RFXY model are still controversial, e.g. the exact form of the $\overline{\langle\phi\phi\rangle}$-correlations in the low-temperature phase. [The 2D RFXY model, and in particular the issue of its $\overline{\langle\phi\phi\rangle}$-correlations, will be considered in detail in part II of this work.] However, all approaches agree in the existence of a high-temperature phase, in which disorder is irrelevant, above a temperature T_g or for $\tau < 0$, where

$$\tau := 1 - \frac{K_c}{K} = \frac{T_g - T}{T_g} \quad \text{with} \quad K_c = \frac{p^2}{4\pi} \tag{3.56}$$

is the *negative reduced temperature*, and a glassy low-temperature phase for $\tau > 0$, which is disorder dominated and exhibits glass-like dynamical properties [22, 23, 54, 57]. The $\overline{\langle\phi\phi\rangle}$-correlations have been conjectured either to diverge $\propto \ln r$, i.e. similar to their behaviour in $2 < d < 4$ (3.40) [9, 17, 21, 54] or to exhibit rather a so-called "super-roughness" with a somewhat stronger divergence $\propto \ln^2 r$ [18, 61]:

$$\zeta_{2D} = \mathcal{O}(\sqrt{\log}) - \mathcal{O}(\log)\ . \tag{3.57}$$

Neither from the analytics or from the numerics one or the other could be ruled out so far. Due to the pronounced thermal fluctuations in $d = 2$, which entirely "wipe out" the disorder above T_g, the crossover length to the disorder-dominated phase, i.e., the positional correlation length R_l [which is equivalent to the Larkin length $R_\xi = R_l$ in the single-harmonic approximation (3.36) in (3.35) of the Bragg glass model] is renormalized upwards also in the low-temperature phase [9] (see Appendix, equations (A.20, A.22)):

$$R_{l,2D}(T=0) \sim \frac{K}{g^{1/2}} \tag{3.58}$$

$$R_{l,2D}(\tau) \simeq l \left(\frac{R_{l,2D}(T=0)}{l}\right)^{1/\tau}\ . \tag{3.59}$$

Now, that we have reviewed the properties of the *dislocation-free* disordered FL array in some detail, we have set the stage for the appearance of dislocations in the disordered FL array.

Chapter 4

Variational Calculation for a Layered Superconductor in a Parallel Field

We want to start our study of dislocations in the disordered FL array with a variational calculation for a strongly layered impure HTSC in a magnetic field *parallel* to the superconducting CuO-planes $\mathbf{H} \parallel \mathbf{ab}$ [Figure 4.1] [62, 63, 64, 65, 66, 67]. To avoid shear instabilities of the FL lattice [63], we choose the magnetic field such that the FL lattice is *commensurate* with the layer spacing d of the superconducting planes. The FL distances are $l_\parallel$ and $l_\perp = nd$ (n integer) in the directions parallel and perpendicular to the layers, respectively; the magnetic penetration depths are λ_c and λ_{ab} for magnetic fields parallel and perpendicular to the layers, respectively. The superconducting CuO-planes provide a sufficiently strong confining potential for the Josephson-like vortex lines which exist in the interlayer spacing so that we can exclude to a good approximation the possibility of lines crossing the superconducting layers: In BSCCO with the fields parallel to the ab-planes, typical vortex kink energies are of the order $(\phi_0/4\pi\lambda_{ab})^2 d \approx 10^3(1 - T/T_c)^\circ K$ [64]. This amounts to limiting the vortex displacement field from two components in an isotropic sample to one component (i.e. , parallel to the layers). We will come back in chapter 5 to the usual experimental situation of magnetic fields perpendicular to the CuO-planes of the HTSC, where the displacements are two component.

In what follows, we model each layer of FLs in the HTSC as a planar FL array in $d = 1 + 1$ dimensions subject to point disorder or, by virtue of the mapping described in chapter 3, as 2D RFXY model given by formulae (3.45-3.55). For these layers, we derive an inter-layer coupling between "adjacent" layers, which reduces to an elastic shear coupling of the lattice for a strong inter-layer coupling but allows for the formation of dislocation loops in between each layer. This enables us to explore *quantitatively* the possibility of an instability with respect to a proliferation of dislocation loops by means

of a variational calculation of an effective shear modulus. The effective shear modulus is driven to zero upon a proliferation of dislocation loops. Though the application of the model to a layered HTSC in a *parallel* field is interesting in its own right, we introduce this model as a first step towards a systematic study of the usual experimental situation of a HTSC in a field *perpendicular* to the CuO-planes or, more generally speaking, an anisotropic type-II superconductor in the presence of point disorder with the magnetic field along the symmetry axis. With regard to this generic situation, the layered model we consider in this chapter has limitations based on the uniaxiality of the displacements, which, on the other hand, make an analytic treatment possible at all. However, we can cast the main result of the variational calculation into a *Lindemann-like criterion* comparing the positional correlation length R_l [which is equal to the Larkin length R_ξ in the Bragg glass model we employ, see (3.38)] with the FL spacing. In this form, it can be generalized easily to other more generic models with two-component displacements, which are studied in detail in the following chapters 5 and 6.

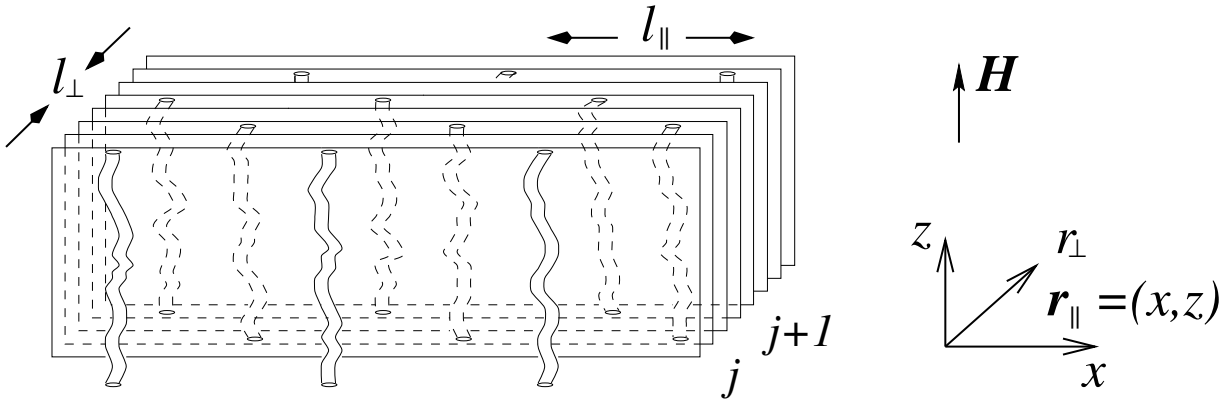

Figure 4.1: FL array in a layered superconductor in a parallel magnetic field

4.1 Hamiltonian for the Layered Uniaxial Geometry

We choose $\mathbf{r}_\parallel = (x, z)$ as in-plane coordinates, such that the z-axis is parallel and the x-axis is perpendicular to the undistorted FLs, and $r_\perp = y$ as coordinate perpendicular to the FL layers, which are labeled with an index j [Figure 4.1]. We adopt for the layered HTSC the "language" of the 2D RFXY model introduced in the last chapter (3.45-3.55) and write down the Hamiltonian in terms of a phase field $\phi_j(\mathbf{r}_\parallel)$ instead of the uniaxial, scalar displacement field $\mathbf{u}_j = \phi_j \, \hat{\mathbf{x}} \, l_\parallel p/2\pi$. Then, the FL array can be described by a

Hamiltonian

$$\mathcal{H}[\{\phi_j\}] \;=\; \sum_j \left\{\mathcal{H}_{el}^{2D}[\phi_j] + \mathcal{H}_d^{2D}[\phi_j]\right\} + \mathcal{H}_{int}[\{\phi_j\}] \tag{4.1}$$

with the (isotropized) elastic energy $\mathcal{H}_{el}^{2D}$ of the disorder-free 2D FL-array introduced above (3.48) and characterized by an isotropic in-plane elastic constant K (3.53).

Pinning effects due to point disorder are described by the disorder part $\mathcal{H}_d^{2D}[\{\phi_j\}]$ of the Hamiltonian, which is the sum of the random potentials of the 2D layers. These are uncorrelated since the range of the disorder in the direction perpendicular to the CuO-planes equals the coherence length ξ_c in that direction and is typically several orders of magnitude smaller than $l_\perp = nd$ in a HTSC. As mentioned in the introductory chapter 2, only *free*, *unbound* dislocation loops induce a melting in the direction perpendicular to the FL layers, so we have to use the approximation (3.50) for the disorder within each 2D FL layer, that describes the large scale properties in the Bragg glass phase correctly:

$$\beta\mathcal{H}_d^{2D}[\phi_j] \;=\; \int d^2\mathbf{r}_\parallel \;\left\{W_j[\mathbf{r}_\parallel, \phi_j(\mathbf{r}_\parallel)] \;-\; \mathbf{w}_j[\mathbf{r}_\parallel]\cdot\boldsymbol{\nabla}\phi_j\right\} \tag{4.2}$$

with $\overline{W_j W_{j'}} = \delta_j j' \overline{WW}$ from (3.51) and $\overline{\mathbf{w}_j \mathbf{w}_{j'}} = \delta_{jj'}\overline{\mathbf{ww}}$ from (3.52).

$\mathcal{H}_{int}[\{\phi_j\}]$ is the (ϕ-dependent part of the) interaction energy between the layers. It can be written in the framework of the London-theory as interaction energy between all pairs of FL-elements. In the continuum description of the planar FL arrays, we can write it in terms of the FL densities $\rho[\mathbf{r}, \phi(\mathbf{r})]$ as

$$\beta\mathcal{H}_{int}[\{\phi_j\}] = \sum_{i>j}\int_{\mathbf{r}_{\parallel,1}}\int_{\mathbf{r}_{\parallel,2}} V_{int}(i-j,\; \mathbf{r}_{\parallel,1}-\mathbf{r}_{\parallel,2})\rho[\mathbf{r}_{\parallel,1}, \phi_i(\mathbf{r}_{\parallel,1})]\rho[\mathbf{r}_{\parallel,2}, \phi_j(\mathbf{r}_{\parallel,2})]. \tag{4.3}$$

For simplicity, we want to consider here the dilute limit, where the FL interaction is effectively a "nearest layer" interaction, i.e., $V_{int}(i, \mathbf{r}_\parallel) \approx \delta_{i,1} l_\parallel^2 v_{int}(\mathbf{r}_\parallel)$. In the dilute limit $\lambda_{ab} \ll l_\perp$, the range of the magnetic interaction given by the magnetic penetration depths λ_{ab} perpendicular to the planes exceeds the FL distance $l_\perp$. Note that in this limit $v_{int} \propto \exp(-l_\perp/\lambda_{ab})$ is small compared to the in-plane elastic energies. The generalization of our results to the dense limit will be discussed below. Using the expression (3.49) for the FL density $\rho[\mathbf{r}_\parallel, \phi]$ as in the disorder part of the Hamiltonian and neglecting fast oscillating terms, we obtain

$$\beta\mathcal{H}_{int}[\{\phi_j\}] \;\approx\; \sum_j \int d^2\mathbf{r}_\parallel \left\{V_j[p(\phi_j(\mathbf{r}_\parallel) - \phi_{j+1}(\mathbf{r}_\parallel))] \;+\; \frac{1}{2}K_\mu \boldsymbol{\nabla}\phi_j \cdot \boldsymbol{\nabla}\phi_{j+1}\right\} \tag{4.4}$$

$$\approx \sum_j \int d^2\mathbf{r}_\parallel \left\{V_j[\phi_j(\mathbf{r}_\parallel) - \phi_{j+1}(\mathbf{r}_\parallel)]\right\} \;, \tag{4.5}$$

where we anticipated in (4.4) that the elastic term can be treated as isotropic in the thermodynamic limit. After switching in every second FL layer to $\phi_j \mapsto \phi_j + \pi$, taking into account the hexagonal structure of the groundstate of the FL lattice, the inter-layer coupling $V_j[p\phi]$ is

$$V_j[\phi] \;=\; -\mu \cos(p\phi) \; . \tag{4.6}$$

This expression can be regarded as the repulsive magnetic interaction energy between the lowest harmonics of density fluctuations between vortex lines in adjacent layers [65]. μ and K_μ, which is in general dispersive $K_\mu = K_\mu[k_\parallel]$, are proportional to the shear energy, that is given by v_{int} and can be expressed in terms of the Fourier transform $\tilde{v}_{int}(k_\parallel)$ as:

$$\mu \;\simeq\; \tilde{v}_{int}(2\pi/l_\parallel) \;\propto\; \frac{1}{T} \tag{4.7}$$

$$K_\mu[k_\parallel] \;=\; \tilde{v}_{int}(k_\parallel) l^2 p^2/8\pi^2 \;\propto\; \frac{1}{T} \tag{4.8}$$

[note that we had absorbed temperature dependencies into $\tilde{v}_{int} \propto 1/T$, see (4.3)]. In the local long wavelength limit $K_\mu \approx K_\mu[0]$ of interest, one recognizes that in the continuum limit of (4.4), the elastic term with the coupling constant K_μ can be absorbed into the elastic constant K in $\mathcal{H}_{el}^{2D}$ (3.48): $K \mapsto K + K_\mu$. Due to $K_\mu \propto \exp(-l_\perp/\lambda_{ab}) \ll K$, we can neglect K_μ completely for the following and arrive at (4.5). Putting everything together, we obtain a Hamiltonian of the form

$$\begin{aligned} \beta\mathcal{H}[\{\phi_j\}] \;=\; \sum_j \int d^2\mathbf{r}_\parallel \Big\{ & \frac{1}{2} K (\boldsymbol{\nabla}_\parallel \phi_j)^2 \;+\; V_j[\phi_j(\mathbf{r}_\parallel) - \phi_{j+1}(\mathbf{r}_\parallel)] \;+ \\ & + W_j[\mathbf{r}_\parallel, \phi_j(\mathbf{r}_\parallel)] - \mathbf{w}_j[\mathbf{r}_\parallel] \cdot \boldsymbol{\nabla} \phi_j \Big\} \end{aligned} \tag{4.9}$$

for the layered HTSC in a parallel field.

Clearly, a coupling of the form (4.6) allows for dislocations, because shifts of $2\pi/p$ in the phase difference $\phi_{j+1} - \phi_j$ between two neighbouring layers (or equivalently by $l_\parallel$ in the relative displacement $u_{j+1} - u_j$) do *not* cost interaction energy. So, a few remarks are in order at this point about where and how dislocations can proliferate in this uniaxial, layered system. Because the FLs are confined to *one* layer (between two CuO-planes) and displacements are thus uniaxial, also the Burgers vectors $\mathbf{b}$ have to be *uniaxial*

$$\mathbf{b} \parallel \hat{\mathbf{x}} \; . \tag{4.10}$$

As discussed in chapter 2, this entails that only dislocation loops *parallel* to the FL layers can form [to which we assign a location on the plaquets formed by the bonds of the FL array, so that dislocation loops are always lying in between two FL layers]. Obviously, such dislocation loops cannot destroy the in-plane order of the FL layers. The in-plane

order of the FLs cannot be destroyed in this uniaxial model at all, because FLs within the same layer cannot cross each other, and the displacement or phase field $\phi_j(\mathbf{r}_\parallel)$ can always be unambiguously defined within each plane j. [Consequences of this peculiarity for the disorder-free system are discussed in detail in Ref. [65].] Therefore, a dislocation-mediated melting will destroy only the positional order in the direction perpendicular to the FL layers and lead rather to a *smectic* phase consisting of effectively decoupled 2D systems, which was analyzed for the disorder-free system in Refs. [66, 67]. However, a proliferation of dislocation loops will lead to a vanishing effective shear modulus, a characteristic of a disorder-induced "melting" into a smectic phase.

4.2 Elastic and Decoupled Limit

In what follows, we study the phase diagram in terms of the inter-layer coupling μ and the in-plane elastic constant $K \propto 1/T$, which plays the role of an inverse temperature, for a fixed strength of the disorder. The behaviour of the system is governed by the competition between the inter-layer coupling and the disorder. The inter-layer coupling tries to bring FLs in neighbouring layers into registry and favors a *dislocation-free*, hexagonal crystalline order of the FL array. On the other hand, the disorder, which is uncorrelated between the layers, tends to decouple the layers to allow for an optimal adjustment to the disorder configuration in each layer separately; for dominating disorder, the FL array looses the lattice order and "melts" into the just mentioned *smectic* glassy phase. Then, typical FL configurations can only be described in terms of a collection of *unbound dislocation loops* in between the layers.

For $\mu \uparrow \infty$, the FL array is *dislocation-free*, and V_{int} can be approximated by an elastic energy

$$V_{j,el}[\phi] \;=\; \frac{1}{2}\mu p^2 \phi^2 \;, \tag{4.11}$$

and μ is related to the shear modulus. The "nearest neighbour" approximation for the dilute limit leads to a *local* elasticity theory, i.e., with dispersion-free elastic modulus μ. The continuum (introducing $\mathbf{r} = (\mathbf{r}_\parallel, r_\perp = j \cdot l_\perp)$) and disorder-free version of (4.9) with (4.11) is just the uniaxial ($n = 1$) standard three-dimensional elastic Hamiltonian $\mathcal{H}_{el}^{(d=3,n=1)}$ (3.12) introduced in the preceding chapter 3. Remembering the in-plane rescaling (3.46), we find the relations

$$\mu \;\approx\; c_{66}(\hat{c}_{44}/\hat{c}_{11})^{1/2} \frac{l_\parallel^2}{(2\pi)^2 l_\perp} \frac{1}{T} \tag{4.12}$$

$$K \;\approx\; (\hat{c}_{44}\hat{c}_{11})^{1/2} \frac{l_\parallel^2 l_\perp}{(2\pi)^2} \frac{1}{T} \tag{4.13}$$

between μ and the shear modulus and between K and the tilt and compression moduli

of the 3D FL array. Whereas it is clear that the elastic energy of the uniaxial, layered superconductor in a parallel field under consideration is completely described by a set three elastic constants, lots of work in the literature has been devoted to the calculation of the larger set of elastic constants for the general case of two-component displacements. In the standard terminology [4] of this more general situation [but for $\mathbf{H} \parallel \mathbf{ab}$], we refer here to the subset of moduli $c_{11}^{\parallel}$, $c_{44}^{\parallel}$ and $c_{66}^{\parallel}$ when specializing to uniaxial displacements with $\mathbf{u} \parallel \mathbf{ab}$. The assumed suppression of vortex kinks crossing the planes is equivalent to taking the remaining elastic constants $c_{11}^{\perp}$, $c_{44}^{\perp}$ and $c_{66}^{\perp}$ to be *infinite*. It can be checked that this is indeed to a good approximation fulfilled for strongly anisotropic materials with $\varepsilon = \lambda_{ab}/\lambda_c \ll 1$ because $c_{11}^{\perp} = c_{11}^{\parallel}/\varepsilon^2$, $c_{44}^{\perp} = c_{44}^{\parallel}/\varepsilon^2$, and $c_{66}^{\perp} = c_{66}^{\parallel}/\varepsilon^4$ [4].

K can be estimated from $\hat{c}_{44} \gtrsim BH_{c1}/4\pi$ and $\hat{c}_{11} \approx B^2/4\pi$ [68] for the dense limit $l_\perp < \lambda_{ab}$; using the relations $B = \phi_0/l_\parallel l_\perp$ and $l_\perp/l_\parallel \approx \lambda_{ab}/\lambda_c$, we obtain for BSCCO typical values

$$KT \;\approx\; \frac{1}{16\pi^3} B^{3/2} H_{c1}^{1/2} l_\parallel^2 l_\perp \;\sim\; (\phi_0/4\pi\lambda_{ab})^2 \lambda_{ab} \;\sim\; 10^5 (1 - T/T_c)^{1/2}\ {}^\circ\mathrm{K}. \tag{4.14}$$

In the 2D RFXY model corresponding to a single FL layer, this estimate implies that the transition temperature T_g, see (3.56), is extremely high,

$$K \gg K_c \quad \text{or} \quad \tau = 1 - \frac{K_c}{K} \simeq 1 \ , \tag{4.15}$$

and we are effectively in the $T{=}0$-limit ($K \uparrow \infty$). However, in the dilute limit $l_\perp \gg \lambda_{ab}$ it is known [65] that within each layer steric repulsion dominates because the FL interaction decays exponentially, and K becomes effectively temperature independent:

$$K \approx K_c \frac{1}{1 - \lambda_c/l_\parallel} \gtrapprox K_c \quad \text{or} \quad \tau = 1 - \frac{K_c}{K} \gtrapprox 0 \ . \tag{4.16}$$

Thus, the physical realization of a HTSC in a parallel field maps *always* to the low-temperature phase $1 \geq \tau > 0$ ($K \geq K_c$) of our model consisting of a stack of coupled 2D RFXY models: $\tau \simeq 1$ is realized in the dense limit of the FL array, and $\tau \gtrapprox 0$ in the dilute limit.

The disordered layered FL array is in the elastic, dislocation-free strong coupling limit equivalent to a uniaxial Bragg glass in $d = 3$, but with a discretized coordinate in the direction perpendicular to the layers[1]. As discussed in the previous chapter 3, it exhibits logarithmic roughness, see (3.40). The asymptotic form of the propagator has been calculated in the framework of a variational approach with an RSB Ansatz for the propagator and by a functional renormalization group (FRG) calculation by Giamarchi and LeDoussal [9, 17].

[1]The additional random bond term associated with the random field $\mathbf{w}$ is irrelevant in 3 dimensions [9].

In the variational calculation one finds ($k_\perp$ runs over the Brillouin zone $[-\pi/l_\perp, \pi/l_\perp]$ of the discrete coordinate)

$$\begin{aligned}
\overline{\langle\phi(\mathbf{k}_\parallel,k_\perp)\phi(\mathbf{k}'_\parallel,k'_\perp)\rangle}_{3D} &= (2\pi)^3\delta^2(\mathbf{k}_\parallel+\mathbf{k}'_\parallel)\delta^1(k_\perp+k'_\perp)\; G_{3D}(k_\parallel,k_\perp) \\
G_{3D}(k_\parallel,k_\perp) &\simeq \frac{2\pi^2 K\mu^{1/2}}{\left(Kk_\parallel^2+2\mu l_\perp^2\,(1-\cos\left(k_\perp l_\perp\right))\right)^{3/2}} \\
G_{3D}(r_\parallel=0,j=0) &\simeq \ln\left(\frac{R_\parallel^2}{R_{l,3D,\parallel}^2}+\frac{R_\perp^2}{R_{l,3D,\perp}^2}\right)^{1/2}
\end{aligned} \tag{4.17}$$

for a finite system of (transversal) size $R_\parallel$ and $R_\perp$. The variational calculation yields a prefactor of the log of exactly unity in the last equation (which we will use henceforth for definiteness), whereas the FRG approach gives the slightly larger value $\pi^2/9$. This asymptotic form holds on lengths scales exceeding the Larkin length $R_{l,3D}$, which can be expressed in terms of K, μ and g as

$$\begin{aligned}
R_{l,3D,\parallel}=R_{\xi,3D,\parallel} &= \bar{c}_{d=3}\frac{K^{3/2}\mu^{1/2}}{g} \\
R_{l,3D,\perp}=R_{\xi,3D,\perp} &= \bar{c}_{d=3}\frac{K\mu}{g}l_\perp
\end{aligned} \tag{4.18}$$

[(for $p=1$); see (3.38, A.23), and for the numerical prefactors the discussion in Appendix A.1.1] with $\bar{c}_{d=3}=8\pi^2$ (A.11). Also, due to the existence of a statistical symmetry [69, 70], it is known that the disorder-averaged responses of the system to various elastic deformations are identical to those of the pure elastic system, i.e., the Hamiltonian (4.9) with $W\equiv 0$. In particular, there is a non-zero response to shear.

In the limit of a very small inter-layer coupling $\mu \ll 1$, we can find perturbatively, whether the inter-layer coupling (4.6) in (4.5) is relevant on large scales by evaluating the correction ΔF_μ to the (disorder-averaged) free energy per layer to leading order in μ, which is the free energy gain due to the coupling in the disordered, *decoupled* FL array:

$$\begin{aligned}
\Delta F_\mu &= -\mu T\int d^2\mathbf{r}_\parallel\overline{\langle\cos\left(p(\phi_j(\mathbf{r}_\parallel)-\phi_{j+1}(\mathbf{r}_\parallel))\right)\rangle}_{\mu=0} \\
&\approx -\mu T\int d^2\mathbf{r}_\parallel\exp\left(-p^2\overline{\langle(\phi_j(\mathbf{r}_\parallel))^2\rangle}_{2D}\right)\,.
\end{aligned} \tag{4.19}$$

The average is calculated with the Hamiltonian of the uncoupled system, therefore the last average is performed with the 2D RFXY Hamiltonian. In (4.19) we applied a cumulant expansion and neglected higher order cumulants, which is exact only for *Gaussian* averages where the connected higher order correlations $\overline{\langle\phi^{2m}\rangle}_{2D,\mathrm{conn}}$ ($m>1$) vanish. Let us discuss the validity of this approximation along with the different results for the 2-point correlation

function of the 2D RFXY model, the correct asymptotic behaviour of which is still a subject of current research and will be one of the main issues in part II of this work.

Up to now, essentially two analytical approaches to the 2D RFXY model are existing as already mentioned, which are (i) a renormalization group (RG) treatment due to Cardy and Ostlund [18] and Goldschmidt and Houghton [19], and (ii) a variational approach with a RSB Ansatz by Korshunov [21] and Giamarchi and LeDoussal [9, 17], which has also been successfully applied to the Bragg glass phase in higher dimensions $2 < d < 4$. However, the results of both approaches are not in agreement regarding important properties of the low-temperature phase, which is in both approaches found for a reduced temperature $\tau > 0$ or $K > K_c = p^2/4\pi$.

In the RG-approach, one finds that the 2-point vertex of the replicated Hamiltonian is renormalizable, i.e., all divergences occuring in the low-temperature phase in a double-expansion in g and the reduced temperature τ can be absorbed in a renormalization of g and Δ; K is unrenormalized due to a statistical tilt symmetry. The long-wavelength properties can be analyzed by studying the RG-flow under a change of scale by a factor e^{ℓ}. One finds a "runaway-flow" for $\Delta(\ell)$ and a perturbative fixed point g^* for $g(\ell)$ with

$$\begin{aligned} \frac{d\Delta}{d\ell} &= \frac{p^2}{16c}(4cl_\parallel^2 g)^2 && (4.20)\\ \frac{dg}{d\ell} &= 2\tau g - 4cl_\parallel^2 g^2 && (4.21)\\ g(\ell) \to g^* &= \frac{2\tau}{4cl_\parallel^2}\ , && (4.22) \end{aligned}$$

where c is a non-universal numerical constant depending on the IR cutoff procedure; we take $c = \pi$ henceforth corresponding to a circular cutoff. Upon integrating the RG-flow up to $e^{-\ell} = k_\parallel l_\parallel/2\pi$, the "runaway-flow" of Δ leads to an additional logarithmic divergence in the 2-point correlation function and a "super-rough" low-temperature phase [61]:

$$\begin{aligned} \overline{\langle\phi(\mathbf{k}_\parallel)\phi(\mathbf{k}'_\parallel)\rangle}_{2D} &= (2\pi)^2\delta^2(\mathbf{k}_\parallel + \mathbf{k}'_\parallel)G(k_\parallel)\\ G_{2D}(k) &\simeq \frac{1}{Kk^2} + \left(\frac{\Delta(\ell)}{K^2k^2} + \frac{g(\ell)e^{-2\ell}}{K^2k^4}\right)\Bigg|_{\ell=\ln(2\pi/kl_\parallel)} \end{aligned} \qquad (4.23)$$

The first term is the propagator of the disorder-free system, the first two terms represent the renormalized bare propagator of the disordered system, and the third term the renormalized self-energy contribution to first order in g. Using

$$\tilde{g}(\ell) \ :=\ 4\pi l_\parallel^2 g(\ell) \ =\ \frac{\tilde{g}\exp(2\tau\ell)}{1 + \frac{\tilde{g}}{2\tau}\exp(2\tau\ell)} \to \tilde{g}^* = 2\tau\ , \qquad (4.24)$$

the first two terms in (4.23) give to leading order in τ the asymptotics

$$\begin{aligned} G_{2D}(k) &\simeq \frac{1}{Kk^2} + \tau^2 \frac{\ln\left(\frac{2\pi}{kl_\parallel}\right)}{k^2} \\ G_{2D}(r_\parallel = 0) &\simeq \frac{1}{2\pi K} \ln\left(\frac{R_\parallel}{l_\parallel}\right) + \frac{\tau^2}{4\pi} \ln^2\left(\frac{R_\parallel}{l_\parallel}\right) \end{aligned} \tag{4.25}$$

for a finite system of (transversal) size $R_\parallel$. The $\log^2$-divergence is the signature of the "super-rough" low-temperature phase. The asymptotic $\log^2$-behaviour sets in above the Larkin length $R_{l,2D}$, i.e., the scale where the mean square phase-shift exceeds $(2\pi/p)^2$, and perturbation theory breaks down. This scale is determined by the last term in (4.23), which dominates the perturbative regime, and given by (3.58, 3.59).

Applying these results to higher order correlations $\overline{\langle\phi^{2m}\rangle}_{2D,\mathrm{conn}}$ $(m > 1)$, we argue that by means of the renormalization of the 2-point vertex all essential divergences should have been removed (if renormalizability holds). Using renormalized vertices in a diagrammatic calculation, one finds, similar to the asymptotics of the third term in (4.23), *finite* results of the order of $g^* \propto \tau$ for the connected correlations $\overline{\langle\phi^{2m}\rangle}_{2D,\mathrm{conn}}$ in the thermodynamic limit. Therefore, averages with the 2D RFXY Hamiltonian, i.e., the *decoupled* system ($\mu = 0$), are approximately *Gaussian* on large scales apart from finite corrections, and the neglect of the higher order cumulants in (4.19) is justified. Using the asymptotic expression (4.25), we obtain for layers of (transversal) size $R_\parallel$

$$\Delta F_\mu \sim -\mu T \left(R_\parallel/l_\parallel\right)^{2\tau - K_c\tau^2 \ln\left(R_\parallel/R_{l,2D}(\tau)\right)} , \tag{4.26}$$

which is clearly *irrelevant* in the thermodynamic limit. A small coupling $\mu \ll 1$ does not lead to an energy gain in the disordered FL array, and the layers remain *decoupled* and optimally configured with regard to the disorder in each layer.

In the variational approach, one uses an RSB Ansatz to calculate the optimal *quadratic* approximation to the full propagator in replica space, i.e., the full propagator is approximated by a *hierarchically* organized set of quadratic propagators. This leads a priori to Gaussian averages and the cumulant expansion in (4.19) becomes exact in this framework. The result for the asymptotic propagator is [9, 21]

$$\begin{aligned} G_{2D}(k) &\simeq \frac{1}{Kk^2} + \frac{K}{K_c}(\tau + y/2) \frac{1}{Kk^2\left(1 + \left(\frac{kR_{l,2D}(\tau)}{2\pi}\right)^2\right)} \\ G_{2D}(r_\parallel = 0) &\simeq \frac{1}{2\pi K} \ln\left(\frac{R_\parallel}{l_\parallel}\right) + \frac{\tau + y/2}{p^2} \ln\left(\frac{R_\parallel^2 + R_{l,2D}^2(\tau)}{l_\parallel^2 + R_{l,2D}^2(\tau)}\right) \end{aligned} \tag{4.27}$$

again for a finite system of size $R_\parallel$ and with $y := (l_\parallel/R_{l,2D}(\tau))^2 \propto g^{1/\tau} \ll 1$ measuring the disorder strength. Thus the variational approach gives only a log-divergence for the

correlations in the low-temperature phase much like in the disorder-free high-temperature phase, only with an increased prefactor. The Larkin length $R_{l,2D}$ is in terms of K and g given by (3.38, 3.58, 3.59):

$$R_{l,2D}(T=0) = R_{\xi,2D}(T=0) \;\simeq\; \bar{c}_{d=2}\frac{K}{g^{1/2}} \tag{4.28}$$

$$R_{l,2D}(\tau) = R_{\xi,2D}(\tau) \;\simeq\; l_{\parallel}\left(\frac{R_{l,2D}(T=0)}{l_{\parallel}}\right)^{1/\tau} \tag{4.29}$$

[(for $p = 1$); see (A.20), and for the numerical prefactors the discussion in Appendix A.1.1] with $\bar{c}_{d=2} = (2\pi)^{3/2}$ (A.11).

As for the coupling energy ΔF_{μ}, also with the result (4.27) from the variational approach, we find that the inter-layer coupling is *irrelevant* in the thermodynamic limit:

$$\Delta F_{\mu} \;\sim\; -\mu T\left(R_{\parallel}/R_{l,2D}\right)^{-y/2} \;. \tag{4.30}$$

4.3 Variational Calculation

The above findings suggest the existence of a transition from a decoupled phase for small inter-layer couplings to an elastically coupled phase at a *non-zero* inter-layer coupling μ_c. For $\mu \uparrow \infty$, the system should be equivalent to the elastically coupled Bragg glass with a non-zero shear modulus and free of unbound dislocations. In an underlying RG analysis, we would expect a stable "glassy", "elastic" fixed point at $T = 0$ with a relevant interlayer-coupling $\mu(L) \uparrow \infty$ [Figure 4.2]. But we know from the above perturbative calculations that at small enough couplings the RG flow of the inter-layer coupling μ is in a different basin of attraction and flows to a "decoupled", "glassy" ($\tau > 0$) fixed point $\mu(L) \downarrow 0$ [Figure 4.2]. The above result $\mu(L) \downarrow 0$ (4.26, 4.30) is a signature of a *vanishing shear modulus* in the decoupled phase. The underlying physical mechanism for the downward-renormalization of the shear modulus is clearly the existence of plastic deformation mediated by unbound dislocation loops. The "elastic" and "decoupled" RG sinks must be separated by a phase transition at a critical non-zero inter-layer coupling μ_c.

We want to explore the outlined scenario by a variational calculation, where we determine an *effective shear modulus* $\widetilde{\mu}$. To this end, we define an elastic "trial" Hamiltonian $\mathcal{H}_{el}[\widetilde{\mu}]$ with an harmonic inter-layer coupling $V_{j,el}[\widetilde{\mu}] = \frac{1}{2}\widetilde{\mu}\phi^2$, where $\widetilde{\mu}$ is proportional to the shear modulus of the FL array. [Henceforth, we will set

$$p \equiv 1 \tag{4.31}$$

for simplicity.] To calculate an optimal shear modulus $\widetilde{\mu}$ with respect to the original Hamiltonian $\mathcal{H}[\mu]$ with the cos-coupling $V_j[\mu] = -\mu\cos(\phi)$ derived above (4.6), we use the

Jensen-inequality for the disorder-averaged free energies

$$\overline{F[\mu]} \;\leq\; F_{var} \;:=\; \overline{F[\widetilde{\mu}]} + \overline{\langle \mathcal{H}[\mu] - \mathcal{H}_{el}[\widetilde{\mu}]\rangle_{\widetilde{\mu}}} \tag{4.32}$$

[where $\overline{\langle \ldots \rangle}_{\widetilde{\mu}}$ means an average with the elastic trial Hamiltonian $\mathcal{H}_{el}[\widetilde{\mu}]$]. Minimizing the variational free energy F_{var} with respect to $\widetilde{\mu}$ gives the following self-consistency equation for $\widetilde{\mu}$, which establishes a relation $\widetilde{\mu} = \widetilde{\mu}(\mu)$ between the effective shear modulus $\widetilde{\mu}$ and the "bare" inter-layer coupling parameter μ:

$$\begin{aligned} 0 \;=\; \frac{\partial F_{var}}{\partial \widetilde{\mu}} \;&=\; -\frac{1}{2}\sum_j \int_{\mathbf{r}_\parallel} \overline{\left\langle (\mathcal{H}[\mu] - \mathcal{H}_{el}[\widetilde{\mu}]) \left((\phi_{j+1} - \phi_j)|^2_{\mathbf{r}_\parallel} \right) \right\rangle}_{\widetilde{\mu},\mathrm{conn}} \\ &\approx\; \frac{1}{2}\sum_{j,i} \int_{\mathbf{r}_\parallel} \int_{\tilde{\mathbf{r}}_\parallel} \overline{\left\langle \widetilde{\mu} - \mu \cos\left(\phi_{j+1} - \phi_j\right)|_{\mathbf{r}_\parallel} \right\rangle}_{\widetilde{\mu}} \times \\ &\qquad \times \overline{\left\langle \left((\phi_{j+1} - \phi_j)|^2_{\mathbf{r}_\parallel} \right) \left((\phi_{i+1} - \phi_i)|^2_{\tilde{\mathbf{r}}_\parallel} \right) \right\rangle}_{\widetilde{\mu},\mathrm{conn}} \end{aligned}$$

$$\Rightarrow \quad \widetilde{\mu} \;\approx\; \mu \overline{\langle \cos\left(\phi_{j+1} - \phi_j\right)\rangle}_{\widetilde{\mu}} \;\approx\; \mu \exp\left(-\frac{1}{2} \overline{\langle (\phi_{j+1} - \phi_j)^2 \rangle}_{\widetilde{\mu}} \right) . \tag{4.33}$$

In deriving the self-consistency equation we treated the combined disorder and thermal averages $\overline{\langle \ldots \rangle}_{\widetilde{\mu}}$ as approximately *Gaussian* and applied the Wick-theorem. Similarly, we employed in (4.33) a cumulant expansion on the cos-average and neglected higher-order cumulants. These approximations will be justified below.

The form of the elastic trial Hamiltonian induces some peculiarities for the mechanism of dislocation proliferation, which we have to comment on. To keep the following calculations tractable, we used a *single* variational parameter $\widetilde{\mu}$ characterizing the effective shear modulus. In particular, this means that the effective shear modulus in $V_{j,el}[\widetilde{\mu}]$ is *layer-independent*. This has the important consequence that a possible decoupling transition where $\widetilde{\mu}$ vanishes corresponds to a proliferation of dislocation loops in between *every* pair of neighbouring layers. Thus, at the transition, the distance between the unbound dislocations is the FL spacing $l_\perp$ perpendicular to the layers, and the variational Ansatz envisions a first-order "melting" scenario on the shortest scale $l_\perp$.

Let us now address the basis of our above assumption in deriving the self-consistency equation (4.33), namely that averages $\overline{\langle \ldots \rangle}_{\widetilde{\mu}}$ are to a good approximation Gaussian averages. To this end, we have to investigate in detail the behaviour of the connected correlations $\overline{\langle (\phi_{j+1} - \phi_j)^{2m} \rangle}_{\widetilde{\mu},\mathrm{conn}}$, i.e., thermodynamic averages in the disordered elastic layered FL array with a shear modulus given by $\widetilde{\mu}$. For the purpose of solving (4.33), we are interested in $m = 1$; to show that averages $\overline{\langle \ldots \rangle}_{\widetilde{\mu}}$ are to a good approximation Gaussian, we have to show that correlations with $m > 1$ are sufficiently small. Essentially, we expect

contributions from three sorts of fluctuations, which are closely related to the elastic and decoupled limits discussed in the previous section 4.2 [henceforth, we refer to the Larkin lengths of the elastic trial system depending on $\widetilde{\mu}$ as $\widetilde{R}_{l,3D} := R_{l,3D}[\widetilde{\mu}]$; note that $R_{l,2D}$ is *independent* of $\widetilde{\mu}$]:

(i) For large shear moduli $\widetilde{\mu}$, the system is on large length scales $R_\parallel > \widetilde{R}_{l,3D,\parallel}$ well described as a discretized version of the elastic uniaxial Bragg glass model in $d = 3$, discussed above as the elastic limit.

(ii) However, for small enough shear moduli, quasi-two-dimensional fluctuations start to dominate the averages. These fluctuations become available on scales $R_\perp \sim (\widetilde{\mu} l_\perp^2/K)^{1/2} R_\parallel \lesssim l_\perp$ and are for $R_\parallel > R_{l,2D}(\tau)$ essentially the large scale, disorder-induced fluctuations of the single layer Bragg glass in $d = 2$, i.e., the 2D RFXY model, which has been analyzed above as the decoupled limit $\widetilde{\mu} = 0$.

(iii) On length scales smaller than the Larkin lengths $\widetilde{R}_{l,3D}$, $R_{l,2D}$, the disorder can be treated as perturbation, and thermal fluctuations dominate [for $T > 0$, at $T = 0$ we get only disorder contributions, which can, however, be neglected on small scales beyond the Larkin length].

Note that we refer here always to the Larkin lengths of the elastic trial system with shear modulus $\widetilde{\mu}$. When studying equation (4.19), we discussed already in detail the validity of the Gaussian approximation for the averages contributing in (ii) when the layers can be regarded as decoupled. Furthermore, it is clear that the averages over the thermal fluctuations (iii) are Gaussian. For the elastic limit of the 3D Bragg glass encountered in (i), the combined disorder and thermal averages in (4.33) can be treated as approximately Gaussian in the variational treatment with an RSB Ansatz for the propagator because the propagator is approximated by a set of harmonic propagators leading directly to Gaussian averages. In the framework of an FRG in $4 - \epsilon$ dimensions for the 3D Bragg glass, the system is dominated by a $T = 0$ fixed point, where the fixed point disorder correlator is perturbative in $\epsilon = 4 - d$. The correlations $\overline{\langle(\phi_{j+1} - \phi_j)^{2m}\rangle}$ can be calculated by integrating their RG flow equation and evaluating them at the fixed point perturbatively, as done in Ref. [9] for $m = 1$. At the fixed point, the disorder correlator is perturbatively *quadratic* in ϕ, which leads immediately to an asymptotically *Gaussian* field theory, and the averages are approximately Gaussian also in the FRG treatment of the contributions (i). This result can be supplemented by a second argument based on the observation that at a $T = 0$ fixed point only diagrams with #internal lines = #vertices contribute because vertices in the FRG formalism are the disorder correlators carrying a factor T^{-2}, and each bare propagator carries a factor T^1. One can derive for the asymptotic fixed point form of the vertex, as obtained in Ref. [9], and for *connected* diagrams contributing to higher order ($m > 1$) correlations $\overline{\langle(\phi_{j+1} - \phi_j)^{2m}\rangle}$ the rule: #vertices $> m$. Thus, the higher order correlations

are of the order $\lesssim \mathcal{O}(\epsilon^m)$, i.e., can be neglected in a controlled manner in the framework of the FRG based on the ϵ-expansion.

To evaluate the right hand side of equation (4.33), we have to use the proper generalization of the 3D elastic trial Bragg glass propagator ((4.17) with $\widetilde{\mu}$) taking correctly into account the crossover to the decoupled limit (4.27 with $\widetilde{\mu}$) as $\widetilde{\mu} \downarrow 0$. In the framework of the variational RSB approach to the 3D Bragg glass [9], we obtain the following propagator for the correct interpolation to the decoupled limit:

$$\begin{aligned} G(\mathbf{k}_\parallel, k_\perp) &\approx \frac{1}{G_0^{-1}(k_\parallel, k_\perp)} \Bigg(1 + \frac{\tau + y/2}{1-\tau}\, \mathrm{f}_{2D}\left[\frac{R_{l,2D}(\tau) k_\parallel}{2\pi}\right] + \\ &\quad + \frac{2\pi^2 K \widetilde{\mu}^{1/2}}{\left(G_0^{-1}(k_\parallel, k_\perp)\right)^{1/2}}\, \mathrm{g}_{3D}\left[\frac{\widetilde{R}_{l,3D,\parallel}}{2\pi}\left(\frac{G_0^{-1}(k_\parallel, k_\perp)}{K}\right)^{1/2}\right] \Bigg) \\ G_0^{-1}(k_\parallel, k_\perp) &= K k_\parallel^2 + 2\widetilde{\mu}\left(1 - \cos\left(l_\perp k_\perp\right)\right) \ , \end{aligned} \tag{4.34}$$

where the functions f_{2D} (A.33) and g_{3D} (A.34) control the crossover from the asymptotic behaviour on scales exceeding the Larkin lengths to the perturbative regime on small scales. They are normalized to give $\mathrm{f}_{2D}[x], \mathrm{g}_{3D}[x] \simeq 1$ for $x \gg 1$ and essentially produce a cutoff at small length scales, where $\mathrm{f}_{2D}[x], \mathrm{g}_{3D}[x] \simeq 0$ for $x \ll 1$. The first term in the sum (4.34) represents contributions from thermal fluctuations (iii), the second term from the quasi-2D fluctuations of the disordered system (ii), described by the 2D RFXY model, and the third term from the elastic fluctuations of the 3D Bragg glass (i).

Using the expression (4.34), we have to solve the following self-consistency equation according to (4.33) to obtain the effective shear modulus $\widetilde{\mu}(\mu)$ as a function of the interlayer coupling μ:

$$0 = \frac{\partial F_{var}}{\partial \widetilde{\mu}} \propto \widetilde{\mu} - \mu\ \exp\left(-\frac{\mathrm{I}[\widetilde{\mu}]}{2}\right)$$

with

$$I[\widetilde{\mu}] = \int_{-\pi}^{\pi} \frac{d\varphi}{2\pi}\, 2(1-\cos(\varphi)) \int_0^{2\pi/l_\parallel} \frac{k\ dk}{2\pi}\, G\left(|\mathbf{k}_\parallel| = k,\ k_\perp l_\perp = \varphi\right) \ . \tag{4.35}$$

It is clear that the integral $I[\widetilde{\mu}]$ splits into three contributions from the corresponding terms in the propagator (4.34),

$$I[\widetilde{\mu}] \ = \ I^{th}[\widetilde{\mu}] + I_{2D}^{dis}[\widetilde{\mu}] + I_{3D}^{dis}[\widetilde{\mu}] \ . \tag{4.36}$$

As shown in the Appendix A.2, equation (4.35) has for $\widetilde{\mu} \uparrow \infty$ the strong coupling solution $\widetilde{\mu} \approx \mu$, where the FL array is dislocation-free and described by elasticity theory as discussed

above, section 4.2. Furthermore, $\widetilde{\mu} = 0$ is *always* a solution of the self-consistency equation, which is essentially mirroring the perturbative result presented in 4.2. Hence, the point of interest is whether coupled solutions of (4.35), similar to $\widetilde{\mu} \approx \mu \uparrow \infty$, can persist for *finite* inter-layer couplings μ, i.e., whether extrema of $F_{var}[\widetilde{\mu}]$ can be found, which have a smaller free energy $\Delta F_{var}[\widetilde{\mu}] = F_{var}[\widetilde{\mu}] - F_{var}[0] < 0$ than the decoupled solution $\widetilde{\mu} = 0$. When no other solutions of (4.35) exist, $\widetilde{\mu} = 0$ is the global minimum, and the system is effectively *decoupled*.

Whereas the details of the quite lengthy calculation for the solution of (4.35) are presented in Appendix A.2, let us comment here on the most important features and results. In (4.34), we used in the decoupled 2D limit the propagator (4.27) as it is obtained in the variational RSB approach for consistency, because the propagator used in the elastic 3D limit is the result of the same approach. However, quantitatively similar results are obtained when we use in the 2D limit the propagator (4.25) from the RG calculation. Thus, the lack of a consensus regarding the properties of the 2D RFXY model influences only weakly the outcome of our calculation. Before presenting the results derived in the Appendix A.2, let us give a more heuristic argument, which nevertheless captures the main features of the calculation and gives a qualitatively correct estimate of the critical value μ_c, below which the layers decouple.

From the self-consistency equation (4.33), it is clear that the effective shear modulus $\widetilde{\mu}$ is reduced most strongly by fluctuations with $\phi_{j+1} - \phi_j \sim \mathcal{O}(1)$, i.e., quasi-2D fluctuations on scales $R_\perp \lesssim l_\perp$ from the decoupled regime (ii), where neighbouring layers fluctuate independently. This is essentially due to the fact that the inter-layer coupling (4.5) is a "nearest-layer" interaction. Furthermore, we know from the work by Mikheev and Kolomeisky [65], that the disorder-free system is *always* unstable with respect to a small inter-layer coupling for $\tau > 0$ or $K > K_c$ [which is the physical parameter range of interest for a layered HTSC in a parallel field (see 4.15, 4.16)]: It exists a *second order* phase transition at $\mu_c = 0$ producing a scaling relation

$$\left(\frac{\mu l_\parallel^2}{4\pi^2 K}\right) \simeq C_{3D}^{dis} e^{-1+\tau} \left(\frac{\widetilde{\mu} l_\parallel^2}{4\pi^2 K}\right)^\tau \tag{4.37}$$

giving $\widetilde{\mu} = \widetilde{\mu}(\mu)$. For the disorder-free system, $C_{3D}^{dis} = 1$. Inclusion of 3D disorder fluctuations from the Bragg glass regime (i) does not change the phase transition qualitatively because the fluctuations between neighbouring layers $\phi_{j+1} - \phi_j$ are *finite*. Hence, the only modification compared to the disorder-free case is the *finite* factor $C_{3D}^{dis} = \exp(-I_{3D}^{dis}/2)$. It can be easily checked that $0 \leq I_{3D}^{dis} \leq I_{3D}^{dis}[\widetilde{\mu} \downarrow 0] = 4$, see (A.48), such that $1 \leq C_{3D}^{dis} \leq e^2$.

Therefore, only quasi-2D disorder fluctuations can change this picture qualitatively. As the perturbative calculation indicates (4.26, 4.30), they can indeed lead to a vanishing effective shear modulus $\widetilde{\mu} = 0$ for small μ (which is explicitly checked in the detailed calculation in the Appendix A.2), and the phase transition becomes *first order*. Below a

non-zero $\mu_c > 0$, the layers decouple, and the effective shear modulus drops from $\widetilde{\mu}(\mu_c) = \Delta\widetilde{\mu}$ to zero. To obtain an upper bound for the jump $\Delta\widetilde{\mu}$, let us consider for a moment exclusively quasi-2D fluctuations on the shortest scale perpendicular to the layers. For these fluctuations, the main effect of the elastic coupling to the neighbouring layer in the trial Hamiltonian is to produce effectively a mass-term $\widetilde{\mu}\phi_j^2$ for the single layer fluctuations described by the 2D RFXY model. This mass-term allows only for quasi-2D fluctuations on scales $R_\parallel \lesssim 2\pi\sqrt{K/\widetilde{\mu}}$. On the other hand, it is clear that on scales $R_\parallel \lesssim R_{l,2D}(\tau)$ smaller than the Larkin length, thermal fluctuations dominate and the disorder can be treated as perturbation; the 2D fluctuations are effectively disorder-free. However, as explained above (4.37), the disorder-free system is *always* coupled. It follows that a decoupling is possible only for couplings $\widetilde{\mu} \lesssim K(2\pi/R_{l,2D}(\tau))^2$ such that disordered quasi-2D fluctuation regime becomes accessible on scales $R_{l,2D}(\tau) \lesssim R_\parallel \lesssim 2\pi\sqrt{K/\widetilde{\mu}}$. Thus, we obtain as upper bound for the jump $\Delta\widetilde{\mu}$

$$\Delta\widetilde{\mu} \;\lesssim\; K\left(\frac{2\pi}{R_{l,2D}(\tau)}\right)^2 . \tag{4.38}$$

The first order transition occurs at a critical inter-layer coupling $\mu_c > 0$. Because for $\widetilde{\mu} \geq \Delta\widetilde{\mu}$, the system behaves effectively disorder-free regarding the quasi-2D fluctuations, we can essentially apply the above relation (4.37) for the disorder-free case to $\mu = \mu_c$ and $\widetilde{\mu}(\mu_c) = \Delta\widetilde{\mu}$. With $C_{3D}^{dis} \leq e^2$ in (4.37), this yields the following estimate for an upper bound for the critical inter-layer coupling in our variational approach:

$$\mu_c \;\lesssim\; eK\left(\frac{2\pi}{l_\parallel(R_{l,2D}(\tau)/l_\parallel)^\tau}\right)^2 \overset{(4.29)}{\simeq}\; eK\left(\frac{2\pi}{R_{l,2D}(T=0)}\right)^2 . \tag{4.39}$$

As it is shown in the Appendix A.2, where the variational calculation, i.e., the solution of the self-consistency equation (4.35) is performed, one finds indeed a *first order transition* at a critical interlayer coupling μ_c, below which the layers decouple. The decoupling manifests in a jump of the effective shear modulus $\widetilde{\mu}(\mu)$, that drops from the finite value $\Delta\widetilde{\mu} = \widetilde{\mu}(\mu_c) > 0$ to zero at the transition. In the Appendix A.2, μ_c and the jump $\Delta\widetilde{\mu}$ in the effective shear modulus are calculated in detail for the two limiting cases $T = 0$ (or $\tau = 1$) and $\tau \gtrapprox 0$ (see the above discussion and (4.16, 4.15)), which describe the dense and dilute limit, respectively, in the physical realization of a HTSC in a parallel field. In summary, the following results are found:

- The phase transition is turned into a *first order* transition by the inclusion of the quasi-2D disorder-induced fluctuations. This further supports the above outlined scenario that unbound dislocation loops with a distance $l_\perp$ of the layer spacing proliferate at the decoupling transition. The first order "melting" by unbound dislocations happens on the *shortest* scale $l_\perp$ in the direction perpendicular to the layers.

- The critical inter-layer coupling μ_c is found to be of the form

$$\begin{aligned} \mu_c &\approx \alpha K \left(\frac{2\pi}{R_{l,2D}(T=0)} \right)^2 \\ &\overset{4.28}{\approx} \frac{\alpha_c}{2\pi} \frac{g}{K} \ . \end{aligned} \tag{4.40}$$

  both for $T = 0$ and $\tau \gtrapprox 0$. The numerical factor α is only weakly temperature-dependent due to the fact that the decoupling is essentially disorder-driven. The slight increase of α with temperature mirrors the tendency of thermal fluctuations to decrease the effective shear modulus. The analytical and numerical results for α from (A.55, A.59) can be summarized to

	$\alpha(\mu_c)$	$\alpha(\mu_{c2})$
$T = 0$	0.7–1.0	0.8–1.1
$\tau \gtrapprox 0$	2.7	

(4.41)

  $\mu_{c2} > \mu_c$ is the critical inter-layer coupling where the solution of the self-consistency equation (4.35), which gives only the zeros of $\partial F_{var}/\partial\widetilde{\mu}$, becomes a thermodynamically stable, *absolute* minimum of the free energy. Note that all given values are in accordance with the upper bound (4.39) obtained above. Furthermore, α is only *weakly* temperature dependent.

- The jump $\Delta\widetilde{\mu}$ in the effective shear modulus is strongly depending on the temperature. Whereas we find for $T = 0$ that $\Delta\widetilde{\mu} \sim K/R^2_{l,2D}(T=0)$, the first order transition is much *weaker* for $\tau \gtrapprox 0$, where $\Delta\widetilde{\mu} \sim K/\tau R^2_{l,2D}(\tau)$, which is several orders of magnitude smaller than the $T = 0$ value (remember that $R_{l,2D}(\tau)/l_\parallel \simeq (R_{l,2D}(T = 0)/l_\parallel)^{1/\tau} \sim (K^2/gl^2_\parallel)^{1/2\tau}$). For $\tau \downarrow 0$, $\Delta\widetilde{\mu}$ vanishes, and the phase transition becomes second order: The phase boundary in the low-temperature phase terminates in a critical point at

$$\mu_c \ = \ eK \left(\frac{2\pi}{R_{l,2D}(T=0)} \right)^2 \ = \ (e/2\pi)g/K \quad , \quad \tau \ = \ 0 \tag{4.42}$$

  [Figure 4.2].

- For completeness, we remark that upon entering the high-temperature phase $\tau < 0$ or $K < K_c$ of the model, which is, however, not accessible in the physical realization under consideration, we also find a first order decoupling, that is induced by *thermal* fluctuations and happens below a much higher critical coupling $\mu_c \approx eK(2\pi/l_\parallel)^2$ [Figure 4.2]. It exhibits a jump $\Delta\widetilde{\mu} \sim |\tau|K/l^2_\parallel$.

Since variational calculations tend to underestimate fluctuations, we expect the actual value for α to be larger than the results (4.41) or the upper bound (4.39) gained from the variational calculation. This is connected to the above mentioned problem that we have only *one* variational parameter $\widetilde{\mu}$ in our Ansatz for the elastic trial Hamiltonian. Hence, it is impossible to capture features connected to fluctuations on more than *one* length scale, which are, however, typical for critical phenomena. Such systems are handled best by an RG approach, where a successive integration of fluctuations from the shortest to the largest scale is performed, and the interplay of fluctuations on different length scales is accounted for in the RG flow of the coupling constants of the Hamiltonian. The first order phase transition that we find in the variational calculation may be an artefact of our one-parameter approximation.

However, it is indeed possible to do an RG calculation along the line of the work of Cardy and Ostlund [18] for a model of *two* interacting planar FL arrays. The Hamiltonian is again given by (4.9), but with the layer-index running over $j = 1, 2$ only. The two-layer system is studied in detail in part II, chapter 11, where we find for small $\tau > 0$ a Kosterlitz-Thouless-like *second order* phase transition at an inter-layer coupling

$$\mu_c \;\approx\; \frac{1}{8\pi}\,\frac{g}{K}\;. \tag{4.43}$$

In the variational calculation, the disorder strength g enters essentially in form of the Larkin lengths, see Appendix A.2. To compare (4.43) to the results of the variational calculation, one has to use the results (A.20, A.21, A.18) of Appendix A.1.1, and finds $\mu_c \approx (\pi^2/2)K\,(2\pi/R_{l,2D}(T=0))^2$ corresponding to

$$\alpha \approx \frac{\pi^2}{2} \approx 4.9\;, \tag{4.44}$$

which is considerably higher than the values given in (4.41). Taking into account the discrepancies in the results (4.41, 4.44), it is reasonable (and sufficient) to work with the rough estimate $\alpha \approx \mathcal{O}(4)$ in the following.

These findings can be summarized in a criterion for the stability of the elastically coupled ($\widetilde{\mu} > 0$) Bragg glass phase in the layered geometry with uniaxial displacements, which takes on the form

$$\frac{\mu}{K} > \alpha \left(\frac{2\pi}{R_{l,2D}(T=0)}\right)^2 \overset{4.28}{\simeq} \alpha \frac{4\pi^2}{\bar{c}^2_{d=2}}\,\frac{g}{K^2} \tag{4.45}$$

with

$$\alpha \approx \mathcal{O}(4)\;. \tag{4.46}$$

The criterion (4.45) gives immediately a phase diagram in the μ/K-$1/K$-plane, as shown in Figure 4.2. The inverse elastic constant $1/K \propto T$ measures the temperature in units

of the elastic energy; remembering that $g \propto 1/T^2$ and $\mu \propto 1/T$, it is useful to consider the temperature independent coupling strength μ/K and to choose a fixed temperature independent disorder strength g/K^2, or equivalently a fixed Larkin length $R_{l,2D}(T=0)$. In Figure 4.2, we also show the phase diagram in the temperature independent quantities μ/K and g/K^2.

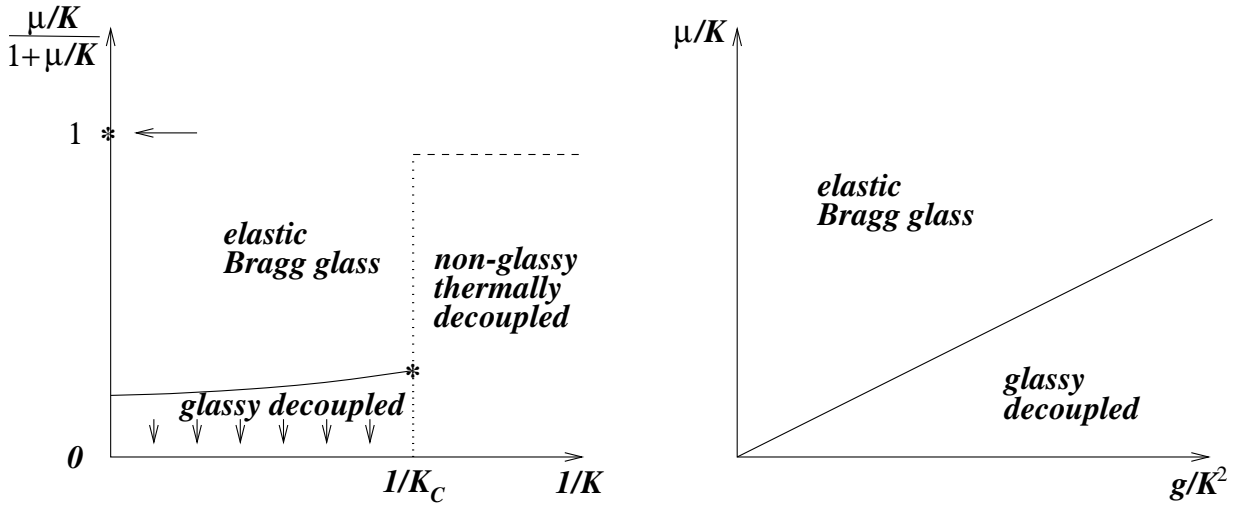

Figure 4.2: Left: Phase diagram in the μ/K-$1/K$-plane for fixed temperature independent disorder strength g/K^2, as obtained from the variational calculation; the arrows indicate the perturbative results from section 4.2 and the $T = 0$ fixed point found in the FRG calculation, see chapter 3. The solid line μ_c/K represents first order transitions from the glassy decoupled to the elastic Bragg glass phase in the low-temperature phase $K > K_c$ and terminates in a critical point (4.42) with a second order transition at K_c^{-1}. According to the results (4.41), the line μ_c/K slightly increases with temperature. The dashed line gives the first order decoupling transitions by thermal fluctuations in the high-temperature phase $K < K_c$. The nature of the transition from the glassy decoupled or Bragg glass phase to the thermally decoupled phase at $K = K_c$ (dotted line) has not been determined. Right: Phase diagram in the temperature independent quantities μ/K and g/K^2 (for $K > K_c$).

However, in the above form (4.45), this criterion is not very meaningful because it is formulated in terms of the in-plane Larkin length, and we know already that in the layered, uniaxial system the in-plane topological order is always preserved, and only the topological order *perpendicular* to the layers is destroyed in the decoupling transition. Hence, it is more meaningful to formulate (4.45) as

$$\begin{aligned} R_{l,3D,\perp} &\overset{(4.18)}{\simeq} \bar{c}_{d=3} \frac{K\mu}{g} l_\perp \\ &> c \cdot l_\perp \end{aligned} \tag{4.47}$$

with

$$\begin{aligned} c &\approx \alpha(4\pi^2 \bar{c}_{d=3}/\bar{c}_{d=2}^2) \;\simeq\; 4\pi\alpha \\ &\approx \mathcal{O}(50)\ . \end{aligned} \tag{4.48}$$

This criterion can be viewed as a disordered analog of the *Lindemann-criterion* [38], because it compares the positional correlation length R_l characterizing the strength of the disorder-induced fluctuations with the length scale of the FL spacing set by the ordered state of the lattice. c is a number playing a similar role as the Lindemann-number in the conventional Lindemann-criterion.

The Lindemann-like criterion (4.47) is the main result of the variational calculation in this chapter, which was devoted exclusively to a layered, uniaxial geometry realized in a HTSC in a parallel field. In the above form, the criterion can be readily generalized in a naive way to the experimentally more interesting situation of a HTSC in a field *perpendicular* to the layers where displacements have two components. However, the underlying variational calculation cannot be generalized, mainly due to the fact that one has to allow for dislocations with *three* possible orientations (or Burgers vectors) compared to *one* for uniaxial displacements (see (4.10)). The next chapter is devoted to scaling arguments which will give a criterion of the same form (4.47) (however, it is not possible to fix the numerical factor α in a scaling argument), but which can indeed be formulated for both uniaxial *and* "biaxial" displacements.

Chapter 5

Scaling Arguments

In this chapter, we explore the stability of the Bragg glass phase with respect to a spontaneous formation of large dislocation loops on scales exceeding the positional correlation length R_l by Imry-Ma-type scaling arguments. In a functional renormalization group (FRG) treatment, the Bragg glass phase is characterized by a $T=0$ fixed point, indicating that thermal fluctuations are irrelevant for the large scale properties. This means that the free energy is equal to the energy of a large dislocation loop, and the entropy gain of the dislocation loop by meandering does *not* lead to a free energy gain in the disordered system. In many disordered systems described by $T=0$ fixed points, Imry-Ma-type [71] arguments, in which the energy cost of a perturbation is compared to the energy gain from advantageous disorder fluctuations, have proven a powerful tool to test the stability of ordered phases. In this chapter we want to check the stability of the Bragg glass with respect to the formation of large unbound dislocation loops. Therefore, our "ordered" phase is the elastic dislocation-free Bragg glass phase, which is highly non-trivial in itself. It exhibits the typical features of a disordered, glassy system, characterized in the literature by catchwords like the existence of "many metastable states" [52] or "droplet excitations" [8], depending on the analytical approach to the problem. Both terms indicate that the behaviour of the disordered system is dominated by the low-lying excitations above a complex ground state and involves large scale fluctuations which are accompanied by diverging energy fluctuations. We expect large dislocations to enable such large scale fluctuations. This mechanism allows the dislocations to gain disorder energy because the FL array can adapt a more optimal configuration on scales exceeding the positional correlation length R_l. If the gain in disorder energy can compensate for the elastic energy cost, that is accumulated on the small scales $\lesssim R_l$ due to the elastic deformation around the core of the dislocation, unbound dislocations will proliferate. The difficulty of the issue is caused by the limited knowledge about the statistics of the low-lying excitations of the Bragg glass and the existence of non-trivial pre-asymptotic regimes, the random force (RF) regime and the random manifold (RM) regime, which have to be taken into account in a

realistic model as we have seen in chapter 3.

We will consider only *single* large dislocations or allow for dislocations only in a *single* plane of the FL array. This should be sufficient to detect the *onset* of an instability or the locus of a *second order* phase transition. However, it may be possible (as it is seen for example in the variational calculation presented in the preceding chapter 4 or for the disorder-free case discussed in chapter 2) that a *first order* transition is favorable, where we have to consider *many* dislocation loops at the transition point. Such first order transition scenarios will not be considered in this chapter though the results turn out to be in agreement with our findings from the variational calculation. In particular, the stability condition for the Bragg glass can be casted again in the form of a Lindemann-like criterion (4.47) obtained already by the variational calculation. In the last part of this chapter we show again by a scaling argument that this Lindemann-like criterion is in fact equivalent to the Lindemann criterion in its conventional form $u^2(l) < c_L^2 l^2$, where $u^2(l)$ is the (disorder-averaged) mean square displacement of the FLs on the *shortest scale*, and c_L is the Lindemann-number. This will provide us with a possibility to check "a posteriori" the value for c (4.48) obtained in the variational calculation.

5.1 The Layered, Uniaxial Model

Before discussing the experimentally more common situation of a HTSC in a perpendicular field with two-component displacements of the FLs, we want to begin with a scaling argument for the uniaxial system introduced in the preceding chapter with the Hamiltonian (4.9). We want to investigate the possibility of a spontaneous formation of dislocation loops in a *single* plane. For this purpose, we cut the system into two halves, within which the system is elastically coupled, and allow dislocation loops to form in the contact plane, say between the j_0^{th} and $(j_0+1)^{\text{th}}$ FL layer. Analytically, this can be implemented by considering in the Hamiltonian (4.9) an inter-layer coupling

$$V_j[\phi] \;=\; \begin{cases} \frac{1}{2}\mu\phi^2 & j \neq j_0 \\ -\mu' \cos(\phi) & j = j_0 \;, \end{cases} \tag{5.1}$$

which is elastic except for the one layer. We are interested in the behaviour for *finite* $\mu \approx \mu'$, however it is useful to discuss arbitrary values of μ' first.

If the two halves of the system are decoupled for $\mu' = 0$, the configuration of the flux array in each half is *individually optimized*, and each of them forms a Bragg glass because couplings for $j \neq j_0$ are *elastic*. The properties of the Bragg glass have been discussed in some detail in chapter 3, and for this particular layered geometry in 4.2, where we considered an elastic coupling (4.11), exactly of the above form (5.1) with $j \neq j_0$, that applies to each of the half-systems. Let us shortly recapitulate these results and consider

in addition free energy fluctuations, which will be particularly important for the Imry-Ma argument. For the following, it is useful to rescale the perpendicular coordinate and to go over to the standard continuum description to obtain a three-dimensional isotropic elastic part of the Hamiltonian. This is achieved by the transformation

$$r'_\perp = r_\perp(\mu/K)^{1/2} = (j \cdot l_\perp)(\mu/K)^{1/2} \ , \tag{5.2}$$

leading to a Hamiltonian[1]

$$\beta\mathcal{H}[\{\phi_j\}] \ = \ \int d^3\mathbf{r}\left\{\frac{1}{2}\gamma(\boldsymbol{\nabla}\phi)^2 + W[\mathbf{r},\phi(\mathbf{r})]\right\} \tag{5.3}$$

with an effective isotropic elastic constant $\gamma = (\mu K)^{1/2}$ and a random potential

$$\overline{W[\mathbf{r},\phi]W[\mathbf{r}',\phi']} = 2g_{3D} \ \cos(\phi-\phi') \ \delta^3(\mathbf{r}-\mathbf{r}') \tag{5.4}$$

with

$$g_{3D} = g(\mu/K)^{1/2} \ . \tag{5.5}$$

Note that under this rescaling also the positional correlation lengths (or Larkin lengths) become isotropic (see (4.18))

$$R_l = R_\xi \ := \ R_{l,3D,\parallel} \ = \ R'_{l,3D,\perp} \ \sim \ \frac{K\mu}{g_{3D}} \ \sim \ \frac{K^{3/2}\mu^{1/2}}{g} \ . \tag{5.6}$$

As discussed already in chapter 3, the three-dimensional uniaxial isotropic Bragg glass (5.3) has logarithmic correlations (3.40)

$$\overline{\langle(\phi(\mathbf{r})-\phi(\mathbf{r}'))^2\rangle} \ = \ 2A\ln\left(\frac{|\mathbf{r}-\mathbf{r}'|}{R_l}\right) \ , \tag{5.7}$$

where A is a numerical constant of order unity. A variational calculation with RSB yields a value $A = 1$, slightly smaller than the result from the FRG, $A = \pi^2/9$ [9], due to the fact that variational calculations tend to underestimate fluctuations. In Fourier-space, the logarithmic divergence corresponds to a k^{-d}-divergence of the propagator, and in $d = 3$ we have (see also (4.17))

$$\begin{aligned} \overline{\langle\phi(\mathbf{k})\phi(\mathbf{k}')\rangle} \ &= \ (2\pi)^3\delta^3(\mathbf{k}+\mathbf{k}') \ G_{3D}(\mathbf{k}) \\ G_{3D}(\mathbf{k}) \ &\simeq \ 2\pi^2 \ A \ \frac{1}{k^3} \ . \end{aligned} \tag{5.8}$$

[1]The additional random bond term associated with the random field $\mathbf{w}$ is irrelevant in 3 dimensions [9].

The logarithmic fluctuation in displacement causes an anomalously large elastic energy cost of the order

$$\begin{aligned} \int_L d^3\mathbf{r} \frac{\gamma}{2} \overline{\langle (\boldsymbol{\nabla}\phi)^2 \rangle} &\simeq \frac{\gamma}{2} \sum_{\mathbf{k}} k^2 G_{3D}(\mathbf{k}) \\ &\sim \gamma A L \end{aligned} \tag{5.9}$$

in an (isotropic) volume of the order L^3. This energy is compensated by the disorder energy gained from the anomalous displacement of the flux array. Thus

$$\Delta E \sim \gamma L \tag{5.10}$$

gives the order of variation in free energy for configurations of the field *phi* which differ by $\mathcal{O}(\sqrt{\log(L/R_l)})$. Note that this expression is *independent* of the disorder strength g. However, one has to be careful in identifying this as the order of the sample-to-sample free energy fluctuation of the Bragg glass, as one would naively do following standard scaling arguments in the theory of elastic manifolds [52]. These arguments are based on the assumption that the manifold "sees" a *completely* different, statistically independent disorder configuration when it undergoes at a given point larger fluctuations in the displacement than the typical ones, that are logarithmic in our case. But this *cannot* be the case for the Bragg glass due to the discrete translational symmetry under $\phi \mapsto \phi + 2\pi$ of the Hamiltonian (5.3) with (5.4), which is just the defining property of the Bragg glass, where the symmetry of the FL lattice is retained, see chapter 3. Rather (5.10) gives the typical free energy fluctuations *within* a sample. The fluctuations between *different* samples should be much larger, probably scaling with the square-root of the volume, i.e., an exponent $\theta = 3/2$.

So far we have considered the limit $\mu' = 0$, where the two half-systems are decoupled, each of them individually optimized and in a Bragg glass phase. Now, let us compare the free energy difference between the completely coupled and completely decoupled limit. When we tie the two halves together by letting $\mu' \uparrow \infty$, then the constraint across the contact plane forces a *complete* re-optimization of the flux array, resulting in a *higher* free energy for each half. The constraint effectively leads to a change in the boundary condition $\phi_{j_0}(\mathbf{r}_\parallel)$ of the half-systems by an amount which is given by the typical size of the displacement fluctuation in the unconstrained system. According to (5.7), this is $\mathcal{O}(\sqrt{\log(L/R_l)})$. Therefore, the typical free energy increase in each half due to the constraint is given by $\Delta E \sim \gamma L$ (5.10).

The scaling argument is based on the observation that the process of the re-optimization upon lifting the constraint at the contact plane, i.e., decoupling the two half-systems is closely related to the formation of dislocation loops. This relation can be made clear in a very pictorial way: The change in the optimal configuration of each half system

resulting from the removal of the constraint at j_0 can be described by a collection of "vortex sheets", such as the one depicted in Figure 5.1. A dislocation loop, which describes phase mismatches across the contact plane, is just the boundary of a vortex sheet at the contact plane. It is possible to estimate the number of generated "sheets" N_{sheet} in a typical rearrangement of the half system. Since the order of the difference in the boundary condition $\phi_{j_0}(\mathbf{r}_\parallel)$ is $\mathcal{O}(\sqrt{\log(L/R_l)})$, i.e., logarithmically growing with the system size, a likely scenario for the vortex sheet structure is to have at the contact plane one *statistically independent* vortex sheet terminating at each scale $R_l, 2R_l, 4R_l, \ldots$ up to L. This yields $N_{sheet} = \log_2(L/R_l)$, which is only logarithmically growing with system size.

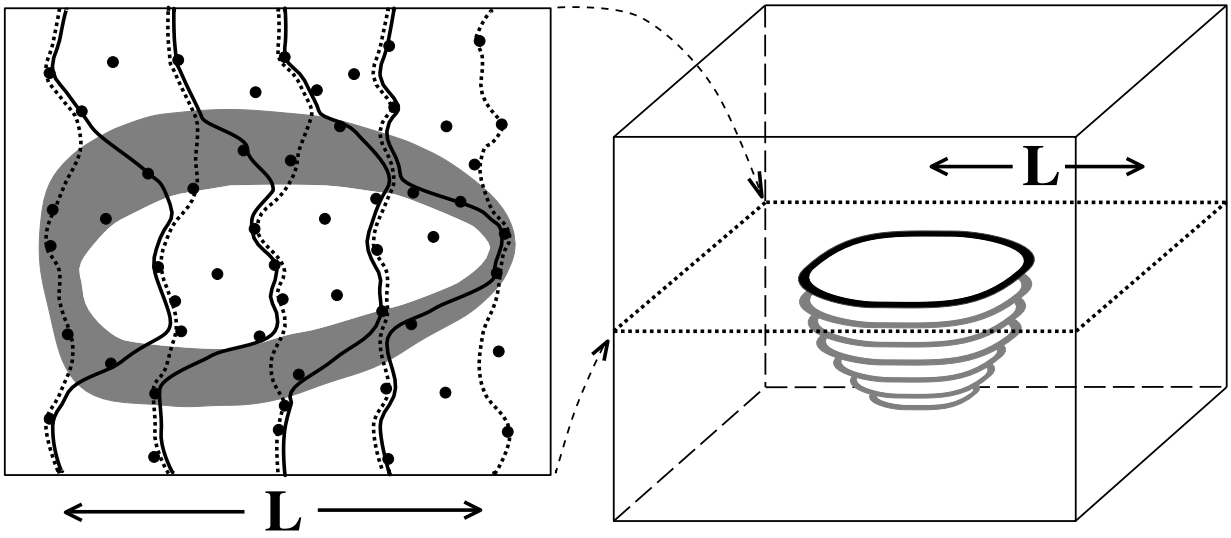

Figure 5.1: Left: The elastic rearrangement of each planar flux array can be represented by a number of vortex *loops* (shaded region). Right: Aligned vortex loops in successive layers form a vortex *sheet*. The boundary of the sheet (dark loop on top) is a *dislocation loop*.

The argument above thus shows that the disorder energy gained from the *proliferation* of dislocations loops at the contact plane, resulting in a *complete* decoupling, is ΔE. The disorder energy *gained* from the formation of a *single* dislocation loop of size L_{loop} is just the energy gained from the formation of a vortex sheet E_{sheet}, resulting from the *elastic deformation* of the half-system [Figure 5.1]. E_{sheet} clearly cannot exceed $\Delta E \sim \gamma L_{loop}$, which is the disorder energy gained from *complete* optimal elastic rearrangement of the half-system at the scale L_{loop}. Consequently, the disorder energy gained from the formation

of a single dislocation loop is $E_{dis} \lesssim \Delta E$. Assuming scaling of this energy,

$$E_{dis} \sim \gamma' L_{loop}^{\omega} \ , \tag{5.11}$$

it follows that $\omega \leq 1$.

On the other hand, the creation of dislocation loops at the contact plane is associated with an interaction energy cost for finite μ' due to the resulting phase mismatch. For the moment, let us start from the decoupled situation, where many dislocations are present at the contact plane. To find whether or not the two half systems actually couple for a given finite μ', it is necessary to balance the cost in disorder energy due to coupling with the *reduction* in interaction energy ΔE_{int} due to phase matching. The latter can be readily computed for small μ' perturbatively using (5.7). One finds for the contact plane of size L^2

$$\begin{aligned} \Delta E_{int} &= \mu' \int_L d^2\mathbf{r}_\parallel \overline{\langle \cos\left(\phi_{j_0+1} - \phi_{j_0}\right)\rangle} \\ &\simeq \mu' \int_L d^2\mathbf{r}_\parallel \exp\left(\overline{\langle \left(\phi_{j_0+1} - \phi_{j_0}\right)^2\rangle}_{\mu'=0}\right) \\ &\sim \mu' R_l^A L^{2-A} \ , \end{aligned} \tag{5.12}$$

where we used in the cumulant expansion again the property that the combined disorder and thermal averages with the Bragg glass Hamiltonian are approximately Gaussian (see the discussion in section 4.3). Since $A \geq 1$ [9], we obtain $\Delta E_{int} \lesssim L$. As the disorder energy cost due to coupling, $\Delta E \sim \gamma L$ (5.10), exceeds the interaction energy to be gained at small μ' and large L, the two half systems will remain decoupled.

In the large (but finite) μ' limit of interest, the perturbative result is no longer valid. Since the energy cost of phase mismatch is large there, we consider the stability of a *single* optimally-configured dislocation loop of extent $L_{loop} \gg R_l$ at the contact plane of the two half systems that are otherwise elastically coupled . The energy cost of the core of the dislocation loop due to the inter-layer interaction is extensive. For a stretched circular loop of linear size L_{loop}, we expect

$$E_{core} \sim \mu' R_l L_{loop} \ . \tag{5.13}$$

Here, the Larkin length R_l appears as "thickness" of the loop because the flux array is elastically coupled at smaller scales. The distortions of order $l_\parallel/2$ or phase-mismatches of order π in the very core of the dislocation cannot be screened on scales smaller than R_l, since this is the length scale upon which typical displacement differences become of the order $l_\parallel$: $\overline{\langle (u(R_l) - u(0))^2\rangle} \sim l_\parallel^2$ (3.33).

More generally, if we allow the dislocation loop to take on fractal shapes, say with the total loop length scaling as L_{loop}^D for $L_{loop} \gg R_l$ ($D \geq 1$ being the fractal dimension), then the core energy becomes

$$E_{core} \sim \mu' R_l^{2-D} L_{loop}^D \ . \tag{5.14}$$

[This expression has a similar structure as the result (5.12), but a quite different meaning: (5.14) is the *cost* in interaction energy due to the phase-mismatch of a *single* dislocation loop with respect to the situation, where both halves are tied together ($\mu' \uparrow \infty$), whereas (5.12) is the *gain* in interaction energy due to phase-matching with respect to the decoupled situation ($\mu' = 0$) when *many* dislocations are present.]

The existence or not of dislocation loops can now be determined by comparing the core energy (5.14) with the gain in disorder energy (5.11), $E_{dis} \sim \gamma' L_{loop}^{\omega}$. The value of the exponent ω depends on the structure of the dislocation loop that we allow, i.e., on the fractal dimension D: $\omega = \omega(D)$. We expect that the upper bound $\omega(D) \leq 1$, set by the disorder energy gain in a *complete* rearrangement at the contact plane when the coupling at the contact plane is changed from $\mu' \uparrow \infty$ to $\mu' = 0$, may only be reached if the structure of the associated vortex sheet is similar to those that arise in a complete rearrangement. This amounts to assuming that $\omega(D)$ is monotonously increasing with D. As explained above, we expect also in a complete rearrangement only *one* loop to form at each scale $R_l, 2R_l, 4R_l, \ldots$ up to L; assuming that the largest loop of size $L_{loop} \sim L$ dominates the large scale properties, it is plausible that it is not so much the *number* of loops (as one could naively expect) as rather the *structure* of the loops that may cause $\omega < 1$ to be smaller than the upper bound. The structure of the loop for a complete rearrangement can be deduced as follows: Denote the difference in the configuration before and after the change in μ' by $\varphi(\mathbf{r})$. The vortex sheets are then the equal-φ contours of $\varphi(\mathbf{r})$, and the associated dislocation loops are the contours of $\varphi(\mathbf{r}_\parallel, r_\perp = j_0 l_\perp)$ at the contact plane. The relationship between a rough "landscape" and the fractal geometry of its contours has recently been examined [72]. The φ-landscape is expected to be logarithmically rough since the typical size of the displacement fluctuation in the unconstrained system is logarithmic according to (5.7). For such a logarithmically rough φ-landscape an exact calculation yields $D = 3/2$ [73, 72]. Thus we have $\omega(D = 3/2) = 1$. Let us summarize our knowledge about the exponent ω:

$$\begin{aligned} \omega = \omega(D) &\leq 1 \\ \omega(D) & \quad \text{monotonously increasing with } D \\ \omega(D = 3/2) &= 1 \end{aligned} \tag{5.15}$$

This leads to the conclusions

$$\begin{aligned} \omega(D) < D & \qquad \text{for } D > 1 \\ \omega(D = 1) \leq D = 1 & \qquad \text{for } D = 1 \end{aligned} \tag{5.16}$$

about $\omega(D)$. The total energy of the dislocation loop [remember that the system is at a $T = 0$ fixed point and the free energy equal to the energy]

$$F_{loop} \;=\; E_{loop} \;=\; E_{core} - E_{dis} \;\sim\; \mu' R_l^{2-D} L_{loop}^{D} - \gamma' L_{loop}^{\omega(D)} \tag{5.17}$$

does not admit a stable solution with $L_{loop} \gg R_l$ for large $\mu' \approx \mu$ for $D > 1$ due to the results (5.16). Hence the Bragg glass is *stable* to the spontaneous formation and proliferation of large *fractal* dislocation loops due to the anomalously large core energies. However, though from the above analysis it is tempting to assume that also $\omega(D = 1) < 1$, we find that for a *stretched* dislocation (i.e., $D = 1$) we may well be in a *marginal* situation with $\omega = D = 1$ and both energies scaling in the same way $\sim L_{loop}$. It follows that dislocation loops will be *non-fractal* if they occur, and *stretched* loops with $\omega = D = 1$ are the preferred "channel" of any instability to dislocation loop formation. In investigating the stability of the Bragg glass with respect to large non-fractal, stretched dislocation loops, we consider this "worst case" with $\omega = D = 1$ in the following, which is the marginal case so that the behaviour of the prefactors has to be studied further.

Assuming $\mu' \approx \mu$ and $\gamma' \approx \gamma$ for $\omega(D = 1) = D = 1$, we obtain from the prefactors (which can be specified up to numerical factors) in F_{loop} (5.17) the stability criterion

$$\begin{aligned} E_{core} &> E_{dis} \\ \mu R_l &> c \cdot \gamma \end{aligned} \tag{5.18}$$

for the Bragg glass, where c is a numerical prefactor, the determination of which is beyond the scope of the scaling argument. Using (4.18, 5.6), this can again be reformulated in terms of the more meaningful length scales perpendicular to the layers as

$$R_{l,3D,\perp} \sim \frac{K\mu}{g} l_\perp \; > \; c \cdot l_\perp \; . \tag{5.19}$$

This criterion is exactly of the same form as the Lindemann-like criterion (4.47) found by means of the variational calculation in the previous chapter, where we were able to give an estimate $c \approx \mathcal{O}(50)$ (4.48) for the numerical prefactor.

Though the underlying picture for the topological transition is quite different, we obtain a Lindemann-like criterion of the same form. In the scaling approach for a *single* large dislocation loop we have a second order transition in mind whereas in the variational calculation the decrease of the effective shear modulus is dominated by fluctuations on the shortest scale $l_\perp$ perpendicular to the layers such that *many* loops with a perpendicular distance $\sim l_\perp$ are expected to proliferate in a first order transition. At this point, we cannot give a definite answer which scenario is more likely. For the applications, i.e., the calculation of a phase diagram in the next chapter 6, the question of the nature of the topological transition is important but not necessary to know. The situation is somewhat analogous to the role the usual phenomenological Lindemann criterion plays in describing the melting transition of the disorder-free FL lattice: It is a a powerful and simple phenomenological tool to determine the melting line but can give *no* information about the order of the melting transition. But it has to be emphasized that the Lindemann-like criterium (4.47, 5.19) has been *derived* by two different approaches whereas there exists *no* underlying theory for the usual phenomenological Lindemann criterion.

5.2 Scaling Approach to Realistic Models

So far we considered only the model (4.9) for the layered geometry of a HTSC in a parallel field. Clearly, this model has the two main limitations

- displacements are uniaxial,
- dislocation loops occur only in planes parallel to the vortex layers,

in comparison to the usual experimental situation of the magnetic field perpendicular to the layers leading to a two-component system, where dislocation loops can occur with three different orientations in the hexagonal Abrikosov lattice. In addition, the existence of a RM regime has so far not been considered in our model based on the Bragg glass approximation (see the discussion in chapter 3).

As for the first point, we expect the difference between one- and two-component displacements to be analogous to the difference between scalar and vector charges in a Coulomb gas representation of the dislocations. This is the three-dimensional analog to the the well-known difference in two dimensions between vortices in the XY-model (one-component spin-angle) and dislocations in a two-dimensional crystal (two-component displacements), where both of the systems can be mapped onto Coulomb gases; the XY model is described by scalar charges and a two-dimensional crystal with hexagonal symmetry by vector charges with the three possible orientations of the elementary Burgers vectors of the dislocations [35]. For the two-dimensional analog, we know that the critical behaviour is the same for scalar and vector charges. Thus, we expect also the scaling of the relevant energy scales of a dislocation loop, E_{dis} and E_{core}, to be unchanged for two-component displacements.

Regarding the second point, also for two-component displacements, a dislocation loop *always* has to lie within a single plane spanned by its Burgers vector and the applied field [31], see (2.1) and the discussion in chapter 2, if we exclude vacancies and interstitials [32].

Therefore, the scaling argument we presented for the layered system can essentially also be applied to study the stability of the Bragg glass in the more common experimental situation of flux lines perpendicular to the CuO planes. A naive generalization of our results to the isotropic system yields $R_l > c \cdot l$, where we expect a larger numerical factor c compared to the uniaxial case, since the two-component system is less stable: $c \gtrapprox \mathcal{O}(50)$.

Nevertheless, it is useful to reformulate a few aspects of the scaling argument for the uniaxial system to allow also the inclusion of the RM regime in our argumentation. This turns out to be crucial to make contact to experiments as we want to in the next chapter 6. The scaling relations for the energy gain E_{dis} from the disorder and the core energy cost E_{core} in the most relevant case of a large stretched, non-fractal (i.e. $D = 1$) dislocation

loop of size $L_{loop} \gg R_l$ are: $E_{dis} \sim \gamma L_{loop}$ (5.11) and $E_{core} \sim \mu R_l L_{loop}$ (5.13), where we consider again the most favorable case $\omega = D = 1$ for dislocation loop formation, and $\mu' \approx \mu$, $\gamma' \approx \gamma$. We gained these relations by inspecting a rearrangement of the FL array induced by the removal of the elastic coupling between a single pair of layers. On the other hand, we can interpret them also in the following slightly different way, not making explicitly use of the layered geometry.

Consider a typical configuration of the dislocation-free elastic Bragg glass phase, and add a large, stretched dislocation loop of extent L_{loop}. In the Bragg glass regime on scales $R > R_l$, the dislocation loop allows to gain disorder energy by a partial re-optimization of the configuration of the FL array. If the formation of a *single* loop leads to the full energy gain comparable to the fluctuations in the free energy for changes in displacements by $\mathcal{O}(\sqrt{\log(L_{loop}/R_l)})$ as in a typical rearrangement, we obtain $E_{dis} \sim \Delta E \sim \gamma L_{loop}$ (5.11). These anomalously large energy fluctuations are only possible in the Bragg glass regime on scales $R > R_l$. On the other hand, taking a configuration optimal with respect to variations on scales $R > R_l$ leads to a non-optimal configuration on scales $R < R_l$ and hence an energy cost in a dislocation-core of extent R_l. On these length scales, the FL array is described by the RF regime in the Bragg glass model as discussed in chapter 3. Displacements scale with a roughness exponent $\zeta_{RF} = 1/2$ (3.24) in $d = 3$. The core of the dislocation forms around the actual topological defect with displacement-gradients of order unity. We denote the radial coordinate in the direction transversal to the dislocation line with ρ and take the topological defect to be at $\rho = 0$ with $u(\rho = l_\parallel) \sim b = l_\parallel$. Now, we assume that the distortion in the core of the dislocation, at $\rho = 0$, "propagates" with the k^{-4}-divergent propagator of the RF regime up to $\rho = R_l$. This amounts to applying the scaling relation for displacements in the RF regime $\overline{\langle(\mathbf{u}(\mathbf{r}) - \mathbf{u}(0))^2\rangle} \sim r^{2\zeta_{RF}}$ to the core region $\rho < R_l$, and we obtain

$$\overline{\langle u^2(\rho < R_l)\rangle} \simeq b^2 \left(\frac{R}{l_\parallel}\right)^{2\zeta_{RF}} \quad . \tag{5.20}$$

Then, we can evaluate E_{core} for $\zeta_{RF} = 1/2$ in $d = 3$:

$$E_{core} \;\sim\; \gamma \left(\frac{2\pi}{l_\parallel}\right)^2 \int_0^{L_{loop}} ds \int_0^{R_l} d^2\rho \overline{\langle(\boldsymbol{\nabla} u)^2\rangle} \;\sim\; \gamma R_l L_{loop} \;, \tag{5.21}$$

which is just (5.13). Via (5.18), we obtain again the criterion (5.19).

In this form, the scaling argument can be readily generalized to the usual two-component system with the magnetic field perpendicular to the layers and described by a Hamiltonian $\mathcal{H}[\mathbf{u}] = \mathcal{H}_{el}^{3D}[\mathbf{u}] + \mathcal{H}_{d}^{3D}[\mathbf{u}]$ as discussed in chapter 3 with the elastic Hamiltonian

(3.7)

$$\mathcal{H}_{el}^{3D}[\mathbf{u}] \;\approx\; \frac{1}{2}\int_{BZ}\frac{d^2\mathbf{K}}{(2\pi)^2}\int\frac{dk_z}{2\pi}\;\Big\{c_{66}\;\left[K^2|u_T(\mathbf{K},k_z)|^2\right]+ \\ \hat{c}_{44}(1+K^2\tilde{\lambda}_c^2)^{-1}\;\left[k_z^2|u_T(\mathbf{K},k_z)|^2\right]\Big\} \tag{5.22}$$

and a disorder part (3.16)

$$\mathcal{H}_{d}^{3D}[\mathbf{u}] \;=\; \sum_{\boldsymbol{\nu}}\int dz\; v(\mathbf{R}_{\boldsymbol{\nu}}+\mathbf{u}_{\boldsymbol{\nu}}(z),z)\;, \tag{5.23}$$

modeling the interaction of the FLs with the pinning potential $v(\mathbf{r})$ generated by the point defects. The typical "aspect ratio" of a large dislocation loop of longitudinal length $L_{loop} \gg L_l$ and transversal length $R_{loop} \gg R_l$ is given by $L_{loop} \sim (\hat{c}_{44}/c_{66})^{1/2}R_{loop}$ in the non-dispersive long-wavelength limit, see (3.8). The longitudinal pieces of the dislocations are *edge* dislocations, the elastic energy of which is determined essentially by the tilt modulus c_{44}, and the transversal parts are *screw* dislocations, which couple to the shear modulus c_{66}. Again, it is convenient to go over to an *isotropic* Bragg glass by a rescaling

$$\begin{aligned} k_z' &= k_z(\hat{c}_{44}/c_{66})^{1/2} \\ L' &= L(\hat{c}_{44}/c_{66})^{-1/2} \;\sim\; R\;. \end{aligned} \tag{5.24}$$

Typical dislocation loops are isotropic then and of size R_{loop}, and the elastic part of the Hamiltonian is characterized again by one elastic constant γ, which is $\gamma = (\hat{c}_{44}c_{66})^{1/2}$ in the long-wavelength limit. Also for two-component displacements, we find logarithmic correlations (3.40) for the three-dimensional isotropic Bragg glass

$$\overline{\langle(u(\mathbf{r})-u(\mathbf{r}'))^2\rangle} \;=\; \frac{4A}{K_0^2}\ln\left(\frac{|\mathbf{r}-\mathbf{r}'|}{R_l}\right) \tag{5.25}$$

or a k^{-d}-divergence of the propagator in Fourier-space. By arguments analogous to the ones presented above, this leads to the result

$$E_{dis} \;\sim\; \Delta E \;\sim\; \gamma l^2 R_{loop} \;\sim\; (\hat{c}_{44}c_{66})^{1/2}l^2R_{loop} \tag{5.26}$$

for the scaling of the *gain* in disorder energy of the dislocation loops of size L', which can be achieved by a more optimal adjustment to the disorder on scales exceeding R_l. Following exactly the above given argumentation, we argue that this leads to non-optimal configurations on small scales $R < R_l$ and hence an energy cost in the core region. To tackle realistic models of superconductors with the scaling argument, we have to take into account the existence of the RM regime on scales $R < R_l$, as it was discussed in chapter 3 in detail. In evaluating the cost, we concentrate on the case of *single vortex pinning* in the

RF regime, where the pinning is strong such that the single vortex Larkin length $L_\xi^s \lesssim L^*$ is smaller than the FL-interaction-induced length scale L^*. This is the generic situation in extreme high-T_c materials like the Bi-compounds, as we will see in the next chapter 6. For single vortex pinning, we have a "collective RM regime" with $d = 3$ and $n = 2$ on scales $l \lesssim R \lesssim R_l$, i.e., on the relevant scales for fluctuations in the dislocation core. Therefore, in order to estimate the core energy, we have to use the scaling relation (3.31)

$$\overline{\langle u^2 \rangle}(R) \;\sim\; \left(R^2 + \tilde{\lambda}_c^2 \right)^{\zeta} \tag{5.27}$$

for displacements in the collective RM regime with the roughness exponent (3.32)

$$\zeta := \zeta(d = 3, n = 2) \approx 1/5 \; . \tag{5.28}$$

In (5.27), the additional scale $\tilde{\lambda}_c$ (3.5) for the onset of non-local effects occurs due to the *dispersion* of the tilt modulus $c_{44} = c_{44}[K]$ (3.4). Using the scaling relation (5.27) together with $u(\rho = l) \sim b = l$, we obtain for the typical displacements in the core region $\rho < R_l$ and the core energy E_{core} analogously to the results (5.20, 5.21):

$$\overline{\langle u^2(\rho < R_l) \rangle} \;\simeq\; b^2 \left(\frac{\rho^2 + \tilde{\lambda}_c^2}{l^2 + \tilde{\lambda}_c^2} \right)^{\zeta} \tag{5.29}$$

$$\begin{aligned} E_{core} \;&\sim\; \gamma b^2 \int_0^{R_{loop}} ds \int_0^{R_l} d^2\rho \, \overline{\langle (\boldsymbol{\nabla} u)^2 \rangle} \\ &\sim\; (\hat{c}_{44} c_{66})^{1/2} l^2 \left(\frac{R_l^2}{l^2 + \tilde{\lambda}_c^2} \right)^{\zeta} R_{loop} \; , \end{aligned} \tag{5.30}$$

where we anticipated that $R_l \gg \tilde{\lambda}_c$ (see chapter 6). We find thus a *reduction* in the dislocation loop core energy due to the existence of the collective RM regime with the smaller roughness exponent $\zeta \approx 1/5$ (3.32) compared to the RF regime. Comparing E_{core} (5.30) and E_{dis} (5.26), we obtain a stability criterion

$$\begin{aligned} E_{core} \;\sim\; (\hat{c}_{44} c_{66})^{1/2} l^2 R_{loop} \left(\frac{R_l^2}{l^2 + \tilde{\lambda}_c^2} \right)^{\zeta} \;&>\; E_{dis} \;\sim\; (\hat{c}_{44} c_{66})^{1/2} l^2 R_{loop} \\ R_l \;&>\; c^{1/2\zeta} \cdot (l^2 + \tilde{\lambda}_c^2)^{1/2} \; . \end{aligned} \tag{5.31}$$

with a numerical constant c. The criterion (5.31) is again a Lindemann-like criterion very similar to the criteria (4.47, 5.19) for the uniaxial, layered model. We can regain the previous results (4.47, 5.19) when we go over to the local limit, i.e., with the scale for the onset of dispersion $\tilde{\lambda}_c \ll l$ much smaller than the FL spacing, and replace ζ by its value $\zeta_{RF} = 1/2$ in the RF regime. This is in accordance with our modeling leading to (4.47, 5.19), where we used the Bragg glass approximation, i.e., let the disorder vary on

the scale of the FL spacing and thereby lost the intermediate RM regime and where we excluded dispersion. But in principle, the results (4.47, 5.19) naively generalize to the realistic model.

By comparison with the result (4.47) from the variational calculation, we estimate $c \approx \mathcal{O}(50)$ (4.48), but notice that the determination of the numerical c is beyond the scope of the scaling argument. We expect $c \gtrapprox \mathcal{O}(50)$ for two-component displacements, because fluctuations should be stronger and the topologically ordered Bragg glass less stable compared to the uniaxial model. The increased numerical factor $c^{1/2\zeta} \approx c^{5/2}$ indicates a *reduced* stability regime for the Bragg glass, resulting from the reduced core energy when we take into account the RM regime properly. Below, we derive the relation $c \approx c_L^{-2}$ between c and the Lindemann-number c_L, which will allow us to confirm the value $c \approx \mathcal{O}(50)$ (4.48) found by the variational calculation.

In the dense limit $\tilde{\lambda}_c \gg l$, the FL spacing l is replaced by the range of the magnetic interaction $\tilde{\lambda}_c$. This leads to a further reduction of E_{core} by a factor $(l/\tilde{\lambda}_c)^{2\zeta}$. The Bragg glass cannot be stable in the limit $\tilde{\lambda}_c \uparrow \infty$ [or at scales below $\tilde{\lambda}_c$ for finite $\tilde{\lambda}_c$'s; note that $\tilde{\lambda}_c \uparrow \infty$ for $B \uparrow B_{c2}$, see (3.5)] since the long-ranged magnetic interaction gives rise to a much stronger disorder energy, $\Delta E \sim {L_{loop}}^2$ [9], which always exceeds E_{core}.

5.3 Lindemann Criteria

We can summarize the findings accumulated so far in the previous chapters in the Lindemann-like criterion for the stability of the Bragg glass

$$R_l \;>\; c^{1/2\zeta} \cdot \left(l^2 + \tilde{\lambda}_c^2\right)^{1/2} \;\simeq\; c^{1/2\zeta} \max\left\{l, \tilde{\lambda}_c\right\} \tag{5.32}$$

$$c \;\gtrapprox\; \mathcal{O}(50)\ . \tag{5.33}$$

When this criterion is violated, dislocations proliferate in a topological transition, the order of which could not be determined unambiguously.

Let us demonstrate now that the criterion (5.32) is equivalent to the Lindemann criterion in its conventional phenomenological form [38]

$$2\overline{\langle u^2(R=l)\rangle} \;<\; c_L^2 l^2\ , \tag{5.34}$$

where $2\overline{\langle u^2(R=l)\rangle} = \overline{\langle(\mathbf{u}(\mathbf{R}+\mathbf{l}) - \mathbf{u}(\mathbf{R}))^2\rangle}$ is the (disorder-averaged) mean square displacement of the FLs on the *shortest scale* ($\mathbf{l}$ is a primitive lattice vector of the Abrikosov lattice). c_L is the Lindemann-number of the FL lattice, which is only phenomenologically known; for thermal melting, values $c_L \approx 0.1-0.2$ are used in the literature. The Lindemann criterion has been proven as a very efficient phenomenological tool to obtain the thermal melting curves of lattices, e.g. the disorder-free FL lattice. In writing down (5.34), we

have generalized to a disordered system by complementing the average over the quenched randomness hoping that (5.34) gives the stability range of the topologically ordered phase in the disordered system in a similar way as the conventional Lindemann-criterion gives the ordered phase in a thermally fluctuating system. The derivation of the criterion (5.32) based on the variational calculation demonstrates, that unbound dislocations proliferate indeed on the shortest scale at the topological transition described by (5.32), i.e., in between every layer and thus with a distance l. This suggests that the use of the conventional phenomenological Lindemann criterion in the form (5.34) might be one possibility to obtain the topological transition line, thereby interpreting the proliferation of dislocation loops as disorder-induced "melting". An approach very similar to this, has actually be taken in a recent work by Ertaş and Nelson [34]. They use a "cage model" to mimic the interactions between FLs, which yields an effective theory for a single FL in a random potential. To this single FL, they apply the Lindemann criterion directly in its phenomenological form (5.34). As we will see, the quantity $u(l)$ is equivalent to the mean square displacement of the "effective" FL studied in their cage model. However, let us stress that the conventional Lindemann-criterion (5.34) is purely phenomenological, whereas the criterium (5.32) was *derived* on the basis of a variational calculation and detailed scaling arguments.

The equivalence of (5.32) and (5.34) can be shown by employing the scaling properties in the RM regime on scales $l \lesssim R \lesssim R_l$. Here we consider again a pinning strong enough that we have single vortex pinning in the RF regime ($L_\xi^s \lesssim L^*$), the generic situation in extreme high-T_c materials so that we have a "collective RM regime" with $d = 3$ and $n = 2$ on scales $l \lesssim R \lesssim R_l$ and the scaling (5.27) of displacements,

$$\overline{\langle u^2 \rangle}(R) \;\sim\; \left(R^2 + \tilde{\lambda}_c^2\right)^{\zeta} \;. \tag{5.35}$$

Applying this relation on the scales $R = l$ and $R = R_l$, where per definitionem (3.33) of the positional correlation length R_l

$$2\overline{\langle u^2 \rangle}(R_l) \simeq l^2 \;, \tag{5.36}$$

yields the relation

$$2\overline{\langle u^2 \rangle}(R_l) \;\simeq\; l^2 \;\simeq\; 2\overline{\langle u^2(R=l) \rangle} \left(\frac{R_l^2 + \tilde{\lambda}_c^2}{l^2 + \tilde{\lambda}_c^2}\right)^{\zeta} \;. \tag{5.37}$$

Using $R_l \gg \tilde{\lambda}_c$ (which will be shown in the following chapter 6), our Lindemann-like criterion (5.32) can be written as

$$2\overline{\langle u^2(R=l) \rangle} \;<\; c^{-1} l^2 \;, \tag{5.38}$$

and it becomes immediately clear that (5.32) is the analog of the Lindemann criterion (5.34), formulated in terms of the underlying transversal scales rather than the corresponding displacements. Furthermore, we can identify

$$c \approx c_L^{-2} \ . \tag{5.39}$$

We see that the equivalence of the criterion (5.32) to the phenomenological Lindemann criterion (5.34) includes the agreement of the appearing numerical factors. The value for the Lindemann-number $c_L \approx 0.15$, widely used in the literature, produces a good agreement in (5.39) with the value $c \approx \mathcal{O}(50)$ obtained by the variational calculation. This equivalence to a scenario where disorder-induced fluctuations on the shortest scale "melt" the FL array favours a first order transition scenario for the topological transition, which could not be excluded in the experiments [30].

Using (5.39) and $\zeta \approx 1/5$ (3.32), we can rewrite the Lindemann-like criterion (5.32) as

$$R_l \ > \ c_L^{-5} \cdot \max\left(l, \tilde{\lambda}_c\right) \ . \tag{5.40}$$

As the very concept of collective pinning in the Bragg glass breaks down when R_l is decreased to the order of the FL spacing l or the range of the magnetic interaction $\tilde{\lambda}_c$, (5.40) reaches only within a large factor $c_L^{-5} \approx \mathcal{O}(10^5)$ of the maximally possible stability regime for the Bragg glass. So the Bragg glass is only *weakly stable* with respect to dislocation formation.

The remainder of this part of the work is devoted to the experimental consequences of the Lindemann-like criterion (5.32, 5.40), i.e., to the calculation of a phase diagram in the B-T plane for a typical HTSC such as BSCCO, displaying the phase boundaries of the Bragg glass. This requires an explicit evaluation of the positional correlation length R_l in terms of the microscopic parameters of the HTSC and the disorder strength.

Chapter 6

Phase Diagram for a Typical HTSC

The main result of part II is the Lindemann criterion (5.32, 5.40) for the stability of the Bragg glass with respect to dislocation loop formation. It has been derived by a variational calculation and detailed scaling arguments in the preceding chapters. Here, we want to explore essentially the experimental consequences of this criterion for the phase diagram of a typical HTSC, such as $Bi_2Sr_2CaCu_2O_{8+x}$ (BSCCO), in the usual experimental situation $\mathbf{H}||\mathbf{c}$ of a magnetic field perpendicular to the CuO-planes of the HTSC.

The purpose of this chapter is twofold. Firstly, we express R_l in terms of the microscopic parameters of the HTSC and the disorder strength, and obtain its dependence on magnetic induction B and temperature T. To this end, we consider in detail the crossovers between the different pre-asymptotic regimes of the FL array subject to point disorder on scales smaller than the positional correlation length R_l, as they were introduced in chapter 3. Secondly, and most importantly from the experimental point of view, we calculate the region of the phase diagram in the B-T plane [Figure 6.1] where the Bragg glass phase is stable and should be observable experimentally or numerically according to the Lindemann-like criterion (5.40). We find good agreement with the experiments [25, 30]. The upper phase boundary of the Bragg glass, which we obtain using (5.40), turns out to be identical to the one obtained by Ertaş and Nelson [34]. They apply the conventional phenomenological Lindemann criterion to a single "effective" FL in a random potential within a "cage model" which mimics the interaction between FLs.

6.1 Experimental Facts

Let us begin with reviewing the known experimental and numerical results regarding the stability of the topological order in the Bragg glass phase. The algebraically decaying

Bragg peaks with a structure factor (3.44)

$$S(\mathbf{k}) \sim \frac{1}{|\mathbf{k}-\mathbf{K}|^{d-j^2\cdot A(4-d)}} \tag{6.1}$$

at the j^{th} reciprocal lattice vector $\mathbf{k} \approx \mathbf{K} = j \cdot \mathbf{K}_0$ have been observed in the neutron diffraction experiments on BSCCO of Cubitt et al. [25] up to the second order peak at low magnetic fields. However, upon increasing the magnetic field, the Bragg peaks vanish, indicating an instability of the Bragg glass phase. For this transition they find a midpoint of $B \sim 650$G. As opposed to Cubitt et al.}, who assigned this transition to a decomposition of the flux lines into pancake vortices, we want to explain their data by the existence of the topological phase transition and the proliferation of dislocation loops when the criterion (5.40) is violated.

Critical current measurements of Khaykovich et al. [30] show a sharp drop in the (local) critical current j_c upon decreasing the magnetic induction below a critical value. This critical value is shown to decrease with increasing anisotropy of the material. The observed transition, the order of which could not determined unambiguously, happens around $B \sim$ 400G. It can be attributed to the "disentanglement" of FLs in the absence of dislocations when topological order is regained, and dislocation loops vanish upon lowering the magnetic field.

The existence of such a transition has also been demonstrated in recent numerical studies [28, 29]. In the closely related 3D XY model in a random field, Gingras and Huse [28] find that vortex loops occur in a topological phase transition at a critical strength of the random field.

A direct simulation of a model flux line lattice of Ryu et al. [29] demonstrated explicitly the existence of a "topological glass transition", where unbound large dislocations proliferate. In addition, the existence of Bragg peaks and their vanishing upon increasing the magnetic field could be confirmed numerically in good agreement with the experimental results of Cubitt et al. [25].

6.2 Positional Correlation Length R_l

To find the phase boundaries of the Bragg glass in the B-T plane as given by the criterion (5.40), we have to relate R_l to experimentally accessible quantities, i.e., the microscopic parameters of the superconductor (the magnetic penetration depths λ_{ab} and λ_c and the coherence lengths ξ_{ab} and ξ_c), the disorder strength, the magnetic induction B (or the FL spacing l), and the temperature T. To this end, we have to take into account the crossover between the different pre-asymptotic regimes of the dislocation-free disordered FL array preceding the asymptotic Bragg glass phase, and the associated crossover length scales,

which have been introduced in chapter 3 and have to be expressed in experimentally accessible quantities, too. As discussed in detail in chapter 3, we have essentially two different pre-asymptotic regimes: The random force (RF) regime of Larkin and Ovchinnikov [6, 48], which crosses over to the so-called random manifold (RM) regime at the Larkin length, before the asymptotic Bragg glass behaviour sets in on the largest scales exceeding the positional correlation length. In between this sequence of crossovers, the FL interaction sets a length scale L^*, which describes a crossover from a "single vortex" behaviour to a "collective" behaviour. The relations between these length scales are visualized for an extreme HTSC as BSCCO in Figure 3.3 (a)&(c).

For the following, it turns out to be convenient to use the *reduced induction* $b \equiv B/B_{c2}(T) = 2\pi\xi_{ab}^2/l^2$ to measure the strength of the magnetic field.

6.2.1 Interaction-Induced Length Scale L^*

In chapter 3, it has been argued that the three-dimensional elastic theory is valid only on scales $R \gtrsim l$ or

$$L \gtrsim L^* \simeq \left(\frac{c_{44}^s}{c_{66}}\right)^{1/2}, \tag{6.2}$$

see (3.9). When we consider fluctuations on scales $L \lesssim L^*$, the FL array breaks up into single FLs described by 1-dimensional elasticity, and the effects of FL interaction become irrelevant. The interaction-induced length scale L^* separates a regime of "collective" behaviour described by 3D elasticity from a "single vortex" behaviour described by 1D elasticity. L^* starts to increase exponentially for $l/\lambda_{ab} = (b/2\pi)^{-1/2}/\kappa \gg 1$ in the dilute limit, (with $\kappa = \lambda_{ab}/\xi_{ab} \approx 100$ for BSCCO [4]) due to the exponential decay of $c_{66} \propto \exp(-l/\lambda_{ab})$. The length scale L^*, given by (6.2), can be calculated with the expressions given in Appendix A.3 for c_{44}^s and c_{66}. This yields the following useful interpolation formula:

$$L^* \approx \varepsilon l \, \mathrm{f}_\kappa\left(\frac{b}{2\pi}\right) \tag{6.3}$$

$$\mathrm{f}_\kappa(x) = \begin{cases} x < \kappa^{-2}: & 1 \\ x > \kappa^{-2}: & (x\kappa^2)^{3/8} \exp\left(\frac{(x\kappa^2)^{-1/2}-1}{2}\right), \end{cases} \tag{6.4}$$

where $\varepsilon = \lambda_{ab}/\lambda_c$ is the anisotropy ratio of the HTSC and $\varepsilon \approx 1/100$ for BSCCO [4].

6.2.2 Larkin Length L_ξ

The Larkin length L_ξ is the crossover length between the RF and the RM regime and has been discussed in detail in chapter 3. When considering an extreme HTSC as BSCCO, it is important to note, and will be checked explicitly below, that the pinning by point disorder

is typically such strong that we have *single vortex pinning* in the RF regime. This means that

$$L_\xi = L_\xi^s \lesssim L^* \ . \tag{6.5}$$

The Larkin length is smaller than L^*, and each FL is pinned *independently* in the RF regime so that the Larkin length is equal to the single vortex Larkin length L_ξ^s.

The single vortex Larkin length L_ξ^s is at low temperatures given by (3.28):

$$L_\xi^s \ \sim \ \xi_{ab} \ \left(\frac{c_{44}^{s\ 2} \xi_{ab}^2}{\Delta_{pin}^2} \right)^{1/3} \ . \tag{6.6}$$

As proposed in Ref. [4], it is convenient for what follows to introduce the basic energy (per length) scale

$$\epsilon_0 = (\phi_0 / 4\pi\lambda_{ab})^2 \tag{6.7}$$

and the dimensionless disorder strength δ as

$$\delta \ = \ \frac{\Delta_{pin}^2}{(\epsilon_0 \xi_{ab})^2} \ . \tag{6.8}$$

In terms of these parameters and using results from the Appendix A.3 for c_{44}^s, we find for the Larkin length L_ξ at low temperatures [4]

$$L_\xi(0) \ \simeq \ \varepsilon \xi_{ab} \ \left(\frac{(\varepsilon \epsilon_0 \xi_{ab})^2}{\varepsilon \Delta_{pin}^2} \right)^{1/3} \ \simeq \ \varepsilon \xi_{ab} \ \left(\frac{\delta}{\varepsilon} \right)^{-1/3} \ . \tag{6.9}$$

This result holds as long as the range of the single vortex pinning potential $v(\mathbf{r})$ (3.14), is given by the core-diameter ξ_{ab} of a single FL. However, at higher temperatures thermal fluctuations start to weaken the pinning by effectively broadening the cores of the FLs such that the effective range r_T of the single vortex pinning potential becomes

$$r_T \approx \max \left\{ \xi_{ab}, \langle u^2 \rangle_{th}^{1/2}(L_\xi) \right\} \ . \tag{6.10}$$

As opposed to its definition (3.25) at low temperatures, L_ξ is at higher temperatures properly defined as the crossover scale, at which the average FL displacement becomes of order of the *effective* range r_T of the point disorder:

$$u(L_\xi) \simeq r_T \approx \max \left\{ \xi_{ab}, \langle u^2 \rangle_{th}^{1/2}(L_\xi) \right\} \ . \tag{6.11}$$

Here, we introduced the notation

$$u(R, L) \equiv \overline{\langle (\mathbf{u}(\mathbf{r} + (\mathbf{R}, L)) - \mathbf{u}(\mathbf{r}))^2 \rangle}^{1/2} \tag{6.12}$$

for displacement correlations (and $\langle \ldots \rangle_{th}$ for a purely thermal average).

The low-temperature result (6.9) holds as long as $r_T \simeq \xi_{ab}$. However, above the *depinning temperature* T_{dp} of the single vortex, r_T grows beyond ξ_{ab} [4]:

$$r_T^2 \simeq \xi_{ab}^2 \exp\left((T/T_{dp})^3\right) , \tag{6.13}$$

where the depinning temperature T_{dp} is given by [4]

$$T_{dp} \;\simeq\; \varepsilon\epsilon_0\xi_{ab}\,\frac{\varepsilon\xi_{ab}}{L_\xi(0)} \;\simeq\; \varepsilon\epsilon_0\xi_{ab}\,\left(\frac{\delta}{\varepsilon}\right)^{1/3} . \tag{6.14}$$

Above T_{dp}, $L_\xi(T)$ increases exponentially with temperature due to the fact that random forces are only marginally relevant for a single FL with two-component displacements [4]:

$$L_\xi(T) \simeq L_\xi(0) \begin{cases} T \ll T_{dp}: & 1 \\ T > T_{dp}: & (T/T_{dp})^{-1} \exp\left((T/T_{dp})^3\right) \end{cases} \tag{6.15}$$

Let us discuss estimates of the quantities L_ξ and T_{dp} at this point, which provide alternative measures of the disorder strength for BSCCO. As estimates in BSCCO, we use $\xi_{ab} \approx 20$Å, $\epsilon_0\xi_{ab} \approx 1000$K, $\varepsilon \approx 1/100$, which is in accordance with Refs. [4, 34]. In Ref. [34], the disorder strength is given by $T_{dp} \approx 10K$, which leads to $\delta/\varepsilon \approx 1$ with (6.14). This estimate is considerably higher than typical values given in Ref. [4] for weak pinning. We will adopt these estimates of Ref. [34], that may apply for a relatively strong intrinsic disorder and thus strong pinning in BSCCO. This yields a small (longitudinal) Larkin length of the order of $L_\xi(0) \approx \varepsilon\xi_{ab}$ in BSCCO such that $L_\xi(0) \approx \varepsilon\xi_{ab} \ll \varepsilon l \lesssim L^*$. Thus the condition (6.5) is fulfilled, and single vortex pinning in the RF regime is realized in BSCCO.

6.2.3 Positional Correlation Length R_l

On scales exceeding the Larkin length L_ξ, we enter the RM regime (for a detailed discussion see again chapter 3). Because we consider the case of single vortex pinning in the RF regime, we have *two* RM regimes with somewhat different scaling properties. On scales $L_\xi \lesssim L \lesssim L^*$, we find a single vortex RM regime, where the FLs are described as 1-dimensional elastic manifolds, i.e., $d = 1$ and $n = 2$. In this regime, the scaling behaviour of the $\overline{\langle uu\rangle}$-correlations is (3.31)

$$u(L) \sim L^{\zeta(1,2)} . \tag{6.16}$$

In the collective RM regime on scales $L^* \lesssim L \lesssim L_l$ (or transversal scales $l \lesssim R \lesssim R_l$), the scaling relation (6.16) gets slightly modified by the dispersion of c_{44} to (3.31, A.26)

$$u^2(R) \sim \left(\tilde{\lambda}_c^2 + R^2\right)^{\zeta(3,2)} . \tag{6.17}$$

The best available estimates for the roughness exponents are [7] (3.32)

$$\zeta(1,2) \approx 5/8 \qquad \text{and} \qquad \zeta := \zeta(3,2) \approx 1/5 . \tag{6.18}$$

The scaling relations (6.16, 6.17) enable us to obtain the relation between the (transversal) positional correlation length R_l and the (longitudinal) Larkin length L_ξ, which will allow us to express R_l in terms of microscopic parameters. Applying the scaling relation (6.16) for the $\overline{\langle uu \rangle}$-correlations to the single vortex RM regime on the longitudinal scales $L = L_\xi$ and $L = L^*$, we obtain with (6.11)

$$u_* := u(R{=}l, L{=}L^*) \simeq r_T \left(\frac{L^*}{L_\xi(T)} \right)^{\zeta(1,2)} . \tag{6.19}$$

In the same manner, we can use (6.17) in the collective RM regime on transversal scales $R = R_l$:

$$l^2 \simeq u^2(R{=}R_l) \simeq u_*^2 \left(\frac{\tilde{\lambda}_c^2 + R_l^2}{\tilde{\lambda}_c^2 + l^2} \right)^{\zeta(3,2)} . \tag{6.20}$$

Using (6.19, 6.20), R_l can be expressed as

$$R_l(T) \simeq (\tilde{\lambda}_c^2 + l^2)^{1/2} \left(\frac{l}{r_T} \right)^{1/\zeta(3,2)} \left(\frac{L_\xi(T)}{L^*} \right)^{\zeta(1,2)/\zeta(3,2)} . \tag{6.21}$$

With the results (6.13) for r_T, (6.3) for L^*, and (6.15) for $L_\xi(T)$, together with $\zeta(3,2) \approx 1/5$ and $\zeta(1,2) \approx 5/8$ (6.18), this yields the desired expression for R_l:

$$\begin{aligned} R_l(0) &\approx \left(\tilde{\lambda}_c^2 + l^2 \right)^{\frac{1}{2}} \left(\frac{b}{2\pi} \right)^{-15/16} \left(\mathrm{f}_\kappa \left(\frac{b}{2\pi} \right) \right)^{-25/8} \left(\frac{\delta}{\varepsilon} \right)^{-25/24} \\ R_l(T) &\approx R_l(0) \begin{cases} T \ll T_{dp}: & 1 \\ T > T_{dp}: & (T/T_{dp})^{-25/8} \exp\left(\frac{5}{8} (T/T_{dp})^3 \right) \end{cases} \end{aligned} \tag{6.22}$$

For inductions $b = 10^{-4} \ldots 10^{-1}$ in the dense limit $b \gtrsim 2\pi/\kappa^2$, we obtain with $\delta/\varepsilon \approx 1$ and $\lambda_c \approx 2 \cdot 10^5$Å (transversal) positional correlation lengths $R_l(0) \approx (10^5 \ldots 10^2) \cdot \lambda_c \approx 2 \cdot (1 \ldots 10^{-3})$cm, which is extremely large and indicates that over a wide range of length scales the pre-asymptotic RM regimes should be observable rather than the asymptotic Bragg glass regime.

6.3 Phase Diagram

Let us now address the issue of phase boundaries of the topologically ordered Bragg glass in the B-T plane as they follow from the Lindemann-like criterion (5.40). The results are summarized in Figure 6.1. The boundary of the regime given by (5.40) defines a *topological transition line* $B_t(T)$, where dislocations proliferate and the topological order of the Bragg

glass phase is lost. The upper branch $b_{t,u}(T)$ of this line can be obtained by applying the expression (6.22) for the positional correlation length R_l in the dense limit $b \gtrsim 2\pi/\kappa^2$ (i.e. $\mathrm{f}_\kappa \equiv 1$ in (6.22)) to the criterion (5.40), which finally yields a condition $b < b_{t,u}(T)$ in the b-T plane with

$$\begin{aligned} b_{t,u}(0) &\approx 2\pi \left(\frac{\delta}{\varepsilon}\right)^{-10/9} c_L^{16/3} \approx 2\pi \left(\frac{\varepsilon\epsilon_0\xi_{ab}}{T_{dp}}\right)^{10/3} c_L^{16/3} \\ b_{t,u}(T) &\approx b_{B,u}(0) \begin{cases} T \ll T_{dp}: & 1 \\ T > T_{dp}: & (T/T_{dp})^{-10/3} \exp\left(\frac{2}{3}\,(T/T_{dp})^3\right). \end{cases} \end{aligned} \tag{6.23}$$

Note that the transition line (6.23) is identical to the one obtained by Ertaş and Nelson [34] by applying the conventional phenomenological Lindemann criterion to a "cage model" for a single FL. The estimates $c_L \approx 0.17$ and $\delta/\varepsilon \approx 1$ lead to $b_{t,u}(0) \approx 5 \cdot 10^{-4}$ or $B_{t,u}(0) \approx 400$G [34], which is in good agreement with the experiments [25, 30]. Good agreement is also obtained for the overall transition line shape [Figure 6.1] [30]. For stronger anisotropy or effectively larger disorder strength δ/ε, the transition line $b_{t,u}$ decreases in magnetic field, and the stability region of the topologically ordered Bragg glass shrinks in accordance with the experimental findings in Ref. [30]. For temperatures $T < T_{dp}$, the transition line is essentially temperature-independent because the mechanism for the proliferation of dislocation loops is purely disorder-driven at low temperatures as we have seen in the preceding chapters. For $T > T_{dp}$, it increases exponentially due to the very effective weakening of the pinning effects by thermal fluctuations in the single vortex regime, and at some temperature slightly above T_{dp}, the transition line will terminate in the upper branch of the melting curve $b_{m,u}(T)$, which is

$$b_{m,u}(T) \approx 30 \frac{(\varepsilon\epsilon_0\xi_{ab})^2 {c_L}^4}{T^2} \tag{6.24}$$

in this regime [4]. Beyond the melting curve $b_{m,u}(T)$, the FL array melts into a disordered FL liquid, and the Bragg glass order is destroyed by the thermal fluctuations, whereas above the transition line $b_{t,u}(T)$ the Bragg glass "melts" by disorder-induced fluctuations, when unbound dislocation loops proliferate. As noted in [34], $b_{t,u}(T)$ is well below the so-called "decoupling field", beyond which the layered structure of the HTSC requires a discrete description in the **c**-direction.

At low inductions in the dilute limit $b \ll 2\pi/\kappa^2$, the criterion (5.40) will be violated due to the exponential decrease of the shear modulus c_{66}, or increase of the interaction-induced length scale L^* (6.3) encoded in the function f_κ (6.4). At low temperatures $T \lesssim T_{dp}$, the temperature independent lower branch of the topological transition line $b_{t,l}(T) \approx b_{t,l}(0)$

can be determined as the smaller of the two solutions of

$$\left(\mathrm{f}_\kappa\left(\frac{b_{t,l}(0)}{2\pi}\right)\right)^{10/3}\frac{b_{t,l}(0)}{2\pi} \;\approx\; \left(\frac{\delta}{\varepsilon}\right)^{-10/9} c_L^{16/3}. \tag{6.25}$$

At temperatures $T \gg T_{dp}$ well above the depinning temperature, the asymptotics

$$b_{t,l}(T) \;\sim\; \frac{25\pi}{2\kappa^2}\left(\frac{T}{T_{dp}}\right)^{-6} \tag{6.26}$$

is obtained. Thus, $b_{t,l}(T)$ will terminate in the lower branch of the melting curve $b_{m,l}(T)$, which increases logarithmically with temperature [4]

$$b_{m,l}(T) \;\approx\; \frac{2\pi}{\kappa^2}\ln^{-2}\left(\frac{(\varepsilon\epsilon_0\xi_{ab})^2 {c_L}^4\kappa^2}{T^2}\right). \tag{6.27}$$

Beyond the lower branch of the melting curve $b_{m,l}(T)$, the vortex array is essentially well-described as a collection of independently fluctuating single FLs, which may be individually pinned and form a glassy phase in the presence of point disorder. However, for virtually single vortices, the issue of dislocations is not of primarily interest. With $c_L \approx 0.17$ and $\delta/\varepsilon \approx 1$, we can obtain from (6.25) numerically $b_{t,l}(0) \approx 0.03(2\pi/\kappa^2) \approx 2\cdot 10^{-5}$, which is by a factor of 25 smaller than $b_{t,u}(0)$ and experimentally hard to verify due to the small inductions $B_{t,u}(0) \approx 16$G. From (6.25), it is clear that the transition line $b_{t,u}(T)$ increases with the disorder strength so that the stability region of the topologically ordered Bragg glass shrinks.

In conclusion, we have obtained the region in the phase diagram of BSCCO in the B-T plane, where the topologically ordered vortex glass should be observable according to the Lindemann-criterion (5.32, 5.40) derived in the preceding chapters, and the topological transition lines $B_{t,u}(T)$ and $B_{t,l}(T)$, where dislocation loops proliferate. The resulting phase diagram, as given by the formulae (6.23, 6.25, 6.26) and depicted in Figure 6.1, is in reasonable agreement with the experimental data of Refs. [25, 30] as well as the simulation data of Ref. [29]. Our results for the upper branch of the topological transition line $B_{t,u}(T)$ agree with Ref. [34], where the conventional phenomenological Lindemann-criterion was applied to the disorder-induced "melting" in the framework of a "cage model".

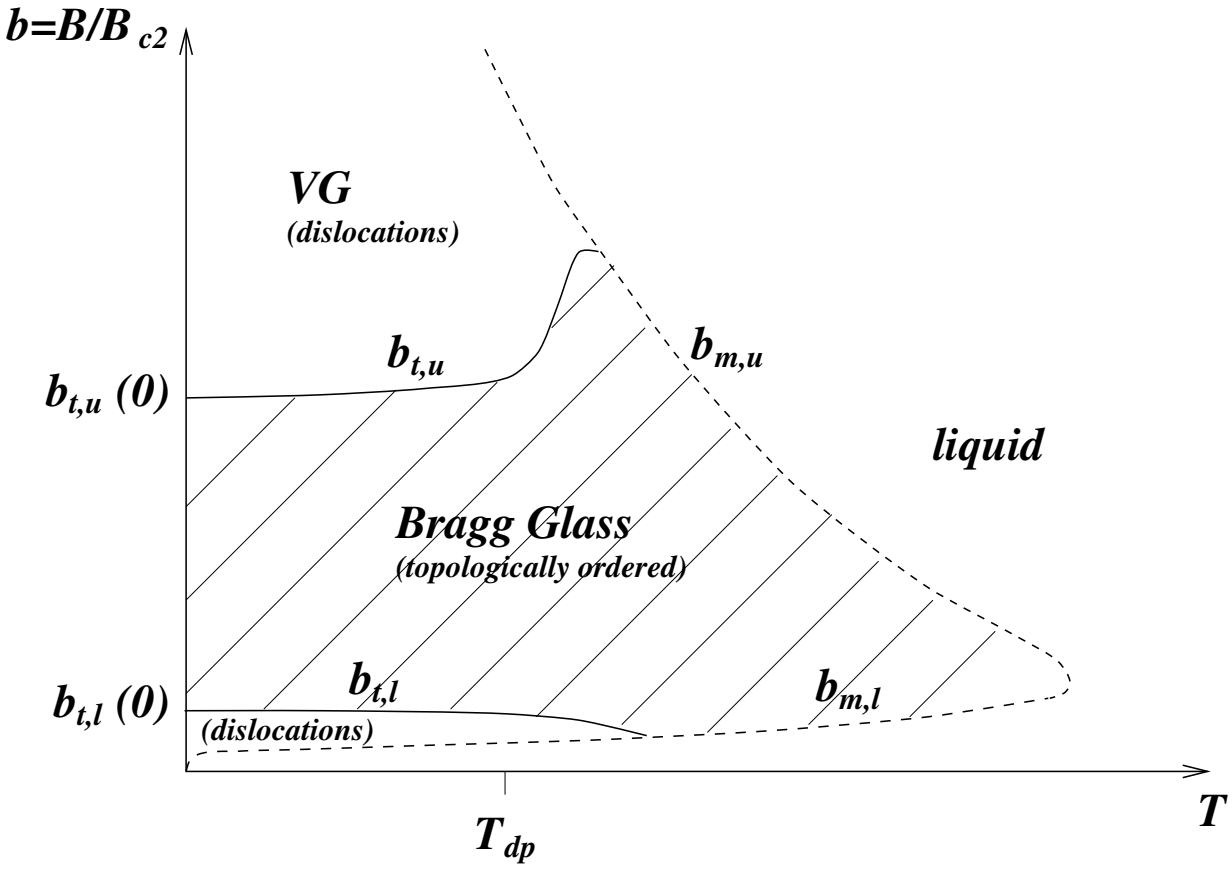

Figure 6.1: Schematic phase diagram in the b-T plane ($b \equiv B/B_{c2}(T)$) showing the stability regime of the topologically ordered Bragg glass phase (hatched region). Its phase boundaries are given by the upper and lower branch $b_{t,u}(T)$ and $b_{t,l}(T)$ (solid lines) of a *topological* transition line, where dislocations proliferate. They terminate in the two branches $b_{m,u}(T)$ and $b_{m,l}(T)$ (dashed lines) of the *melting* curve, where the FL array melts into a (disordered) FL liquid.

Chapter 7

Conclusion

In this first part of the work we tried to shed some light on the issue of topological defects, in particular dislocations, in a disordered FL array. The main result of this part is the simple Lindemann-like criterion (5.32, 5.40) comparing the positional correlation length to the FL spacing (in the dilute limit) or magnetic penetration depth (in the dense limit), which has been derived by a variational calculation (chapter 4) and detailed scaling arguments (chapter 5). In chapter 6, it was transformed into the phase diagram 6.1 for a typical extreme high-T_c material such as the Bi-compound, which is in agreement with existing experiments [25, 30] and numerical simulations [29] but should be subject of further verification. We stress once again that the Lindemann-like criterion (5.32, 5.40) has been *derived* on the basis of a variational calculation and detailed scaling arguments as opposed to the conventional Lindemann criterion [38] which is purely phenomenological.

Let us comment at this point on the limitations of the employed methods in deriving the Lindemann-like criterion. Essentially, all of them are due to the fact that already the dislocation-free FL array is a highly non-trivial disordered system as the short overview in chapter 3 demonstrated: The physics of the dislocation-free FL array (at low enough inductions to be the positional degrees of freedom of the vortices the only relevant degrees of freedom) subject to point disorder can be mapped onto elastic manifolds in $d = 3$ (FL lattice) or $d = 1$ (single FL) dimensions with $n = 2$ (two-component displacements) codimensions in various types of random media, differing in their modeling of the point disorder in the cospace of the displacement components: These types ranges from random forces, over "classical" random manifolds with short-range point disorder, to CDW-like periodic disorder-potentials.

A rigorous analysis for an ensemble of dislocations with fixed coordinates would require to optimize the FL configurations, i.e., redo the analysis for the dislocation-free elastic FL array, in the presence of the topological constraints imposed by the ensemble of dislocations which is certainly an unsolvable problem for complicated enough dislocation configurations but has been studied for a *single* dislocation and random-bond-like disorder

in Ref. [74]. Such an analysis should end up with an effective partition sum for the ensemble of dislocations in the disordered medium, i.e., a many-"particle" path integral summing up the statistical weights of the many-dislocation configurations, which is in principle the disordered analog of the transfer-matrix procedure of Ref. [37]. Due to disorder-induced long-range interactions between dislocations and additional interactions between dislocations and quenched randomness [74], such a calculation is probably impossible to perform.

To be able to do a statistical mechanics calculation, we have taken in chapter 4 a much simpler approach in limiting ourselves to only *one* possible orientation of dislocation loops with only *one* possible Burgers vector by studying a layered uniaxial model, which can indeed be realized in layered HTSCs in a *parallel* field. We derived an inter-layer coupling going beyond the elastic theory, which allows for dislocations on the one hand and is simple enough to make analytic progress (even without specifying certain dislocation configurations) on the other hand. This has enabled us to perform a variational calculation for an effective shear modulus, the vanishing of which is a manifestation of proliferating unbound dislocations. As we will see in the next part II of the work, the layered geometry can also be studied by an RG approach, which takes fluctuation effects from many scales correctly into account, and we are able to analyze the RG-flow for a "toy"-model consisting of only 2 layers in detail. The findings in the RG-approach agree with the results of the variational calculation and give further evidence for the Lindemann-like criterion (5.32, 5.40). The main shortcoming of the variational calculation of chapter 4 is the use of a *single* variational parameter, namely an effective shear modulus. Such an approximation cannot account for phenomena where an optimization on more than one length scale is necessary. By our "one-parameter" Ansatz for the shear modulus, dislocations occur simultaneously in between *all* layers because it is not dependent on the length scale perpendicular to the layers, i.e., the layer index. The first order transition found in such a calculation may be an artefact of such an approximation; on the other hand, we explored the *opposite* extreme in the scaling argument by considering a *single* dislocation and obtained a criterion of the same form. Potentially, this difficulty can be overcome in the RG calculation for many layers [75], where it is in principle also possible to go beyond the "nearest layer" approximation of chapter 4. However, as we will get a flavor when considering the two-layer model in part II, chapter 11, it is very hard to analyze the resulting RG flows. For future work on an improvement of the variational calculation one could perform similar calculations for inter-layer couplings which allow for dislocations every n^{th} layer for comparison.

The approach in chapter 5 was based on scaling arguments. In considering large dislocations of size L in an elastic manifold in a random medium, one induces a large scale re-optimization of the FL configurations on a scale L, simply due to the fact that topological defects have a long-range, non-local effect on the deformation of the lattice and cannot be annihilated by simple elastic deformation. For this reason, one is left with a similar task as if an additional interaction is introduced which requires a large scale re-optimization

of the pinned elastic manifold. Examples for such interactions are additional long-range interactions within the manifold or with "replicas" of the manifold and the presence of additional, random or non-random, quenched defect types apart from the point disorder, e.g. defect planes or columnar defects in a superconductor. These types of problems have been successfully approached over the last years in a more rigorous analytical manner, and at least in the case of single elastic lines ($d = 1$) in a random medium containing point disorder, the problems of depinning from a single columnar defect [44, 45] or two interacting lines [76] could be solved analytically by applying RG or scaling concepts to the additional interaction *at* the $T=0$ fixed point of the interaction-free, point-disordered system. In principle, our scaling argument follows the same avenue as these approaches, balancing the disorder energy *gained* in the large re-optimization against the *cost* imposed by the additional interaction. However, due to the fact that for the FL array in $d = 3$ much less is known about the dislocation-free disordered system as in $d = 1$ about directed paths in a random medium and that the existence of the nontrivial pre-asymptotic random manifold and random force regimes further complicate the analysis, it is hard to formulate an analytically more rigorous RG treatment, which would put the scaling-concepts used in chapter 5 on a more "solid" basis. Furthermore, it is likely that for a stretched dislocation we are in the marginal case where the prefactors of the involved energies determine whether unbound dislocations occur, which makes the scaling-analysis sensitive to possible logarithmic corrections. In the present formulation, such corrections do not seem to emerge, but a detailed RG approach would be desirable also to clarify this point.

Despite these potential points of criticism, the presented Lindemann-criterion (5.32, 5.40) produces good agreement with experiments and seems to capture the physics involved in the instability of the topologically ordered Bragg glass phase with respect to dislocation loop formation sufficiently well.

Part II

Planar Arrays of Steps and Lines in Random Media: The 2D Random Field XY Model

Chapter 8

Introduction

In part I we have introduced one prominent example of a "planar array of lines", namely the planar array of flux lines (FL) in a superconductor with point impurities which was realized in form of a planar array of Josephson-like vortices confined between the superconducting CuO-planes of a high-T_c superconductor (HTSC) in a parallel field. This system can be modeled in the Bragg glass regime on scales exceeding the positional correlation length by the Hamiltonian of the two-dimensional XY model in a random symmetry breaking field (2D RFXY model) in the absence of vortices. The mapping has been discussed in detail in chapter 3, but let us shortly recapitulate the main points. Displacements of the lines in the planar geometry are *uniaxial* and described by the scalar field $u(\mathbf{r})$ defined over two dimensions ($\mathbf{r} \in \mathbb{R}^2$), which can be reinterpreted as a phase field $\phi(\mathbf{r}) = 2\pi u(\mathbf{r})/l$, where l is the line spacing. Single lines are elastic with a given stiffness (due to the core energy cost proportional to their length) and interactions between lines are modeled within the framework of elasticity theory, such that we arrive at an *elastic* Hamiltonian describing the disorder-free array of interacting lines, which can be chosen isotropic with one elastic constant K[1], see (3.48):

$$\beta\mathcal{H}_{el}[\phi] \;=\; \frac{1}{2}\int d^2\mathbf{r}\;\left\{K(\boldsymbol{\nabla}\phi)^2\right\} \tag{8.1}$$

The lines interact with point impurities, which generate the short-ranged disorder potential $v(\mathbf{r})$, assumed to be Gaussian distributed with mean zero and correlations $\overline{v(\mathbf{r})v(\mathbf{r}')} = g_0\;\delta^2(\mathbf{r}-\mathbf{r}')$, see (3.14). In terms of the line density $\rho(\mathbf{r})$ (with average $\rho_0 = 1/l$) the interaction of the lines with the randomness is described by

$$\mathcal{H}_d[\phi] \;=\; \int d^2\mathbf{r} v(\mathbf{r})\rho[\mathbf{r},\phi(\mathbf{r})]\;. \tag{8.2}$$

In the asymptotic regime on scales beyond the positional correlation length, where the average displacement exceeds the FL spacing l, we want to preserve the discrete translational

[1] As opposed to chapter 3, we want to start directly from an *isotropic* elastic Hamiltonian for simplicity.

symmetry of the line lattice under $u(\mathbf{r}) \mapsto u(\mathbf{r}) + l$. In the periodic line array, this is vital to take the competition of different lines for the same minima of the disorder potential $v(\mathbf{r})$ correctly into account [11]. Therefore, the Poisson formula is used to take the continuum limit. As can be checked by "power counting", the first harmonic of the line density fluctuations is most relevant [9]. Keeping only the first harmonic and a gradient term describing the long-wavelength fluctuations in the density ρ, we obtain the approximation (see (3.49))

$$\rho[\mathbf{r}, \phi(\mathbf{r})] \approx \rho_0\big(1 - (\partial_x \phi(\mathbf{r}))/(2\pi\rho_0) + 2\cos\left(2\pi\rho_0 x - \phi(\mathbf{r})\right)\big) \; . \tag{8.3}$$

Finally, we arrive at the following Hamiltonian, the disorder part of which is periodic in the phase field ϕ, see (3.50-3.52),

$$\mathcal{H}[\phi] = \mathcal{H}_{el}[\phi] + \mathcal{H}_d[\phi] \tag{8.4}$$

$$= \int d^2\mathbf{r} \left\{ \frac{1}{2} K (\boldsymbol{\nabla}\phi)^2 \; - \; \mathbf{w}[\mathbf{r}] \cdot \boldsymbol{\nabla}\phi \; + \; W[\mathbf{r}, \phi(\mathbf{r})] \right\} \tag{8.5}$$

with

$$\overline{W[\mathbf{r}, \phi] W[\mathbf{r}', \phi']} = 2g \; \cos\left(\phi - \phi'\right) \; \delta^2(\mathbf{r} - \mathbf{r}') \tag{8.6}$$

$$\overline{w_i[\mathbf{r}] w_j[\mathbf{r}']} = \Delta \; \delta_{ij} \delta^2(\mathbf{r} - \mathbf{r}') \; , \tag{8.7}$$

where W and $\mathbf{w}$ are Gaussian distributed with mean zero, uncorrelated $\overline{\mathbf{w}W} = 0$, and have a (bare) strength proportional to g_0:

$$g = g_0 \rho_0^2 \frac{1}{T^2} \tag{8.8}$$

$$\Delta = g_0 \frac{1}{8\pi^2} \frac{1}{T^2} \; . \tag{8.9}$$

The Hamiltonian (8.5) defines the 2D XY model in a random symmetry breaking field of strength g. In the literature, it is often represented as the 2D random phase sine-Gordon model in writing the disorder part of the Hamiltonian as

$$\beta \mathcal{H}_d[\phi] = \int d^2\mathbf{r} 2\sqrt{g} \cos\left(\phi(\mathbf{r}) - \alpha(\mathbf{r})\right) \tag{8.10}$$

with a quenched random phase $\alpha(\mathbf{r})$, uncorrelated between different points $\overline{\alpha(\mathbf{r})\alpha(\mathbf{r}')} \propto \delta^2(\mathbf{r} - \mathbf{r}')$ and uniformly distributed at each point. For FLs, we study this model in the *absence* of vortices in the ϕ-field, which correspond to lines ending in the plane and which are excluded for energetical reasons as argued in chapter 4.

Clearly, the derivation of the Hamiltonian (8.5) applies not only to flux lines but in general to arrays of *elastic lines* with the additional ingredients of an *inter-line interaction*,

a *periodic lattice* in the ground state and a random medium containing *point disorder*. Such arrays of lines occur in a variety of physical contexts. In the field of superconductivity alone, one can think also of a thin superconducting type-II film in a parallel field [53, 77] or Josephson vortices between two planar Josephson junctions in an artificially grown SNS ("superconducting-normal-superconducting") sandwich structure [78]. In the first example, point disorder is generated by point-like defects, in the second by inhomogeneities in the thickness of the normal-conducting middle layer.

Another prominent example of elastic lines are steps on crystal surfaces. These steps possess a stiffness because they cost a certain energy per length which can be related to the number of broken bonds in the crystal lattice. These steps occur either on a miscut or *vicinal* surface, usually cut along a "high-index" crystal plane slightly misoriented with respect to a closed packed plane, where steps occur to accommodate the misorientation [Figure 8.1]. Point disorder can originate from crystalline defects in the underlying substrate, as shown for example in Figure 8.1 due to pinning of the steps by a randomly distributed ensemble of quenched screw dislocations threading the bulk of the crystal. Because double-steps are energetically costly, steps are forbidden to cross and interact via a hard-core repulsion. Along the steps of the mapping for flux lines described above, also this system can be mapped onto a 2D RFXY model. However, for steps on crystal surfaces, vortices in the ϕ-field correspond to terminating steps and are principally allowed, but require the presence of unpaired, single screw dislocations in the bulk as one can easily convince oneself with Figure 8.1.

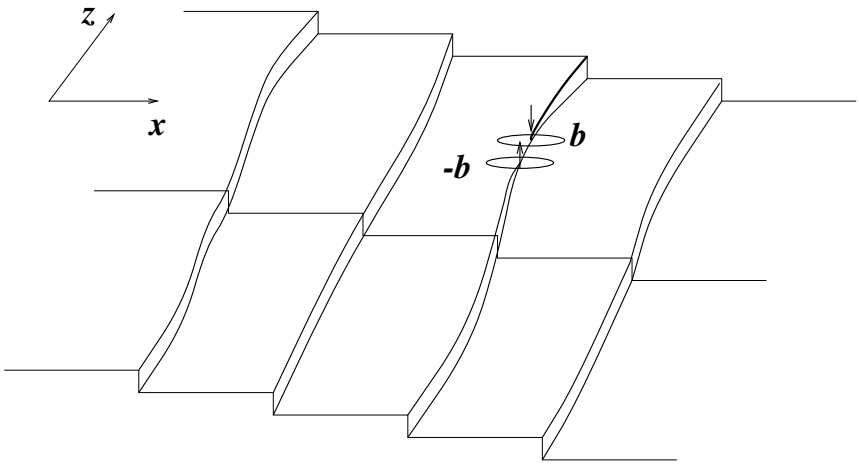

Figure 8.1: Vicinal surface (along the "high index" crystal plane $[1\bar{6}0]$) with steps due to the slight misorientation with respect to a close packed crystal plane. The two circle show a pair of quenched screw dislocations (with Burgers vectors $\mathbf{b}$ and $-\mathbf{b}$) threading the crystal-bulk and terminating at the surface that try to "pin" the step.

Let us mention another important application of the 2D RFXY model, though not directly related to steps or lines, which is the description of the roughening of a surface due to the presence of quenched bulk disorder in the crystal. Here, the ϕ-field corresponds to the height of the surface [61, 79] and the 2D RFXY model describes a (2+1)-dimensional elastic manifold which is pinned by a periodic random potential generated by the crystal planes of the disordered bulk. Because the ϕ-field is a height-field, vortices correspond to screw dislocations in the crystal.

The inclusion of vortices into the 2D RFXY model is crucial, when it is applied to disordered XY magnets, Josephson junction arrays with positional disorder, or the melting in disordered two-dimensional crystals. Only recently, interest has renewed due to new findings regarding the stability of the disordered system with respect to free vortices [80, 81] for a related model, the 2D XY model with random phase shifts, which can be obtained from the Hamiltonian given above for $W \equiv 0$, i.e., only with the random bond term coupling to the random field w.

As should be clear by now, the 2D RFXY model is one of the basic models for disordered systems in two dimensions, and of particular interest due to its applications to vortex glass phases of disordered FL arrays. So far the two-dimensional FL array is the only FL system for which the existence of a vortex glass (VG) phase has been proven analytically, namely in form of the glassy, low-temperature phase of the vortex-free 2D RFXY model [5, 53]. This is because topological imperfections are excluded in $1+1$ dimensions where the labeling of the lines, and therefore also the displacement field, is always unambiguously defined such that the elastic description in the 2D RFXY model is fully justified.

Despite all its applications, its relatively long history going back until the early 80s [18, 19, 82], and numerous analytical and numerical approaches, important features of the vortex-free 2D RFXY model are still under debate. To motivate some of the work in chapters 9 and 10, it is helpful to take a closer look into the history of this model.

All approaches are based in one or the other way on the replica method, in order to perform the average over the disorder by writing for the disorder-averaged logarithm of the partition sum

$$\overline{\ln Z} \;=\; \lim_{n\to 0} \frac{\overline{Z^n} - 1}{n} \;. \tag{8.11}$$

$\overline{Z^n}$ is the disorder-averaged partition sum of the n-times replicated system. This partition sum $\overline{Z^n} = Z_R$ corresponds to a translationally invariant replica Hamiltonian $\mathcal{H}_R[\{\phi_\alpha\}]$ depending on the fields ϕ_α in each replica (labeled by $\alpha \in \{1, \ldots, n\}$), where the averaging over the disorder induces an interaction between the replicas: Instead with a system coupling to a disorder potential, we have to deal now with a translationally invariant system consisting of n *interacting* replicas of the original system in the peculiar limit $n \downarrow 0$.

The first works [18, 19, 82] on this model use renormalization group (RG) approaches on the replica Hamiltonian $\mathcal{H}_R$. Goldschmidt and Houghton (GH) [19] employ a diagrammatic

field theoretic framework developed by Amit, Goldschmidt, and Grinstein [83] for the pure 2D sine-Gordon model, whereas Cardy and Ostlund (CO) [18] map the system onto a Coulomb gas with $n(n-1)/2$ types of $(n-1)$-dimensional vector charges, and use the formalism introduced by Kosterlitz [84] for vortices in the pure XY model. Both approaches yield the same RG equations and establish the existence of a glassy low-temperature phase for $K > K_c = 1/4\pi$ [18, 19]. In the low-temperature phase fluctuations in the ϕ-field are enhanced because the manifold can gain disorder energy in making anomalously large excursions: Toner and DiVincenzo [61] later worked out the result $\overline{\langle(\phi(\mathbf{r}) - \phi(\mathbf{r}'))^2\rangle} \propto \ln^2 |\mathbf{r} - \mathbf{r}'|$ by integrating the RG flow of the correlations as it follows from the results of CO and GH. For this $\log^2$-divergence, as compared to the log-divergence of the high-temperature phase, the glassy phase has also been termed "super-rough" phase, with regard to the above mentioned application to the roughening of a crystal surface in the presence of bulk disorder. The findings of CO and GH have been confirmed in a positional space RG in Ref. [20], and by dynamical RG treatments of a corresponding Langevin equation in Refs. [22, 23], where in addition to the super-roughness a vanishing mobility and an increased dynamical exponent $z > 2$ have been found in the low-temperature phase, further establishing the picture of a *glassy* phase.

In the RG treatment by CO and GH, the peculiar limit $n \downarrow 0$ of the replica method (8.11) can easily be taken in the RG recursion relations *after* having performed a renormalization of the divergences that occur in the perturbation theory in the thermodynamic limit. On the other hand, we know from the theory of spin glasses [85] that the procedure of the limit $n \downarrow 0$ requires some care and may involve a breaking of the replica symmetry which was tacitly assumed to be preserved in the renormalization scheme by CO and GH when performing the limit $n \downarrow 0$ in the RG equations. As we know, for example from the mean-field theory of spin glasses, this might cause an insufficient treatment of the large scale optimization that is required when many metastable or nearly degenerate minima exist in a disordered system separated in phase space by large scale excitations. Such a scenario has been further explored by applying the work of Mézard and Parisi [52] on elastic manifolds in random media to the 2D RFXY model, which provides a mean-field-like treatment where a breaking of the replica symmetry might occur to accommodate to the rough energy landscape exhibited by the model. Mézard and Parisi developed a variational approach with a replica symmetry breaking (RSB) Ansatz for the propagator of the random manifold. This method applies a Hartree-Fock like approximation to the replicated Hamiltonian $\mathcal{H}_R$ (which becomes exact in the limit of an infinite number of components of the field ϕ), to determine self-consistently a constant self-energy contribution in the propagator of $\mathcal{H}_R$. Their Ansatz for the propagator is harmonic, however they allow for a breaking of the replica symmetry which is originally present in the Hamiltonian $\mathcal{H}_R$ in their Ansatz for the self-energy. Such spontaneous breaking of the replica symmetry is known from the theory of spin glasses [85] where it correctly describes the mean-field theory of spin glasses. In

the variational approach, it amounts to approximating the full propagator of the random manifold by a *hierarchically* organized set of Gaussian propagators, i.e., describing the large scale energy landscape as a hierarchically organized set of parabolas. For random manifolds, The variational method reproduces the Flory-results for the roughness and free-energy fluctuations (see the discussion in chapter 3). Though it can be doubted that it gives the right scaling behaviour for a manifold with a low-dimensional cospace, such as the 2D RFXY model with the one-component field ϕ [for the paradigm of such a low-dimensional manifold, namely a single $1+1$-dimensional directed line in a random medium, the Flory-results are wrong], this method can be applied to the 2D RFXY model [9, 17, 21]. At low temperatures for $K > K_c$, an instability of the replica symmetric solution is found [9, 17]. Instead, Korshunov (K) [21] and Giamarchi and Le Doussal (GL) [9, 17] obtain, for $K > K_c$, a glassy low-temperature phase, the signature of which is the stability of a one-step RSB solution. The $\overline{\langle\phi\phi\rangle}$-fluctuations are also found to be enhanced in the low-temperature regime, but still a divergence $\overline{\langle(\phi(\mathbf{r}) - \phi(\mathbf{r}'))^2\rangle} \propto \ln|\mathbf{r} - \mathbf{r}'|$ is found as in the high-temperature phase; however, the prefactor of the logarithm starts to *increase* slightly upon lowering the temperature further in the low-temperature phase. Also in the framework of the self-consistent Hartree-approximation, the dynamics of the model has been studied [54], and the log-divergence of the correlations has been confirmed; in addition, a violation of the fluctuation-dissipation theorem indicates non-ergodic behaviour on large time scales, another characteristic of a glassy phase.

Although for many applications, as one can see for example in chapter 4, differences in the results of CO/GH and K/GL may be qualitatively irrelevant, this contradiction remains a puzzling theoretical problem of broad interest. Its solution, which is yet to be found, may throw some light on the validity of one or the other method: The RG approach, where replica symmetry is preserved throughout the whole calculation, and the variational approach with RSB in the low-temperature phase. In particular, it would provide a test of the concept of RSB that has still to be shown to describe correctly realistic, non-mean-field, low-dimensional glassy systems.

The difference in the results of CO/GH and K/GL for the $\overline{\langle\phi\phi\rangle}$-correlation has also led to a strong interest in a *numerical* testing of the contradictory analytical predictions [57, 58, 59, 60]. But so far no decisive answer could be given, mainly due to problems in accessing the asymptotic limit. We expect the asymptotics to be seen on scales exceeding the positional correlation length $R_l \sim (K^2/g)^{K/2(K-K_c)}$ (see (3.59)), which can be extremely large for K close to K_c and weak disorder. Note that the analytic results of CO/GH and K/GL are all derived for *weak* disorder.

Let us give an outline of the results in this part of the work regarding these open questions in the theory of the 2D RFXY model and some novel applications. Before investigating the differences between the RG approach and the self-consistent Hartree-approximation of the variational approach to the vortex-free 2D RFXY model, it will

be useful to start in the next **chapter 9** with the derivation of a set of RG equations for a generalized form of the replica Hamiltonian $\mathcal{H}_R$, as suggested in Ref. [55]. This is done using a diagrammatic method similar to that of GH. This method has the advantage that we can find also a systematic expansion of the free energy in terms of renormalized quantities, which may cause problems in the Coulomb gas representation of CO where only contributions from bound vector charge pairs can be taken into account [86]. The RG equations can be used to include various RSB schemes in the RG treatment [55], of which we discuss a one-step scheme (as found in the variational approach) in chapter 10 and to study a system consisting of two coupled 2D RFXY models, the applications of which are the subject of chapter 11.

In **chapter 10**, we present two calculations, which serve to get a better understanding of the differences between the RG approach and the self-consistent Hartree-approximation of the variational approach to the vortex-free 2D RFXY model. Firstly in **section 10.1**, we extend the replica symmetric RG calculation of CO/GH by allowing for a one-step RSB, as it is found by K/GL in the self-consistent variational calculation, and check the stability of the RG flow with respect to RSB. This is also of interest conceptually, because it opens up the possibility to study the viability of the idea of RSB in a system exhibiting strong fluctuation effects which are *not* describable by a mean-field-like theory. Rather the strong disorder and thermal fluctuations of the vortex-free 2D RFXY model can be correctly described only by a RG treatment and lead to "phases of critical points" already in the pure system [35, 87]. Similar ideas have been applied to random ferromagnets [88, 89]. We find that the renormalization group flow is *unstable* with respect to replica asymmetric perturbations, and new fixed points with a broken replica symmetry are obtained. It is possible to calculate the $\overline{\langle\phi\phi\rangle}$-correlation functions for the case of a broken replica symmetry. Interestingly, the one-step RSB scheme opens up the possibility of *both* correlations diverging as $\ln r$ and $\ln^2 r$, depending on the choice of the block size parameter m of the one-step RSB scheme. However, we are not able to identify a *physical mechanism* for the generation of the replica asymmetric perturbations which are necessary to evoke the instability. In the physical models where RSB has been found so far, such as the mean-field theory of spin glasses or the variational approach to random manifolds, the RSB parameter m is determined by *extremizing* the free energy. In both of these theories a detailed study of the fluctuations around the extremal solutions [52, 85] reveals that the stable solution *maximizes* the free energy. However, in the RG treatment of the problem, where m occurs as a free parameter initially, it is not clear a priori whether similar mechanisms are at work which sort out an "optimal" RSB parameter m by an extremization of the free energy. Nevertheless, it is possible to study the free energy of the system in the RG framework, and we obtain block size parameters m for the one-step RSB scheme, which extremize the free energy. Finally, it is possible to identify the approximations needed within the one-step RSB RG treatment to reproduce the results of the variational approach using RSB.

Secondly in **section 10.2**, we extend the self-consistent Hartree-approximation of the variational approach by accounting also for higher order vertex- and propagator-corrections, as they occur in the diagrammatic RG calculation by GH. This leads to an improved set of self-consistency equations consisting of a Dyson equation for the propagator *and* for a dressed vertex. In the replica symmetric case, the solution of the two self-consistency equations gives results *identical* to the RG treatment. In particular, it reproduces the phase transition to a low-temperature phase for $K > K_c$ which could not be obtained within the replica symmetric Hartree-approximation. For the one-step RSB case it is found that the solution obtained by K/GL no longer fulfills the extended set of self-consistency equations and has to be modified strongly with a result being similar to the RG treatment with a one-step RSB. In particular, the result hints to a $\log^2$-divergence in the $\overline{\langle\phi\phi\rangle}$-correlations.

The investigation of two coupled 2D RFXY models in **chapter 11** is also of interest regarding the glassy low-temperature phase of a single 2D RFXY model. In other disordered systems, it is already known that the introduction of two interacting *physical* replicas of a system allows to gain some knowledge about important properties of the glassy phase of the system itself, for example the properties of low-lying excitations [90, 91]. This becomes clear if one considers the system at $T = 0$, where a repulsive interaction prevents both replicas from occupying independently the ground state of the system; rather both replicas have to re-optimize and explore other low-lying states.

Furthermore, in view of the discussion of dislocations in part I, such a system represents the "toy"-model of two magnetically coupled FL layers, where we can study an instability with respect to dislocation formation leading to a decoupling on large scales by RG methods. We find good agreement with the results elaborated in chapters 4 and 5. While it is in principle possible to study also many layers by means of the RG equations derived in chapter 9, the RG flow of two layers can still be analyzed by analytical methods and a complete picture of the topology of fixed points, sinks and separatrices can be obtained.

Another application of such a system consisting of two coupled 2D RFXY models is the investigation of anisotropically reconstructed surfaces, in particular a (2×1) reconstructed gold (110) surface [92, 93]. There, we study the interplay between the roughening and deconstruction of the surface in the presence of point disorder which may again originate from crystal defects in the underlying substrate. Steps occur in this system in form of (3×1) microfacets, which can be regarded as "defects" in the (2×1) reconstruction, in terms of which the deconstruction can be described [92, 93, 94, 95] as depicted in Figure 11.1. However, *two* sorts of microfacets can occur, which will lead to a modeling by two interacting 2D RFXY models. By a detailed analysis of the RG flow derived in chapter 9, we can obtain the phase diagram of the surface. Among the findings are the stability of a flat anisotropically reconstructed surface, a novel second-order phase transition with continuously varying critical exponents, and the generic disappearance of the glassy, superrough phase which is found for a system with a single species of steps or two non-interacting

sorts of steps as discussed above. The results are also relevant to the issue of RSB in the 2D RFXY model because they demonstrate that the glassy low-temperature phase is extremely "fragile", since already a small interaction with a second "physical" replica changes the nature of the glassy phase drastically (it can even lead to a loss of the "glassiness"). Vortices cannot be excluded here as opposed to the corresponding flux line system and correspond, on the surface, to *loops* of steps. We will discuss also the stability of the surface with respect to the formation of such vortices or loops.

Chapter 9

Renormalization of a Generalized Replica Hamiltonian of the Vortex-Free 2D RFXY Model

The goal of this chapter is to derive a set of RG equations for the replica Hamiltonian of the vortex-free 2D RFXY (or, synonymously, 2D random phase sine-Gordon) model. In view of the subsequent chapters 10 and 11, it will turn out to be advantageous to study a somewhat generalized version of the replicated Hamiltonian. Conditioned by the subject, this chapter is rather technical; nevertheless, the RG equations (9.24, 9.25) for the coupling constants of the replicated vortex-free 2D RFXY model, the RG results (9.28) for the propagator and (9.34) for the free energy, which are provided in this chapter, are vital for the further analysis of the physical problems in chapters 10 and 11.

9.1 Replica Hamiltonian

The replica Hamiltonian $\mathcal{H}_R$ of the 2D RFXY model is obtained by writing the disorder averaged partition sum of the n-times replicated model $\overline{Z^n}$ as

$$\overline{Z^n} \;=\; \prod_{\alpha=1}^{n} \int \mathcal{D}\phi_\alpha(\mathbf{r}) \exp\left(-\mathcal{H}_R[\{\phi_\alpha\}]\right) . \tag{9.1}$$

Henceforth Greek indices are running from 1 to n and are replica indices. For the 2D RFXY model with the Hamiltonian (8.5), this yields in the absence of vortices in the ϕ-field

$$\mathcal{H}_R[\{\phi_\alpha\}] \;=\; \int d^2\mathbf{r} \sum_{\alpha,\beta=1}^{n} \left\{ \frac{1}{2} K_{\alpha\beta} \boldsymbol{\nabla}\phi_\alpha \cdot \boldsymbol{\nabla}\phi_\beta \;+\; g_{\alpha\beta} \cos\left(\phi_\alpha - \phi_\beta\right) \right\} . \tag{9.2}$$

Using the definitions of the random potential W (8.6) and the random field $\mathbf{w}$ (8.7), we obtain for the matrices of the coupling constants the specific (replica symmetric) forms $K_{\alpha\beta} = K\delta_{\alpha\beta} - \Delta$ and $g_{\alpha\beta} = g(1 - \delta_{\alpha\beta})$. However, as suggested in Ref. [55], we want to consider the replica Hamiltonian in its most general form as it is given by (9.2) and derive the renormalization group equations for virtually *arbitrary* matrices $K_{\alpha\beta}$ and $g_{\alpha\beta}$, only requiring that the matrices are symmetric with $g_{\alpha\alpha} \equiv 0$ and $K_{11} \equiv \ldots \equiv K_{nn}$. [The two special cases of the RG equations relevant for the analysis in chapters 10 and 11 have been obtained in Refs. [77, 86, 96].] Such a generalization will prove useful for what follows in the subsequent chapters 10 and 11.

9.2 Renormalization

In deriving the RG equations, we follow a diagrammatic approach similar to that of GH [19], which is on its part based on the RG approach to the pure 2D sine-Gordon model worked out by Amit, Goldschmidt, and Grinstein [83]. We start with the diagrammatic perturbation theory for the 2-point vertex function $\Gamma_{\alpha\beta}(k)$ by expanding in the parameters $g_{\alpha\beta}$, and isolate the divergent diagrams. The divergences can be absorbed into renormalized parameters $K^R_{\alpha\beta}$, $g^R_{\alpha\beta}$, which are properly defined on the basis of a suitably chosen renormalization condition for a renormalized 2-point vertex $\Gamma^R_{\alpha\beta}(k)$. The divergences can be systematically classified by expanding in the small parameters

$$\epsilon_{\alpha\neq\beta} \;:=\; 2 - \frac{1}{4\pi}\left(K^{-1}_{\alpha\alpha} + K^{-1}_{\beta\beta} - 2K^{-1}_{\alpha\beta}\right) \qquad (\alpha \neq \beta)\ . \tag{9.3}$$

The $\epsilon_{\alpha\beta}$ are the analog of the $\epsilon = 4 - d$ in the ϕ^4-theory [but note that opposed to the ϕ^4-theory, $\epsilon_{\alpha\beta}$ may change here under the RG transformation together with the $K_{\alpha\beta}$]. Thus, to set up a renormalized theory, we perform a double-expansion in the $\epsilon_{\alpha\beta}$ and $g_{\alpha\beta}$. The renormalized quantities $K^R_{\alpha\beta}$, $g^R_{\alpha\beta}$ are defined with respect to some arbitrarily chosen length scale serving as IR-cutoff. Usually in field theory this cutoff is provided by an arbitrarily chosen mass. In the field theory for 2D sine-Gordon models, diagrams are evaluated in position space, and we implement the IR-cutoff for simplicity by putting the system into a box of size L cutting off all real-space integrations at L. The UV-cutoff is given by the lattice constant l. Following the flow of the renormalized quantities $K^R_{\alpha\beta}$, $g^R_{\alpha\beta}$ upon a change of the scale L by a factor e^ℓ, finally gives the RG equations of the model (9.2). Pursuing this program, we start with the diagrammatic perturbation theory for the 2-point vertex function $\Gamma_{\alpha\beta}(k)$ in the parameters $g_{\alpha\beta}$. The peculiarity of sine-Gordon models is the form of the vertex in the diagrammar, which is given by the whole *power series* $g_{\alpha\beta}\cos(\phi_\alpha - \phi_\beta)$,

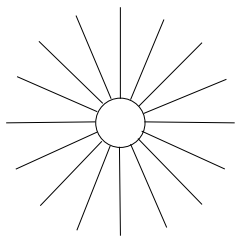

Figure 9.1: Graphical representation of the vertex.

i.e., it contains *all* powers of the field ϕ_α (which makes the treatment considerably different from a ϕ^4-theory, for example). Graphically, we represent this vertex as shown in Figure 9.1. The bare 2-point vertex function can be read off from (9.2)

$$\Gamma^{(0)}_{\alpha\beta}(k) \;=\; K_{\alpha\beta}k^2 \;=\; K_{\alpha\beta}G_0^{-1}(k)\;, \tag{9.4}$$

where we introduced the bare propagator $G_0(k) = 1/k^2$.

As already mentioned, we will mainly work in real space, and use a simple cutoff procedure in putting the system into a box of size L. The cutoff procedure introduces a geometry-dependent non-universal factor c, giving the volume of the box as $A = cL^2$. The standard choice is a circular "box" of radius L, which corresponds to $c = \pi$. Implementing the UV cutoff by the lattice with spacing l, we obtain for the Fourier-transformed $G_0(r)$ [87]

$$G_0(k) \;=\; k^{-2} \tag{9.5}$$

$$G_0(r=0) \;\simeq\; \frac{1}{2\pi}\ln\left(L/Cl\right) \tag{9.6}$$

$$G_0(0) - G_0(r) \;\simeq\; \frac{1}{2\pi}\ln\left(r/Cl\right)\;, \tag{9.7}$$

where C is a non-universal constant[1] depending on the cutoff procedure. It is convenient for the following to switch to dimensionless quantities in the Hamiltonian (9.2) by setting $\tilde{l} := Cl \equiv 1$ or absorbing factors of $\tilde{l}$ into

$$\begin{aligned} g_{\alpha\beta}\tilde{l}^2 \;&\mapsto\; g_{\alpha\beta} \\ \mathbf{r}/\tilde{l},\; L/\tilde{l} \;&\mapsto\; \mathbf{r},\; L\;. \end{aligned} \tag{9.8}$$

The corrections to the bare result (9.4) are the one-particle irreducible self-energy contributions $\Sigma_{\alpha\beta}(k)$ from the Dyson equation

$$\Gamma_{\alpha\beta}(k) = \Gamma^{(0)}_{\alpha\beta}(k) - \Sigma_{\alpha\beta}(k)\;. \tag{9.9}$$

Due to a "statistical tilt symmetry" of the problem [19, 69, 70], $\Gamma_{\alpha\beta}$ obeys the *exact* relation

$$\frac{1}{n}\sum_{\alpha\beta}\Gamma_{\alpha\beta} \equiv \frac{1}{n}\sum_{\alpha\beta}\Gamma^{(0)}_{\alpha\beta}\;, \tag{9.10}$$

and it is sufficient to consider the case $\alpha \neq \beta$ in (9.9); $\Gamma_{\alpha\alpha}(k)$ can be determined by (9.10). The symmetry (9.10), or the non-renormalization of the combination $(1/n)\sum_{\alpha\beta}\Gamma_{\alpha\beta}$, emerges in the replica language because the mode $\phi_1 \equiv \ldots \equiv \phi_n$ does *not* couple to the vertex $g_{\alpha\beta}\cos\left(\phi_\alpha - \phi_\beta\right)$, and thus the "replica center of mass" $\Phi = n^{-1/2}\sum_\alpha \phi_\alpha$ is a *free* field [19].

[1] $C \approx e^{-\gamma}/\sqrt{8}$, where γ is Euler's constant [87].

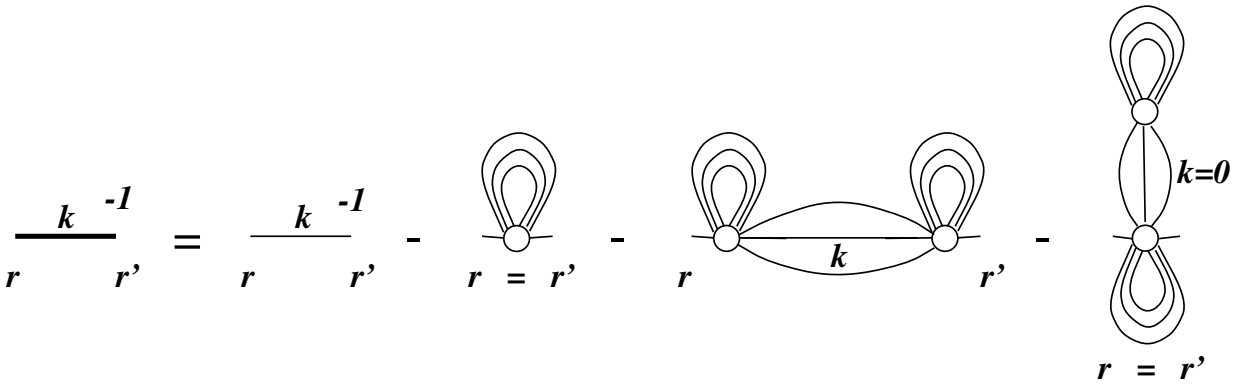

Figure 9.2: Graphical representation of the Dyson equation (9.9) up to second order in the vertex drawn in Figure 9.1. Thin lines are bare propagators $(\Gamma^{(0)})^{-1}$, the thick line the full propagator, a line^{-1} denotes the corresponding 2-point vertex function $\Gamma^{(0)}$ or Γ, respectively. The two diagrams with $\mathbf{r} = \mathbf{r}'$ are independent of k; the diagram in the middle is k-dependent.

Up to second order in the vertex, the Dyson equation (9.9) can be graphically represented as in Figure 9.2. The corresponding analytic expressions can be derived by using the following theorem for Gaussian averages of an arbitrary function $F[\{\phi_\gamma\}]$ of the fields ϕ_γ, of which $\phi_\alpha(\mathbf{r})$ and $\phi_\beta(\mathbf{r}')$ are connected to the rest of the diagram:

$$\langle \ldots F[\{\phi_\gamma\}]\rangle_{\mathrm{conn}[\phi_\alpha(\mathbf{r}),\phi_\beta(\mathbf{r}')]} = \sum_{\alpha,\beta} \int_{\mathbf{r}} \int_{\mathbf{r}'} \left\langle \ldots \phi_\alpha(\mathbf{r})\phi_\beta(\mathbf{r}') \right\rangle \left\langle \frac{\delta^2}{\delta\phi_\alpha(\mathbf{r})\delta\phi_\beta(\mathbf{r}')} F[\{\phi_\gamma\}] \right\rangle \quad (9.11)$$

or in words: If a "ϕ_α-leg" is "pulled" out of the function (or vertex) $F[\{\phi_\gamma\}]$ in a diagram, the corresponding functional derivative of $F[\{\phi_\gamma\}]$ is "left over". By using this theorem, we can derive the first order contribution $\Sigma^{(1)}_{\alpha\beta}(k)$ to the self-energy corresponding to the first, k-independent diagram in Figure 9.2:

$$\begin{aligned} \Sigma^{(1)}_{\alpha\neq\beta}(k) &= 2g_{\alpha\beta} \left\langle \cos\left(\phi_\alpha(0) - \phi_\beta(0)\right)\right\rangle_0 \\ &= L^{-2}\, 2g_{\alpha\beta} L^{\epsilon_{\alpha\beta}} \,, \end{aligned} \quad (9.12)$$

where $\langle \ldots \rangle_0$ is an average with the bare propagator obtained from (9.4). The factor $L^{\epsilon_{\alpha\beta}}$ in (9.12) yields an additional power-law divergence in the propagator $G_{\alpha\beta}$ in the thermodynamic limit and will be absorbed into the renormalized $g^R_{\alpha\beta}$. Since the first order contribution (9.12) is k-independent, corrections to the $\epsilon_{\alpha\beta}$ are of second order in the $g_{\alpha\beta}$ such that we can use the bare $\epsilon_{\alpha\beta}$ given by (9.3) in setting up the perturbation theory up to

second order. The second order contribution $\Sigma^{(2)}_{\alpha\beta}(k)$ corresponds to the last two diagrams in Figure 9.2 and is most conveniently derived first in real space (again using the theorem (9.11)) and then Fourier-transformed yielding

$$\begin{aligned}\Sigma^{(2)}_{\alpha\neq\beta}(k) \;=\; & 4\int_{(\mathbf{r}-\mathbf{r}')} e^{i\mathbf{k}\cdot(\mathbf{r}-\mathbf{r}')}\times \\ & \times\left\{\sum_{\gamma,\delta} g_{\alpha\gamma}g_{\beta\delta}\left\langle\sin\left(\phi_\gamma(\mathbf{r})-\phi_\alpha(\mathbf{r})\right)\sin\left(\phi_\delta(\mathbf{r}')-\phi_\beta(\mathbf{r}')\right)\right\rangle_{0,1\mathrm{PI}}\right\} \\ & +\; 2\int_{\mathbf{r}'}\left\{\sum_{\gamma,\delta} g_{\alpha\beta}g_{\gamma\delta}\left\langle\cos\left(\phi_\alpha(\mathbf{r})-\phi_\beta(\mathbf{r})\right)\cos\left(\phi_\gamma(\mathbf{r}')-\phi_\delta(\mathbf{r}')\right)\right\rangle_{0,1\mathrm{PI}}\right\}.\end{aligned} \tag{9.13}$$

[$\langle\ldots\rangle_{0,1\mathrm{PI}}$ shall be defined as the one-particle irreducible (1PI) contribution to the average.] While the second term is k-independent, the first term depends on k. In what follows, we split off the $(k=0)$-part $\Sigma^{(2)}_{\alpha\neq\beta}(k=0)$ containing the k-independent second term and the $(k=0)$-part of the first term of (9.13). Together with the k-independent $\Sigma^{(1)}_{\alpha\neq\beta}$ (9.12), the k-independent contribution $\Sigma^{(1)}_{\alpha\neq\beta}(k=0)+\Sigma^{(2)}_{\alpha\neq\beta}(k=0)$ to $\Sigma_{\alpha\neq\beta}$ renormalizes the vertex coupling constant $g_{\alpha\beta}$. The k-dependent part $\Sigma^{(2)}_{\alpha\neq\beta}(k)-\Sigma^{(2)}_{\alpha\neq\beta}(k=0)$ can be expanded in k, and the leading term $\propto k^2$ renormalizes the propagator coupling constant $K_{\alpha\beta}$. Before performing the renormalization, we have to isolate the singular $1/\epsilon$-divergences of these terms. After a lengthy but straightforward calculation, one finds that the only singular contribution to $\Sigma^{(2)}_{\alpha\neq\beta}(k=0)$ that does not cancel is

$$\Sigma^{(2)}_{\alpha\neq\beta}(k=0) \;\simeq\; L^{-2}\,4c\sum_{\gamma,(\alpha\neq\gamma\neq\beta)} g_{\alpha\gamma}g_{\gamma\beta}L^{\epsilon_{\alpha\gamma}+\epsilon_{\gamma\beta}}\frac{1}{\epsilon_{\gamma\beta}+\epsilon_{\alpha\gamma}-\epsilon_{\alpha\beta}}. \tag{9.14}$$

Expanding $\Sigma^{(2)}_{\alpha\neq\beta}(k)-\Sigma^{(2)}_{\alpha\neq\beta}(k=0)$, the only divergent contribution proportional to k^2 is found to be

$$\begin{aligned}\Sigma^{(2)}_{\alpha\neq\beta}(k)-\Sigma^{(2)}_{\alpha\neq\beta}(k=0) \;&=\; k^2\left.\frac{\partial}{\partial k^2}\right|_{k=0}\Sigma^{(2)}_{\alpha\neq\beta}(k)+\mathcal{O}(k^4) \\ &\simeq\; k^2\; cg^2_{\alpha\beta}L^{2\epsilon_{\alpha\beta}}\frac{1}{2\epsilon_{\alpha\beta}}+\mathcal{O}(k^4)\;.\end{aligned} \tag{9.15}$$

These divergences can be absorbed into renormalized coupling constants $K^R_{\alpha\beta}$ and $g^R_{\alpha\beta}$, in terms of which all diagrams should be free of divergences if the theory is renormalizable. The renormalized quantities are defined properly by imposing the following conditions on

the renormalized 2-point vertex $\Gamma^R_{\alpha\beta}(k)$ warranting its analycity:

$$\Gamma^R_{\alpha\neq\beta}(k=0,L) \;=\; -\Sigma^R_{\alpha\neq\beta}(k=0,L) \;=\; -2g^R_{\alpha\beta}L^{-2} \tag{9.16}$$

$$\left.\frac{\partial}{\partial k^2}\right|_{k=0}\Gamma^R_{\alpha\neq\beta}(k,L\uparrow\infty) \;=\; -\left.\frac{\partial}{\partial k^2}\right|_{k=0}\Sigma^R_{\alpha\neq\beta}(k,L\uparrow\infty) \;=\; K^R_{\alpha\beta} \tag{9.17}$$

Essentially, the conditions ensure that the prefactor of the "mass" L^{-2} (in a more refined treatment of the IR-cutoff, one would introduce a mass-term with $m^2 \sim L^{-2}$ [19]) and the elastic term stay *finite*. It follows from our perturbative calculation of the divergent contributions (9.12, 9.14, 9.15) that these conditions can be met by defining

$$g^R_{\alpha\neq\beta} \;=\; g_{\alpha\beta}L^{\epsilon_{\alpha\beta}} + 2c\sum_{\gamma,(\alpha\neq\gamma\neq\beta)}\left(g_{\alpha\gamma}L^{\epsilon_{\alpha\gamma}}\right)\left(g_{\gamma\beta}L^{\epsilon_{\gamma\beta}}\right)\frac{1}{\epsilon_{\gamma\beta}+\epsilon_{\alpha\gamma}-\epsilon_{\alpha\beta}} \tag{9.18}$$

$$K^R_{\alpha\neq\beta} \;=\; K_{\alpha\beta} - c\left(g_{\alpha\beta}L^{\epsilon_{\alpha\beta}}\right)^2\frac{1}{2\epsilon_{\alpha\beta}}\;. \tag{9.19}$$

We define analogously to (9.3) renormalized $\epsilon^R_{\alpha\beta}$ using $K^R_{\alpha\neq\beta}$. Equations (9.18) and (9.19) yield immediately the following β-functions:

$$\begin{aligned}\beta^g_{\alpha\neq\beta}\left(\{g^R_{\sigma\rho},\;K^R_{\sigma\rho}\}\right) \;&\equiv\; \frac{dg^R_{\alpha\beta}}{d\ln L}\\ &=\; \epsilon^R_{\alpha\beta}g^R_{\alpha\beta} + 2c\sum_{\gamma,(\alpha\neq\gamma\neq\beta)}g^R_{\alpha\gamma}g^R_{\gamma\beta} + \;\mathcal{O}\left(\left(g^R\right)^3,\epsilon^R\left(g^R\right)^2\right)\end{aligned} \tag{9.20}$$

$$\begin{aligned}\beta^K_{\alpha\neq\beta}\left(\{g^R_{\sigma\rho},\;K^R_{\sigma\rho}\}\right) \;&\equiv\; \frac{dK^R_{\alpha\beta}}{d\ln L}\\ &=\; -c\left(g^R_{\alpha\beta}\right)^2 + \;\mathcal{O}\left(\left(g^R\right)^3,\epsilon^R\left(g^R\right)^2\right)\end{aligned} \tag{9.21}$$

The β-functions give the RG equations of the coupling constants under a change of scale $L \mapsto Le^{\ell}$. It is convenient to define (remember that we included the factor $\tilde{l}^2$ into $g_{\alpha\beta}$ already in (9.8))

$$\begin{aligned}\tilde{g}_{\alpha\beta} \;&:=\; 4c(\tilde{l}^2 g_{\alpha\beta})\\ \tilde{K}_{\alpha\beta} \;&:=\; 8cK_{\alpha\beta}\;.\end{aligned} \tag{9.22}$$

Furthermore, the tilt symmetry (9.10) yields (to all orders) the *exact* result

$$\beta^K_{\alpha\alpha} \;\equiv\; -\frac{1}{n}\sum_{\gamma\neq\delta}\beta^K_{\gamma\delta}\;, \tag{9.23}$$

and we obtain finally the following set of RG equations

$$\begin{aligned}\frac{d\tilde{g}_{\alpha\neq\beta}}{d\ell} &= 4c\beta^{g}_{\alpha\neq\beta}\left(\left\{\tilde{g}_{\sigma\rho}/4c,\ \tilde{K}_{\sigma\rho}/8c\right\}\right) \\ &= \epsilon_{\alpha\beta}\tilde{g}_{\alpha\beta}+\frac{1}{2}\sum_{\gamma,(\alpha\neq\gamma\neq\beta)}\tilde{g}_{\alpha\gamma}\tilde{g}_{\gamma\beta} \qquad (9.24)\\ \frac{d\tilde{K}_{\alpha\beta}}{d\ell} &= 8c\beta^{K}_{\alpha\neq\beta}\left(\{\tilde{g}_{\sigma\rho}/4c\}\right) \\ &= \begin{cases} -\frac{1}{2}\left(\tilde{g}_{\alpha\beta}\right)^2 & (\alpha\neq\beta) \\ \frac{1}{2n}\sum_{\gamma\neq\delta}\left(\tilde{g}_{\gamma\delta}\right)^2 & (\alpha=\beta)\ . \end{cases} \qquad (9.25)\end{aligned}$$

Notice that the $\epsilon_{\alpha\beta}$ depend on $K_{\alpha\beta}$ by (9.3) and feed back into the RG equation for $\tilde{g}_{\alpha\beta}$ in general. These RG equations are valid as long as $\epsilon_{\alpha\beta}(\ell)\ll 1$ and $\tilde{g}_{\alpha\beta}(\ell)\ll 1$ so that our double-expansion in these parameters is justified. In Refs. [77, 86, 96], the same RG equations (9.24, 9.25) have been derived for various sub-cases by means of a Coulomb gas representation of the cos-coupling in (9.2) in terms of $n(n-1)/2$ types of interacting vector charges.

9.3 Correlation Functions

With the above results, we can calculate the asymptotic behaviour of the $\langle\phi\phi\rangle$-correlation function

$$\langle\phi_\alpha(\mathbf{k})\phi_\beta(\mathbf{k}')\rangle = (2\pi)^2\delta^2(\mathbf{k}+\mathbf{k}')\ G_{\alpha\beta}(k) \qquad (9.26)$$

with the propagator $G_{\alpha\beta}(k)=\Gamma^{-1}_{\alpha\beta}(k)$. Solving the RG (Callan-Symanzik) equation of the 2-point vertex function $\Gamma_{\alpha\beta}(k)$ yields

$$\Gamma_{\alpha\beta}\left(k,\ \{g_{\sigma\rho},\ K_{\sigma\rho}\}\right)\simeq\ e^{-2\ell}\Gamma^R\left(ke^{\ell},\{g_{\sigma\rho}(\ell),\ K_{\sigma\rho}(\ell)\}\right)$$

and in the asymptotic limit with $\ell=\ln(1/kl)$

$$\begin{aligned}&\simeq\ (kl)^2\Gamma^R\left(\frac{1}{l},\left\{g_{\sigma\rho}\left(\ell=\ln\tfrac{1}{kl}\right),\ K_{\sigma\rho}\left(\ell=\ln\tfrac{1}{kl}\right)\right\}\right)\\ &\simeq\ k^2K_{\alpha\beta}\left(\ell=\ln\frac{1}{kl}\right)\ . \qquad (9.27)\end{aligned}$$

The large scale behaviour of the propagator is obtained by inverting the 2-point vertex function:

$$G_{\alpha\beta}(k) \;\simeq\; k^{-2}\; K^{-1}_{\alpha\beta}\left(\ell{=}\ln\frac{1}{kl}\right)\;. \tag{9.28}$$

Apart from this RG relation, the statistical tilt symmetry of the problem [19, 69, 70] gives an additional *exact* result for the propagator of the *free* "replica center of mass" field Φ,

$$\frac{1}{n}\sum_{\alpha\beta} G_{\alpha\beta}(k) \;=\; \frac{1}{n}\sum_{\alpha\beta} G^{(0)}_{\alpha\beta}(k) \;=\; \frac{1}{n}\sum_{\alpha\beta}\frac{K^{-1}_{\alpha\beta}(\ell=0)}{k^2}\;, \tag{9.29}$$

which follows directly from (9.10).

9.4 Free Energy

One advantage of the diagrammatic approach to the RG presented here over the Coulomb gas representation of the cos-coupling in terms of vector charges is to enable a more systematic expansion of the free energy. This aspect of the problem becomes important in the next chapter 10 in the context of RSB, where it is generally believed that the extremum of the free energy determines the choice for the RSB-scheme. In the Coulomb gas picture only the renormalization of the free energy from contributions due to bound vector charge pairs can be considered [86]. The leading order contributions from such pairs are of the order $\mathcal{O}(g^2_{\alpha\beta})$, whereas free unbound charges may give already a contribution $\mathcal{O}(g_{\alpha\beta})$ as it occurs also in the variational approach to leading order [21]. This potential drawback of the Coulomb gas representation is circumvented in the diagrammatic RG approach where we can expand the free energy systematically in powers of $g_{\alpha\beta}$, and re-sum the resulting perturbation series in terms of the renormalized $g^R_{\alpha\beta}$.

The perturbation theory for the free energy $F = -\log\overline{Z^n}$[2] of the replicated system up to second order in the vertex can be graphically represented by Figure 9.3. The diagrams correspond to the expression

$$\begin{aligned} F \;=\; F^{(0)} &- \int_{\mathbf{r}}\left\{\sum_{\alpha\beta} g_{\alpha\beta}\left\langle\cos\left(\phi_\alpha(\mathbf{r})-\phi_\beta(\mathbf{r})\right)\right\rangle_0\right\} \\ &- \frac{1}{2}\int_{\mathbf{r}}\int_{\mathbf{r}'}\left\{\sum_{\alpha\beta}\sum_{\gamma\delta} g_{\alpha\beta}g_{\gamma\delta}\left\langle\cos\left(\phi_\alpha(\mathbf{r})-\phi_\beta(\mathbf{r})\right)\cos\left(\phi_\gamma(\mathbf{r}')-\phi_\delta(\mathbf{r}')\right)\right\rangle_{0,\mathrm{conn}}\right\}, \end{aligned} \tag{9.30}$$

where $F^{(0)}$ is he bare Gaussian free energy of the disorder-free model.

[2] Strictly speaking, this is the free energy divided by T.

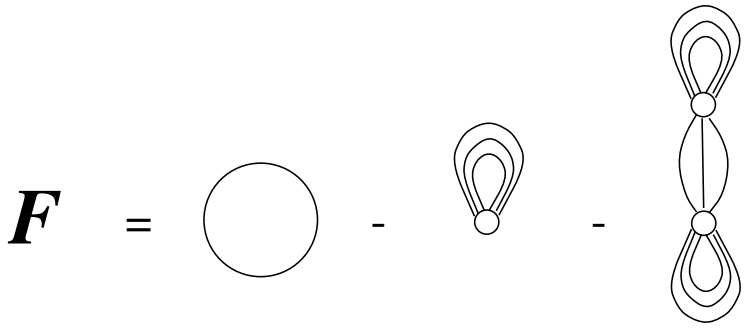

Figure 9.3: Graphical representation of the perturbation series (9.30) for the free energy up to second order in the vertex. The circle (closed bare propagator) represents the bare Gaussian free energy of the disorder-free model.

The divergent terms of the series for the free energy difference $\Delta F = F - F^{(0)}$ with respect to the disorder-free Gaussian model can be re-summed similarly to the $(k = 0)$-part of the 2-point vertex function. Using our above choice (9.18) for the renormalized $g^R_{\alpha\beta}$, we obtain

$$\begin{aligned}
\Delta F &= F - F^{(0)} \\
&\simeq -\sum_{\alpha\neq\beta} c g_{\alpha\beta} L^{\epsilon_{\alpha\beta}} \\
&\quad - 4c^2 \sum_{\alpha\neq\beta} \sum_{\gamma,(\alpha\neq\gamma\neq\beta)} g_{\alpha\beta} g_{\alpha\gamma} L^{\epsilon_{\alpha\beta}+\epsilon_{\alpha\gamma}} \frac{1}{\epsilon_{\alpha\beta}+\epsilon_{\alpha\gamma}-\epsilon_{\gamma\beta}} \\
&\simeq F^{(0)} - \sum_{\alpha\neq\beta} c g^R_{\alpha\beta} \, .
\end{aligned} \tag{9.31}$$

We recognize that the free energy is renormalized already by the same partial re-summation of diagrams leading to the expression (9.18) for the renormalized $g^R_{\alpha\beta}$ except for the divergence stemming from the bare Gaussian contribution $F^{(0)}$.

This leads to the following RG equation for the free energy density f of a system with UV-cutoff l

$$\Delta f\left(l, \{\tilde{g}_{\sigma\rho},\ \tilde{K}_{\sigma\rho}\}\right) = \tag{9.32}$$

$$\simeq \Delta f\left(le^{\ell}, \{\tilde{g}_{\sigma\rho}(\ell),\ \tilde{K}_{\sigma\rho}(\ell)\}\right) - \left(le^{\ell}\right)^{-2} \frac{1}{4} \sum_{\alpha\neq\beta} \tilde{g}_{\alpha\beta}(\ell) \tag{9.33}$$

and in the thermodynamic limit with $\ell = \ln(L/l) \uparrow \infty$ to

$$\begin{aligned} \simeq \ \text{const} \ + \ L^{-2} \ \tfrac{1}{2} \ln \left(\det_{\alpha\beta} \tilde{K}_{\alpha\beta} \left(\ell = \ln \tfrac{L}{l} \right) \right) \ - \\ - \ L^{-2} \ \tfrac{1}{4} \sum_{\alpha \neq \beta} \tilde{g}_{\alpha\beta} \left(\ell = \ln \tfrac{L}{l} \right) \ . \end{aligned} \tag{9.34}$$

Thus, Δf is determined solely by the RG asymptotics, i.e., the RG fixed points if they exist, of $\tilde{g}_{\alpha\beta}(\ell \uparrow \infty)$ and $\tilde{K}_{\alpha\beta}(\ell \uparrow \infty)$.

The main goal of this chapter has been to provide the above RG equations (9.24, 9.25) and the relations (9.28, 9.34). In the subsequent chapters 10 and 11, we will perform a thorough analysis of the RG flow for two sub-cases of (9.24, 9.25) [these two special cases of the RG equations have been obtained in Refs. [77, 86, 96]]. For potential applications of these equations, it is important to note that the structure of the matrix $g_{\alpha\beta}$ has been left entirely unspecified apart from requiring symmetry (and $g_{\alpha\alpha} \equiv 0$, $K_{11} \equiv \ldots \equiv K_{nn}$). In particular, it will be possible to generalize from the "auxiliary" replicas of the replica trick (8.11) to "physical" replicas of the model in chapter 11.

Chapter 10

Replica Symmetry Breaking and Renormalization of the Vortex-Free 2D RFXY Model

In the two parts of this chapter we present in each an approach, which aims at clarifying the differences between the two basic approaches to the vortex-free 2D RFXY model, the RG approach of CO/GH [18, 19] and the self-consistent variational approach with RSB of K/GL [9, 17, 21]. In the first part of this chapter, we extend the replica symmetric RG calculation of CO/GH by allowing for a one-step RSB, as it is found by K/GL in the self-consistent variational calculation and check the stability of the RG flow with respect to RSB. In the second part, we develop a self-consistent diagrammatic approach to the problem, which goes beyond the self-consistent Hartree-approximation of the variational approach by accounting also for vertex-corrections, as they occur in the diagrammatic RG calculation presented in the previous chapter 9.

10.1 Replica Symmetry Breaking in Renormalization

In this section, we study how the concept of RSB could enter into the RG analysis of the vortex-free 2D RFXY model. Equipped with the flow equations for the generalized replica Hamiltonian (9.2) derived in the previous chapter 9, we can analyze the behaviour of different RSB schemes under the RG treatment by choosing an appropriate Ansatz for the couplings $g_{\alpha\beta}$, $K_{\alpha\beta}$ *before* performing the subtle limit $n \downarrow 0$ of the replica method (8.11). However, it is important to note that the bare unrenormalized couplings $g_{\alpha\beta}(\ell=0)$

and $K_{\alpha\beta}(\ell=0)$, as they are obtained from the very definition of the vortex-free 2D RFXY model, (8.5, 8.6, 8.7) are *replica symmetric* and of the form

$$K_{\alpha\beta} = K\delta_{\alpha\beta} - \Delta \tag{10.1}$$

$$g_{\alpha\beta} = \begin{cases} g & (\alpha \neq \beta) \\ 0 & (\alpha = \beta)\ . \end{cases} \tag{10.2}$$

Therefore, this represents also the natural replica symmetric Ansatz for the coupling matrices in the RG analysis as it was used by CO/GH. Furthermore, replica symmetry is *conserved* under the RG flow as can be checked with the general RG equations (9.24, 9.25). Exploiting the statistical tilt symmetry (9.29) [69, 70] of the 2D RFXY model, one finds that K is unrenormalized. Because of $K \propto 1/T$,

$$\tau_0 := 1 - \frac{K_c}{K} \quad \text{with} \quad K_c = \frac{1}{4\pi} \tag{10.3}$$

defines a *negative reduced temperature*, which is *not* renormalized. $2\tau_0$ is the the expansion parameter $2\tau_0 = \epsilon_{\alpha\neq\beta}$ (9.3) of the renormalization scheme as introduced in the last chapter 9 and classifies the divergences of the corresponding field theory. Employing the RG equations (9.24, 9.25), we reproduce for the set of dimensionless parameters (9.22) $\tilde{\Delta} := 8c\Delta$ (similarly we define $\tilde{K}_c := 8cK_c$), $\tilde{g} := 4c\tilde{l}^2 g$ and τ_0 the RG equations of CO/GH, for which we can perform easily the peculiar limit $n \downarrow 0$ of the replica trick (8.11) [see also part I, (4.20), CO/GH use $c = \pi$ corresponding to a circular IR-cutoff]:

$$\frac{d\tilde{g}}{d\ell} = 2\tau_0\tilde{g} + \frac{n-2}{2}\tilde{g}^2 \overset{n\downarrow 0}{\to} 2\tau_0\tilde{g} - \tilde{g}^2 \tag{10.4}$$

$$\frac{d\tilde{\Delta}}{d\ell} = \frac{1}{2}\tilde{g}^2 \tag{10.5}$$

$$\frac{d\tau_0}{d\ell} = \frac{n}{2\tilde{K}_c}(1-\tau_0)^2\tilde{g}^2 \overset{n\downarrow 0}{\to} 0\ . \tag{10.6}$$

These flow equations are valid as long as $\tau_0 \ll 1$ and $\tilde{g}(\ell) \ll 1$.

The physical properties of the vortex-free 2D RFXY model are essentially encoded in the RG flow of the disorder strength g [Figure 10.1] and change at a critical value $K = K_c$ or at the temperature $\tau_0 = 0$. It is interesting to note that $\tilde{\Delta}$ does *not* feed back into the RG flow of $\tilde{g}$. This is due to the fact that the random bond field $\mathbf{w}$ in the Hamiltonian (8.5) can be shifted away by the transformation $\phi'(\mathbf{r}) = \phi(\mathbf{r}) - \sigma(\mathbf{r})$ with $K\boldsymbol{\nabla}^2\sigma = \boldsymbol{\nabla}\cdot\mathbf{w}$ [70]. For $\tau_0 < 0$ or $K < K_c$, the model is in a high-temperature phase, where the disorder strength $\tilde{g}$ is irrelevant on large scales and the Gaussian fixed point $\tilde{g}^* = 0$ stable. Therefore, properties of the model in the high-temperature phase are essentially identical to those of the disorder-free Gaussian model in 2D. However, for $\tau_0 > 0$ or $K > K_c$ in the low-temperature phase, a *line* of disorder-dominated fixed points

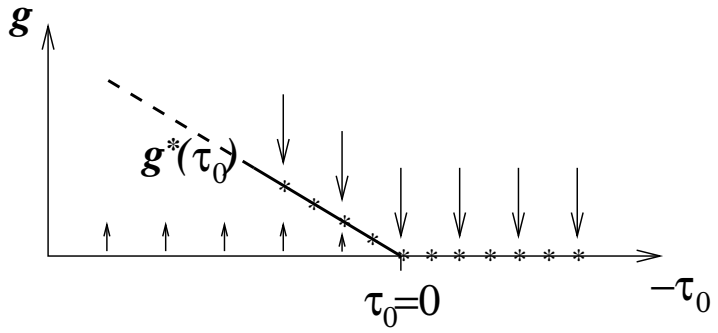

Figure 10.1: Replica symmetric RG flow as found by CO.

$\tilde{g}^*(\tau_0) = 2\tau_0$ becomes attractive, which can be interpreted as fixed points characterizing a *glassy* phase, and $\tilde{\Delta}$ exhibits asymptotically the characteristic "runaway-flow" $\tilde{\Delta}(\ell) \sim 2\tau_0^2\ell$ [which does not affect the flow of the other parameters as discussed above]. Right at $\tau_0 = 0$, the disorder is marginally irrelevant and $\tilde{g}(\ell) \propto 1/\ell$.

Using the RG result (9.28) for the propagator in the low-temperature phase $\tau_0 > 0$ (in the limit $n \downarrow 0$),

$$G_{\alpha\beta}(k) \;\simeq\; \delta_{\alpha\beta}\frac{1}{Kk^2} + \frac{\Delta(\ell=\ln(\frac{1}{kl}))}{K^2k^2} \;\propto\; \tau_0^2\frac{\ln(1/kl)}{k^2}\;, \tag{10.7}$$

a direct consequence of the "runaway-flow" of $\tilde{\Delta}(\ell)$ is the "super-roughness" [61]

$$\overline{\langle(\phi(\mathbf{r})-\phi(0))^2\rangle} \;=\; \int d^2\mathbf{k}\; 2(1-\cos(\mathbf{k}\cdot\mathbf{r}))G_{\alpha\alpha}(k) \propto \tau_0^2\ln^2(r/l) \tag{10.8}$$

in the phase- or displacement-correlations. Although Δ does not feed back into the RG flow of the other parameters, it determines the divergence of the $\overline{\langle\phi\phi\rangle}$-correlations. On the other hand, due to the statistical tilt symmetry (9.29), the thermal fluctuations of ϕ given by the *connected* correlations

$$\begin{aligned}\overline{\langle(\phi(\mathbf{r})-\phi(0))^2\rangle_{\rm conn}} \;&=\\ &= \int d^2\mathbf{k}\; 2(1-\cos(\mathbf{k}\cdot\mathbf{r}))\left(\lim_{n\to 0}\frac{1}{n}\sum_{\alpha,\beta}G_{\alpha\neq\beta}(k)\right)\\ &= 4(1-\tau_0)\ln(r/l)\end{aligned} \tag{10.9}$$

are unrenormalized by the disorder and identical to the $\langle\phi\phi\rangle$-correlations of the disorder-free Gaussian model, which diverge as $\ln r$. In the high-temperature phase $\tau_0 < 0$, disorder is irrelevant, and we obtain as in the disorder-free system $\overline{\langle(\phi(\mathbf{r})-\phi(0))^2\rangle} \simeq \overline{\langle(\phi(\mathbf{r})-\phi(0))^2\rangle_{\rm conn}} \propto \ln r$.

So far we recapitulated the RG analysis of CO with a replica symmetric Ansatz for the couplings $g_{\alpha\beta}$ and $K_{\alpha\beta}$. Armed with the powerful tool of the general RG equations (9.24, 9.25), it is now possible to explore various RSB schemes *within* the RG analysis. Whereas it was demonstrated in Ref. [55] that even continuous RSB can be included, we want to analyze in this section in detail the case of a one-step RSB, as it occurs also in the variational approach by K/GL as stable solution for a harmonic RSB propagator. Technically speaking, the origin of a RSB may be connected to a proper treatment of the subtleties involved in taking the limit $n \downarrow 0$. In particular, the classification of the divergences in the RG calculation, which is done in the thermodynamic limit, is performed *before* the limit $n \downarrow 0$. However, it is difficult to sketch a "physical picture" underlying the RSB. Let us compare the situation with the theory of random ferromagnets, where similar ideas regarding RSB in a RG analysis have been applied to the RG in $4 - \epsilon$ dimensions [88, 89]. For such systems, it has been argued [88, 89] that RSB effects come from the multiple local minima solutions of the mean-field equations; the RG treats fluctuations in an expansion around these minima and thus "inherits" RSB in the initial values of the RG flow from the mean-field solution. It is an important difference of those approaches compared to the situation in the 2D RFXY model that due to the pronounced fluctuations typical for a two-dimensional system, even a "local" description by a mean-field theory is impossible in the 2D RFXY model. Therefore, the energy landscape is rather "smeared out" by thermal fluctuations, and it is unclear what physical mechanism can be responsible for a breaking of the replica symmetry in the initial couplings $g_{\alpha\beta}(\ell=0)$ and $K_{\alpha\beta}(\ell=0)$. We will further discuss this question below along with an analysis of the large scale behaviour of the free energy. We start our discussion of RSB in the RG approach with a discussion of the consequences of a replica asymmetric perturbation, that is put into the bare values of the couplings $g_{\alpha\beta}(\ell=0)$ "by hand".

10.1.1 RG Analysis of a One-Step RSB

In order to investigate a one-step RSB scheme within the RG analysis, we generalize to Parisi-type [85] coupling matrices of the form

$$K_{\alpha\beta} = K\delta_{\alpha\beta} + K_m\widetilde{\delta}_{\alpha\beta} - \Delta \tag{10.10}$$

$$g_{\alpha\beta} = \begin{cases} g_1\widetilde{\delta}_{\alpha\beta} + g_2\left(1 - \widetilde{\delta}_{\alpha\beta}\right) & (\alpha \neq \beta) \\ 0 & (\alpha = \beta)\ . \end{cases} \tag{10.11}$$

The matrix $\widetilde{\delta}_{\alpha\beta}$ is specified by the *RSB parameter* m determining the block size of the one-step RSB matrices. Elements of the matrix $\widetilde{\delta}_{\alpha\beta}$ are 1 if α and β belong to the same block of size m and 0 otherwise:

$$\widetilde{\delta}_{\alpha\beta} := \begin{cases} 1 & \alpha = \beta \ (\mathrm{mod}\ m) \\ 0 & \alpha \neq \beta \ (\mathrm{mod}\ m)\ . \end{cases} \tag{10.12}$$

Applying the general RG equations (9.24, 9.25), one can check that the one-step Parisi-type form of the couplings is *conserved* under the RG flow. The statistical tilt symmetry (9.29) [69, 70] yields the *invariant* quantity

$$\tau_m \;:=\; 1 - \frac{K_c}{K + mK_m} \quad \text{with} \quad K_c \;=\; \frac{1}{4\pi}\;, \tag{10.13}$$

which defines analogously to τ_0 in the replica symmetric case a negative reduced temperature. Similarly, we define a reduced elasticity parameter

$$\kappa \;:=\; 1 - \frac{K_c}{K}\;. \tag{10.14}$$

κ and τ_m are the expansion parameters $\epsilon_{\alpha\neq\beta}$ (9.3) in the RG calculation of chapter 9. The RG equations (9.24, 9.25) derived in chapter 9, take on the following form for the coupling constants κ, τ_m, $\tilde{\Delta} = 8c\Delta$ ($\tilde{K}_c := 8cK_c$), $\tilde{g}_i := 4c\tilde{l}^2 g_i$ ($i = 1, 2$), and the limit $n \downarrow 0$ is performed straightforwardly [the same set of equations has been obtained in Ref. [86] by a mapping onto a Coulomb gas of vector charges]:

$$\frac{d\tilde{g}_1}{d\ell} \;=\; 2\kappa\tilde{g}_1 - \frac{2-m}{2}\tilde{g}_1^2 - \frac{m}{2}\tilde{g}_2^2 \tag{10.15}$$

$$\frac{d\tilde{g}_2}{d\ell} \;=\; \frac{2}{m}\left(\tau_m - (1-m)\kappa\right)\tilde{g}_2 - m\tilde{g}_2^2 - (1-m)\tilde{g}_1\tilde{g}_2 \tag{10.16}$$

$$\frac{d\kappa}{d\ell} \;=\; \frac{1}{2\tilde{K}_c}(1-\kappa)^2 m\left(\tilde{g}_1^2 - \tilde{g}_2^2\right) \tag{10.17}$$

$$\frac{d\tilde{\Delta}}{d\ell} \;=\; \frac{1}{2}\tilde{g}_2^2 \tag{10.18}$$

$$\frac{d\tau_m}{d\ell} \;=\; 0\;. \tag{10.19}$$

These flow equations are valid for $\tau_m,\ \kappa(\ell) \ll 1$ and $\tilde{g}_i(\ell) \ll 1$. As already discussed for the replica symmetric case and for the same reasons given above, $\tilde{\Delta}$ does not feed back into the RG flow of the other quantities. For the moment, m is a *free* parameter in the RG equations with $0 \leq m \leq 1$ in the limit $n \to 0$. In the mean-field theory of spin glasses [85] or the variational approach to random manifolds [52], the stable solution of the self-consistency equations turns out to maximize the free energy of the system. A naive adaption of these results would suggest that m can be determined by maximizing the free energy. Possible choices for m, based on an analysis of the free energy, will be discussed below.

The replica symmetric RG flow (10.4-10.6) is reproduced for $m = 1$ and $m = n \downarrow 0$ if the invariant negative reduced temperatures are identical $\tau_m = \tau_0$ [note that at $m = 0$ also $\kappa = \tau_m$ is invariant]. In the RG equations for $m = 1$ [$m = 0$], $\tilde{g}_2$ [$\tilde{g}_1$] plays the role of the single disorder strength parameter $\tilde{g}$ of the replica symmetric flow. Also the off-diagonal

matrix elements Δ $[K_m + \Delta]$ and $\tilde{g}_2$ $[\tilde{g}_1]$ renormalize as in in the replica symmetric case. The system exhibits the known fixed points $\tilde{g}_2^* = 0$ $[\tilde{g}_1^* = 0]$ and $\tilde{g}_2^* = 2\tau_m$ $[\tilde{g}_1^* = 2\tau_m]$. For $m = 1$, the RG flow is sketched in Figure 10.2a. $\tilde{g}_1$ $[\tilde{g}_2]$ does not feed back into the RG flow of the other quantities and does therefore not enter physical results like correlation functions (see below). For this reason the introduction of a small replica asymmetric perturbation

$$\Delta g = g_1 - g_2 \tag{10.20}$$

has no effect on physical results if $m = 1$ $[m = 0]$, although Δg turns out to be a relevant perturbation under RG as we will see.

Let us also stress once again that, *independently* of the value of m, the replica symmetric subspace given by $\tilde{g}_1 \equiv \tilde{g}_2 \equiv \tilde{g}$ and $\kappa \equiv \tau_m$ is *closed* also under the one-step RSB RG flow (10.15-10.19). Within this subspace one finds the *trivial fixed point* $\tilde{g}_1^* = \tilde{g}_2^* = 0$ and the *replica symmetric CO fixed point*

$$\tilde{g}_1^* = \tilde{g}_2^* = 2\tau_m \quad , \quad \kappa^* = \tau_m \tag{CO}$$

However, what happens to the RG flow when we introduce a small RSB perturbation $\Delta g(\ell = 0) \neq 0$ of the bare parameters $g_{\alpha\beta}(\ell = 0)$ if $0 < m < 1$? Then, the RG flow (10.15-10.19) develops for $\tau_m > 0$ an *instability* with respect to RSB. The system flows for $\Delta\tilde{g}(0) > 0$ to a regime with $\tilde{g}_1 > \tilde{g}_2$ and for $\Delta\tilde{g}(0) < 0$ to a regime $\tilde{g}_1 < \tilde{g}_2$, entering on large length scales the unphysical regime of negative disorder strengths $\tilde{g}_1$. In particular, the replica symmetric CO fixed point (CO) is *unstable* against small replica asymmetric perturbations. A linear stability analysis of the CO fixed point yields ($\Delta\kappa = \kappa - \tau_m$)

$$\frac{d\Delta\kappa}{d\ell} = m\frac{2}{\tilde{K}_c}(1-\tau_m)^2\tau_m \; \Delta\tilde{g} \tag{10.21}$$

$$\frac{d\Delta\tilde{g}}{d\ell} = 2\frac{1}{m}4\tau_m \; \Delta\kappa \; . \tag{10.22}$$

These equations describe an instability of the CO fixed point with respect to perturbations $\Delta\tilde{g}$ with a positive crossover exponent λ_m

$$\lambda_m = \sqrt{8/\tilde{K}_c}(1-\tau_m)\tau_m > 0 \; . \tag{10.23}$$

Note that λ_m vanishes upon approaching the transition $\tau_m \downarrow 0$ indicating that such an RSB instability is *absent* in the high-temperature phase $\tau_m < 0$. To avoid entering the unphysical regime of negative $\tilde{g}_1$, we consider only perturbations $\Delta\tilde{g}(0) > 0$. As it is seen from (10.21, 10.22), such a perturbation causes the reduced elasticity parameter κ and the replica asymmetry $\Delta\tilde{g}$ to increase. As we will see below, κ is renormalized towards $\kappa^* = 1$ following (10.17) and $\Delta\tilde{g} \sim \mathcal{O}(\kappa^*)$ following (10.15, 10.16). This demonstrates that upon

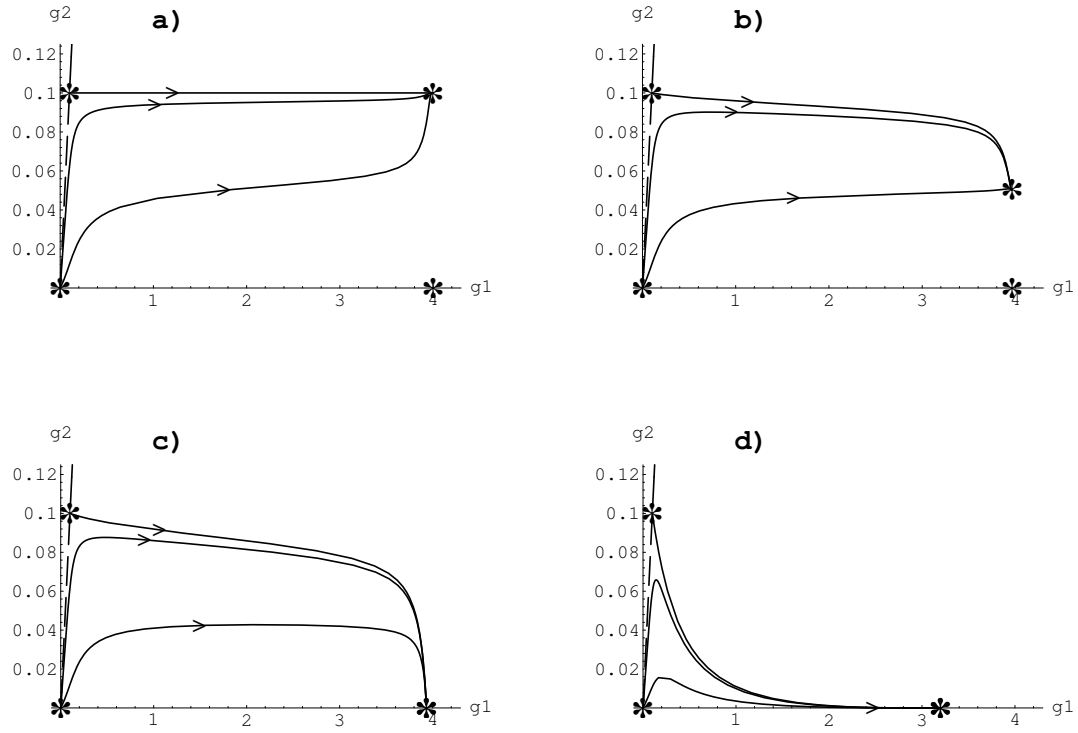

Figure 10.2: RG flow trajectories for $\tau_m = 0.05$ and different values of m with an initial replica asymmetry $\Delta\tilde{g}(0) = \tilde{g}_1(0) - \tilde{g}_2(0) = \tau_m^2$; a) $m = 1$, b) $m = (1 + m^*)/2$, c) $m = m^*$, d) $m = 1 - 5\tau_m$. The dashed line is the line $\tilde{g}_1 = \tilde{g}_2$ of replica symmetric values. The trivial fixed point and the replica symmetric fixed point (CO) are located on this line. The RSB fixed points (RSB1) (upper right fixed point) and (RSB2) (lower right fixed point) are plotted as well.

the instability the RG flow is attracted by a novel RG sink characterized by a *strong RSB* with $\kappa^* = 1$, which implies a strongly enhanced stiffness $K \uparrow \infty$.

We can find from (10.15, 10.16) two additional non-trivial RSB fixed points (RSB1) and (RSB2) with $\kappa^* = 1$ in the physical regime $\tilde{g}_2 > 0$:

$$\tilde{g}_1^* = 2\kappa^* - \frac{2(1-m)}{m}(\kappa^* - \tau_m) + 2(\kappa^* - \tau_m)\left(1 - \frac{2}{m} + \frac{2}{\kappa^* - \tau_m}\right)^{1/2}$$

$$\tilde{g}_2^* = 2\kappa^* - \frac{2(2-m)}{m}(\kappa^* - \tau_m) - \frac{2(1-m)}{m}(\kappa^* - \tau_m)\left(1 - \frac{2}{m} + \frac{2}{\kappa^* - \tau_m}\right)^{1/2}$$

$$\kappa^* = 1 \qquad \text{(RSB1)}$$

and

$$\begin{aligned} \tilde{g}_1^* &= \frac{4\kappa^*}{2-m} \\ \tilde{g}_2^* &= 0 \\ \kappa^* &= 1 \ . \end{aligned} \tag{RSB2}$$

At a certain

$$m^* = 1 - \tau_m/3 + \mathcal{O}(\tau_m^2) \ , \tag{10.24}$$

the fixed points (RSB1) and (RSB2) fall exactly together. These fixed points are still perturbative in κ and τ_m, but due to the flow of $\kappa(\ell) \uparrow \kappa^* = 1$, the fixed point $\tilde{g}_1^*$ becomes of order unity and we obtain a strong RSB $\Delta\tilde{g} \sim \mathcal{O}(\kappa) \uparrow \mathcal{O}(1)$. Though the RG flow is strictly speaking valid only for $\kappa \ll 1$, we assume for the following that it mirrors the *qualitative* features, i.e., the topology of the RG sinks, correctly also in the limit of $\kappa \uparrow \kappa^* = 1$.

Only for $m^* \leq m \leq 1$, the RSB fixed point (RSB1) is in the physical regime $\tilde{g}_2^* \geq 0$ of non-negative $\tilde{g}_2$. Moreover, the fixed point (RSB1) is in this range of m stable with respect to perturbations in $\tilde{g}_1$ and $\tilde{g}_2$ (becoming marginal with respect to perturbations in $\tilde{g}_2$ at $m = m^*$ where it coincides with (RSB2)), whereas the fixed point (RSB2) is unstable with respect to perturbations $\tilde{g}_2 > 0$. Thus, for $m^* \leq m \leq 1$, the fixed point (RSB1) represents the RSB RG sink for all RG trajectories with bare parameters $\tilde{g}_1(0) > \tilde{g}_2(0) > 0$ [Figure 10.2b] while the fixed point (RSB2) is attractive only for RG trajectories with $\tilde{g}_1(0) > \tilde{g}_2(0) = 0$.

For $0 < m \leq m^*$, (RSB2) is the only RSB fixed point in the physical regime of non-negative $\tilde{g}_2 \geq 0$. It is in this range of m the RSB RG sink for all RG trajectories with $\tilde{g}_1(0) > \tilde{g}_2(0) \geq 0$ [Figures 10.2c, 10.2d]; furthermore, it is stable with respect to perturbations in $\tilde{g}_1$ and $\tilde{g}_2$.

In the high-temperature phase for $\tau_m < 0$, the system flows to the stable trivial replica symmetric fixed point $\tilde{g}_1^* = \tilde{g}_2^* = 0$ regardless of an initial asymmetry $\Delta\tilde{g}(0) \neq 0$. In this phase the trivial replica fixed point is stable with respect to the RSB perturbation $\Delta\tilde{g}$ so that RSB cannot occur in the high-temperature phase as it is expected. For $\tau_m = 0$ the trivial fixed point stays marginally stable.

10.1.2 Correlations

The analysis of the RG sinks can directly be used to calculate the $\overline{\langle\phi\phi\rangle}$-correlations following the procedure outlined in the preceding chapter 9 and using the RG result (9.28) for the propagator. We have seen that the RG flow and fixed point structure change significantly

upon introducing a replica asymmetric perturbation $\Delta\tilde{g}(0) > 0$ in the low-temperature phase. As well the behaviour of the $\overline{\langle\phi\phi\rangle}$-correlations changes depending on the value of the fixed point $\tilde{g}_2^*$ and thus m. Using the result (9.28) for the Fourier transformed propagator, we obtain

$$\begin{aligned} G_{\alpha\beta}(k) &\simeq k^{-2}\, K_{\alpha\beta}^{-1}\left(\ell{=}\ln\frac{1}{kl}\right) \\ &\simeq \frac{4\pi}{k^2}\Bigg(\delta_{\alpha\beta}\left(1-\kappa\left(\ell{=}\ln\tfrac{1}{kl}\right)\right)+\widetilde{\delta}_{\alpha\beta}\frac{\kappa\left(\ell{=}\ln\frac{1}{kl}\right)-\tau_m}{m}+ \\ &\quad +\frac{(1-\tau_m)^2}{\tilde{K}_c}\tilde{\Delta}\left(\ell{=}\ln\tfrac{1}{kl}\right)\Bigg) \end{aligned} \tag{10.25}$$

so that the large scale correlations depend essentially only on the asymptotic RG flow of the reduced elasticity parameter $\kappa(\ell)$ and $\tilde{\Delta}(\ell)$.

As in the replica symmetric RG (compare (10.9)), the *connected* correlations are unrenormalized by the disorder and identical to the $\langle\phi\phi\rangle$-correlations of the disorder-free Gaussian model due to the statistical tilt symmetry (9.29):

$$\begin{aligned} &\overline{\langle(\phi(\mathbf{r})-\phi(0))^2\rangle_{\mathrm{conn}}} = \\ &= \int d^2\mathbf{k}\; 2(1-\cos(\mathbf{k}\cdot\mathbf{r}))\left(\lim_{n\to 0}\frac{1}{n}\sum_{\alpha,\beta}G_{\alpha\neq\beta}(k)\right) \\ &= 4(1-\tau_m)\ln(r/l)\;. \end{aligned} \tag{10.26}$$

This result holds for all m and *independently* of the introduction of a $\Delta\tilde{g}(0) > 0$.

In the high-temperature phase, no RSB instability occurs, even if $\Delta\tilde{g}(0) > 0$, and the renormalization of κ, $\tilde{\Delta}$ can essentially be neglected; the connected $(\overline{\langle\phi\phi\rangle - \langle\phi\rangle\langle\phi\rangle})$-correlation function and the $\overline{\langle\phi\phi\rangle}$-correlation function coincide, and $\overline{\langle(\phi(\mathbf{r})-\phi(\mathbf{0}))^2\rangle} \simeq 4(1-\tau_m)\ln(r/l)$.

In the low-temperature phase the asymptotics of $\tilde{\Delta}(\ell)$, which is determined by the flow equation (10.18), is of special interest because in the replica symmetric case, i.e., without a replica asymmetric perturbation ($\Delta\tilde{g}(0) = 0$), the "runaway-flow" $\tilde{\Delta}(\ell) \sim \tau_m^2\ell$ diverging linearly is the reason for the super-roughness in the correlations $\overline{\langle(\phi(\mathbf{r})-\phi(\mathbf{0}))^2\rangle} \sim \tau_m^2\ln^2(r/l)$, see (10.8).

With an induced RSB instability by a small replica asymmetry $\Delta\tilde{g}(0) > 0$ in the bare parameters (and $\tilde{g}_2(0) > 0$), $\tilde{\Delta}(\ell)$ has also a linearly divergent asymptotics $\tilde{\Delta}(\ell) \sim (\tilde{g}_2^*)^2\ell/2$ for $m^* < m \leq 1$ because the stable RSB fixed point (RSB1) has $\tilde{g}_2^* > 0$. For the RSB RG sink (RSB1), we obtain to a good approximation $\tilde{g}_2^* \simeq 6(m-m^*)$ such that

$$\tilde{\Delta}(\ell) \;\sim\; \frac{1}{2}(\tilde{g}_2^*)^2\ell \;\sim\; 18(m-m^*)^2\ell\;. \tag{10.27}$$

Using (10.25), this entails $\overline{\langle\phi\phi\rangle}$-correlations

$$\overline{\langle(\phi(\mathbf{r})-\phi(0))^2\rangle} \;\propto\; (\tilde{g}_2^*)^2 \ln^2(r/l) \;\propto\; (m-m^*)^2 \ln^2(r/l) \tag{10.28}$$

with a $\log^2$-divergence for this range of m but with the prefactor reduced by a factor $9(m-m^*)^2/\tau_m^2 < 1$ compared to the replica symmetric case. In particular, we get back the replica symmetric CO result (10.7, 10.8) upon choosing $m = 1$ (and $\tau_m = \tau_0$).

The situation changes significantly in the regime $0 < m \leq m^*$, where the stable RSB fixed point is given by (RSB2) with $\tilde{g}_2^* = 0$. Therefore, $\tilde{\Delta}(\ell)$ *saturates* on large scales to a value $\tilde{\Delta}^*$. From a linear stability analysis around the replica symmetric CO fixed point extending (10.21, 10.22) [and neglecting the pre-asymptotic RG-flow towards the replica symmetric CO fixed point], one finds that $\tilde{g}_2(\ell)$ renormalizes to 0 on a scale

$$\ell^* \;\sim\; \frac{1}{\lambda_m} \ln\left(\frac{4\tau_m}{(1-m)\Delta\tilde{g}(0)}\right), \tag{10.29}$$

which leads by equation (10.18) and (10.23) to

$$\tilde{\Delta}^* \;\sim\; 4\tau_m^2 \ell^* \;\sim\; \sqrt{2\tilde{K}_c}\tau_m \ln\left(\frac{4\tau_m}{(1-m)\Delta\tilde{g}(0)}\right) \tag{10.30}$$

for the leading order contribution in τ_m. Hence, we obtain from (10.25), with $\kappa(\ell) \uparrow \kappa^* = 1$, only logarithmically divergent $\overline{\langle\phi\phi\rangle}$-correlations

$$\begin{aligned}\overline{\langle(\phi(\mathbf{r})-\phi(0))^2\rangle} &\simeq \left(4(1-\kappa^*)\frac{4(\kappa^*-\tau_m)}{m} + \frac{4(1-\tau_m)^2}{\tilde{K}_c}\tilde{\Delta}^*\right)\ln(r/l) \\ &\sim \left(\frac{4(1-\tau_m)}{m} + \frac{4\sqrt{2}}{\sqrt{\tilde{K}_c}}\tau_m \ln\left(\frac{4\tau_m}{(1-m)\Delta\tilde{g}(0)}\right)\right)\ln(r/l)\end{aligned} \tag{10.31}$$

with a prefactor *greater* than in the high-temperature phase and increasing upon lowering the temperature.

Our results for the low-temperature phase show that within the one-step RSB RG approach with a small initial replica asymmetry $\Delta\tilde{g}(0) > 0$, it is possible to obtain $\overline{\langle\phi\phi\rangle}$-correlations with a $\log^2$-divergence as well as only log-divergent $\overline{\langle\phi\phi\rangle}$-correlations. For $m = 1$, we reproduce the known super-rough replica symmetric RG result of Ref. [61] for the $\overline{\langle\phi\phi\rangle}$-correlations; similarly, we find a $\log^2$-divergence with a reduced prefactor for the regime $m^* < m \leq 1$ such that $\tilde{g}_2^* > 0$. And finally, we obtain only log-divergent $\overline{\langle\phi\phi\rangle}$-correlations with a prefactor increasing with decreasing temperature if $0 < m \leq m^*$ and $\tilde{g}_2^* = 0$. The latter possibility is of interest with regard to the results of the variational approach of K/GL which produces qualitatively the same behaviour.

10.1.3 Free Energy

As mentioned already, the proper initial values $K_{\alpha\beta}(0) = K\delta_{\alpha\beta} - \Delta$ (10.1) and $g_{\alpha\neq\beta}(0) = g$ (10.2) are replica symmetric with $\Delta g(0) = 0$. It remains unclear in this approach how the initial asymmetry $\Delta g(0) > 0$ necessary for the development of an instability with respect to RSB can be obtained for physical reasons. So far, we have put in this asymmetry "by hand" thereby *explicitly* breaking the replica symmetry. However, to be of physical relevance, the RSB should happen *spontaneously*. For random ferromagnets in $4 - \epsilon$ dimensions, it has been argued in Refs. [88, 89] that a spontaneous RSB arises from an "underlying" rugged energy landscape, which requires an expansion around multiple local minima solutions of the mean-field equations, whereas in the original Hamiltonian an expansion around $\phi \equiv 0$ is tacitly assumed. The existence of multiple local minima requires a description by RSB, which is essentially "passed" to the initial values of the RG flow, that describes the physics of fluctuations around these minima. However, such an argumentation is not possible in two dimensions where a mean-field description is inapplicable due to the pronounced fluctuation effects.

The lack of a clearcut physical picture of the generation of the RSB instability makes it also a difficult task to comment on possible choices of the RSB parameter m. In this context it is useful to remind what determines an "optimal" RSB parameter in physical systems where RSB has been found so far, such as the mean-field theory of spin glasses or the variational approach to random manifolds. In both of these systems, the solutions of the self-consistency equations extremize the free energy. They have been tested in detail for their thermodynamic stability [52, 85], which is properly done by considering fluctuations around the solutions to quadratic order and calculate the eigenvalues of the corresponding excitation-modes in replica space. For the 2D RFXY model in the variational approach, the RSB solution of the self-consistency equations in the low-temperature regime turns out to be *stable* with respect to fluctuations and to *maximize* the free energy [9]. This is similar to the situation in the mean-field theory of spin glasses where the stable RSB mean-field solution also maximizes the free energy. Such behaviour is usually assigned to the fact that the number of parameters describing the fluctuations around the solution becomes *negative* in the limit $n \downarrow 0$, thereby transforming the free energy maximums into stable thermodynamic states. At first sight, this result suggests to determine an optimal parameter m by calculating the free energy in the RG framework and to maximize the free energy with respect to m. However, one should be careful with such a naive adaption of these results from mean-field or variational calculations to a RG analysis. It is plausible from general thermodynamic considerations to seek for an extremum of the free energy if internal *free* parameters are present; for a minimum in the standard case of a positive number of free parameters and presumably for a maximum if the number of free parameters is negative, as it happens in the mentioned glassy systems. In our RG analysis,

the RSB parameter m remains the *only* free parameter of the model in replica space so that it is tempting to conclude that the proper physical choice of m corresponds to a *minimum* of the free energy rather than a maximum as it is suggested by the corresponding variational calculation. However, the final answer to this problem has to be left open to future investigation along with the problem of the physical origin of a possible *spontaneous* RSB. In the following, we will determine maximum *and* minimum of the free energy in dependence of m. This amounts to the plausible assumption that one of the discussed thermodynamic extremum-principles (maximum or minimum) should be applicable to the internal RSB degree of freedom represented by m.

As demonstrated in the previous chapter 9, it is possible to calculate the free energy difference $\Delta F = F - F^{(0)}$ to the disorder-free Gaussian model in the RG framework in terms of the renormalized $g_{\alpha\beta}$ and $K_{\alpha\beta}$. In the thermodynamic limit $L/l \uparrow \infty$ of an infinite system size L, the RG equation (9.34) yields for the free energy difference ΔF per replica with the one-step RSB scheme in the limit $n \downarrow 0$ (apart from a constant independent of m)

$$\begin{aligned}\frac{1}{n}\Delta F &\simeq \frac{1}{2n}\ln\left(\det_{\alpha\beta}\tilde{K}_{\alpha\beta}\left(\ell{=}\ln\frac{L}{l}\right)\right) - \frac{1}{4n}\sum_{\alpha\neq\beta}\tilde{g}^*_{\alpha\beta} \\ &= \frac{1-m}{2m}\ln\left(1-\kappa\left(\ell{=}\ln\tfrac{L}{l}\right)\right) - \frac{1}{2m}\ln\left(1-\tau_m\right) - \\ &\quad -\frac{1}{2}(1-\tau_m)\tilde{\Delta}\left(\ell{=}\ln\tfrac{L}{l}\right) + \frac{1}{4}\left((1-m)\tilde{g}^*_1 + m\tilde{g}^*_2\right) \ . \end{aligned} \tag{10.32}$$

For the replica symmetric case, the free-energy in the low-temperature phase is determined by the CO fixed point disorder strengths $\tilde{g}^*_1 = \tilde{g}^*_2 = 2\tau_m$ and dominated by the "runaway-flow" of $\tilde{\Delta}$ with the linearly divergent asymptotics $\tilde{\Delta}(\ell) \sim 2\tau_m^2\ell$, which yields in (10.32)

$$\frac{1}{n}\Delta F_{RS} \ \sim \ -(1-\tau_m)\tau_m^2\ln\left(L/l\right) \ . \tag{10.33}$$

Upon inducing a one-step RSB by introducing a bare replica asymmetric perturbation $\Delta\tilde{g}(0) > 0$, the RG sink becomes one of the RSB fixed points (RSB1) and (RSB2) depending on our choice of m. For both sinks we obtain from 10.17 the asymptotics

$$1-\kappa(\ell) \ \propto \ \frac{1}{\ell} \ \downarrow \ 1-\kappa^* = 0 \ . \tag{10.34}$$

For $m^* < m \leq 1$ (and $\tilde{g}_2(0) > 0$), the RSB fixed point (RSB1) represents the RG sink of the model, and we have $\tilde{g}^*_2 > 0$ giving again a "runaway-flow" of $\tilde{\Delta}(\ell)$ with a linearly divergent asymptotics (10.27). The corresponding term in (10.32) gives as in the replica

symmetric case the dominant contribution to the free energy in the thermodynamic limit

$$\begin{aligned}\frac{1}{n}\Delta F_{RSB}(m^* < m \leq 1) &\sim -\frac{1}{4}(1-\tau_m)(\tilde{g}_2^*)^2 \ln(L/l) \\ &\simeq -9(1-\tau_m)(m-m^*)^2 \ln(L/l)\ . \end{aligned} \tag{10.35}$$

For $0 < m \leq m^*$, (RSB2) is the RSB RG sink with $\tilde{g}_2^* = 0$. This changes not only the behaviour of the $\overline{\langle\phi\phi\rangle}$-correlations drastically, as discussed above, but has similar consequences for the free energy. In this regime $\tilde{\Delta}(\ell)$ saturates on large scales, see (10.30), and the dominant contribution in the free energy (10.32) comes from the weak logarithmic divergence stemming from the asymptotics of $\kappa(\ell)$, see (10.34):

$$\frac{1}{n}\Delta F_{RSB}(0 < m \leq m^*) \sim -\frac{1-m}{2m}\ln(\ln(L/l))\ . \tag{10.36}$$

Interestingly, the results (10.35, 10.36) with $\Delta F(L) \sim (\ln L)^\theta$ for the free energy and (10.28, 10.31) with $\overline{\langle\phi^2\rangle}(L) \sim (\ln L)^\zeta$ obey the simple scaling law $\theta = 2\zeta - 1$ in terms of the logarithm $(\ln L)$ of the system size L for all m. This could have been naively guessed by equating $\Delta F(L)$ with the average elastic energy though a "power" counting in logarithms is certainly a delicate issue.

From the results (10.35, 10.36) for $\frac{1}{n}\Delta F_{RSB}(m)$ in the thermodynamic limit, we find that $\frac{1}{n}\Delta F_{RSB}(m)$ is monotonously increasing in the interval $0 < m \leq m^*$ and monotonously decreasing in $m^* < m \leq 1$. Thus the *maximum* of $\frac{1}{n}\Delta F_{RSB}(m)$ is reached for $m = m^*$. It is also obvious that $\frac{1}{n}\Delta F_{RSB}(m)$ takes its *absolute minimum* for the replica symmetric $m = 1$. If the optimal RSB parameter m is given by a maximal free energy, i.e., $m = m^*$, only log-divergent $\overline{\langle\phi\phi\rangle}$-correlations (10.31) should be found. If, on the other, hand simple thermodynamics still holds in the disordered system and m is obtained from minimizing the free energy, we would recover the replica symmetric result $m = 1$, that means the $\log^2$-divergence and hence super-roughness in the $\overline{\langle\phi\phi\rangle}$-correlations.

However, without a clear picture of the underlying physical mechanism for a spontaneous RSB in the RG treatment, i.e., the generation of the replica asymmetric perturbation, it is not clear which of the two extrema represents the physical one.

10.1.4 Comparison with Variational RSB Approach

It sheds some light onto the approximations underlying the variational approach of K/GL with a RSB Ansatz for the propagator [9, 17, 21] to examine what has to be neglected and how $\Delta\tilde{g}(0)$ has to be chosen to *reproduce* its results by the RSB RG treatment presented before.

One can re-derive the results given by K/GL for the free energy and the correlations using: (i) *Truncated* RG equations, i.e., only the first order terms $\mathcal{O}(\tilde{g}_1^1,\ \tilde{g}_2^1)$ in (10.15-10.19) and (ii) for the disorder strengths *replica asymmetric* bare values $\tilde{g}_2(0) = 0$, $g_1(0) =$

$\Delta g(0) = g > 0$. Due to the truncation of the RG equations, one has in particular $\kappa \equiv \tau_m$. It follows immediately that $g_2 \equiv 0$ and $\tilde{g}_1(\ell) = \tilde{g} \exp(2\tau_m \ell)$. Due to the neglect of second order terms, fixed points are absent in such a treatment. Therefore, the renormalization of $\tilde{g}_1$ has to be stopped at some scale ℓ^*, which we want to fix by $\tilde{g} \exp(2\tau_m \ell^*) \sim K^2$ and $L^*/l \sim (K^2/g)/2\tau_m$, where we apply a Debye-Hückel approximation and replace the cos-term in the Hamiltonian (9.2) by a mass term

$$-g_1(\ell^*) \cos(\phi_\alpha - \phi_\beta) \widetilde{\delta}_{\alpha\beta} \;\mapsto\; g_1(\ell^*) \left(-m\delta_{\alpha\beta} + \widetilde{\delta}_{\alpha\beta} \right) \phi_\alpha \phi_\beta \; . \tag{10.37}$$

By applying the RG equations for the 2-point vertex function (9.27) and the free energy (9.34) derived in the previous chapter 9 with $\tilde{g}_2 \equiv 0$

$$\Gamma_{\alpha\beta}(k,\; \{\tilde{g}_1,\; K\}) \sim (\frac{l}{L^*})^2 \Gamma^{DH}\left(k\frac{L^*}{l}, \{\tilde{g}_1 \sim K^2,\; K\} \right) \tag{10.38}$$

$$\Delta F(L/l,\; \{\tilde{g}_1,\; K\}) \sim (L/L^*)^2 (1-m) \tilde{g}_1(\ell^*) + \Delta F^{DH}\left(L/L^*,\; \{K^2,\; K\} \right) \; , \tag{10.39}$$

one obtains the correlations and the free energy. The quantities with a superscript "DH" are evaluated within the Debye-Hückel approximation with a mass term (10.37).

Such a procedure reproduces the results of the variational approach for the correlations and the free energy. Thus maximization of the free energy yields also the same value $m \simeq 1 - \tau_m$ [9, 17, 21]. However, it should be stressed that all terms occuring in the second order $\mathcal{O}(g_1^2,\; g_1 g_2,\; g_2^2)$ have been neglected, which give in the perturbation theory serious $1/\tau_m$- and $1/\kappa$-singularities as we have seen in the previous chapter 9; in the next section 10.2 we will further clarify this point. As another remarkable result of the demonstrated equivalence, one recognizes that in the variational calculation, being equivalent to a RSB RG approach with $\Delta g(0) = g_1(0) > 0$, the replica symmetry seems to be effectively broken "by hand". On the other hand, we have seen in this section that it is not at all clear for which physical reason the replica asymmetry $\Delta g(0)$ should occur within the RG framework. This casts in turn doubt on the applicability of a widening of the Ansatz for the propagator in the variational approach by using RSB. It may be an effect of this "mathematical tool" to break the replica symmetry *explicitly* and to induce a RG flow to a different fixed point with strongly different physical properties, which would be fixed point (RSB2) if the RG flow had not been truncated. Thus the drastic change in the physical behaviour, with fixed point (RSB2) exhibiting strong RSB and $\kappa^* = 1$, as opposed to the replica symmetric CO fixed point, and with accordant consequences for the $\overline{\langle\phi\phi\rangle}$-correlations as discussed earlier, may be a result of subtle interactions induced by the widening of the variational Ansatz.

Such a view will be further supported in chapter 11, where we study *two* interacting physical replicas of the 2D RFXY model. There, it is also found that RSB results are consistent with the physics obtained if a small repulsion between the physical replicas is

introduced, which corresponds to a small replica asymmetric perturbation in a single 2D RFXY model. Although we expect similar physical properties of the RG sink for the two weakly interacting physical replicas, we will find in chapter 11, similar to our findings here, pronounced instabilities in the RG flow leading to RG sinks with very different physical properties.

10.2 Self-Consistent Diagrammatic Approach

Whereas we tried in the last section 10.1 to widen the replica symmetric RG treatment of CO/GH [18, 19], the remainder of this chapter is devoted to an extension of the variational approach with RSB used by K/GL [9, 17, 21], both aiming at a more unified view of the subject. In the previous section we were able to *reproduce* the results of the variational approach within the RSB RG treatment using certain approximations. Vice versa our goal in this section is to obtain the RG results by an extended self-consistent calculation.

In the form it has been developed in Ref. [52], we want to interpret the variational approach as a tool to derive in a controled manner [the approach can be shown to be exact in the limit of infinite number of components N of the field ϕ] a set of self-consistency equations for the propagator in replica space, which are essentially equivalent to a self-consistent Hartree-approximation. Though exact in the limit $N \uparrow \infty$, it is clear that in the case $N = 1$ under consideration in the vortex-free 2D RFXY model important classes of diagrams (we use throughout this section essentially the diagrammatic "language" of chapter 9) have been neglected. In particular, no $1/\tau$-singularities arise, where the negative reduced temperature

$$\tau \;:=\; 1 - \frac{K_c}{K} \quad \text{with} \quad K_c \;=\; \frac{1}{4\pi} \tag{10.40}$$

is the small expansion parameter of the renormalization classifying the divergences of the diagrams [as defined here, τ coincides in the replica symmetric RG with τ_0 (10.3) and in the one-step RSB RG with κ (10.14)]. The $1/\tau$-singularities stem from higher order diagrams in the vertex $g\cos(\phi_\alpha - \phi_\beta)$. Therefore, the self-consistent Hartree-approximation does *not* give a self-consistency equation for the vertex, which arises naturally, as we will see, if the higher order vertex-corrections are taken into account. Including such corrections, one is able to partly reconcile an extended self-consistent approach and the RG treatment presented in chapter 9. A similar idea has been followed in Ref. [56], where it is shown that for a N-component vortex-free 2D RFXY model the $\log^2$-divergence of the RG equations derived by CO/GH for $N = 1$ is suppressed by a factor $1/N^3$ for large N. This indicates that upon inclusion of more classes of diagrams into the self-consistent approach, which can in fact be interpreted as a $1/N$-expansion as shown in Ref. [52], the corresponding term should emerge in higher orders in the vertex.

We want to start, as in chapter 9, from the most general form (9.2) of the replica Hamiltonian. The self-consistent diagrammatic approach presented here, is based on an extension of the theorem (9.11) used already in the diagrammar in chapter 9. The essence of this theorem applied to the vertex $g_{\alpha\beta}\cos(\phi_\alpha - \phi_\beta)$ is the following: "Pulling" a "ϕ_α-leg" out of the vertex in any diagram leaves behind the functional derivative of the vertex. The vertex $g_{\alpha\beta}\cos(\phi_\alpha - \phi_\beta)$ [Figure (9.1)] is peculiar since it is a $\cos(\phi)$-vertex, i.e., a

whole *power series*, and every functional derivative leaves (apart from the sign) a $\sin(\phi)$- or $\cos(\phi)$-vertex behind in the diagram. Therefore, one can formulate a self-consistency equation for a *dressed vertex* or *vertex part* $g^V_{\alpha\beta}\cos(\phi_\alpha - \phi_\beta)$ by summing up sub-classes of diagrams but conserving the cos-form of the vertex at the same time. The dressed vertex is calculated using the *full* propagator, for which in turn a Dyson equation can be formulated in terms of the dressed vertex. Thereby, we obtain a closed set of two diagrammatic equations that should be self-consistently solved for the full propagator, which encodes the physical properties we are interested in.

We represent the bare vertex $g_{\alpha\beta}\cos(\phi_\alpha - \phi_\beta)$ graphically as in chapter 9 by Figure (9.1) with a white circle for the $g_{\alpha\beta}$ whereas we choose in the dressed vertex for $g^V_{\alpha\beta}$ a filled black circle. Bare propagators $G^{(0)}_{\alpha\beta}(k)$ are represented by thin lines and full propagators $G_{\alpha\beta}(k)$ by thick ones. Graphically, we can write the Dyson equation and the vertex part as shown in Figure 10.3. The analytic expression for the vertex part equation of Figure 10.3 is

$$
\begin{aligned}
&g^V_{\alpha\neq\beta}\cos(\phi_\alpha - \phi_\beta) \;= \\
&\quad = g_{\alpha\beta}\cos(\phi_\alpha - \phi_\beta)\exp\Big(-\tfrac{1}{2}\big(G_{\alpha\alpha}(0) + G_{\beta\beta}(0) - 2G_{\alpha\beta}(0)\big)\Big) + \\
&\qquad + g_{\alpha\beta}\cos(\phi_\alpha - \phi_\beta)\Big\{\sum_{\mu\neq\nu}\int_{\mathbf{r}}\exp\Big(-\tfrac{1}{2}\big(G_{\alpha\alpha}(0) + G_{\beta\beta}(0) - 2G_{\alpha\beta}(0)\big)\Big)\times \\
&\qquad\quad \times g^V_{\mu\nu}\Big[\cosh^*\Big(G_{\alpha\mu}(\mathbf{r}) + G_{\beta\nu}(\mathbf{r}) - G_{\alpha\nu}(\mathbf{r}) - G_{\beta\mu}(\mathbf{r})\Big)\Big]\Big\} - \\
&\qquad - 2\sum_{\mu(\neq\beta),\nu(\neq\alpha)}\int_{\mathbf{r}} g^V_{\alpha\nu}g_{\mu\beta}\exp\Big(-\tfrac{1}{2}\big(G_{\mu\mu}(0) + G_{\beta\beta}(0) - 2G_{\mu\beta}(0)\big)\Big)\times \\
&\qquad\quad \times\Big[\sinh^*\Big(G_{\alpha\mu}(\mathbf{r}) + G_{\beta\nu}(\mathbf{r}) - G_{\nu\mu}(\mathbf{r}) - G_{\alpha\beta}(\mathbf{r})\Big)\Big]\;, \qquad \text{(V)}
\end{aligned}
$$

where $\cosh^* x = (\cosh x - 1)$ and $\sinh^* x = (\sinh x - x)$ count only one-particle irreducible graphs.

In order not to overcount graphs we have to subtract the $(k = 0)$-part in the second order contribution to the self-energy in the Dyson equation ($\tilde{\Sigma}(k) := \Sigma(k) - \Sigma(k = 0)$, which is taken into account already in the vertex part equation. The analytic expression for the Dyson equation of Figure 10.3 is [note the similarities to equations (9.13) and (9.12)]

$$
G^{-1}_{\alpha\beta}(k) = \big(G^{(0)}\big)^{-1}_{\alpha\beta} - \Sigma^{(1)}_{\alpha\beta} - \tilde{\Sigma}^{(2)}_{\alpha\beta}(k)
$$

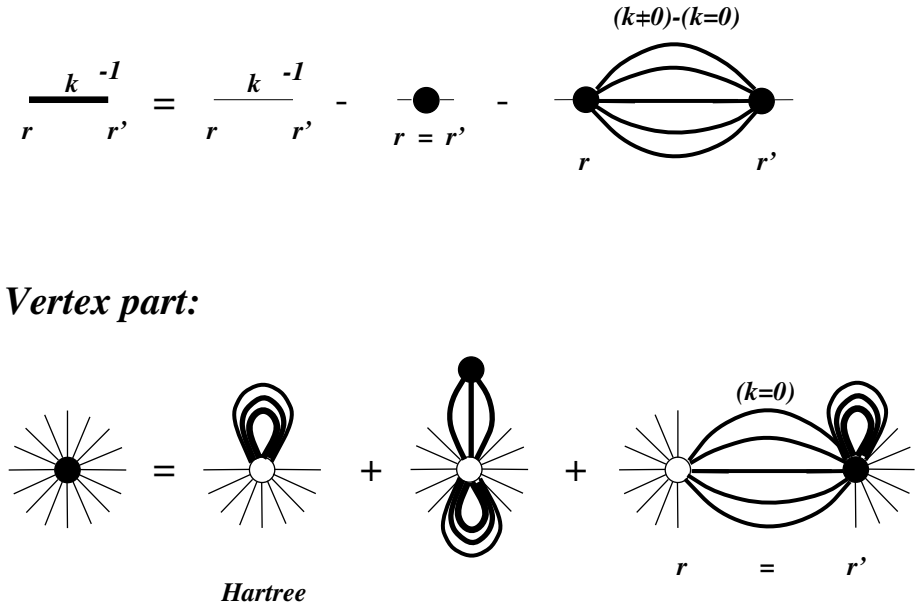

Figure 10.3: Graphical representation of the Dyson equation and the vertex part $g^V_{\alpha\beta}\cos(\phi_\alpha - \phi_\beta)$. Thin lines are bare propagators $G^{(0)}$, thick lines full propagators G, a line^{-1} denotes the corresponding 2-point vertex function $\Gamma^{(0)}$ or Γ, respectively.

with

$$\begin{aligned}
\Sigma^{(1)}_{\alpha\neq\beta} &= 2g^V_{\alpha\beta} \\
\tilde{\Sigma}^{(2)}_{\alpha\neq\beta} &= \int_{\mathbf{r}} \left(e^{i\mathbf{k}\cdot\mathbf{r}} - 1\right) \Sigma^{(2)}_{\alpha\beta}(\mathbf{r}) \\
\Sigma^{(2)}_{\alpha\neq\beta}(\mathbf{r}) &= 4 \sum_{\gamma(\neq\alpha),\nu(\neq\beta)} g^V_{\alpha\gamma} g^V_{\nu\beta} \times \\
&\quad \times \left[\sinh^*\left(G_{\alpha\beta}(\mathbf{r}) + G_{\gamma\nu}(\mathbf{r}) - G_{\alpha\nu}(\mathbf{r}) - G_{\gamma\beta}(\mathbf{r})\right)\right] \qquad \text{(D)}
\end{aligned}$$

The bare propagator $G^{(0)}$ can be read off from (9.2)

$$G^{(0)}_{\alpha\beta} \;=\; K^{-1}_{\alpha\beta}\; k^{-2}\;. \tag{10.41}$$

Due to the "statistical tilt symmetry" (9.10) [19, 69, 70], $\Sigma_{\alpha\alpha}$ obeys (for Parisi-type matrices) to all orders the *exact* relation

$$\Sigma_{\alpha\alpha} \equiv \sum_{\beta(\neq\alpha)} \Sigma_{\alpha\beta}\;. \tag{10.42}$$

Though not very handy at first sight, the two equations (V) and (D) provide a closed set of equations for the full propagator $G_{\alpha\beta}(k)$. The self-consistent variational approach as used by K/GL is contained in these equations when we set $\Sigma^{(2)} \equiv 0$ and only the first term in equation (V) is considered in the determination of $g^V_{\alpha\beta}$. Then, the only diagram contributing to the self-energy is the Hartree-diagram [see Figure 10.3] contributing to $\Sigma^{(1)}$ and giving the variational approach the alternative name *self-consistent Hartree-approximation*. However, as should have become clear in the diagrammatic approach to the RG treatment the second order contribution $\Sigma^{(2)}$ bears essential singularities which *cannot* be taken into account in a Hartree-approximation. In the RG equations, these additional terms are responsible for the existence of non-trivial fixed points. Though the work of Bauer and Bernard [56] suggests that it should be possible to derive the above scheme (V) and (D) in a controled manner in a $1/N$-expansion (N being the number of components of ϕ), this has not been achieved so far. In the form presented here, the extensions with respect to the Hartree-approximation are not based on a systematic expansion (though the results of Ref. [56] indicate that they are $1/N^3$-corrections to the leading order $1/N$ of the Hartree-approximation) but rather incorporate a novel class of diagrams into the self-consistent scheme, which has proven to be essential in the RG calculation. In considering *more* diagrams than before, (V) and (D) should *improve* the self-consistent approach.

10.2.1 Replica Symmetric Solution

For the following, we want to specialize to the proper bare replica symmetric vertex $g_{\alpha\beta} = g(\delta_{\alpha\beta} - 1)$ (10.2) as obtained from replicating the Hamiltonian (8.5). That means we do *not* break the replica symmetry "by hand" as in the RG approach.

First, we use (V) and (D) to re-examine the replica symmetric solution within the self-consistent framework. We make a replica symmetric Ansatz for the propagator:

$$G^{-1}_{\alpha\beta} = \left(G^{(0)}\right)^{-1}_{\alpha\beta}(k) - \Sigma(k) \;=\; KG_0^{-1}(k)\delta_{\alpha\beta} - \Sigma(k)\;, \tag{10.43}$$

where [83]

$$G_0(k) = (k^2 + \mu^2)^{-1} \tag{10.44}$$

$$G_0(r) = \int \frac{d^2k}{(2\pi)^2} G_0(k) e^{i\mathbf{k}\cdot\mathbf{y}}\Big|_{y^2=r^2+l^2} \overset{\mu r \ll 1}{\to} -\frac{1}{4\pi}\ln\left(C\mu^2(r^2+l^2)\right) \tag{10.45}$$

with $\mu^2 \sim 1/L^2$ as a regularizing mass serving as IR-cutoff (as opposed to the hard cutoff L in real space used in chapter 9) and an UV-cutoff l. C is a non-universal constant[1] introduced by the UV-cutoff procedure [for similar reasons a constant C (with a different

[1] $C = \frac{1}{4}e^{2\gamma}$, where γ is Euler's constant [83].

value) occurs in the RG calculation in chapter 9]. Henceforth, we absorb factors of the UV-cutoff l to obtain dimensionless quantities, analogously to the RG calculation (see (9.8)), such that $l \equiv 1$.

The Hartree-approximation of K/GL *fails* to find a phase transition to a low-temperature phase [9, 17, 21] for $\tau > 0$ with the above replica symmetric Ansatz. Using the extended self-consistency equations (V) and (D), we find that $\Sigma(k)$ drops out of equation (V) [which is analogous to $\tilde{\Delta}$ not feeding back in the replica symmetric RG equations (10.4-10.6)] and keeping only the most divergent terms for $\mu,\ \bar{\mu} \downarrow 0$ and $\tau \ll 1$, we obtain

$$
\begin{aligned}
g^V_{\alpha\neq\beta} &= g^V \\
g^V[\bar{\mu}] &\simeq\ g(C\mu^2)^{1-\tau} + g\, g^V[\bar{\mu}]\,(n-2) I_\tau[\bar{\mu}] && (10.46)\\
\Sigma^{(1)}_{\alpha\neq\beta} &\simeq 2 g^V[\mu] && (10.47)\\
\tilde{\Sigma}^{(2)}_{\alpha\neq\beta}(k) &\simeq k^2\, \frac{\pi}{2} (C\mu^2)^{-2(1-\tau)} \int^{1/\mu^2} dr^2 r^2 (r^2+1)^{-2(1-\tau)} (g^V[\bar{\mu}])^2\ . && (10.48)
\end{aligned}
$$

with

$$
I_\tau[\mu] :=\ \frac{\pi}{\tau}\left(\mu^{-2\tau} - 1\right)\ .
$$

The similarity with corresponding expressions (9.18) and (9.19) in the RG treatment is already obvious. Note particularly the $1/\tau$-singularity contained in I_τ, which is neglected in the Hartree-approximation but included and renormalized in the RG treatment of chapter 9. On the other hand, also an inherent shortcoming of the self-consistent approach as compared to a RG calculation becomes apparent, which is the reason for the distinction between the two masses $\mu,\ \bar{\mu}$: When $\mu = \bar{\mu}$, the self-consistency equations (V) and (D) are evaluated at *one* large length scale $1/\mu$, whereas the RG is based on the idea to consider the interaction between *many* length scales by integrating out successively fluctuations on smaller scales. The self-consistency equations with a single $\mu = \bar{\mu}$ can be regarded as a RG treatment, where the successive integrations of the RG steps are implemented in a *single* step.

Nevertheless, already with $\mu = \bar{\mu}$, we get the result

$$
g^V (C\mu^2)^{-1}\ \simeq\ \frac{g(C\mu^2)^{-\tau}}{g\frac{(n-2)\pi}{\tau}\,(\mu^{-2\tau}-1)}\ \overset{\mu\downarrow 0}{\longrightarrow}\ \tau\frac{C^{-\tau}}{(2-n)\pi}\ , \qquad (10.49)
$$

which is *identical* to the renormalized $g^R(L \sim 1/\mu)$ or the solution $g(\ell = \ln 1/\mu)$ of the RG equation (10.4) in the RG calculation for the replica symmetric case [apart from factors C due to the different cutoff procedures used in the two calculations]. In the limit $n \downarrow 0$ of the replica trick, it gives the known replica symmetric CO fixed point for $\tau > 0$. In particular,

we find the existence of a transition from $g^V = 0$ in the high-temperature phase $\tau < 0$ to $(g^V \mu^{-2}) \sim \tau$ in the low-temperature phase. Using (10.47), equation (10.49) yields also the result $\Sigma^{(1)} \sim g^V \sim \mu^2$, which is nothing else then the renormalization condition (9.16), keeping the renormalization of the mass *finite*. Therefore, the contribution $\Sigma^{(1)}$ leaves the asymptotic behaviour of the propagator unchanged in the thermodynamic limit $\mu \downarrow 0$, and it remains to investigate effects coming from the next order $\tilde{\Sigma}^{(2)}(k)$.

For $\mu = \bar{\mu}$, the self-consistency equations (V) and (D) *fail* to reproduce the replica symmetric RG result for the renormalized propagator (10.7), which exhibits the characteristic additional $\log k$-divergence leading to the super-roughness. This is due to the above mentioned problem that the RG is effectively performed in a single step and can be cured by introducing the auxiliary mass $\bar{\mu} > \mu$, which allows interaction between *two* kinds of fluctuations in the calculation of the propagator, fluctuations on scales $l \lesssim r \lesssim 1/\bar{\mu}$ and on scales $1/\bar{\mu} \lesssim r \lesssim 1/\mu$: Following the RG philosophy, it is reasonable to set $\bar{\mu} \sim 1/r$ in the integral in (10.48), which yields in the limit $n \downarrow 0$

$$\tilde{\Sigma}^{(2)}_{\alpha \neq \beta}(k) \;\propto\; \tau^2 \; k^2 \ln(1/k) \;, \tag{10.50}$$

in accordance with (10.7).

Thus it is possible to reconcile the self-consistent approach with the RG calculation in the replica symmetric case if the extended set of equations (V) and (D) is used. Interestingly, this is possible just by considering a new class of diagrams, which give essential singularities in the RG treatment and have not been considered in the self-consistent Hartree-approximation used by K/GL.

10.2.2 One-Step RSB Solution

Due to the technical difficulties involved in solving the equations (V) and (D) for a one-step RSB Ansatz for the propagator $G_{\alpha\beta}(k)$, we do not aim at a full solution but rather check the viability of the solution found by K/GL with the Hartree-approximation within the extended set of equations (V) and (D). Therefore, we start with an one-step RSB Ansatz for the 2-point vertex function containing only a *k-independent* self-energy [21]

$$G^{-1}_{\alpha\beta} = \; K G_0^{-1}(k)\delta_{\alpha\beta} - K\left[\sigma_2 + (\sigma_1 - \sigma_2)\widetilde{\delta}_{\alpha\beta} - \Delta_1 \delta_{\alpha\beta}\right] \tag{10.51}$$

$$\Delta_1 = \; (n\sigma_2 + m(\sigma_1 - \sigma_2)) \tag{10.52}$$

with $G_0(k)$ from (10.44). In the limit $n \downarrow 0$, this yields a propagator

$$\begin{aligned} G_{\alpha\beta}(k) = \; & \frac{1}{K}\Bigg\{ \frac{1}{(k^2+\mu^2)+\Delta_1}\delta_{\alpha\beta} + \\ & + \frac{1}{m}\left(\frac{1}{k^2+\mu^2} - \frac{1}{(k^2+\mu^2)+\Delta_1} \right) \widetilde{\delta}_{\alpha\beta} + A(k) \Bigg\} \;. \end{aligned} \tag{10.53}$$

Inserting this into the equations (V) and (D), one finds that the last term $A(k)$, which has not been explicitly displayed above, drops out of equation (V). Collecting only the most divergent terms for $\mu \downarrow 0$ and $\tau \ll 1$, and using only a *single* mass as opposed to the replica symmetric calculation we obtain from (V) after some lengthy algebra the following equations for the dressed vertex in the limit $n \downarrow 0$ of the replica trick:

$$\begin{aligned} g^V_{\alpha\neq\beta} &= g^V_1 \widetilde{\delta}_{\alpha\beta} + g^V_2 \left(1 - \widetilde{\delta}_{\alpha\beta}\right) \\ g^V_1 &\simeq gD_\tau - ((2-m) - mM_\tau)\, I_\tau\, g\, g^V_1 - \left(\frac{m}{M_\tau} + m\right) I_\tau\, g\, g^V_2 \qquad (10.54) \\ g^V_2 &\simeq gD_\tau M_\tau - 2(1-m) M_\tau I_\tau\, g\, g^V_1 - 2m I_\tau\, g\, g^V_2 \qquad (10.55) \end{aligned}$$

with

$$\begin{aligned} D_\tau &= D_\tau[\mu, \Delta_1] \;:=\; (C(\mu^2 + \Delta_1))^{1-\tau} \\ M_\tau &= M_\tau[\Delta_1/\mu] \;:=\; \left(1 + \frac{\Delta_1}{\mu}\right)^{-(1-\tau)/m} \leq 1 \qquad (10.56) \\ I_\tau &= I_\tau[\mu] \;:=\; \frac{\pi}{\tau}\left(\mu^{-2\tau} - 1\right) . \end{aligned}$$

Note again the similarities with the corresponding RG equations (10.15) and (10.16).

With these equations, one finds for $\tau < 0$ in the high-temperature phase that $g^V_1 = g^V_2 = 0$, whereas we obtain in the low-temperature phase for $\tau > 0$

$$\begin{aligned} g^V_1 (C\mu^2)^{-1} &\simeq \tau \frac{C^{-\tau}}{2\pi} M_\tau^{-m} \\ g^V_2 (C\mu^2)^{-1} &\simeq \tau \frac{C^{-\tau}}{2\pi} M_\tau^{1-m} \; . \qquad (10.57) \end{aligned}$$

Simultaneously with (10.57), we have to fulfill the equation (D), where we neglect for the moment the second order contribution $\tilde{\Sigma}^{(2)}(k)$ to stay consistent with our Ansatz of a k-independent self-energy. This yields in the limit $n \downarrow 0$ using (10.51, 10.52)

$$\begin{aligned} K\sigma_i &= 2g^V_i \qquad (i = 1, 2) \\ \Delta_1 &= \frac{\sigma_1 - \sigma_2}{m} \end{aligned}$$

and finally with (10.56, 10.57)

$$M_\tau^{-m/(1-\tau)} \simeq 1 + \frac{4\tau(1-\tau)}{m} C^{1-\tau} M_\tau^{-m} (1 - M_\tau) \; . \qquad (10.58)$$

From the last equation we can determine $M_\tau[\Delta_1/\mu] \leq 1$ and thus the vertices g^V_i and self-energies σ_i $(i = 1, 2)$.

The above replica symmetric result (10.49) for $g_1^V = g_2^V$ is recovered with the solution $M_\tau = 1$ of (10.58). A RSB solution of (10.58), i.e., a solution with $M_\tau < 1$ can exist only for a RSB-parameter $m < m_c$ smaller than a critical value

$$m_c \;:=\; 2C^{(2-\tau)/2}(1-\tau)\,\sqrt{\tau}\;. \tag{10.59}$$

This indicates a possible RSB instability for a certain parameter regime $m < m_c$ of the RSB parameter m though the RSB solution found here exhibits striking differences to the solution found by K/GL, and the *failure* of the Hartree-approximation becomes apparent. The major difference are vanishing RSB masses $\sigma_i \sim g_i^V \sim \mu^2$ in the thermodynamic limit $\mu^2 \sim 1/L^2 \downarrow 0$, such that they leave the asymptotic behaviour of the propagator and hence the $\overline{\langle\phi\phi\rangle}$-correlation *unchanged* as compared to the high-temperature phase. Thus we have to consider contributions from the k-dependent next order $\tilde{\Sigma}^{(2)}(k)$. K/GL, however, find a *finite* σ_1 for $\mu \downarrow 0$ such that the leading order of the self-energy is k-*independent* resulting in a log-divergence (in position space) of the $\overline{\langle\phi\phi\rangle}$-correlation. The RSB solution described by (10.58) has $g_1^V(C\mu^2)^{-1} > g_2^V(C\mu^2)^{-1} > 0$, and it is tempting to assume in the light of our replica symmetric calculation regarding the behaviour at the fixed point (RSB1) that one finds an additional $\log k$-divergence in the propagator if $\tilde{\Sigma}^{(2)}(k)$ is considered in the self-consistency equations, which should lead to super-roughness in the $\overline{\langle\phi\phi\rangle}$-correlations. This is suggested by the results from the RSB RG calculation because $g_2^V(C\mu^2)^{-1} > 0$ corresponds to $\tilde{g}_2^* > 0$ there, which produces a $\log^2$-divergence in the $\overline{\langle\phi\phi\rangle}$-correlations, see (10.28). This point certainly needs further verification. It is well possible that the self-consistent approach can be reconciled with the RSB RG approach as in the replica symmetric case, which requires however a detailed knowledge of the solution for $\tilde{\Sigma}^{(2)}(k)$ to reproduce results associated with a renormalization of τ in the RSB RG analysis. One important difference to the RG calculation is yet to be emphasized: It seems *not* to be necessary to break the replica symmetry of the bare vertex "by hand" to obtain a self-consistent RSB solution. This is contrary to the RG analysis where the instability in the RG flow is only obtained with a small replica asymmetric perturbation of the bare vertex. But also to answer this question with certainty, a complete solution of the Dyson equation (D) including the second order contribution $\tilde{\Sigma}^{(2)}(k)$ has to be found.

The scenario which is suggested by the results obtained so far in the self-consistent approach in this section as well as with the RG calculation with one-step RSB in the previous section 10.1 is the following:

- RSB instabilities, which have been examined for a one-step RSB, are present in both treatments. RSB-unstable RG trajectories require a small replica asymmetric perturbation of the bare couplings. However, the physical mechanism underlying the occurrence of such perturbations and thus the existence of a *spontaneous* RSB is unclear so far. On the other side, the self-consistent approach yields a RSB solution for the dressed vertex even for a replica symmetric bare vertex.

- In the RG approach, the replica symmetric RG flow for $m = 1$ is associated with the *minimum* of the free energy in the free RSB parameter m in the limit $n \downarrow 0$ of the replica trick.

- The extended set of two self-consistency equations (V) and (D) and the renormalization include the same classes of divergent diagrams and should yield identical results, which has been explicitly shown for the replica symmetric case. The self-consistent Hartree-approximation of K/GL is recovered when second order diagrams in the Dyson equation and the equation for the dressed vertex are neglected [and hence $1/\tau$-singularities], which can also be demonstrated within the RG analysis.

- In the low-temperature phase $\tau > 0$, the asymptotic propagator acquires *no* k-independent mass to leading order in the vertex such that higher order self-energy contributions have to be considered and additional $\log k$-divergences likely occur as in the replica symmetric RG result. The same result can be obtained by the one-step RSB RG approach in a certain parameter range. This is in contradiction to results from the self-consistent Hartree-approximation of K/GL and favors the existence of a *super-rough* low-temperature phase in the vortex-free 2D RFXY model.

Chapter 11

Two Interacting Arrays of Lines and Steps in Random Media

Planar arrays of lines and steps in a random medium containing point impurities can be mapped onto the 2D RFXY model with a Hamiltonian (8.5) as discussed already in the introductory chapter 8. So far in this second part, we have mainly addressed theoretical aspects of the vortex-free 2D RFXY model regarding the possibility of RSB in the glassy, low-temperature phase of the model. In this chapter we come back to the issue of planar line-arrays and consider a novel application regarding planar arrays of directed lines, which is the effect of point disorder on *two* interacting species of lines in a plane.

This problem arises in the study of the interplay between the roughening and deconstruction of anisotropically (2×1) reconstructed (110) surfaces of gold [92], or other fcc crystals. It has been argued that both the deconstruction and the roughening of the (110) facet can be described in terms of *steps* on the crystal surface, which occur in form of *two* kinds of (3×1) microfacets corresponding to upward and downward steps and representing "defects" in the (2×1) reconstruction [92, 93, 94, 95]. These defects separate different domains of (2×1) reconstruction, which have a choice of *four* different sublattices on the surface [Figure 11.1]. To define an order parameter of the reconstruction, it is useful to introduce a *domain phase* $\varphi(\mathbf{r})$, that counts the number $n(\mathbf{r}) = 1, \ldots, 4$ of the sublattice at point $\mathbf{r}$ in multiples of $\pi/2$:

$$\varphi(\mathbf{r}) \;:=\; n(\mathbf{r})\frac{\pi}{2}\;. \tag{11.1}$$

An order parameter capturing the ordering of the domains is $R(\mathbf{r}) = e^{i\varphi(\mathbf{r})}$, which decays algebraically in the disorder-free system when the domain phase starts to fluctuate at the deconstruction transition. On the other hand, the (3×1) microfacets induce upward and downward steps of the surface and thus height fluctuations, which can lead to a roughening

transition. To explain the possibility of a *simultaneous* deconstruction and roughening, it is important to realize that on a (110) reconstructed facet of a fcc crystal (like gold) the steps affect *both* the order parameter of the roughening transition, i.e., the height of the surface *and* the order parameter of the deconstruction, i.e., the domain phase [92, 93, 94, 95] (as opposed to steps on a reconstructed sc crystal surface, which do *not* couple to the reconstruction degrees of freedom [94, 95]). This is illustrated in Figure 11.1, where upon advancing to the right, the domain phase changes by $+\pi/2$ at each (3×1) microfacet, regardless whether an up or down step, whereas the height changes by +1 at an upward step and -1 at a downward step.

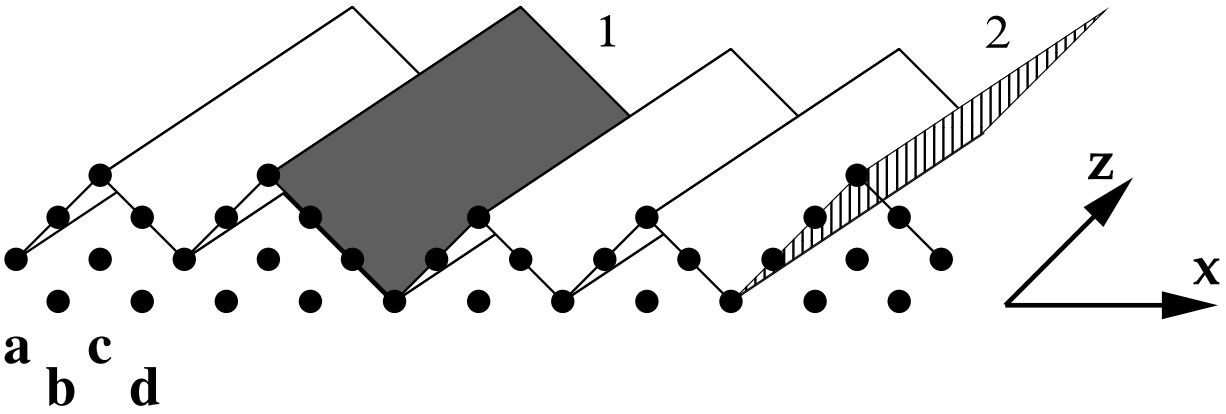

Figure 11.1: Two kinds of (3x1) microfacets on a (2x1) reconstructed crystal surface. The background (2x1) facets can be on four possible sublattices (marked "**a**"–"**d**"). Each (3x1) facet shifts the phase by one sublattice.

Previous studies of the pure system have revealed a rich phase diagram with a variety of possible phases as a function of the interaction parameters [92, 93, 94, 95]. In this chapter, we study the system in the presence of point disorder, which can originate from crystalline defects on a disordered underlying substrate. These point defects induce deformations in the trajectories of the microfacets. As we will show the two interacting arrays of steps in the presence of point disorder can be described by *two coupled* 2D RFXY models.

The investigation of two coupled 2D RFXY models is also of interest for a number of other issues. As already pointed out in chapter 4 in part I, a stack of many coupled 2D RFXY models describes the physics of the FL array in a strongly layered impure HTSC in a magnetic field *parallel* to the superconducting CuO-planes, $\mathbf{H} \parallel \mathbf{ab}$ [Figure 11.2]. This model has been studied by a variational calculation in chapter 4 though it is desirable to perform a RG analysis, which is more suited to describe fluctuations effects on *many* length scales. In this chapter we perform a detailed RG analysis for the corresponding two-layer model, which can be regarded as a "toy"-model of the many-layer system [Figure 11.2]. Due

to the fact that quasi-2D fluctuations play a prominent role also in the many-layer model as demonstrated in chapter 4, two layers should already capture much of the physics contained in the full many-layer system. But the model has also other applications in the field of vortices in superconductors: Josephson vortices in between planar Josephson junctions in an artificial grown SNSNS sandwich structure [Figure 11.2] are another realization, where point disorder is generated by randomly distributed inhomogeneities in the thickness of the middle layer.

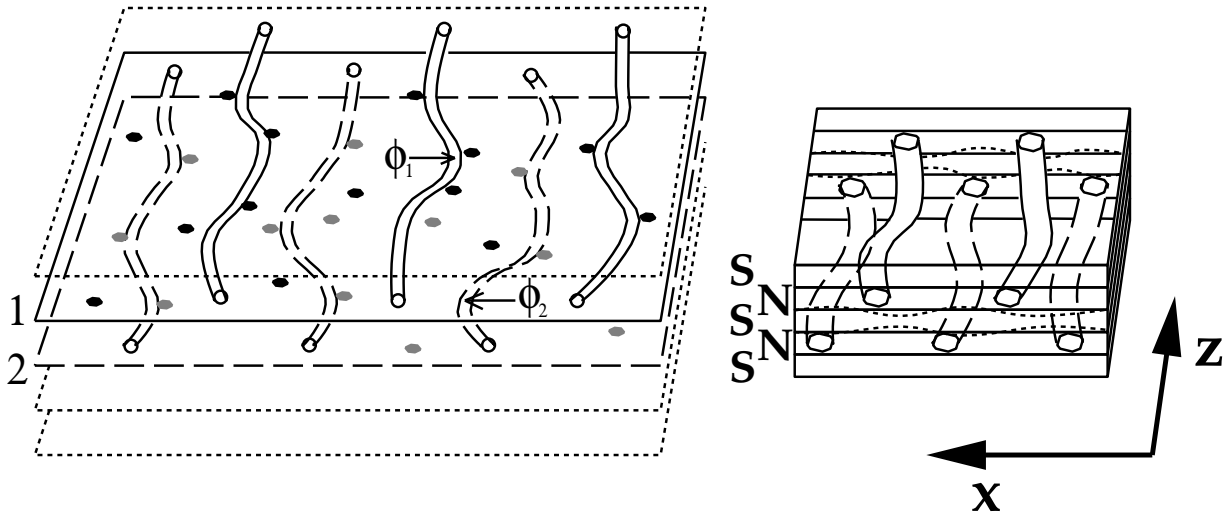

Figure 11.2: Left: Two magnetically interacting arrays of FLs in an impure superconductor. Right: Josephson vortices in an artificial SNSNS sandwich structure with inhomogeneities in the thickness of the middle layer.

It is also of interest for the subject of RSB in a single vortex array, that we discussed already in the previous chapter 10, to consider two *physical* replicas of the system coupled by a small interaction.

We model a single species of directed lines confined in a plane containing quenched point disorder by the 2D RFXY model given by the Hamiltonian (8.5) as discussed already in chapters 3 and 8 in detail. The interaction between the two species of lines is taken to be short-ranged so that we can write in terms of the line density $\rho[\mathbf{r}_i, \phi_i(\mathbf{r}_i)]$ in layer i $(i = 1, 2)$:

$$\beta\mathcal{H}_{int}[\phi_1, \phi_2] \;=\; \int_{\mathbf{r}_1}\int_{\mathbf{r}_2} V_{int}(\mathbf{r}_1 - \mathbf{r}_2)\rho[\mathbf{r}_1, \phi_1(\mathbf{r}_1)]\rho[\mathbf{r}_1, \phi_1(\mathbf{r}_1)] \;, \tag{11.2}$$

with a short-ranged potential V_{int}. Using expression (8.3) for the line density and neglecting

fast oscillating terms, this leads to

$$\beta\mathcal{H}_{int}[\phi_1,\phi_2] \approx \int_{\mathbf{r}} \left\{ 2\mu\rho_0^2 \cos(\phi_1-\phi_2) \; + \; K_\mu \boldsymbol{\nabla}\phi_1\cdot\boldsymbol{\nabla}\phi_2 \right\} \tag{11.3}$$

with

$$\mu = \int_{\mathbf{r}} V_{int}(\mathbf{r}) \tag{11.4}$$

$$K_\mu = \mu/8\pi^2 \; . \tag{11.5}$$

Here we have anticipated that the elastic term becomes *isotropic* in the thermodynamic limit. We assume the disorder potentials $v_i(\mathbf{r})$ (see (8.2) and (3.14)) acting on species i to be statistically identical, i.e., $\overline{v_i(\mathbf{r})v_i(\mathbf{r}')} = g_0\;\delta^2(\mathbf{r}-\mathbf{r}')$, with cross-correlations $\overline{v_1(\mathbf{r})v_2(\mathbf{r}')} = g_{\mu,0}\delta(\mathbf{r}-\mathbf{r}')$ to be specified below. The full Hamiltonian of our system, $\mathcal{H}[\phi_1,\phi_2] = \sum_{i=1}^2 \mathcal{H}[\phi_i] + \mathcal{H}_{int}[\phi_1,\phi_2]$, can then be written in a succinct form [after neglecting fast oscillating terms and anticipating isotropy of the elastic terms],

$$\begin{aligned}\beta\mathcal{H}[\phi_1,\phi_2] \;\; = \;\; & \int_{\mathbf{r}} \Big\{ \frac{1}{2} K_{ij} \boldsymbol{\nabla}\phi_i\cdot\boldsymbol{\nabla}\phi_j \; - \; \mathbf{w}_i[\mathbf{r}]\cdot\boldsymbol{\nabla}\phi_i \\ & + \; W_i[\mathbf{r},\phi_i] \; + \; 2\mu\cos(\phi_1-\phi_2) \Big\},\end{aligned} \tag{11.6}$$

with random potentials W_i and $\mathbf{w}_i$, whose correlators are

$$\overline{W_i[\mathbf{r},\phi]W_j[\mathbf{r}',\phi']} = \; 2g_{ij}\cos(\phi-\phi')\,\delta^2(\mathbf{r}-\mathbf{r}')\overline{\mathbf{w}_i[\mathbf{r}]\mathbf{w}_j[\mathbf{r}']} \tag{11.7}$$

$$= \; \Delta_{ij}\delta^2(\mathbf{r}-\mathbf{r}') \; . \tag{11.8}$$

The parameters of the theory are contained in the 2x2-matrices

$$\Delta_{ij} = \begin{cases} \Delta & (i=j) \\ \Delta_\mu & (i\neq j) \end{cases} \tag{11.9}$$

$$g_{ij} = \begin{cases} g & (i=j) \\ g_\mu & (i\neq j) \end{cases} \tag{11.10}$$

and have bare values

$$g = \; g_0\rho_0^2\frac{1}{T^2} \tag{11.11}$$

$$g_\mu = \; g_{\mu,0}\rho_0^2\frac{1}{T^2} \tag{11.12}$$

$$\Delta_{ij} = g_{ij}/(8\pi^2) \; . \tag{11.13}$$

Notice that all cosine couplings appearing in (11.6) reflect the discrete translational symmetry of the line arrays. The derivation of the above Hamiltonian is analogous to the derivation of the interaction Hamiltonian (4.5, 4.6) for the many-layer system of FLs apart from the additional parameter g_μ, which allows to consider different types of cross-correlation besides the uncorrelated disorder $g_\mu \equiv 0$ considered in chapter 4.

A physical observable of interest for the crystal surface is the height profile $h(\mathbf{r})$ of the surface. It is given by

$$h(\mathbf{r}) \;=\; \left[\phi_1(\mathbf{r}) - \phi_2(\mathbf{r})\right]/2\pi \tag{11.14}$$

since lines from species 1 and 2 represent upward and downward (3×1) microfacets respectively [Figure 11.1], and it is the *difference* of the two that determines the height profile [93]. The other quantity of interest characterizing the domain order is the domain phase φ, which can also be expressed in terms of the fields ϕ_i as

$$\varphi(\mathbf{r}) \;=\; \left[\phi_1(\mathbf{r}) + \phi_2(\mathbf{r})\right]/4 \;. \tag{11.15}$$

Because the domain phase changes in the same way when crossing an upward or downward microfacet [Figure 11.1], it is the *sum* of the number of steps of species 1 and 2 that determines the domain phase φ and thus the domain order parameter $R = e^{i\varphi}$.

In the following analysis, we shall characterize the system by excluding *all* forms of topological defects in ϕ_1 and ϕ_2. This approximation is reasonable for FLs and vortices in Josephson junctions, where it describes the complete confinement of vortex lines between the junctions, and is easily realized experimentally. For FLs in a HTSC, it is the generic situations due to the large energy cost of vortex kinks across the superconducting CuO-planes as discussed in chapter 4. However, it is not always valid for the reconstructed surfaces where vortices in the phase field φ can play an important role [92, 93, 94]. For the latter case, the results of our analysis will be used to determine the relevancy of the vortices in the presence of quenched disorders.

To find the large scale behaviors of the system in the absence of topological defects, we use the replica method and apply the RG equations (9.24, 9.25) derived in chapter 9 for the generalized replicated Hamiltonian of a *single* vortex-free 2D RFXY model. This Hamiltonian is applicable because we have *not* specified the form of the coupling matrices in the RG calculation in chapter 9, and we are thus free to interpret the n-times replicated system consisting of *two* layers as a $2n$-times replicated *single* layer with a specific form of the couplings among the replicas given by the parameters g_{ij} and μ. We are not considering the possibility of RSB here and perform a replica symmetric RG analysis. For the two-layer Hamiltonian (11.6), the RG equations (9.24, 9.25) take on the following form (to bilinear order) [the same set of equations has been derived in Ref. [86] by a mapping onto

a Coulomb gas of vector charges]:

$$\frac{dg}{d\ell} = (\kappa - \tau)g - g^2 - g_\mu\mu \tag{11.16}$$

$$\frac{dg_\mu}{d\ell} = (\kappa - \tau - \delta)g_\mu - gg_\mu - g\mu \tag{11.17}$$

$$\frac{d\mu}{d\ell} = (2\kappa - \delta)\mu - (\tau + \kappa)g_\mu - g\mu \tag{11.18}$$

$$\frac{d\kappa}{d\ell} = \mu(\mu - 2g_\mu)/2 \tag{11.19}$$

$$\frac{d\delta}{d\ell} = (g^2 - g_\mu^2)/2 \tag{11.20}$$

$$\frac{d\overline{\delta}}{d\ell} = (g^2 + g_\mu^2)/2 \ . \tag{11.21}$$

We absorbed a factor $4\pi/\rho_0^2$ into g, μ and g_μ, where π is a non-universal numerical factor appropriate for a circular IR-cutoff as discussed in chapter 9. τ is a *positive* reduced temperature

$$\tau := \frac{1}{4\pi(K + K_\mu)} - 1 \tag{11.22}$$

and

$$\kappa := 1 - \frac{1}{4\pi(K - K_\mu)} \tag{11.23}$$

a reduced elasticity parameter[1]. The parameters

$$\delta := 8\pi(\Delta - \Delta_\mu) \tag{11.24}$$

$$\overline{\delta} := 8\pi(\Delta + \Delta_\mu) \tag{11.25}$$

are a measure of the effect of disorder on the elastic properties of the arrays. While $\overline{\delta}$ does not feedback into (11.16-11.20), its flow controls the scaling of the phase field φ and will be crucial in determining the relevancy of vortices in φ. The RG flow is controlled by the reduced temperature τ, which is *not* renormalized due to the statistical tilt symmetry (9.29) [69, 70]. The parameter δ characterizes the effects of the disorder on the height profile $h(\mathbf{r})$, whereas $\overline{\delta}$ describes the effect of the disorder on the domain phase φ or the order parameter $R = e^{i\varphi}$.

[1] As defined above in (11.22), τ has to be distinguished from the τ (10.40) used in the previous chapter 10. Note the difference in the sign in the definition of the *positive* reduced temperature τ as compared to the *negative* reduced temperatures τ_0 (10.3), τ_m (10.13), τ (10.40) used previously in this part.

At this point, the relation between the system of two coupled *physical* replicas of the 2D RFXY model in *identical* disorder for the two species ($g_\mu \equiv g$, $\delta \equiv 0$) and the replica Hamiltonian with a one-step RSB of a *single* 2D RFXY model can be made explicit on a formal level: The one-step RSB equations (10.15-10.19) with an RSB parameter $m = 2$ corresponding to two species yield with $g = \tilde{g}_1$ and $\mu = \tilde{g}_2 - \tilde{g}_1$ RG equations *identical* to (11.16-11.20) in the limit $n \downarrow 0$.

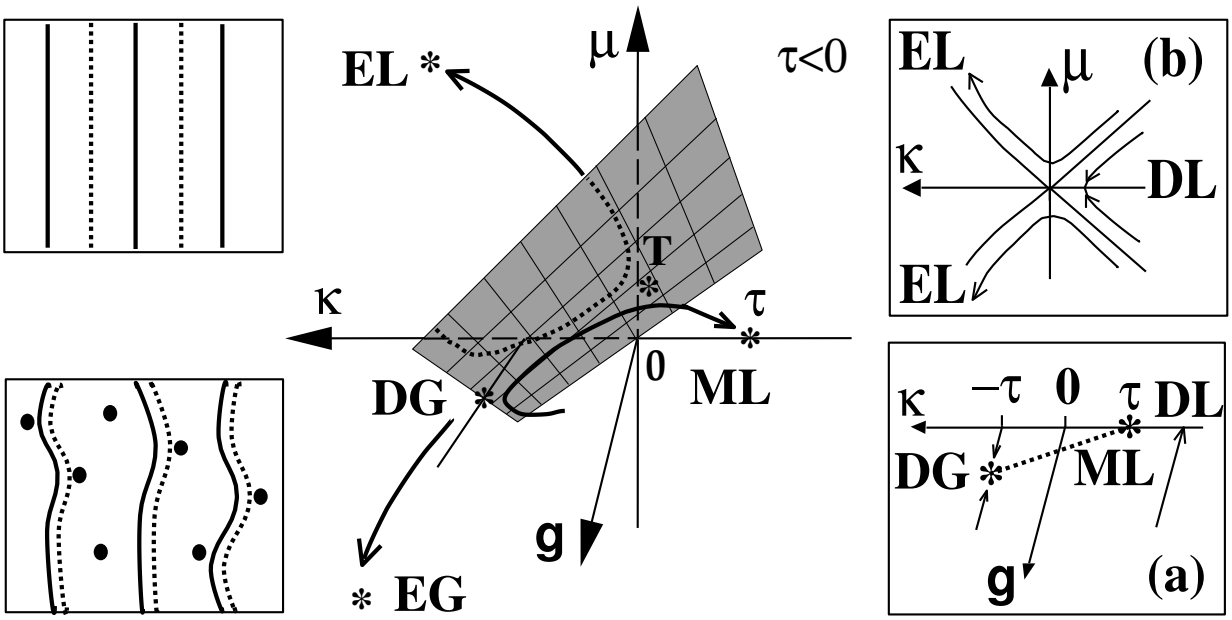

Figure 11.3: RG-flow for identical disorder ($g_\mu = g, \Delta = \Delta_\mu$). Inlets (a) and (b) describe the flow for the sub-case with no inter-species coupling ($\mu = 0$) and no disorders ($g = 0$), respectively.

Before delving into the structure of the RG flow, we first mention two limiting subproblems which have been studied previously. In the limit μ, $g_\mu = 0$, the elasticity parameter κ is also not renormalized, and the RG equation has the same structure as that obtained for a single species of lines by CO [18], with an effective temperature $\tau - \kappa$. As shown in Figure 11.3 (inlet (a)), the disorder (g) is irrelevant at high temperatures ($\tau > \kappa$), yielding the usual logarithmic roughness for 2D surfaces, accompanied by a quasi-long-ranged domain order, i.e., algebraically decaying correlations of $R = e^{i\varphi}$. We refer to this as the decoupled line (DL) phase. At $\tau = \kappa$, the marginal irrelevance of g yields a marginally-coupled line phase (ML), which again has logarithmic roughness and quasi-long-ranged domain ordering. At low temperatures ($\tau < \kappa$), the disorder is relevant. The resulting glass phases are described by the line of fixed points $g^*(\kappa) = \kappa - \tau$, which are perturbatively accessible for $|\kappa|, |\tau| \ll 1$. Since complete decoupling implies also [see equation (11.3)] that

$K_\mu = 0$, or $\kappa + \tau = 0$, only the point $g^* = 2|\tau|$ (and $\mu^* = 0$, $\kappa^* = |\tau|$) along the line $g^*(\kappa)$ is the physical fixed point; it describes a decoupled glass (DG) phase. The surface is *super-rough* [61] in the DG phase, with $\overline{\langle h^2 \rangle} \sim \log^2 L$ on large scales L. The glassiness is also reflected by a disordered (short-ranged) domain order, due to the anomalous scaling of the domain phase $\overline{\langle \varphi^2 \rangle} \sim \log^2 L$. The logarithmic singularities in $\overline{\langle h^2 \rangle}$ and $\overline{\langle \varphi^2 \rangle}$ both result from the divergence of $\overline{\delta}$ when g^* is finite.

Another well known limit of our problem is that of vanishing disorder ($g, g_\mu = 0$), where a Kosterlitz-Thouless (KT) transition occurs independent of τ [see Figure 11.3 inlet (b)]. For large coupling $|\mu|$, the two species become locked together, forming elastically-coupled line (EL) phases with $|\mu^*|, \kappa^* \to \mathcal{O}(1)$. Since the up and down steps are now paired, in phase ($\phi_1 = \phi_2$) for $\mu > 0$ or out of phase ($\phi_1 = \phi_2 + \pi$) for $\mu < 0$, the surface is *flat*, with quasi-long-ranged domain order.

The issue of vortices in the phase field φ has been addressed in Ref. [93]. The vortices are equivalent to *loops* involving the intersection of the four types of domain walls. The relevance of the vortices is controlled by the scaling of $\overline{\langle \varphi\varphi \rangle}$, which depends only on τ in the pure problem. Simple power counting along the line of Ref. [93] indicates that the vortices are relevant if $\tau > 0$ and irrelevant if $\tau < 0$. In the presence of quenched disorders, it naively appears that the vortices might be relevant in the low temperature regime ($\tau < 0$) as well, due to the anomalous variations in φ induced by the disorders. This is however not quite the case as the following analysis will show.

We shall focus on two choices of disorder which are of particular interest: (i) Identical disorder for the two species ($g_\mu \equiv g$, $\delta \equiv 0$), and (ii) completely uncorrelated disorder ($g_\mu \equiv 0$). Case (i) is the generic situation for steps on the anisotropically reconstructed surfaces with disorder. It can also be specifically constructed for the two layers of Josephson vortex lines. In the case of Josephson junctions [Figure 11.2, right] inhomogeneities in the middle layer will lead naturally to identical disorder, whereas for FLs in a layered superconductor in a parallel field, identical disorder can be generated by ion irradiation *perpendicular* to the layers.

The most striking feature of the RG flow in the low temperature ($\tau < 0$) regime [Figure 11.3] is the strong instability of the DG fixed point with respect to inter-species interaction $\mu \neq 0$. An attractive interaction ($\mu < 0$) favors the two species to lock into the same configuration, i.e. $\phi_1 = \phi_2$, or $h = 0$ (flat). Once locked, the system acts effectively as a single species with a doubled elastic constant K, or equivalently a lower effective temperature, so that the effective single species problem is in the glass phase. Correspondingly, (11.16-11.20) yields (for all $\tau < 0$) a RG flow away from the unstable DG fixed point to a sink with strong inter-species coupling *and* strong disorder [$g^*, \kappa^*, -\mu^* \to O(1)$]. We refer to this as the elastically-coupled glass (EG) phase.

Because fluctuation in φ is large for both $\tau > 0$ (entropy driven) and $\tau < 0$ (disorder driven), vortices in φ are *always relevant* for attractive inter-species interactions.

Proliferation of vortices (or loops of domain walls) restores the isotropy of the surface at large scales, rendering the anisotropic treatment meaningless. In the asymptotic isotropic phase, coupling to bulk disorder is likely to roughen the surface as investigated in Ref. [61]. However, a detailed description in that regime is beyond the scope of this work.

A repulsive interaction ($\mu > 0$) competes with fluctuations in the random potential, which still attempts to lock the two species into the same configuration. At low temperatures ($\tau < 0$) [by "low temperatures", we mean $T \lesssim T_c$ or $|\tau| \ll 1$, where the perturbative RG calculation is valid. At much lower temperatures, coupling of the random potential to higher harmonics become relevant and the surface eventually become dominated by disorders], this competition leads to *two* RG sinks separated by a second-order phase transition: If the repulsive interaction dominates, the two species avoid each other by locking into a configuration with $\phi_1 = \phi_2 + \pi$, i.e., with one species displaced by half a line spacing with respect to the other. Such a configuration can be interpreted again as a single species, but now with a doubled line density. This leads to a *higher* effective temperature, such that the effective single species system is *not* glassy, with $g^* = 0$. Corresponding to this scenario, we find for weak bare disorder a RG-flow away from DG towards the fixed point EL, and the RG trajectories approach their pendants in the disorder-free sub-problem. For stronger disorders, however, we obtain a RG flow from DG towards the fixed point ML, since the disorder weakens the inter-species coupling μ and κ, while the coupling μ in turn weakens the disorder g. Note that both the EL and ML phases are *stable* to the formation of dislocations in the phase field φ at low temperatures, since $\bar{\delta}^*$ is finite when $g^* = 0$. The phase transition separating the EL-phase and the ML-phase is governed by an unstable fixed point (T) at $(\kappa^*, g^*, \mu^*) = (-1, 2, 4)\,|\tau|\,/7$, which is the attractor of the plane of separatrix $g \simeq \mu + 2\kappa$. The phase transition is second order for $\tau < 0$, with an algebraically diverging correlation length (characterized by an exponent $\nu = 2\,|\tau|\,/7$) upon crossing the separatrix. It is a remarkable feature of this system that while both RG sinks are (at least marginally) *disorder-free*, the unstable fixed point governing the transition is *disorder-dominated*.

The phases can be characterized quantitatively by examining the linear response of the line density to changes of the line density in the other layer, i.e., the mutual magnetic susceptibility, similarly to the "self"-susceptibility of a layer, which is studied in Ref. [70]. For density changes $\delta\rho$ on scales exceeding the line spacing, only the gradient part of the expression for $\rho[\mathbf{r}_i, \phi_i(\mathbf{r}_i)]$ (8.3) is relevant: $\delta\rho_i = -\partial_x\phi_i/2\pi$. Adding a generating term

$$\beta\mathcal{H}_h = \beta\mathcal{H} - \sum_{i=1}^{2} \int_{\mathbf{r}} h_i \delta\rho_i \tag{11.26}$$

to the Hamiltonian (11.6) [for Josephson vortices, $h_i = \delta H_i \Phi_0/4\pi$ is related to the change δH_i in the applied magnetic field in layer i], we define the mutual susceptibility as $\chi =$

$(\partial/\partial h_1)(\int_{\mathbf{r}} \overline{\langle\delta\rho_2\rangle}/L^2)$ for a system of linear dimension L. $\chi = \int_{\mathbf{r}} \overline{\langle\delta\rho_1(0)\delta\rho_2(\mathbf{r})\rangle_c}$ is related to the (connected) density correlations and can be calculated to lowest order in the renormalized theory as

$$\chi = \pi \frac{(\kappa^* + \tau) - 2\mu^*(1+\tau)(1-\kappa^*)}{1 - 2\mu^*(1-\kappa^*)} \quad , \tag{11.27}$$

where the coupling constants X take on their asymptotic values X^* in the various RG-sinks. Using the above results from our RG analysis for the low temperature ($\tau < 0$) regime, one obtains for the two phases EL and EG the single layer result [70] $\chi_{EL,EG} = 1/2K_{eff}$ with an effectively doubled $K_{eff} = 2(K + K_\mu)$, demonstrating again a locking in these phases. For the ML-phase ($\chi_{ML} = 2\pi\tau$) and the transition point T ($\chi_T = \chi_{ML} \cdot 8/7$), we obtain small negative values $\sim -\tau$ for the susceptibility indicating a small tendency of the lines in layer 2 to avoid places of high line-density in layer 1 and vice versa. At the unstable DG fixed point, one finds $\chi_{DG} = 0$ corresponding to a decoupling of the layers.

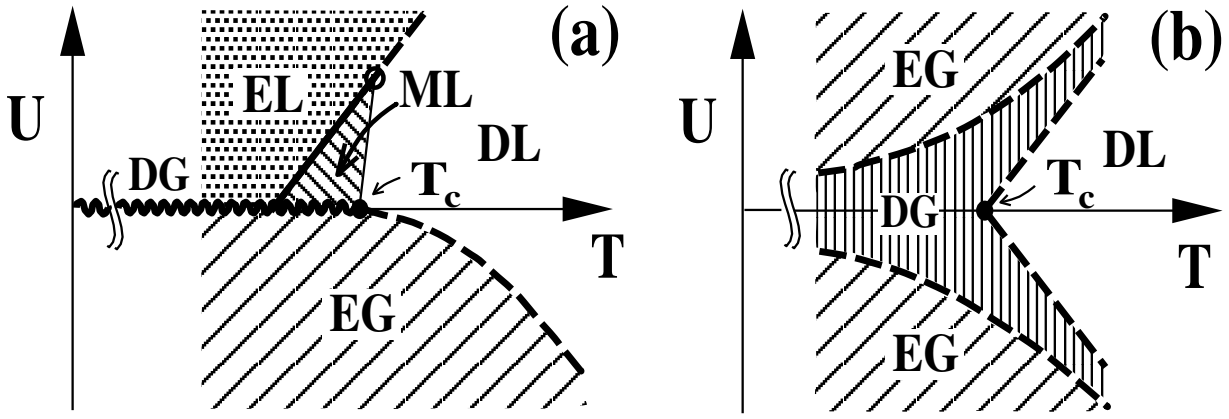

Figure 11.4: Phase diagram for two species of lines in (a) identical and (b) uncorrelated random media.

The above analysis of the RG flow can be straightforwardly turned into a phase diagram. We define an inter-species interaction energy $U = \mu T$, and present the phase diagram in the (U, T) space, at a fixed disorder strength g [see Figure 11.4]. The super-rough DG phases exist at $U = 0$ below a critical temperature T_c given by $K_c = 1/(4\pi)$. These phases are marked by the thick wavy line in Figure 11.4(a) and are unstable to dislocations in φ. For $U > 0$, a separatrix $g = \mu + 2\kappa$ separates the flat, pure phase (EL) at low temperature and large repulsion from the two high temperature phases. At very high temperatures ($T \gg T_c$), the system is in the pure decoupled phase (DL), which is unstable to dislocations in φ. (For surfaces, this phase belongs to the Ising universality class [93].) Upon lowering the temperature beyond the line $\tau = 0$ (thin solid line), the system settles into the *stable*

ML phase for weak repulsive interaction (compared to the strength of disorders). Further lowering the temperature beyond the separatrix (the thick solid line), the system makes a second-order transition from the ML to the EL phase which is also stable with respect to dislocations. Note that because the critical properties there are controlled by the fixed point T which depends on τ, the critical exponents governing this transition actually vary *continuously* along the thick solid line. The second-order transition terminates at a point where the separatrix intersects the line $\tau = 0$ (the open circle in Figure 11.4(a). The transition between DL and EL at higher temperatures is expected to be the same as that of the disorder-free case.

Perhaps the most striking result of the above analysis is the suppression of glass order below T_c by applying a small repulsion between the two species of lines. This induces always a RG flow *away* from the glassy DG phase with the signature of the super-roughness to one of the *disorder-free* RG sinks EL or ML. This effect stabilizes the anisotropy of the reconstruction and the flatness of the surface. The generic suppression of glass order by the repulsive interaction is also quite interesting from a more general theoretical perspective of the discussion of RSB in a *single* array of lines, i.e., the 2D RFXY model: Whereas the super-rough DG phase is identical to the fixed point found by CO in the replica symmetric RG analysis [18, 19, 61], the variational method with RSB [9, 17, 21] seem to find the ML phase instead, which appears naively to be consistent with our findings here. However, our result can in fact be used to question the internal consistency of the RSB scheme: As described in Refs. [90, 91], a physical way of probing the existence of RSB is to take two *physical* replicas of a system in identical random potentials, and monitor the response to a small repulsion between the replicas. If there is a degeneracy of low free energy states (which the RSB scheme attempts to describe), then an infinitesimal repulsion between the replicas will force the two to occupy different states which have *similar glassy properties* and little overlap. The system we have analyzed so far can be interpreted as two physical replicas in the same random potential. In our case, we note that a small repulsion has a much stronger effect in that it gives rise to qualitatively different behaviors, i.e., from DG to ML. This indicates that the glass order of a single line array is extremely fragile, making it quite different from the usual scenario expected of stable (zero-temperature) glass phases. Thus from the view point of the replica symmetric RG analysis, the absence of glass order from the solution of the variational treatment is not surprising, as it may be the result of subtle interactions introduced by the RSB scheme itself. This is in accordance with our findings in chapter 10 where we could reproduce the results of the variational treatment in a RG analysis with RSB if a small initial replica asymmetry was introduced.

We continue with a short discussion of the case where the disorder potentials acting on the two species are uncorrelated, i.e. with the bare $g_\mu = 0$. This is the generic case for two layers of Josephson vortex lines in planar Josephson junctions containing point impurities. Uncorrelated disorder tends to *decouple* the two species of lines and competes with the

locking effect of the inter-species interaction. (Here attractive and repulsive interactions are qualitatively similar, up to a relative π-phase shift between the two species.) The RG analysis is more complicated than before, because one has to consider the full set of equations (11.16-11.21) [note that g_μ is generated by μ and g]. The basic features of the phase diagram can be obtained by observing that the RG-flow is dominated by two KT transitions which can be found in two sub-problems of the RG equations (11.16-11.21): (i) The KT transition of the disorder-free sub-problem. (ii) The KT transition which occurs in the space (g_μ, δ), when $g = \mu = \kappa + \tau = 0$. The latter has a critical separatrix $g_\mu/\sqrt{2} = \delta + 2\tau$ which isolates two regions of flow to a sink with $g_\mu = 0$ and $\delta > 0$, and another sink where g_μ grows. The first sink is consistent with a decoupled glass (DG) phase as the eigenvalue for the flow of μ becomes negative there, while the second sink is consistent with the elastically-coupled glass (EG) phase where $|g_\mu| \to g$. It is difficult to find analytically a continuation of this separatrix to the regime of physical initial conditions (e.g., $g, \mu \gg g_\mu$) in a controled approximation. However, we determined it numerically to be well described by the form

$$\mu \;\simeq\; \tilde{\alpha}\frac{gK_c}{K} \;=\; \frac{\tilde{\alpha}}{4\pi}\frac{g}{K} \tag{11.28}$$

with the numerical constant $\tilde{\alpha} \approx 0.5$. This condition, combined with sub-problem (i) leads to the phase diagram depicted in Figure 11.4(b). The condition (11.28) separating the decoupled and coupled glass phases is of the same form as the criterion (4.40) found by a variational calculation for the system consisting of *many* layers in chapter 4. This similarity includes the numerical value $\tilde{\alpha}$ as we have shown there. In view of the very general RG equations (9.24, 9.25) provided in chapter 9, it is tempting to attack such a many layer system [say with N layers, where also more realistic non-local layer-interactions can be considered in principal] by an analogous RG treatment as performed here for two layers; such a calculation was proposed in Ref. [75]. Though the formulation of RG equations is straightforward, starting from (9.24, 9.25) with the correct choices for the coupling matrices for a replicated system containing nN coupled layers, the RG analysis will be very difficult as this example of two layers already demonstrates.

In conclusion, we have presented a detailed RG analysis for a model of two interacting planar line arrays in random media. Among the findings are a novel second-order phase transition with continuously varying critical exponents, the stability of the anisotropic flat phase for repulsive interactions, and the replacement of the super-rough glass phase by a marginally-coupled phase. These findings along with the structure of the proposed phase diagrams should be accessible by experimental or numerical investigations.

Chapter 12

Conclusion

From a theoretical point of view, our interest in this part of the work has been focused on the development of a more consistent picture regarding the two main analytic approaches to the vortex-free 2D RFXY or random phase sine-Gordon model: The replica symmetric RG analysis of CO/GH [18, 19] and the variational approach using RSB of K/GL [9, 17, 21] that results in a self-consistent Hartree-approximation. In chapter 10, this aim could be met to a certain extent by clarifying the approximations and extensions needed in each of the approaches to reproduce the results of the other. In section 10.1, we generalized the replica symmetric RG analysis to a one-step RSB scheme and found in the low-temperature, glassy phase of the model an *instability* with respect to RSB similar to the findings of the variational calculation of K/GL, who find the thermodynamically stable solution of the self-consistency equations to have a broken replica symmetry with a one-step RSB scheme. In fact, their results can be reproduced by choosing appropriate bare values for the disorder correlator in replica space. On the other hand, we demonstrated that the RG calculation considers higher order terms in the disorder strength, which can give essential singularities and are neglected in the self-consistent Hartree-approximation. In section 10.2, these contributions are identified in a diagrammatic "language" and included into an extended set of self-consistency equations, the main features of which are the appearance of an equation for a dressed vertex and a momentum-dependent higher order correction to the propagator. This extended set of equations can reproduce the RG results for the replica symmetric case. For a one-step RSB scheme we have shown that the solution of the Hartree-approximation is at least strongly modified such that the appearance of a super-rough low-temperature phase, which is the characteristic result of the replica symmetric RG approach [61], cannot be excluded any more.

This may be important in the light of very recent numerical results on the ground state of solid-on-solid models on disordered substrates [97, 98], where clear evidence for the existence of a super-rough low-temperature has been found. These models are believed to be in the same universality class as the random-phase sine-Gordon model if one is

close enough to the transition point ($K \gtrapprox K_c$) that higher harmonics in the density [such as in (3.34)] are *irrelevant*. Though this is not evident for the ground-state at $T = 0$ ($K/K_c \uparrow \infty$), the numerical results of Refs. [97, 98] are more conclusive than previous studies because the *asymptotic* behaviour can be easier accessed at $T = 0$. This is mainly because the crossover length set by the positional correlation length $R_l \sim (K^2/g)^{K/2(K-K_c)}$ (see (3.59)) is much smaller for $T = 0$ or $K/K_c \uparrow \infty$ than in the regime close to the transition $K \gtrapprox K_c$. In addition, a fast algorithm determining the exact ground state of a given sample enables averaging over over many realizations of larger systems.

However, from the analytic point of view, the question of an eventual super-roughness of the low-temperature phase of the vortex-free 2D RFXY model is far from a final answer at the present stage. It would certainly be useful to continue the investigations performed in this work to a study of continuous RSB schemes. For the RG analysis, the corresponding RG recursion relations for a continuous RSB have already been derived in Ref. [55] but a thorough analysis of the RG sinks is yet to be performed. Due to technical difficulties, it is not clear whether a generalization of the extended self-consistency equations given in section 10.2 for the replica symmetric case and a one-step RSB scheme to continuous Parisi-type matrices is possible and amenable to further analysis. It would also be very useful to obtain the extended self-consistency equations given in section 10.2 in a systematic expansion, probably a $1/N$-expansion in the number of components N of the phase field ϕ. That such a derivation might be possible is suggested by the RG calculation for the N-component vortex-free 2D RFXY model in Ref. [56]. Another question arises naturally in view of the RSB instability in the RG treatment of the *equilibrium* system: Can similar instabilities be found in the dynamical RG treatment of Refs. [22, 23] and if so, how are they related to the findings in Ref. [54] regarding a possible violation of the fluctuation-dissipation theorem in the low-temperature regime?

We considered here mainly the vortex-free version of the 2D RFXY model. A further complication occurs if one allows for vortices. It has not yet been investigated in detail how possible RSB instabilities affect the Kosterlitz-Thouless transition describing the proliferation of vortices. This synthesis is of special interest regarding novel findings about the Kosterlitz-Thouless transition in the 2D XY model with random phase shifts [80]. Presumably, the work of CO who discussed the full 2D RFXY model including vortices needs further modifications regarding these points.

Regarding possible applications, chapter 11 is certainly most interesting, where an array of two interacting species of lines in a random medium has been considered. Such a model has important applications in describing simultaneous roughening and deconstruction of reconstructed fcc crystal surfaces in the presence of randomness due to an underlying disordered substrate. We could obtain for this system a phase diagram based on the results of a detailed RG analysis. Moreover, this model represents the link between both parts of the thesis because it can be regarded also as simplified version of an FL array

in a layered superconductor in a parallel field. In this simplified model, we can confirm the Lindemann-criterion (5.32, 5.40) derived in part I for the stability of a topologically ordered Bragg glass phase in superconductors containing point defects.

Appendix A

Part I

A.1 Random Force, Bragg Glass and Random Manifold Regime

A.1.1 Correlations and Larkin Lengths in the Random Force and Bragg Glass Regime

In this Appendix we first calculate the $\overline{\langle uu \rangle}$-correlations in the RF regime, and deduce the Larkin lengths L_ξ and R_ξ for low temperatures and a dispersion-free tilt modulus $c_{44}[K] = \hat{c}_{44}$ in the cases $n \geq 2$ and $n = 1$. Afterwards, we discuss the Larkin lengths and RF regime in the single-harmonic Bragg glass model defined by (3.35, 3.36).

$n \geq 2$

We consider first the case $n \geq 2$, and use the elastic Hamiltonian $\mathcal{H}_{el}^{(d,n\geq 2)}$ from (3.11) with an inverse elastic propagator

$$G_{el}^{-1}(\mathbf{K}, k_z) \;=\; c_{66}K^2 + \hat{c}_{44}k_z^2 \;. \tag{A.1}$$

From the scaling relation (3.8) between longitudinal scales L and transversal scales R follows $L_\xi \simeq (\hat{c}_{44}/c_{66})^{1/2} R_\xi$. The Larkin lengths are defined as the crossover length scales where

$$\overline{\langle (\mathbf{u}(R_\xi, L_\xi) - \mathbf{u}(\mathbf{0}))^2 \rangle} \;\simeq\; 2\overline{\langle u^2 \rangle}(R_\xi, L_\xi) \;\simeq\; \xi_{ab}^2 \tag{A.2}$$

at low temperatures (i.e., below the depinning temperature such that $\xi_{ab}^2 \gtrsim \langle u^2 \rangle_T (R_\xi, L_\xi)$, where $\langle \ldots \rangle_T$ denotes the thermal average).

We start with the Hamiltonian

$$\mathcal{H}^{(d,n)}[\mathbf{u}] = \mathcal{H}_{el}^{(d,n)}[\mathbf{u}] + \mathcal{H}_{d,RF}^{(d,n)}[\mathbf{u}] \tag{A.3}$$

with $\mathcal{H}_{d,RF}^{(d,n)}$ in the approximation (3.21) appropriate for the RF regime.

Using the replica method (8.11), we introduce m replicas of the system (with indices $\alpha, \beta = 1, \ldots, m$) and perform the (Gaussian) disorder average with the random force distribution (3.23) characterized by the mean-square random force strength f_0^2. This leads to a replica Hamiltonian $\mathcal{H}_{R,RF}[\{\mathbf{u}_\alpha\}]$ *quadratic* in the displacements $\mathbf{u}_\alpha$:

$$\begin{aligned} \mathcal{H}_{R,RF}[\{\mathbf{u}_\alpha\}] &= \sum_{\alpha,\beta=1}^{m} \int_{BZ} \frac{d^{d-1}\mathbf{K}}{(2\pi)^{d-1}} \int \frac{dk_z}{2\pi} \\ &\quad \frac{1}{2} \left\{ \delta_{\alpha\beta} G_{el}^{-1}(\mathbf{K}, k_z) - \frac{f_0^2}{nT} \right\} \mathbf{u}_\alpha(\mathbf{K}, k_z) \cdot \mathbf{u}_\beta(-\mathbf{K}, -k_z) \end{aligned} \tag{A.4}$$

The quantity of interest is the replica-diagonal part of the propagator in the limit $m \downarrow 0$, which is obtained straightforward as

$$\begin{aligned} \overline{\langle \mathbf{u}(\mathbf{k}) \cdot \mathbf{u}(\mathbf{k}') \rangle} &= \langle \mathbf{u}_\alpha(\mathbf{k}) \cdot \mathbf{u}_\alpha(\mathbf{k}') \rangle_R \\ &= (2\pi)^d \delta^d(\mathbf{k} + \mathbf{k}') \left(\frac{nT}{G_{el}^{-1}(\mathbf{K}, k_z)} + \frac{f_0^2}{\left(G_{el}^{-1}(\mathbf{K}, k_z)\right)^2} \right), \end{aligned} \tag{A.5}$$

where $\langle \ldots \rangle_R$ denotes an average with the replica-Hamiltonian $\mathcal{H}_R[\mathbf{u}_\alpha]$. At temperatures below the depinning temperature, we can neglect the first term. To calculate $2\overline{\langle u^2 \rangle}(R, L)$ ($L \sim (\hat{c}_{44}/c_{66})^{1/2} R$), we introduce an appropriate IR-regularization in the denominator of (A.5) by using $G_{el}^{-1}(\mathbf{K}, k_z) + \alpha$ with

$$\alpha := \hat{c}_{44} \, (2\pi/L)^2 \, , \tag{A.6}$$

and obtain after substituting $K \to K(c_{66}/\hat{c}_{44})^{1/2}$ and extending the integration over $\mathbf{K}$ to infinity

$$\begin{aligned} 2\overline{\langle u^2 \rangle}(R, L) &= 2 \int \frac{d^{d-1}\mathbf{K}}{(2\pi)^{d-1}} \int \frac{k_z}{2\pi} \frac{f_0^2}{\left(G_{el}^{-1}(\mathbf{K}, k_z) + \alpha\right)^2} \\ &= L^{4-d} \left(\frac{f_0^2}{\hat{c}_{44}^{(5-d)/2} c_{66}^{(d-1)/2}} \right) \left(2c_d (2\pi)^{d-4} \right) \, , \end{aligned} \tag{A.7}$$

where

$$c_d = \int \frac{d^d\mathbf{k}}{(2\pi)^d} \frac{1}{(1 + k^2)^2} = (2\pi)^{-d} \pi^{d/2} \Gamma(2 - d/2) \tag{A.8}$$

with $c_{d=3} = 1/8\pi$, $c_{d=2} = 1/4\pi$ and $c_{d=1} = 1/4$. In particular, we can read off from (A.7) the *roughness exponent*

$$\zeta_{RF} \;=\; \frac{4-d}{2} \;, \tag{A.9}$$

which is independent of n for low temperatures.

We obtain from their definition (A.2) the Larkin lengths

$$\begin{aligned} L_\xi \;&\simeq\; \bar{c}_d \; \xi_{ab} \left(\frac{\hat{c}_{44}^{(5-d)/2} c_{66}^{(d-1)/2} \xi_{ab}^d}{f_0^2 \xi_{ab}^2} \right)^{1/(4-d)} \\ R_\xi \;&\simeq\; L_\xi \; (c_{66}/\hat{c}_{44})^{1/2} \;, \end{aligned} \tag{A.10}$$

where

$$\bar{c}_d \;=\; 2\pi (2c_d)^{-1/(4-d)} \tag{A.11}$$

with $\bar{c}_{d=2} = (2\pi)^{3/2}$ and $\bar{c}_{d=3} = 8\pi^2$.

For $d = 1$, R_ξ is not defined properly, and using $f_0^2 \xi_{ab}^2 = n\Delta_g^2 \xi_{ab}^{-1}$ (3.23), we obtain the *single vortex Larkin length*

$$L_\xi^s \;\simeq\; \bar{c}_{d=1} \; \xi_{ab} \left(\frac{c_{44}^{s\;2} \xi_{ab}^2}{n\Delta_g^2} \right)^{1/3} \;. \tag{A.12}$$

$n = 1$

For $n = 1$, i.e., *uniaxial* displacements $\mathbf{u} = u \cdot \hat{\mathbf{x}}$, we have to include longitudinal compression modes (in the local limit $c_{11}[K] = \hat{c}_{11}$), and use the elastic Hamiltonian $\mathcal{H}_{el}^{(d,n=1)}$ from (3.12) with

$$G_{el}^{-1}(K_\parallel, \mathbf{K}_\perp, k_z) \;=\; \hat{c}_{11} K_\parallel^2 + c_{66} K_\perp^2 + \hat{c}_{44} k_z^2 \;. \tag{A.13}$$

Following the same steps as above, we obtain Larkin lengths

$$\begin{aligned} L_\xi \;&\simeq\; \bar{c}_d \; \xi_{ab} \left(\frac{\hat{c}_{44}^{(5-d)/2} c_{66}^{(d-2)/2} \hat{c}_{11}^{1/2} \xi_{ab}^d}{f_0^2 \xi_{ab}^2} \right)^{1/(4-d)} \\ R_{\xi,\perp} \;&\simeq\; L_\xi \; (c_{66}/\hat{c}_{44})^{1/2} \\ R_{\xi,\parallel} \;&\simeq\; R_{\xi,\perp} \; (\hat{c}_{11}/c_{66})^{1/2} \end{aligned} \tag{A.14}$$

Larkin Lengths of Bragg Glass Model and 2D RFXY Model

Let us discuss the RF regime in the Bragg glass model defined by an elastic Hamiltonian $\mathcal{H}_{el}^{(d,n\geq 2)}$ (3.11) or $\mathcal{H}_{el}^{(d,n=1)}$ (3.12) and a disorder part $\mathcal{H}_{d,B}^{(d,n)}$ with (3.35, 3.36). For the m-times replicated disorder-averaged system, the Bragg glass Hamiltonian reads

$$\begin{aligned}\mathcal{H}_{R,B}[\{\mathbf{u}_\alpha\}] \;=\; \sum_{\alpha,\beta=1}^{m} \Bigg\{ & \int_{BZ} \frac{d^{d-1}\mathbf{K}}{(2\pi)^{d-1}} \int \frac{dk_z}{2\pi} \\ & \frac{1}{2}\left\{\delta_{\alpha\beta} G_{el}^{-1}(\mathbf{K},k_z)\right\} \mathbf{u}_\alpha(\mathbf{K},k_z)\cdot\mathbf{u}_\beta(-\mathbf{K},-k_z) - \\ & - \int d^{d-1}\mathbf{R} \int dz \;\sum_{i=1}^{z} g_B \cos\left(\mathbf{K}_{0i}\cdot(\mathbf{u}_\alpha(\mathbf{R},z)-\mathbf{u}_\beta(\mathbf{R},z))\right)\Bigg\}\end{aligned} \tag{A.15}$$

After expanding for small u_α

$$g_B \;\cos\left(\mathbf{K}_{0i}\cdot(\mathbf{u}_\alpha-\mathbf{u}_\beta)\right) \;\approx\; 1-\frac{1}{2}g_B\left(\mathbf{K}_{0i}\cdot(\mathbf{u}_\alpha-\mathbf{u}_\beta)\right)^2 \tag{A.16}$$

the Bragg glass Hamiltonian (A.15) is found to give the same propagator (A.5) as the RF Hamiltonian (A.4) (in the limit $m \downarrow 0$, for all $n \geq 1$) with an effective coherence length $\xi_{ab,B} \simeq l$ and an effective random force strength $f_{0,B}$

$$f_{0,B}^2 \xi_{ab,B}^2 = f_{0,B}^2 l^2 = c_B \; n g_B, \tag{A.17}$$

where

$$c_B = 8\pi^2 z/n \tag{A.18}$$

is a number. Except for the additional factor c_B, this is just the definition of g_B (3.37) when the effective coherence length $\xi_{ab,B} \simeq l$ is used instead of ξ_{ab}. Thus, the naive expansion of the cos-term, which is correct on the shortest scales $L \ll L_\xi = L_l$, yields Larkin lengths exactly as calculated above in formulae (A.10, A.14), however, with ξ_{ab} replaced by $\xi_{ab,B} \simeq l$ and f_0 replaced by $f_{0,B}$.

On the other hand, in Ref. [9], the asymptotic solution on large scales of this Bragg glass model for $n = 1$ has been worked out by a variational approach with RSB, and the crossover length scale, where the asymptotic logarithmic roughness sets in, was determined. This produces again formulae exactly of the form (A.10, A.14) and with f_0^2 replaced by an effective random force strength as in (A.17). They find

$$c_B = (2\pi)^4 z/n^2. \tag{A.19}$$

In $d = 2$ with $n = 1$ (and $z = 1$) the Bragg glass model is equivalent to the the 2D RFXY model defined in (3.45-3.54), after the transformation $p\phi = u(2\pi/l)$. The transversal

Larkin length $R_\xi = R_l$ at $T = 0$ can now be expressed in terms of $KT = (\hat{c}_{11}\hat{c}_{44})^{1/2}(pl/2\pi)^2$ (see 3.53) and $gT^2 = (\hat{c}_{44}/\hat{c}_{11})^{1/2} g_B$ (see 3.54) instead of the 2D elastic moduli c_{11} and c_{44} (see (A.14) as

$$R_l(T=0) = R_\xi(T=0) \simeq \bar{c}_{d=2}\bar{c}_B^{1/2}\frac{K}{g^{1/2}} \quad \text{with} \tag{A.20}$$

$$\bar{c}_B := \frac{(2\pi)^4}{p^4 c_B} \tag{A.21}$$

with c_B from perturbation theory (A.18) or from the variational calculation (A.19). Because disorder is only marginally relevant in $d = 2$, we obtain for $0 < T < T_g$ in the low-temperature phase a strongly increased Larkin length. This is obtained both in the variational calculation and in perturbation theory by applying the RG-equations (4.20) to include the renormalization of the disorder in the correlation function as in (4.23). One finds

$$R_l(\tau) = R_\xi(\tau) \simeq l\left(\frac{R_l(T=0)}{l}\right)^{1/\tau} . \tag{A.22}$$

The continuum version of the layered model of section 4 is equivalent to the Bragg glass model with $d = 3$ and $n = 1$ (also $z = 1$), again by means of a transformation $p\phi = u(2\pi/l_\parallel)$. In terms of the isotropic elastic constant K and the disorder strength g of a single layer together with $\mu T = c_{66}(\hat{c}_{44}/\hat{c}_{11})^{1/2}(l_\parallel/2\pi)^2/l_\perp$ (in terms of the 3D elastic moduli), the transversal Larkin lengths $R_{\xi,\parallel} = R_{l,\parallel}$ (parallel to the layers) and $R_{\xi,\perp} = R_{l,\perp}$ (perpendicular to the layers) are (see (A.14))

$$\begin{aligned} R_{l,\parallel} = R_{\xi,\parallel} &= \bar{c}_{d=3}\bar{c}_B\frac{K^{3/2}\mu^{1/2}}{g} \\ R_{l,\perp} = R_{\xi,\perp} &= \bar{c}_{d=3}\bar{c}_B\frac{K\mu}{g}l_\perp . \end{aligned} \tag{A.23}$$

Throughout section 4, we use the result from the variational calculation (A.19) for c_B in the expressions for the Larkin lengths along with the correlator from the variational calculation as well as $p = 1$ for simplicity; this corresponds to $\bar{c}_B = 1$. However, note that the result for the "Lindemann-number" c (4.48) is *independent* of $\bar{c}_B$.

A.1.2 Correlations in the Random Manifold Regime

We want to obtain the scaling form of the $\overline{\langle uu\rangle}$-correlations in the RM regime (3.31) for the Hamiltonian

$$\mathcal{H}^{(d,n)}[\mathbf{u}] = \mathcal{H}_{el}^{(d,n)}[\mathbf{u}] + \mathcal{H}_{d,RM}^{(d,n)}[\mathbf{u}] , \tag{A.24}$$

where the elastic part (3.11) contains a tilt modulus exhibiting a dispersion (3.4) $c_{44}[K] \simeq \hat{c}_{44}/(1 + K^2\tilde{\lambda}_c^2)$. The disorder part is given by the RM approximation (3.29).

We use here only the simplest possible scaling argument, a so-called "Flory-argument" [52]. Nevertheless, it reproduces the roughness-exponents obtained with the variational calculation using a RSB Ansatz and allows to include the dispersion (3.4) of the tilt modulus in the elastic Hamiltonian (3.11) in the treatment. In a Flory-type argument, we assume that the scaling of the elastic energy $\overline{\langle \mathcal{H}_{el}^{(d,n)} \rangle}$ and the energy from fluctuations in the disorder energy $(\overline{\langle (\mathcal{H}_{d,RM}^{(d,n)})^2 \rangle})^{1/2}$ is determined by *one* dominant large length scale L with (3.8, 3.4) giving the scaling between longitudinal scales L and transversal scales R. This yields the relations [$u^2 := \overline{\langle u^2 \rangle}(R,L)$]

$$\begin{aligned} L &\sim \left(\frac{\hat{c}_{44}}{c_{66}}\right)^{1/2} \left(1+\frac{\tilde{\lambda}_c^2}{R^2}\right)^{-1/2} R \\ \overline{\langle \mathcal{H}_{el}^{(d,n)} \rangle}(R,L) &\sim u^2\ R^{d-3}\ L \sim \left(1+\frac{\tilde{\lambda}_c^2}{R^2}\right)^{-1} u^2\ R^{d-1}\ L^{-1} \\ (\overline{\langle (\mathcal{H}_{d,RM}^{(d,n)})^2 \rangle})^{1/2}(R,L) &\sim u^{-n/2}\ \left(R^{d-1}L\right)^{1/2} . \end{aligned} \tag{A.25}$$

Requiring that elastic and disorder energy scale in the same way, it follows

$$\begin{aligned} u^2\ R^{d-3}\ L &\sim u^{-n/2}\ \left(R^{d-1}L\right)^{1/2} \\ u^2 &\sim R^{2\zeta}\left(1+\frac{\tilde{\lambda}_c^2}{R^2}\right)^{\zeta/(4-d)} \sim L^{2\zeta}\left(1+\frac{\tilde{\lambda}_c^2}{R^2}\right)^{\zeta(5-d)/(4-d)} . \end{aligned} \tag{A.26}$$

This is the scaling form of the $\overline{\langle uu \rangle}$-correlations in the RM regime (3.31) with the Flory-result

$$\zeta = \zeta_{Flory}(d,n) = \frac{4-d}{4+n} \tag{A.27}$$

for the roughness-exponent ζ.

A.2 Details of the Variational Calculation

The propagator (4.34) consists of 3 parts

$$G \approx G^{th} + G^{dis}_{2D} + G^{dis}_{3D} , \tag{A.28}$$

G^{th} from thermal fluctuations, G^{dis}_{2D} from quasi-2D fluctuations of the disordered system, described by the low-temperature phase (we have *always* $\tau > 0$ for the physical realization of a HTSC in a parallel field, see (4.15, 4.16)) of the corresponding 2D RFXY model, and G^{dis}_{3D} from the elastic fluctuations of the 3D Bragg glass. In detail, we have

$$G^{th}(\mathbf{k}_\parallel, k_\perp) = \frac{1}{G_0^{-1}(k_\parallel, k_\perp)} \quad \text{with} \tag{A.29}$$

$$G_0^{-1}(k_\parallel, k_\perp) = K k_\parallel^2 + 2\widetilde{\mu}\left(1 - \cos\left(l_\perp k_\perp\right)\right) , \tag{A.30}$$

$$G^{dis}_{2D}(\mathbf{k}_\parallel, k_\perp) \simeq \frac{1}{G_0^{-1}(k_\parallel, k_\perp)} \, \frac{\tau + y/2}{1-\tau} \, \mathrm{f}_{2D}\left[\frac{R_{l,2D}(\tau) k_\parallel}{2\pi}\right] \tag{A.31}$$

$$G^{dis}_{3D}(\mathbf{k}_\parallel, k_\perp) \simeq \frac{2\pi^2 K \widetilde{\mu}^{1/2}}{\left(G_0^{-1}(k_\parallel, k_\perp)^{3/2}\right)} \, \mathrm{g}_{3D}\left[\frac{\widetilde{R}_{l,3D,\parallel}}{2\pi}\left(\frac{G_0^{-1}(k_\parallel, k_\perp)}{K}\right)^{1/2}\right] \tag{A.32}$$

[for the definition of y, see (A.39)]. The functions f_{2D} and g_{3D} control the crossover from the asymptotic behaviour on scales exceeding the Larkin lengths to the perturbative regime on small scales. In the variational RSB approach of Ref. [9], they are

$$\mathrm{f}_{2D}[x] \simeq \frac{1}{1+x^2} \tag{A.33}$$

$$\mathrm{g}_{3D}[x] \simeq \frac{2}{\pi} \arctan\left(\frac{2\pi}{x}\right) , \tag{A.34}$$

with $\mathrm{f}_{2D}[x], \mathrm{g}_{3D}[x] \simeq 1$ for $x \gg 1$. At small length scales, they produce essentially a cutoff due to $\mathrm{f}_{2D}[x], \mathrm{g}_{3D}[x] \simeq 0$ for $x \ll 1$.

Note that for $\widetilde{\mu} \downarrow 0$also $G^{dis}_{3D} \downarrow 0$, and we have only contributions from 2D thermal and disorder fluctuations.

A.2.1 Self-Consistency Equation

Using the propagator (A.28-A.32), we rewrite the self-consistency equation (4.33), which determines $\widetilde{\mu}(\mu)$ as function of μ, in the form (4.35):

$$0 = \frac{\partial F_{var}}{\partial \widetilde{\mu}} \propto \widetilde{\mu} - \mu \, \exp\left(-\frac{\mathrm{I}[\widetilde{\mu}]}{2}\right)$$

with

$$I[\widetilde{\mu}] = \int_{-\pi}^{\pi} \frac{d\varphi}{2\pi}\, 2(1-\cos(\varphi)) \int_0^{2\pi/l_\parallel} \frac{k\ dk}{2\pi}\, G\left(|\mathbf{k}_\parallel| = k,\ k_\perp l_\perp = \varphi\right)\ , \tag{A.35}$$

where $I[\widetilde{\mu}]$ consists of three contributions corresponding to (A.28):

$$I[\widetilde{\mu}] \ = \ I^{th}[\widetilde{\mu}] + I^{dis}_{2D}[\widetilde{\mu}] + I^{dis}_{3D}[\widetilde{\mu}]\ . \tag{A.36}$$

The evaluation of the three contributions is tedious but straightforward. It is convenient to use the following dimensionless quantities

$$\left\{ \begin{array}{c} m \\ \widetilde{m} \end{array} \right\} \ := \ \left\{ \begin{array}{c} \mu \\ \widetilde{\mu} \end{array} \right\} \frac{1}{K} \left(\frac{l_\parallel}{2\pi}\right)^2 \tag{A.37}$$

$$y_0 \ := \ \left(\frac{l_\parallel}{R_{l,2D}(T=0)}\right)^2 \ \simeq \ \frac{g}{K^2}\ \frac{l_\parallel^2}{\bar{c}_{d=2}} \tag{A.38}$$

$$y \ = \ y(\tau) \ := \ \left(\frac{l_\parallel}{R_{l,2D}(\tau)}\right)^2 \ = \ y_0^{1/\tau} \ \propto \ g^{1/\tau}\ . \tag{A.39}$$

$\widetilde{m}$ and m measure the inter-layer coupling and y the disorder-strength in units of K (energy) and $l_\parallel$ (length); note that y is independent of the inter-layer coupling. We study weak disorder, i.e., $y_0 \ll 1$.

For I^{th}, we obtain

$$\begin{aligned} I^{th} &= (1-\tau) i^{th}[\widetilde{m}] \\ &= \int_{-\pi}^{\pi} \frac{d\varphi}{2\pi}\, 2(1-\cos(\varphi)) \int_0^{2\pi/l_\parallel} \frac{k\ dk}{2\pi}\ \frac{1}{G_0^{-1}(k, \varphi/l_\perp)} \\ i^{th}[\widetilde{m}] &= 2\mathrm{L}[\widetilde{m}] \end{aligned} \tag{A.40}$$

with

$$\begin{aligned} \mathrm{L}[x] &= -\frac{\sqrt{1+4x}-1}{2x} + \ln\left(1 + \frac{2}{\sqrt{1+4x}-1}\right) \\ &\approx \left\{ \begin{array}{ll} x \ll 1: & -1 + \ln\left(\frac{1}{x}\right) \\ x \gg 1: & \frac{1}{2x} \end{array} \right. \end{aligned} \tag{A.41}$$

Note that $i^{th} = 2\mathrm{L}[\widetilde{m}]$ is a function of $\widetilde{m}$ only; a plot of $\mathrm{L}[x]$ is shown in Figure A.1.

The crossover functions $\mathrm{f}_{2D}[x]$ and $\mathrm{g}_{3D}[x]$ in I^{dis}_{2D} and I^{dis}_{3D} are analytically untractable; therefore, we switch from "soft" IR-cutoffs implemented by $\mathrm{f}_{2D}[x]$ and $\mathrm{g}_{3D}[x]$ to "hard"

IR-cutoffs, i.e., $\mathrm{f}_{2D}[x], \mathrm{g}_{3D}[x] \approx \Theta[x-1]$. This yields

$$\begin{aligned} I_{2D}^{dis} &= (\tau + \frac{y}{2}) i_{2D}^{dis} \\ &\approx \int_{-\pi}^{\pi} \frac{d\varphi}{2\pi}\, 2(1-\cos(\varphi)) \int_0^{2\pi/R_{l,2D}} \frac{k\ dk}{2\pi}\, \frac{\tau + y/2}{1-\tau}\, \frac{1}{G_0^{-1}(k, \varphi/l_\perp)} \\ i_{2D}^{dis} &\approx 2\mathrm{L}[\widetilde{m}/y] \end{aligned} \tag{A.42}$$

with $\mathrm{L}[x]$ from (A.41) [Figure A.1]. Note that for $y \ll 1$, i_{dis}^{2D} is a function of $\widetilde{m}/y(\tau)$ only. This becomes explicit when the "hard" IR-cutoff is used yielding (A.42).

In I_{3D}^{dis}, we use again the "hard" IR-cutoff $\mathrm{g}_{3D}[x] \approx \Theta[x-1]$, and obtain

$$I_{3D}^{dis} \approx \int_0^{2\pi a[\widetilde{m}]} \frac{d\varphi}{2\pi}\, 2(1-\cos(\varphi)) \int_0^{b[\widetilde{m}]} \frac{k\ dk}{2\pi} \frac{2\pi^2 \widetilde{m}^{1/2}}{(k^2 + 2\widetilde{m}(1-\cos\varphi))^{3/2}} \tag{A.43}$$

with

$$a[\widetilde{m}] := \min\left\{1, \frac{l_\perp}{\widetilde{R}_{l,3D,\perp}}\right\} = \min\left\{1, \frac{y_0}{4\pi\widetilde{m}}\right\} \tag{A.44}$$

$$b[\widetilde{m}] := \min\left\{1, \frac{l_\parallel}{\widetilde{R}_{l,3D,\parallel}}\right\} = \min\left\{1, \frac{y_0}{2\widetilde{m}^{1/2}}\right\}, \tag{A.45}$$

where the boundaries of the integrals $a[\widetilde{m}]$ and $b[\widetilde{m}]$ depend on $\widetilde{m}$ or $\widetilde{\mu}$ via the IR-cutoff set by the Larkin lengths $\widetilde{R}_{l,3D}$

$$\begin{aligned} \frac{\widetilde{R}_{l,3D,\perp}}{l_\perp} &= \bar{c}_{d=3} \frac{\widetilde{\mu} K}{g} = \frac{4\pi^2 \bar{c}_{d=3}}{\bar{c}_{d=2}^2} \frac{\widetilde{m}}{y_0} = 4\pi \frac{\widetilde{m}}{y_0} \\ \frac{\widetilde{R}_{l,3D,\parallel}}{l_\parallel} &= \bar{c}_{d=3} \frac{\widetilde{\mu}^{1/2} K^{3/2}}{g} \frac{1}{l_\parallel} = \frac{2\pi \bar{c}_{d=3}}{\bar{c}_{d=2}^2} \frac{\widetilde{m}^{1/2}}{y_0} = 2\frac{\widetilde{m}^{1/2}}{y_0}\,. \end{aligned} \tag{A.46}$$

Performing the k-integration, we obtain

$$I_{3D}^{dis} \approx \int_0^{2\pi a[\widetilde{m}]} d\varphi \left\{ \frac{(1-\cos(\varphi))^{1/2}}{\sqrt{2}} - \frac{(1-\cos(\varphi))}{((b^2[\widetilde{m}]/\widetilde{m}) + 2(1-\cos(\varphi)))^{1/2}} \right\}. \tag{A.47}$$

A closed expression for this integral can only be given in terms of elliptic integrals, but a good approximation is

$$I_{3D}^{dis}[\widetilde{m}] \approx \begin{cases} \widetilde{m} \le y_0^2/4: & 4 - 2\pi\ \widetilde{m}^{1/2} \\ y_0^2/4 \le \widetilde{m}: & \mathrm{F}_{3D}[\widetilde{m}/y_0] \end{cases} \tag{A.48}$$

with

$$\mathrm{F}_{3D}[x] \approx \begin{cases} x \leq 1/4\pi: & 4 - 4\pi\ x \\ x > 1/4\pi: & \text{const } \frac{1}{x^2} \\ \text{with} & \text{const} \approx 1 - \sqrt{5} - 4\mathrm{Arsinh}(1/2) \approx 0.0215 \end{cases} \tag{A.49}$$

It is important to note that, except for very small $\widetilde{m} \leq y_0^2/4$, $I_{3D}^{dis} \approx \mathrm{F}_{3D}[\widetilde{m}/y_0]$ depends only on the ratio $\widetilde{m}/y_0$. $I_{3D}^{dis}[\widetilde{m}]$ is shown in Figure A.1.

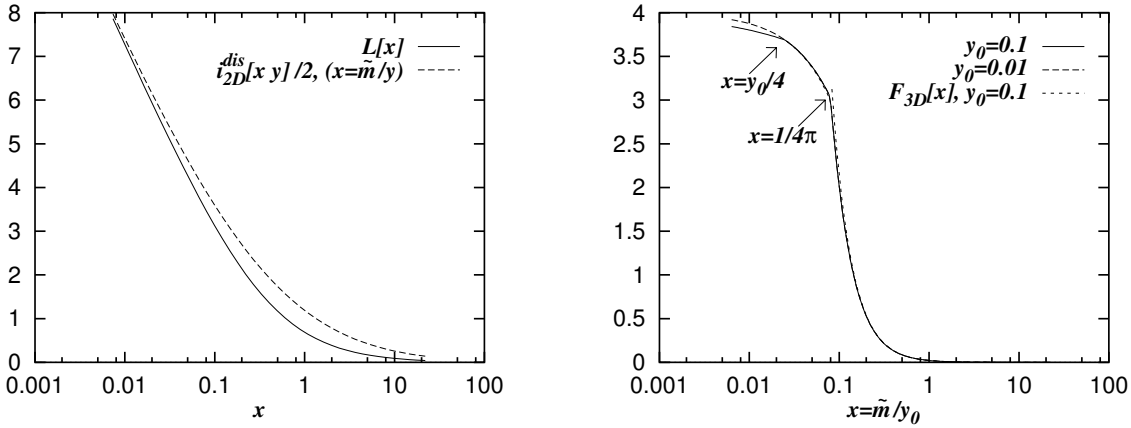

Figure A.1: Left: Function $L[x]$ (solid line) plotted logarithmically. Numerical integration of the integral $i_{2D}^{dis}[xy]/2$ ($x = \widetilde{m}/y$) with the "soft" IR-cutoff function $\mathrm{f}_{2D}[x]$ gives the dashed curve in a logarithmic plot (for $y = 0.1$), whereas the "hard" cutoff gives $L[x]$. Right: Logarithmic plot of a numerical integration of $I_{3D}^{dis}[xy_0]$ ($x = \widetilde{m}/y_0$) using the "hard" IR-cutoff for $y_0 = 0.1$ (solid line) and $y_0 = 0.01$ (dashed line). The two kinks (see arrows) are artefacts of the "hard" cutoff. Except for $x \leq y_0/4$, $I_{3D}^{dis}[xy_0]$ depends on x only. For $y_0 = 0.1$, the dotted curve shows the approximation (A.48), i.e., $\mathrm{F}_{3D}[x]$ for $x > y_0/4$.

Before moving on to a more detailed analysis of the self-consistency equation (A.35), it is instructive to consider the limiting cases $\widetilde{m} \downarrow 0$ and $\widetilde{m} \uparrow \infty$. For $\widetilde{m} \uparrow \infty$, $I[\widetilde{m}] \downarrow 0$, and we obtain the strong coupling limit with $\widetilde{m} \approx m$, where the FL array is dislocation-free and described by elasticity theory as discussed in 4.2. However, in the limit $\widetilde{m} \downarrow 0$, we obtain

$$0 = \frac{\partial F_{var}}{\partial \widetilde{\mu}} \ \propto\ \widetilde{m}\left(1 - me^{-1+y/2}\widetilde{m}^{-\tau}\left(\frac{\widetilde{m}}{y}\right)^{\tau+y/2}\right)\ , \tag{A.50}$$

where the factor $\widetilde{m}^{-\tau}$ comes from purely thermal fluctuations and the factor $(\widetilde{m}/y)^{\tau+y/2}$ from quasi-2D disorder fluctuations (the disorder-induced fluctuations of the 3D elastic Bragg glass give only a constant e^{-2} for $\widetilde{m} \downarrow 0$). Note that we obtain from (A.50) that $\widetilde{m} = 0$ is *always* a solution of the self-consistency equation (4.35). The question is whether

there are other solutions of (4.35), i.e., extrema of $F_{var}[\widetilde{m}]$, which have a smaller free energy $\Delta F_{var}[\widetilde{m}] = F_{var}[\widetilde{m}] - F_{var}[0] < 0$. When no other solutions of (4.35) exist, $\widetilde{m} = 0$ is the global minimum and the system is effectively *decoupled*.

In the disorder-free case, (A.50) reduces for $\widetilde{m} > 0$ to $0 = 1 - me^{-1}\widetilde{m}^{-\tau}$, and one can *always* find a second non-zero solution for small m, namely $\widetilde{m}(m) \sim m^{\tau}$ with $\widetilde{m}(m) \downarrow 0$ for $m \downarrow 0$ (for $\tau > 0$). Thus we have a second order phase transition to an elastically coupled phase at $m_c = 0$. The effective shear modulus $\widetilde{m}$ plays the role of an order parameter fulfilling the scaling law $\widetilde{m} \propto (m - m_c)^{\tau}$ at the critical point.

This is no longer possible if quasi-2D disorder fluctuations are included. Then, (A.50) reduces to

$$m = e^{1-y/2}\widetilde{m}^{\tau}\left(\frac{\widetilde{m}}{y}\right)^{-\tau-y/2} \propto \widetilde{m}^{-y/2} \;, \tag{A.51}$$

and the right hand side is diverging for $\widetilde{m} \downarrow 0$. In addition, we know already that due to $I[\widetilde{m}] \downarrow 0$ for $\widetilde{m} \uparrow \infty$, the right hand side is asymptotically $\propto \widetilde{m}$ and, hence, also diverging for $\widetilde{m} \uparrow \infty$. Therefore, it has a minimum and for a small but finite m (below the minimum of the right hand side) *no* solution of the self-consistency equation can be found. As we will see, we can nevertheless find solutions $\widetilde{m}(m) > 0$ of the self-consistency equation (A.35) for $m > m_c > 0$ above some critical, *non-zero* m_c. At $m = m_c$, this solution has $\widetilde{m}(m_c) = \Delta\widetilde{m} > 0$, and we obtain a *first order* phase transition accompanied by finite jump $\Delta\widetilde{m} > 0$ in the effective shear modulus $\widetilde{\mu}$. Thus it is the inclusion of quasi-2D disorder fluctuations which changes the nature of the phase transition to first order.

It is interesting to note that in the framework of a variational calculation of an effective shear modulus also the high-temperature phase $\tau < 0$ of the disorder-free model exhibits a first order phase transition. Below a critical coupling strength $m_c \approx e^{-1}$, the layers decouple due to *thermal* fluctuations, and the effective shear modulus drops to zero with a jump $\Delta\widetilde{m} \approx |\tau|/3$, which vanishes upon approaching $\tau \downarrow 0$. For $\tau < 0$ in the high-temperature phase of the corresponding single layer system, quasi-2D disorder fluctuations are absent on large scales, $I_{2D}^{dis} \simeq 0$. The effect of the disorder-induced fluctuations of the 3D elastic Bragg glass is to increase m_c for $|\tau| \downarrow 0$ up to $m_c \approx e$.

A.2.2 Quantitative Analysis of the Self-Consistency Equation for $T = 0$ and $\tau \gtrapprox 0$

Next, we want to discuss the self-consistency equation (A.35) in detail for the two limiting cases $T = 0$ (or $\tau = 1$) (4.15) and $\tau \gtrapprox 0$ (4.16), which are possible for the physical realization of an HTSC in a parallel field.

For $\tau = 1$ or $T = 0$, thermal fluctuations are absent and $I^{th} = 0$. Using $y = y_0$ for

$\tau = 1$, the self-consistency equation (A.35) yields (for $\widetilde{m} > 0$)

$$\ln\left(\frac{m}{y_0}\right) \;=\; \ln\left(\frac{\widetilde{m}}{y_0}\right) + \frac{1+y_0/2}{2} i_{2D}^{dis}[\widetilde{m}] + \frac{1}{2} I_{3D}^{dis}[\widetilde{m}] \;, \tag{A.52}$$

see (A.42, A.48). Except for very small $\widetilde{m} \leq y_0^2/4$, $I_{3D}^{dis}[\widetilde{m}] \approx \mathrm{F}_{3D}[\widetilde{m}/y_0]$ (A.48, A.49) is a function of the ratio $\widetilde{m}/y_0$ only. Because $y_0 \ll 1$, $(1+y_0/2) i_{2D}^{dis}[\widetilde{m}] \approx 2L[\widetilde{m}/y_0]$ (A.42, A.41) and the equation (A.52) depends only on $\widetilde{m}/y_0$ and m/y_0 for a wide range of parameters. Reparametrization by

$$m = x y_0 \quad \text{and} \quad \widetilde{m} = \widetilde{x} y_0 \tag{A.53}$$

(for $\widetilde{x} > y_0/4$, and with only weakly y_0-dependent x, $\widetilde{x}$) yields the *parameter-free* equation

$$\ln x \;\approx\; \ln \widetilde{x} + L[\widetilde{x}] + \frac{1}{2}\mathrm{F}_{3D}[\widetilde{x}] \;. \tag{A.54}$$

If quasi-2D fluctuations are neglected, we have $L \equiv 0$ in (A.54) and find solutions $\widetilde{x} \downarrow 0$ for arbitrary small $x \downarrow 0$ [Figure A.2], i.e., a second order transition with $x_c = 0$. Only inclusion of the quasi-2D fluctuations changes this transition into first order: (A.54) has solutions $\widetilde{x}(x)$ only for $x > x_c$ [Figure A.2].

One finds analytically and numerically (for $y_0 \gtrapprox 0$):

	analytically	numerically	
		hard cutoff	soft cutoff
$x_c \approx$	0.76	0.75	1.01
$\widetilde{x}(x_c) \approx$	$(\mathrm{const}/3)^{1/3}\left(1+(\mathrm{const}/3)^{1/3}\right)$	0.23	0.22
$\approx$	0.23		

(A.55)

(with const ≈ 0.0215 (A.49)), where the first numerical result is calculated with the "hard" IR-cutoff in i_{2D}^{dis} used in (A.54), and the second starting from (A.52) with the "soft" IR-cutoff by the cutoff-function $\mathrm{f}_{2D}[x]$ in i_{2D}^{dis} (for I_{3D}^{dis} we used for simplicity always the "hard" cutoff but expect a similar upward-correction for x_c as caused by the use of the "soft" cutoff in i_{2D}^{dis}). This means that at $T = 0$ the self-consistency equation (A.35) has non-zero solutions $\widetilde{m}(m) > 0$ only for $m > m_c = x_c y_0$ above the critical coupling strength m_c. At $m = m_c$, we expect a first order phase transition with a jump in the effective shear modulus $\Delta\widetilde{m} = \widetilde{m}(m_c) = \widetilde{x}(x_c) y_0$. However, solutions of the self-consistency equation (A.35) give only zeros of $\frac{\partial F_{var}}{\partial \widetilde{\mu}}$, and we have to check whether $\Delta F_{var}[\widetilde{m}] = F_{var}[\widetilde{m}] - F_{var}[0] < 0$ for these solutions to be *absolute* minima. Indeed, we expect at the critical value m_c determined above that a *saddle point* occurs in the free energy profile $F_{var}[\widetilde{m}]$. For higher values of m, a minimum develops and only for $m > m_{c2} > m_c$ the minimum is a *global* one. The value

of $m_{c2} = x_{c2} y_0$ can be determined only numerically together with the corrected value for the jump in the effective shear modulus $\Delta\widetilde{m} = \widetilde{m}(m_{c2}) = \widetilde{x}(x_{c2}) y_0$. One finds (for $y_0 \gtrapprox 0$):

		numerically	
		hard cutoff	soft cutoff
x_{c2}	$\approx$	0.82	1.11
$\widetilde{x}(x_{c2})$	$\approx$	0.36	0.37

(A.56)

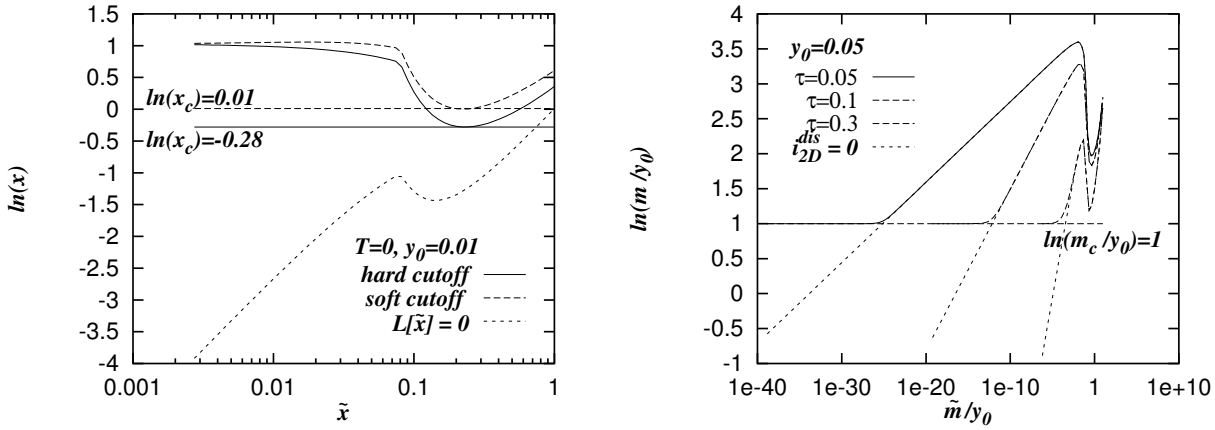

Figure A.2: Left: Logarithmic plot of the right hand side of equation (A.54) for $T = 0$ and $y_0 = 0.01$ (solid line). The left hand side of equation (A.54) gives a horizontal line at $\ln x$. Below the horizontal line $\ln x_c \approx -0.28$ (A.55) no solution of (A.54) can be found. Using the "soft" IR-cutoff in i_{2D}^{dis} we obtain the dashed curve and a corresponding horizontal line of $\ln x_c \approx 0.01$. The dotted curve shows the right hand side of (A.54) when quasi-2D disorder fluctuations are neglected, $L[\widetilde{x}] = 0$: The transition becomes second order with $x_c = 0$. Right: Logarithmic plots of the right hand side of equation (A.57) as function of $\widetilde{m}/y_0$ for $y_0 = 0.05$ and $\tau = 0.05$ (solid line), $\tau = 0.1$ (dashed line) and $\tau = 0.3$ (lower dashed line). The left hand side of equation (A.57) gives a horizontal line at $\ln(m/y_0)$. No solution can be found below the horizontal line $\ln(m/y_0) = 1$ and up to three solutions for sufficiently high inter-layer couplings m. At low enough temperatures the solution with higher $\widetilde{m}$ becomes thermodynamically stable. The dotted curves demonstrate again the absence of the first order transition when quasi-2D disorder fluctuations are neglected, $i_{2D}^{dis} = 0$.

In the other limiting case of interest $\tau \gtrapprox 0$, thermal fluctuations occur explicitly in (A.35) as contribution I^{th}, but also implicitly by weakening the 2D disorder fluctuations in I_{2D}^{dis}, which are now depending on the effectively smaller disorder strength $y = y(\tau) =$

$y_0^{1/tau} \ll y_0 \ll 1$. The self-consistency equation (A.35) yields (for $\widetilde{m} > 0$)

$$\ln\left(\frac{m}{y_0}\right) = \ln\left(\frac{\widetilde{m}}{y_0}\right) + \frac{1-\tau}{2} i^{th}[\widetilde{m}] \frac{\tau + y/2}{2} i_{2D}^{dis}[\widetilde{m}] + \frac{1}{2} I_{3D}^{dis}[\widetilde{m}] \ . \tag{A.57}$$

In this equation there are basically three characteristic values for $\widetilde{m}$: y, y_0 and 1. The quasi-2D disorder fluctuations $i_{2D}^{dis} \approx 2L[\widetilde{m}/y]$ (A.42) vanish for $\widetilde{m} \gtrsim y$, the 3D disorder fluctuations $I_{3D}^{dis}[\widetilde{m}] \approx \mathrm{F}_{3D}[\widetilde{m}/y_0]$ (A.48) from the elastic Bragg glass vanish for $\widetilde{m} \gtrsim y_0 \gg y$, and the thermal fluctuations $i^{th}[\widetilde{m}] = 2L[\widetilde{m}]$ (A.40) vanish for $\widetilde{m} \gtrsim 1 \gg y_0 \gg y$. This allows for the existence of up to 3 solutions of (A.57) in general, two of which are minima of the free energy, as the plot for the right hand side of (A.57) shows in Figure A.2. As we have seen already, the quasi-2D disorder fluctuations are responsible for the transformation of the second order phase transition in the disorder-free system into a first order transition in the presence of weak point disorder. For $\tau \gtrapprox 0$, their interplay with the thermal fluctuations determines the nature of the decoupling transition [Figure A.2]. We find the minimum with the lowest free energy at $\widetilde{\mu} \ll y$, where we can approximate (A.57) by (see (A.41, A.49))

$$\begin{aligned} \ln\left(\frac{m}{y_0}\right) \approx\ & -(1-\tau) + \tau \ln\left(\frac{\widetilde{m}}{y}\right) + (\tau + \frac{y}{2}) L\left[\frac{\widetilde{m}}{y}\right] + \\ & + \left(2 - \pi y^{1/2} \left(\frac{\widetilde{m}}{y}\right)^{1/2}\right) \end{aligned} \tag{A.58}$$

This equation has solutions $\widetilde{m}(m)$ only for $m > m_c$. Analytically, one finds for the critical coupling strength m_c, at which a first order phase transition occurs, and the accompanying jump $\Delta\widetilde{m} = \widetilde{m}(m_c)$ in the effective shear modulus (for $\tau, y_0 \gg y$)

$$m_c \approx e y_0 \approx 2.7 y_0 \tag{A.59}$$

$$\widetilde{m}(m_c) \approx \frac{y^2}{6\tau} \ . \tag{A.60}$$

For completeness, let us mention that the other minimum corresponding to a second solution of (A.58) [Figure A.2] occurs above a considerably higher inter-layer coupling $\bar{m}_c \sim (y_0/2)^\tau/2e \gg y_0$ compared to (A.59). Therefore, it corresponds also to a higher free energy.

For intermediate temperatures, $1 > \tau > 0$, the minimum with the higher free energy found for $\tau \gtrapprox 0$ becomes the thermodynamically stable, global minimum at some intermediate temperature, and crosses over to the $T = 0$ result [Figure A.2].

A.3 Elastic Moduli

We shortly recapitulate the results in the literature for the relevant moduli $c_{44}[\mathbf{k}]$ and c_{66} in (3.2, 3.7) for $\mathbf{H} \parallel \hat{\mathbf{c}}$ (with the z-coordinate $\parallel \hat{\mathbf{c}}$).

To a good approximation for all induction $0 < b = B/B_{c2} < 1$, the tilt modulus c_{44} is given by [68]

$$c_{44}[\mathbf{k}] = \frac{B_{c2}^2}{4\pi} b^2 \frac{1-b}{1-b+K^2\lambda_c^2+k_z^2\lambda_{ab}^2} + \tilde{c}_{44}^s(k_z), \tag{A.61}$$

$$\tilde{c}_{44}^s[k_z] = \frac{B_{c2}^2}{4\pi}\frac{\varepsilon^2}{\kappa^2}\frac{b}{2\pi}\ln\left(\tilde{\kappa}(k_z)+\frac{(1-b)}{2}\right), \tag{A.62}$$

$$\tilde{\kappa}(k_z) := \left(\frac{1+\kappa^2/\varepsilon^2+k_z^2\lambda_{ab}^2}{1+b\kappa^2/\varepsilon^2+k_z^2\lambda_{ab}^2}\right)^{1/2}, \tag{A.63}$$

where $\varepsilon := \lambda_{ab}/\lambda_c = \xi_c/\xi_{ab}$ and $\kappa := \lambda_{ab}/\xi_{ab}$ and

$$c_{44}^s = l^2\,\tilde{c}_{44}^s \tag{A.64}$$

is the tilt modulus of an isolated FL.

As opposed to c_{44}, the shear modulus c_{66} is always *dispersion-free*. In the dilute limit $l \gtrsim \lambda_{ab}$ ($b/2\pi \lesssim 1/\kappa^2$), the interaction between FLs decays exponentially and one obtains [4, 6]:

$$\begin{aligned} c_{66} &= \frac{B_{c2}^2}{4\pi}\frac{\pi^{3/2}6^{1/2}}{4}\kappa^{-7/2}(\frac{b}{2\pi})^{1/4}\exp\left(-\frac{1}{\kappa}(\frac{b}{2\pi})^{-1/2}\right) \\ &\propto \exp\left(-l/\lambda_{ab}\right). \end{aligned} \tag{A.65}$$

Crossing over to the the dense limit $l \lesssim \lambda_{ab}$ ($b/2\pi \gtrsim 1/\kappa^2$) the following expression for c_{66} holds [47]:

$$\begin{aligned} c_{66} &= \frac{B_{c2}^2}{4\pi}\frac{1}{8\kappa^2}b(1-b)^2c(b), \\ c(b) &\simeq 1-0.6b+0.3b^2. \end{aligned} \tag{A.66}$$

The dilute limit is realized only at very low fields a few Gauss above H_{c1}, so that (A.66) is valid in a wide range of inductions b.

The bulk part of (A.61) yields a *dispersive* c_{44}:

$$c_{44}[\mathbf{k}] = \hat{c}_{44}\frac{1-b}{1-b+K^2\lambda_c^2+k_z^2\lambda_{ab}^2}, \tag{A.67}$$

$$\hat{c}_{44} := c_{44}(0) = \frac{B_{c2}^2}{4\pi}b^2. \tag{A.68}$$

The dispersion of c_{44} sets in for $K\tilde{\lambda}_c \gtrsim 1$ with

$$\tilde{\lambda}_c := \frac{\lambda_c}{\sqrt{1-b}}, \tag{A.69}$$

i.e., on scales $R \sim 1/K \lesssim \tilde{\lambda}_c$. When dispersion dominates, (A.67) becomes approximately

$$c_{44}[K] \simeq \hat{c}_{44} \frac{1}{1+K^2\tilde{\lambda}_c^2}. \tag{A.70}$$

On the shortest scales $R \sim 1/K \lesssim l$ this result crosses over to the single vortex contribution in (A.61), which is for $b \ll 1$:

$$\tilde{c}^s_{44} \;\simeq\; \frac{B^2_{c2}}{4\pi}\frac{b}{2\pi}\frac{\varepsilon^2}{\kappa^2}\ln\left(\frac{1}{k_z\xi_c}\right) \;\simeq\; \frac{B^2_{c2}}{4\pi}\frac{b}{2\pi}\frac{\varepsilon^2}{\kappa^2}. \tag{A.71}$$

When we are considering fluctuations on the shortest scales in the dense limit with $K \sim 1/l$, $k_z \sim 1/\varepsilon l$, the neglected logarithmic term becomes of the order $\ln(1/k_z\xi_c) \simeq \ln(1/b)$.

Bibliography

[1] A.A. Abrikosov, Sov. Phys. JETP **5**, 1174 (1957).

[2] J.G. Bednorz and K.A. Müller, Z. Physik B **64**, 189 (1986).

[3] V.L. Ginzburg and L.D. Landau, Zh. Eksp. Teor. Fiz. **20**, 1064 (1950).

[4] G. Blatter *et al*, Rev. Mod. Phys. **66**, 1125 (1994).

[5] M.P.A. Fisher, Phys. Rev. Lett. **62**, 1415 (1989).

[6] A.I. Larkin, Sov. Phys. JETP **31**, 784 (1970).

[7] T. Halpin-Healy and Y.C. Zhang, Phys. Rep. **254**, 215 (1995).

[8] D.S. Fisher, M.P.A. Fisher, and D.A. Huse, Phys. Rev. B **43**, 130 (1991).

[9] T. Giamarchi and P. Le Doussal, Phys. Rev. B **52**, 1242 (1995).

[10] M.V. Feigelman *et al*, Phys. Rev. Lett. **63**, 2303 (1989).

[11] T. Nattermann, Phys. Rev. Lett. **64**, 2454 (1990).

[12] R.H. Koch *et al.*, Phys. Rev. Lett. **63**, 1511 (1989).

[13] P.L. Gammel *et al.*, Phys. Rev. Lett. **66**, 953 (1991).

[14] H. Safar *et al.*, Phys. Rev. Lett. **68**, 2672 (1992).

[15] N.C. Yeh *et al.*, Phys. Rev. B **47**, 6146 (1993); *ibid.* 6150 (1993); *ibid.* 8308 (1993); *ibid.* **49**, 4384 (1994).

[16] H. Safar *et al.*, Phys. Rev. Lett. **70**, 3800 (1993).

[17] T. Giamarchi and P. Le Doussal, Phys. Rev. Lett. **72**, 1530 (1994).

[18] J.L. Cardy and S. Ostlund, Phys. Rev. B **25**, 6899 (1982).

[19] Y.Y. Goldschmidt and A. Houghton, Nucl. Phys. **B210**, 115 (1982).

[20] J. Villain and J.F. Fernandez, Z. Phys. B **54**, 139 (1984).

[21] S.E. Korshunov, Phys. Rev. B **48**, 3969 (1993).

[22] Y.Y. Goldschmidt and B. Schaub, Nucl. Phys. **B251**, 77 (1985).

[23] Y.C. Tsai and Y. Shapir, Phys. Rev. Lett. **69**, 1773 (1992); Phys. Rev. E **50**, 3546 (1994).

[24] C.A. Murray *et al.*, Phys. Rev. Lett. **64**, 2312 (1990)

[25] R. Cubitt *et al.*, Nature **365**, 407 (1993).

[26] U. Yaron *et al.*, Phys. Rev. Lett. **73**, 2748 (1994).

[27] S.L. Lee *et al.*, Phys. Rev. Lett. **71**, 3862 (1993).

[28] M. Gingras and D. A. Huse, preprint cond-mat/9601123.

[29] S. Ryu, A. Kapitulnik, and S. Doniach, preprint cond-mat/9604171.

[30] B. Khaykovich *et al.*, Phys. Rev. Lett. **76**, 2555 (1996).

[31] M.C. Marchetti and D.R. Nelson, phys. Rev. B **41**, 1910 (1990).

[32] E. Frey, D.R. Nelson, D.S. Fisher, Phys. Rev. B **49**, 9723 (1994).

[33] F.R.N. Nabarro and A.T. Quintanilha, in *Dislocations in Solids*, edited by F.R.N. Nabarro (North-Holland, Amsterdam, 1980), Vol. 5.

[34] D. Ertaş and D.R. Nelson, preprint cond-mat/9607142.

[35] D.R. Nelson, in *Phase Transitions and Critical Phenomena*, edited by C. Domb and J.L. Lebowitz (Academic Press, London, 1983), Vol. 7.

[36] L.D. Landau and E.M. Lifshitz, *Theory of Elasticity* (Pergamon, New York, 1970), p. 193.

[37] T. Yamamoto and T. Izuyama, J. Phys. Soc. Jpn. **57**, 3742 (1988).

[38] F. Lindemann, Phys. Z. (Leipzig) **11**, 69 (1910).

[39] L.D. Landau, in *The Collected Papers of L.D. Landau*, edited by D. ter Haar (Pergamon, New York, 1965).

[40] E. Brézin, D.R. Nelson, and A. Thiaville, Phys. Rev. B **31**, 7124 (1985).

[41] M.A. Moore and T.J. Newman, Phys. Rev. Lett. **75**, 533 (1995).

[42] D.R. Nelson, Nature **375**, 356 (1995); E. Zeldov *et al*, *ibid.* 373 (1995).

[43] J. Toner, Phys. Rev. Lett. **66**, 2523 (1991).

[44] T. Hwa and T. Nattermann, Phys. Rev. B **51**, 455 (1995).

[45] H. Kinzelbach and M. Lässig, J. Phys. A: Math. Gen. **28** 6535 (1995).

[46] E.H. Brandt, J. Low Temp. Phys. **26**, 706 and 735 (1977).

[47] E.H. Brandt, J. Low Temp. Phys. **64**, 375 (1986).

[48] A.I. Larkin and Y.N. Ovchinnikov, J. Low Temp. Phys. **34**, 409 (1979).

[49] J. Bouchaud, M. Mézard, and J. Yedidia, Phys. Rev. Lett. **67**, 3840 (1991); *ibid.* Phys. Rev. B **46**, 14686 (1992).

[50] M. Kardar, G. Parisi, and Y.C. Zhang, Phys. Rev. Lett. **56**, 889 (1986).

[51] L. Balents and D.S. Fisher, Phys. Rev. B **48**, 5949, (1993).

[52] M. Mézard and G. Parisi, J. Phys. I France **1**, 809 (1991).

[53] T. Nattermann, I. Lyuksyutov und M. Schwartz, Europhys. Lett. **16**, 265 (1991).

[54] D. Cule and Y. Shapir, Phys. Rev. B **51**, 3305 (1995).

[55] P. Le Doussal and T. Giamarchi, Phys. Rev. Lett. **74**, 606 (1995).

[56] M. Bauer and D. Bernard, Europhys. Lett. **33**, 255 (1996).

[57] G.G. Batrouni and T. Hwa, Phys. Rev. Lett. **72**, 4133 (1994).

[58] D. Cule and Y. Shapir, Phys. Rev. Lett. **74**, 114 (1995).

[59] E. Marinari, R. Monasson, and J.J. Ruiz-Lorenzo, J. Phys. A **28**, 3975 (1995).

[60] H. Rieger, Phys. Rev. Lett. **74**, 4964 (1995).

[61] J. Toner and D.P. DiVicenzo, Phys. Rev. B **41**, 632 (1990).

[62] B.I. Ivlev and N.B. Kopnin, J. Low Temp. Phys. **30**, 161 (1990).

[63] B.I. Ivlev, N.B. Kopnin, and V.L. Pokrovsky, J. Low Temp. Phys. **30**, 187 (1990).

[64] G. Blatter, B.I. Ivlev, and J. Rhyner, Phys. Rev. Lett. **66**, 2392 (1991).

[65] L.V. Mikheev and E. B. Kolomeisky, Phys. Rev. B **43**, 10431 (1991).

[66] L. Balents and D.R. Nelson, Phys. Rev. Lett. **73**, 2618 (1994).

[67] L. Balents and D.R. Nelson, Phys. Rev. B **52**, 12951 (1995).

[68] E.H. Brandt and A. Sudbø, Physica C **180**, 426 (1991); *ibid.* Phys. Rev. Lett. **66**, 1781 (1991).

[69] U. Schulz, J. Villain, E. Brezin, and H. Orland, J. Stat. Phys. **51**, 1 (1988).

[70] T. Hwa and D.S. Fisher, Phys. Rev. Lett. **72**, 2466 (1994).

[71] Y. Imry and S.K. Ma, Phys. Rev. Lett. **35**, 1399 (1975).

[72] J. Kondev and C. Henley, Phys. Rev. Lett. **74**, 4580 (1995).

[73] H. Saleur and B. Duplantier, Phys. Rev. Lett. **58**, 2325 (1987).

[74] M.S. Li, T. Nattermann, H. Rieger, and M. Schwartz,
preprint cond-mat/9604111.

[75] D. Carpentier, P. Le Doussal, and T. Giamarchi, Europhys. Lett. **35**, 379 (1996).

[76] H. Kinzelbach and M. Lässig, Phys. Rev. Lett. **75**, 2208 (1995).

[77] J. Kierfeld, Diplomarbeit, Universität zu Köln, 1993.

[78] V.M. Vinokur and A.E. Koshelev, Zh. Eksp. Teor. Fiz. **97**, 976 (1990) [Sov. Phys. JETP **70**, 547 (1990)].

[79] S. Scheidl, Phys. Rev. Lett. **75**, 4760 (1995).

[80] T. Nattermann, S. Scheidl, S.E. Korshunov, and M.S. Li, J. Phys. (France) I **5**, 565 (1995).

[81] M.C. Cha and H.A. Fertig, Phys. Rev. Lett. **74**, 4867 (1995).

[82] A. Houghton, R.D. Kenway, and S.C. Ying, Phys. Rev. B **23**, 298 (1981).

[83] D.J. Amit, Y.Y. Goldschmidt, and G. Grinstein, J. Phys. A: Math. Gen. **13** 585 (1979).

[84] J.M. Kosterlitz, J. Phys. C **7**, 1046 (1974).

[85] Mézard, G. Parisi, and M. Virasoro, *Spin-Glass Theory and Beyond* (World Scientific, Singapore, 1987).

[86] J. Kierfeld, J. Phys. I France **5**, 379 (1995).

[87] J.V. José, L.P. Kadanoff, S. Kirkpatrick, and D.R. Nelson, Phys. Rev. B **16**, 1217 (1977).

[88] V. Dotsenko, A.B. Harris, D. Sherrington and R.B. Stinchcombe, J. Phys. A: Math. Gen. **28**, 3093 (1995).

[89] V. Dotsenko and D.E. Feldman, J. Phys. A: Math. Gen. **28**, 5183 (1995).

[90] G. Parisi and A. Virasoro, J. Phys. France **50**, 3317 (1990).

[91] M. Mézard, J. Phys. France **51**, 1831 (1990).

[92] J. Villain and I. Vilfan, Europhys. Lett. **12**, 523(1990); Surf. Sci. **257**, 368 (1991).

[93] L. Balents and M. Kardar, Phys. Rev. B, **46**, 16031 (1992).

[94] M. Den Nijs, Phys. Rev. Lett. **66**, 907 (1991).

[95] M. Den Nijs, Phys. Rev. B, **46**, 10411 (1992).

[96] J. Kierfeld and T. Hwa, Phys. Rev. Lett. **77**, 4233 (1996).

[97] H. Rieger and U. Blasum, preprint cond-mat/9608136.

[98] C. Zeng, A.A. Middleton, and Y. Shapir, preprint cond-mat/9609029.

Acknowledgments

I would like to thank Thomas Nattermann and Terry Hwa for supervising this thesis, suggesting many of the problems and strategies to solve them, and innumerable discussions. My special thanks goes to Terry Hwa for his hospitality during my stay at UC San Diego.

I wish to thank Dinko Cule, Thorsten Emig, Igor Lyuksyutov, Tim Newman, Stefan Scheidl, Lei-Han Tang, Andreas Volmer, and all other colleagues of the past years for a pleasant working atmosphere and many helpful discussions. [Special thanks to Thorsten Emig und Andreas Volmer for a reading of the manuscript.]

In particular, I want to mention some of the other graduate students, former graduate students and the system administrator of the Theoretical Physics Institute at Cologne University, who contributed to this work on many levels, not exclusively related to physics. They are Stefan Dahm, Uwe Gropengießer, Jens Kisker, Nikolaus Rajewsky, Andreas Sindermann, Bjoern Strocka, and Peter Wurth.

I am especially grateful to my parents, who supported me during all the years of education.

To Susi, thanks for her patience, understanding and support [and a careful reading of the manuscript].

Zusammenfassung

Die Entdeckung der Hochtemperatursupraleitung im Jahr 1986 durch Bednorz und Müller [2] hat prinzipiell die Möglichkeit eines dissipationsfreien Stromtransports bei Temperaturen bis zu 125K eröffnet. Allerdings zeichnen sich die von Bednorz und Müller entdeckten Materialien neben den hohen Sprungtemperaturen ($\sim$ 100K) durch große magnetische Eindringtiefen und kleine Kohärenzlängen aus. Das Zusammenwirken dieser Charakteristika führt dazu, daß diese Substanzen extreme Typ-II Supraleiter sind. Bei für Anwendungen relevanten Magnetfeldern und Temperaturen befinden sie sich in der gemischten Phase und bilden ein Flußliniengitter aus.

Als Konsequenz des Auftretens von Flußlinien ergibt sich der Zusammenbruch des dissipationsfreien Stromtransports in einer ideal reinen Substanz. Im stromdurchflossenen Supraleiter wirkt auf die Flußlinien, die ein magnetisches Flußquant Φ_0 tragen, eine Lorentzkraft, unter deren Einfluß sie in Bewegung gesetzt werden. Die sich bewegenden Flußlinien generieren ihrerseits ein elektrisches Feld parallel zum angewandten Strom und erzeugen damit einen Widerstand. Auf der anderen Seite ist in Hochtemperaturleitern intrinsisch (bedingt durch die Stöchiometrie der Verbindungen) Unordnung in Form von punktförmigen Defekten vorhanden. Der technologisch bei weitem relevanteste Effekt der Unordnung besteht nun in der Fähigkeit, Flußlinien zu „pinnen“, das heißt der Lorentzkraft eine Pinningkraft entgegenzusetzen, die die Flußlinie „festhält“: Überwiegt die Pinning-Kraft, ist wieder dissipationsfreier Stromtransport möglich. Die Gleichgewichtseigenschaften der gepinnten Phase des Flußliniengitters können im Rahmen der Theorie ungeordneter Systeme durchaus als „glasartig“ charakterisiert werden und führten zu der Bezeichnung „Vortex-Glas-Phase“ für den thermodynamischen Zustand des gepinnten Flußliniengitters [5].

Das technologisch relevante Pinning von Flußlinien ist nur möglich, weil die bereits erwähneten Materialeigenschaften, große magnetische Eindringtiefen, kleine Kohärenzlängen, eine starke Anisotropie in der Kristallstruktur und die hohen Sprungtemperaturen im Hinblick auf Fluktuationseffekte konspirieren. Sie bewirken, daß in weiten Teilen des Phasendiagramms unordnungsinduzierte und thermische Fluktuationen des Flußliniengitters die physikalischen Eigenschaften dominieren. Die durch Unordnung hervorgerufenen Fluktuationseffekte sind im weiteren Sinne auch Thema dieser Arbeit.

Vom phänomenologisch-theoretischen Standpunkt, den wir in dieser Arbeit einnehmen

möchten, hat es sich als sehr fruchtbar erwiesen, daß Flußliniengitter durch eine Elastizitätstheorie zu beschreiben, wie sie auch zur Beschreibung der Deformationen üblicher kristalliner Materialien verwendet wird. Solch eine Beschreibung kann für große Parameterbereiche gerechtfertigt werden, und die Elastizitätsmoduln des Flußliniengitters können im Rahmen der Ginzburg-Landau-Theorie [3] für Supraleiter berechnet werden [4].

In Gegenwart von Punktdefekten führt die elastische Beschreibung auf die Theorie der *gepinnten elastischen Mannigfaltigkeiten*. Deren asymptotisches Verhalten ist im wesentlichen bestimmt durch (i) die Dimension d der Mannigfaltigkeit, (ii) die Kodimension, d.h. die Zahl n der Komponenten des Verschiebungsfeldes und (iii) die Art der Kopplung an die Unordnung. Durch Flußliniengitter in Supraleitern mit Punktdefekten können verschiedenste Kombinationen dieser Parameter realisiert sein, von denen einige in dieser Arbeit untersucht werden. Unterhalb von $d = 4$ Dimensionen, ist die elastische Mannigfaltigkeit instabil bezüglich einer schwachen Punktunordnung [6], wie sie typischerweise von den intrinsisch vorhandenen Punktdefekten erzeugt wird. Die elastische Mannigfaltigkeit befindet sich dann in einer gepinnten glasartigen Phase, der bereits erwähnten Vortex-Glas-Phase. Das Flußliniengitter in Supraleitern wird durch die Parameter $d = 3$ und $n = 2$ beschrieben. Auf großen Längenskalen führt die Periodizität des Flußliniengitters dazu, daß auf die elastische Mannigfaltigkeit ein *periodisches Unordnungspotential* wirkt. Die entsprechende Vortex-Glas-Phase wird auch als „Bragg-Glas“ bezeichnet.

Nach einem einführenden 1. Kapitel befaßt sich Teil I der Arbeit eingehend mit der Frage der *Konsistenz* der elastischen Beschreibung in einem Supraleiter mit Punktunordnung. Eine elastische Beschreibung setzt ein topologisch geordnetes Flußliniengitter voraus. Jedoch kann die topologische Ordnung durch das Auftreten von topologischen Defekten, insbesondere *Dislokationsschleifen*, zerstört werden. Damit das elastische Bragg-Glas eine thermodynamisch stabile Phase darstellt, muß das Flußliniengitter stabil gegenüber einer spontanen Bildung von Dislokationsschleifen sein.

Kapitel 2 dient der Einführung in die Thematik der topologischen Defekte; insbesondere werden Dislokationen und ihre Terminologie eingeführt. Die entropischen Mechanismen, die zum Auftreten von Dislokationen und damit zum Schmelzen im reinen Flußliniengitter führen, werden den rein energetischen Betrachtungen im Flußliniengitter mit Unordnung gegenübergestellt.

In Kapitel 3 werden die verschiedenen Regimes des dislokationsfreien, rein elastischen Flußliniengitters zusammen mit den jeweiligen Crossover-Skalen charakterisiert: Das störungstheoretische Larkin-Regime auf kleinsten Skalen unterhalb der Larkin-Länge, das „Random-Manifold“-Regime auf Skalen bis zur positionellen Korrelationslänge und das asymptotische Bragg-Glas-Regime. Dieses Kapitel dient der Einführung der verschiedenen Modelle gepinnter elastischer Mannigfaltigkeiten, die im weiteren relevant sind.

In Kapitel 4 wird für ein uniaxiales Flußliniengitter der Parameterbereich berechnet, in dem die Bragg-Glas-Phase stabil gegenüber Dislokationen ist. Dazu wird in einer Varia-

tionsrechnung der effektive Schermodul des Gitters selbstkonsistent bestimmt. Uniaxialen Flußliniengitter treten in einem geschichteten Supraleiter im parallelen Feld auf, wo die Auslenkungen der Flußlinien nur in einer Richtung erfolgen können. Der Stabilitätsbereich kann mit Hilfe eines einfachen Kriteriums, ähnlich dem Lindemann-Kriterium für thermisches Schmelzen, quantifiziert werden.

In Kapitel 5 wird mit Hilfe von Scaling-Argumenten eine alternative Herleitung des Lindemann-artigen Kriteriums für das uniaxiale Flußliniengitter gegeben und anschließend auf die im Experiment übliche Situation von zwei-komponentigen Flußlinienauslenkungen verallgemeinert.

In Kapitel 6 wird das Lindemann-Kriterium für die Stabilität der elastischen Bragg-Glas Phase gegenüber spontaner Dislokationsbildung für einen typischen Hochtemperatursupraleiter ($Bi_2Sr_2CaCu_2O_{8+x}$) ausgewertet und der Bereich im Phasendiagramm berechnet, in dem das Bragg-Glas experimentell beobachtbar sein sollte. Das so gewonnene Phasendiagramm wird mit Experimenten verglichen.

Kapitel 7 faßt den ersten Teil zusammen, präsentiert die Schlußfolgerungen und einen Ausblick.

Teil II der Arbeit ist den gepinnten elastischen Mannigfaltigkeiten in $d = 2$ Dimensionen mit uniaxialen ($n = 1$) Auslenkungen in einem periodischen Unordnungspotential gewidmet. Diese sind realisiert in planaren Gittern von elastischen Linien in ungeordneten Medien, wie sie zum Beispiel in den bereits erwähnten geschichteten Supraleitern im parallelen Feld auftreten, aber auch in Form von Stufen auf Kristalloberflächen, die beim Aufrauhen oder Dekonstruieren einer rekonstruierten Oberfläche gebildet werden. Das entsprechende Modell wird auch als zweidimensionales XY-Modell im Zufallsfeld bezeichnet. Weil in planaren Flußliniengittern keine Dislokationen auftreten können, ist die topologische Ordnung perfekt. Es ist somit das einzige System, für das die Existenz einer glasartigen Tieftemperaturphase analytisch gezeigt werden kann. Die Eigenschaften dieser Tieftemperaturphase haben wesentlich zu ersten Vermutungen bezüglich der Existenz einer Vortex-Glas-Phase beigetragen [5]. Jedoch sind trotz zahlreicher analytischer und numerischer Arbeiten zu diesem Modell grundlegende Eigenschaften der Tieftemperaturphase, wie das Verhalten der Verschiebungs-Paarkorrelationen, immer noch unklar. Der zweite Teil der Arbeit beschäftigt sich zu einem großen Teil mit diesen glasartigen Eigenschaften.

In Kapitel 8 wird das zweidimensionale XY-Modell im Zufallsfeld eingeführt und einige seiner Realisierungen vorgestellt. Die bisher erfolgreichsten analytischen Zugänge, eine Variationsrechnung mit Replika-Symmetrie-Bruch und eine Replika-symmetrische Renormierungsgruppenrechnung, werden kurz erläutert. Beide verwenden die Replika-Methode, um die Mittelung über die eingefrorene Unordnung durchzuführen.

In Kapitel 9 wird eine Renormierungsgruppenrechnung für einen verallgemeinerten Replika-Hamiltonian durchgeführt, die die technische Grundlage für die Kapitel 10 und 11 bildet.

In Kapitel 10 wird versucht, die beiden oben genannten Zugänge, die in mehrerer Hinsicht widersprüchliche Resultate liefern, zu erweitern und zu verallgemeinern. Das Ziel dabei ist ein besseres Verständnis der Unterschiede beider Zugänge, die teilweise miteinander vereinbart werden können. Um dies zu zeigen, wird in der Renormierungsgruppenrechnung eine 1-Schritt Replika-Symmetriebrechung zugelassen und die Selbstkonsistenzgleichung der Variationsrechnung verbessert, indem zusätzliche Diagramm-Klassen mitberücksichtigt werden. Die Möglichkeit eines Replika-Symmetrie-Bruches wird eingehend untersucht. Dieses hauptsächlich aus der Spin-Glas-Theorie bekannte Phänomen [85] ist von Bedeutung für die glasartigen Eigenschaften der Tieftemperaturphase.

In Kapitel 11 wird das Aufrauhen und Dekonstruieren einer defektbehafteten Kristalloberfläche untersucht, das durch das Auftreten von zwei Arten von Kristallstufen und damit zwei wechselwirkende planare XY-Modelle im Zufallsfeld beschrieben werden kann. Mit Hilfe einer Renormierungsgruppenrechnung wird ein Phasendiagramm berechnet. Außerdem erlaubt das Studium zweier gekoppelter Modelle weitere Rückschlüsse auf die Glaseigenschaften des Ausgangsmodells.

In Kapitel 12 werden die Ergebnisse von Teil II zusammengefaßt und ein Ausblick gegeben.

Ich versichere, daß ich die von mir vorgelegte Dissertation selbständig angefertigt, die benutzten Quellen und Hilfsmittel vollständig angegeben und die Stellen der Arbeit – einschließlich Tabellen, Karten und Abbildungen –, die anderen Werken im Wortlaut oder dem Sinn nach entnommen sind, in jedem Einzelfall als Entlehnung kenntlich gemacht habe; daß diese Dissertation noch keiner anderen Fakultät oder Universität zur Prüfung vorgelegen hat; daß sie – abgesehen von unten angegebenen Teilpublikationen – noch nicht veröffentlicht worden ist sowie, daß ich eine solche Veröffentlichung vor Abschluß des Promotionsverfahrens nicht vornehmen werde. Die Bestimmungen dieser Promotionsordnung sind mir bekannt. Die von mir vorgelegte Dissertation ist von Prof. Dr. T. Nattermann betreut worden.

Köln, den 2. November 1996

Jan Kierfeld

Teilpublikationen:

J. Kierfeld, Diplomarbeit, Universität zu Köln, 1993.

J. Kierfeld, J. Phys. I France **5**, 379 (1995).

J. Kierfeld and T. Hwa, Phys. Rev. Lett. **77**, 4233 (1996).

J. Kierfeld, T. Nattermann und T. Hwa, Phys. Rev. B **55**, 626 (1997).

J. Kierfeld, preprint cond-mat/9609045, submittiert an Physica C.

Lebenslauf

Persönliche Daten

Name:	Jan Kierfeld
Geburtsdatum:	31. Januar 1969
Geburtsort:	Essen
Eltern:	Prof. Dr. Gerd Kierfeld
	Dr. Elsbeth Kierfeld, geb. Schweer
Familienstand:	ledig

Schulausbildung

1975 - 1979	Gemeinschaftsgrundschule Heinrich-Lübke-Strasse, Leverkusen
1979 - 1988	Freiherr-vom-Stein Gymnasium, Leverkusen
Juni 1988	Abitur

Hochschulstudium

Sept. 1988	Immatrikulation an der Universität zu Köln Studiengänge: Diplom-Physiker und Diplom-Mathematiker
Juni 1990	Diplom-Vorprüfung im Fach Physik
Okt. 1990	Diplom-Vorprüfung im Fach Mathematik
Mai 1992	mündliche Diplom-Hauptprüfung im Fach Physik
Juni 1992 - Juni 1993	Anfertigung der schriflichen Diplomarbeit am Instiut für Theoretische Physik bei Prof. Dr. T. Nattermann, Thema: *Zur Existenz der Vortex-Glas-Phase in Schichtsystemen*
ab Juli 1993	Arbeit an dieser Dissertation
Sep. 1995 - Mai 1996	"research associate" an der University of California, San Diego bei Prof. Dr. T. Hwa.

Arbeitsverhältnisse an der Universität zu Köln

Okt. 1990 - Feb. 1991	Studentische Hilfskraft am Mathematischen Institut
Mai 1992 - Juli 1993	Studentische Hilfskraft am Institut für Theoretische Physik
Aug. 1993 - Dez. 1994	Wissenschaftliche Hilfskraft
Jan. 1995 - Aug. 1995	Wissenschaftlicher Mitarbeiter
ab Juni 1996	Mitarbeiter im SFB 341

Errata

1. In chapter 3, eq. (3.15), a factor ξ_{ab}^2 is missing on the *r.h.s.*:

$$\Delta_{pin}^2 \;:=\; (n_{pin} f_{pin}^2 \xi_{ab}^2)\xi_{ab}^3 \;=\; g_0 \xi_{ab}^{-1} \tag{A.72}$$

2. In chapter 3, eq. (3.40) a prime is missing:

$$\overline{\langle (u(\mathbf{R},L) - u(\mathbf{R}',L'))^2 \rangle} \;=\; 2An(4-d)\frac{1}{K_0^2}\ln\left(\frac{|\mathbf{R}-\mathbf{R}'|^2}{R_l^2} + \frac{(L-L')^2}{L_l^2}\right)^{1/2},$$

3. In chapter 4, eq. (4.25), a factor $p^2/4cK_c^2 = p^2/4\pi K_c^2 = 4\pi/p^2$ ($c=\pi$, $K_c = p^2/4\pi$) is missing:

$$\begin{aligned} G_{2D}(k) &\simeq \frac{1}{Kk^2} + \tau^2 \frac{4\pi}{p^2}\frac{\ln\left(\frac{2\pi}{kl_\parallel}\right)}{k^2} \\ G_{2D}(r_\parallel = 0) &\simeq \frac{1}{2\pi K}\ln\left(\frac{R_\parallel}{l_\parallel}\right) + \frac{\tau^2}{p^2}\ln^2\left(\frac{R_\parallel}{l_\parallel}\right) \end{aligned}$$

4. In chapter 4, in the paragraph *before* eq. (4.34), a factor 2 is missing when determining the diagrams that contribute:

   ... This result can be supplemented by a second argument based on the observation that at a $T=0$ fixed point only diagrams with #internal lines = 2#vertices contribute because vertices in the FRG formalism are the disorder correlators carrying a factor T^{-2}, and each bare propagator carries a factor T^1. ...

5. The argument presented before this sentence is erroneous because the disorder correlator at the fixed point has a *cusp* which has to be taken into account. It cannot be treated as quadratic. However there exists the following improved argument due to Thorsten Emig [private communication] which shows indeed that the averages in eq. (4.33) in the regime (i) can be treated as Gaussian:

   Starting from a replicated Hamiltonian (n = number of replicas)

$$\mathcal{H}_n/T \;=\; \gamma \int d^d x \left\{ \frac{1}{2T}\sum_{\alpha=1}^{n} (\boldsymbol{\nabla}\phi_\alpha)^2 - \frac{\gamma}{2T^2}\sum_{\alpha,\beta=1}^{n} R(\phi_\alpha - \phi_\beta)\right\}. \tag{A.73}$$

we can calculate the correlations $\overline{\langle\Psi(\mathbf{x}_1)\Psi(\mathbf{x}_2)\rangle}$ of the order parameter $\Psi(\mathbf{x}) = \exp(i\phi(\mathbf{x}))$. In the RG approach, the glassy phase is described by a $T = 0$ fixed point where the disorder correlator $R(\phi)$ is uniformly of the order $\epsilon = 4 - d$. This suggests to calculate the Ψ correlations perturbatively in ϵ. In the following we do *not* assume that the field $\phi(\mathbf{x})$ is Gaussian distributed, i.e. we make no direct use of the Wick theorem. Therefore we have to expand the disorder correlator $R(\phi)$ in terms which can be averaged easily with the free Hamiltonian. Since $R(\phi)$ develops a non analyticity at $\phi = 0$ (with $R^{(4)}(0) = \infty$) on length scales beyond the Fukuyama-Lee (or Larkin) length L_Δ, a power series expansion is not available. Instead, we make use of the Fourier expansion

$$R(\phi) = \sum_{m=1}^{\infty} R_m \cos(m\phi) = \frac{1}{2}\sum_{m=1}^{\infty} R_m \left(e^{im\phi} + e^{-im\phi}\right) \tag{A.74}$$

which works also in the non analytic case. To obtain the correlations $\overline{\langle\Psi(\mathbf{x}_1)\Psi(\mathbf{x}_2)\rangle}$ to first order in ϵ, we have to calculate only averages of powers of $\exp(i\phi)$, i.e. terms of the form

$$\langle \exp\left[i\phi_\alpha(\mathbf{x}_1) - i\phi_\beta(\mathbf{x}_2) \pm im\phi_\mu(\mathbf{y}) \mp im\phi_\nu(\mathbf{y})\right]\rangle_0 \tag{A.75}$$

where $\langle\ldots\rangle_0$ denotes the average with respect to the free Hamiltonian with the pure elastic part. Since the free Hamiltonian is Gaussian we can now use Wick's theorem with the bare propagator $\Delta(\mathbf{x}) = \frac{T}{\gamma}\int d^dq e^{i\mathbf{qx}}/q^2$ and obtain for the correlation function

$$\begin{aligned}
&\overline{\langle e^{i(\phi_\alpha(\mathbf{x}_1)-\phi_\beta(\mathbf{x}_2))}\rangle} = \langle e^{i(\phi_\alpha(\mathbf{x}_1)-\phi_\beta(\mathbf{x}_2))}\rangle_0 \\
&+\frac{\gamma^2}{2T^2} e^{-\Delta(\mathbf{0})+\Delta(\mathbf{x}_1-\mathbf{x}_2)\delta_{\alpha\beta}} \sum_{\mu,\nu=1}^{n}\sum_{m=1}^{\infty} R_m e^{-m^2\Delta(\mathbf{0})(1-\delta_{\mu\nu})} \\
&\times \int d^dy \cosh\left[m\Delta(\mathbf{x}_1-\mathbf{y})(\delta_{\alpha\mu}-\delta_{\alpha\nu}) - m\Delta(\mathbf{x}_2-\mathbf{y})(\delta_{\beta\mu}-\delta_{\beta\nu})\right]. \\
&= \langle e^{i(\phi_\alpha(\mathbf{x}_1)-\phi_\beta(\mathbf{x}_2))}\rangle_0 \Bigg(1 + \frac{\gamma^2}{2T^2}\sum_{\mu,\nu=1}^{n}\sum_{m=1}^{\infty} R_m e^{-m^2\Delta(\mathbf{0})(1-\delta_{\mu\nu})} \\
&\times \int d^dy \cosh\left[m\Delta(\mathbf{x}_1-\mathbf{y})(\delta_{\alpha\mu}-\delta_{\alpha\nu}) - m\Delta(\mathbf{x}_2-\mathbf{y})(\delta_{\beta\mu}-\delta_{\beta\nu})\right]. \Bigg)
\end{aligned} \tag{A.76}$$

Now we can make use of the fact that the phase of interest is described by a $T = 0$ fixed point. Since $\Delta(\mathbf{x}) \sim T$, we have to expand the exponentials and the cosh only up to second order in the propagator $\Delta(\mathbf{x})$. Since we have to take the limit $n \to 0$

we can neglect all terms of the order n. Thus we obtain

$$\overline{\left\langle e^{i(\phi_\alpha(\mathbf{x}_1)-\phi_\alpha(\mathbf{x}_2))}\right\rangle} = \left\langle e^{i(\phi_\alpha(\mathbf{x}_1)-\phi_\alpha(\mathbf{x}_2))}\right\rangle_0 - \frac{\gamma^2}{2T^2}\sum_{m=1}^{\infty} m^2 R_m$$
$$\times \int d^d y \left[\Delta^2(\mathbf{x}_1-\mathbf{y}) - 2\Delta(\mathbf{x}_1-\mathbf{y})\Delta(\mathbf{x}_2-\mathbf{y}) + \Delta^2(\mathbf{x}_2-\mathbf{y})\right] \quad \text{(A.77)}$$

Due to $\left\langle e^{i(\phi_\alpha(\mathbf{x}_1)-\phi_\alpha(\mathbf{x}_2))}\right\rangle_0 = 1 + \mathcal{O}(T)$ we end up with

$$\overline{\langle\Psi(\mathbf{x}_1)\Psi(\mathbf{x}_2)\rangle} = 1 + \int d^d q \frac{R''(0)e^{i\mathbf{q}(\mathbf{x}_1-\mathbf{x}_2)}}{q^4} \quad \text{(A.78)}$$

Finally we have to take into account the renormalization of the disorder correlator by using the effective correlator near the fixed point, i.e. replace $R(\phi)$ by $\tilde{R}_q(\phi) = e^{-\epsilon l^*} R_{l^*}(\phi) = (\Lambda/q)^{d-4} R^*(\phi)$ where $l^* = \ln(\Lambda/q)$ corresponds to the length scale (Fukuyama-Lee length) at which $R(\phi)$ has approximatively approached its fixed point value. With $R^{*''}(0) = -\epsilon\frac{\pi^2}{9}\Lambda^{4-d}/K_d$ we obtain

$$\overline{\langle\Psi(\mathbf{x}_1)\Psi(\mathbf{x}_2)\rangle} = 1 - \epsilon\frac{\pi^2}{9}\ln\left(\frac{|\mathbf{x_1}-\mathbf{x}_2|}{L_\Delta}\right) \quad \text{for} \quad |\mathbf{x_1}-\mathbf{x}_2| > L_\Delta. \quad \text{(A.79)}$$

This result agrees to first order in ϵ with the expression

$$\overline{\langle\Psi(\mathbf{x}_1)\Psi(\mathbf{x}_2)\rangle} = \left(\frac{|\mathbf{x_1}-\mathbf{x}_2|}{L_\Delta}\right)^{-\epsilon\pi^2/9} \quad \text{(A.80)}$$

which follows from the assumption of a Gaussian distributed phase $\phi(\mathbf{x})$ by direct use of Wick's theorem. Therefore, to calculate correlations of the order parameter to first order in ϵ it is justified to assume a Gaussian phase field.

6. In chapter 5 after eq. (5.10):

   ... for configurations of the field ϕ ...